THE UNIVERSITY OF MICHIGAN
APR 11 1963
PHOENIX LIBRARY

# REACTOR MATERIALS

*A Quarterly Technical Progress Review*

Prepared for DIVISION OF TECHNICAL INFORMATION, USAEC, by
R. W. DAYTON, E. M. SIMONS, and ASSOCIATES, BATTELLE MEMORIAL INSTITUTE

*February 1963*

● VOLUME 6

● NUMBER 1

FEATURE ARTICLE:

**Recent Developments in Reactor Materials from Powders**

# TECHNICAL PROGRESS REVIEWS

To meet the needs of industry for concise summaries of current atomic developments, the Atomic Energy Commission is publishing this series, Technical Progress Reviews. Issued quarterly, each of the reviews digests and evaluates the latest findings in a specific area of nuclear technology and science.

The four journals published in this series are:

*Nuclear Safety*, Wm. B. Cottrell, W. H. Jordan, and associates, Oak Ridge National Laboratory

*Power Reactor Technology*, W. H. Zinn and J. R. Dietrich, General Nuclear Engineering Corporation

*Reactor Materials*, R. W. Dayton, E. M. Simons, and associates, Battelle Memorial Institute

*Reactor Fuel Processing*, Stephen Lawroski and associates, Chemical Engineering Division, Argonne National Laboratory

Each journal may be purchased ($2.00 per year for subscription and individual issues $0.55) from the Superintendent of Documents, U. S. Government Printing Office, Washington 25, D. C. See back cover for remittance instructions and foreign postage requirements.

The views expressed in this publication do not necessarily represent those of the United States Atomic Energy Commission, its divisions or offices, or of any Commission advisory committee or contractor.

## Availability of Reports Cited in This Review

*Unclassified AEC reports* are available for inspection at AEC depository libraries and are sold by the Office of Technical Services, Department of Commerce, Washington 25, D. C. Some of the reports cited are not available owing to their preliminary nature; however, the information contained in them will eventually be made available in formal progress or topical reports.

*Unclassified reports issued by other Government agencies or private organizations* should be requested from the originator.

*Unclassified British and Canadian reports* may be inspected at AEC depository libraries. British reports are sold by the British Information Service, 45 Rockefeller Plaza, New York, N. Y.; Canadian reports (AECL series) are sold by the Scientific Document Distribution Office, Atomic Energy of Canada, Ltd., Chalk River, Ontario, Canada.

*Classified U. S. and foreign reports* identified in this journal as Classified may be purchased by properly cleared Access Permit Holders from the Division of Technical Information Extension, U. S. Atomic Energy Commission, P. O. Box 1001, Oak Ridge, Tenn. Such reports may be inspected at classified AEC depository libraries.

# REACTOR MATERIALS

## A REVIEW OF RECENT DEVELOPMENTS

Prepared for DIVISION OF TECHNICAL INFORMATION, USAEC,
by R. W. DAYTON, E. M. SIMONS, and ASSOCIATES,
BATTELLE MEMORIAL INSTITUTE

● FEB. 1963
● VOLUME 6
● NUMBER 1

# Foreword

*Reactor Materials* is one of a series of quarterly technical progress reviews broadly covering the field of nuclear science and technology. Under the auspices of the USAEC Division of Technical Information, *Reactor Materials* is prepared by Battelle personnel from worldwide literature. It covers properties, behavior, and fabrication processes of materials applicable to nuclear reactor components and associated equipment.

The reader will recognize that the scope of this Review is too broad to permit detailed coverage of every topic. Rather, the authors and editors attempt to combine the highlights of significant new developments into an informative summary of current research for both management and the technical specialist. As a rule, enough of the results are presented to define the research and summarize the findings. For readers desiring more information on any particular topic, a complete set of references is provided at the end of each section.

Each quarter, a number of bibliographies, monographs, and books appear on subjects within the scope of *Reactor Materials*. Although the main purpose of this Review is to call attention to findings that are new and significant, such publications are noted in the text because they often represent excellent compilations of available information on important materials topics.

R. W. DAYTON
E. M. SIMONS
R. W. ENDEBROCK
*Battelle Memorial Institute*

DEPOSITED BY THE
TED STATES OF AMERICA

# Contents

FEATURE ARTICLE

*Recent Developments in Reactor Materials from Powders* . . . . . 1
**by George W. Cunningham, Battelle Memorial Institute**

Foreword

I. FUEL AND FERTILE MATERIALS . . 19
Uranium Metal and Alloys . . . . . 19
Plutonium . . . . . 24
Thorium . . . . . 28
Dispersion Fuels . . . . . 30
Coated-Particle Fuel Materials . . . . . 31
Refractory Fuel and Fertile Materials . . 41
Basic Studies of Irradiation Effects on Fuel Materials . . . . . 47
References . . . . . 48

II MODERATOR MATERIALS . . . . . 52
Graphite . . . . . 52
Beryllium Metal and Alloys . . . . . 53
Beryllium Oxide . . . . . 58
Solid Hydrides . . . . . 60
References . . . . . 61

III NUCLEAR POISONS . . . . . 63
Metallic Poisons . . . . . 63
Dispersion Control Materials . . . . . 63
References . . . . . 66

IV CLADDING AND STRUCTURAL MATERIALS . . . . . 67
Corrosion . . . . . 67
Metal-Water Reactions . . . . . 73
Radiation Effects in Nonfuel Materials . . 74
Selected Mechanical Properties of Cladding and Structural Materials . . . 86
Selected Metallurgical Aspects of Cladding and Structural Materials . . . 87
Diffusion Studies . . . . . 88
Ceramic Technology . . . . . 89
References . . . . . 90

V SPECIAL FABRICATION TECHNIQUES . . . . . 96
Melting and Casting . . . . . 96
Fabrication and Heat-Treatment . . . . 97
Cladding . . . . . 98
Explosive Forming . . . . . .101
Nondestructive Testing . . . . . .108
References . . . . . .108

Issued quarterly by the U. S. Atomic Energy Commission. Use of funds for printing this publication approved by the Director of the Bureau of the Budget on November 1, 1960.

FEATURE ARTICLE

# Recent Developments in Reactor Materials from Powders

By George W. Cunningham*

[*Editor's Note: Continuing the Policy inaugurated in the last issue, of including a timely review or state-of-the-art article in* Reactor Materials *each quarter, the editors submit the article below on powder techniques as applied to reactor materials. The subject is a "natural" for this series (in view of the substantial strides made during the past few years), and it has been spurred on by the heightened interest in dispersion fuels and high-temperature materials.*

*Obviously a review paper such as this is not intended to be a comprehensive treatise. It is written to give readers who are not specialists in the field a general picture of the developments to date and their applications. From the following descriptions of the newer powder techniques, it will become apparent to the reader that we have come a long way since the old die press-and-sinter days.*]

## Introduction

Powder techniques have been utilized for the development of reactor materials since the time of the Manhattan Project. Initially the work did not represent a major effort, and it was usually temporary in nature. In recent years, however, many fuel and poison-material components have been fabricated by powder techniques. Before the development of suitable melting and casting procedures, powder techniques were often used for primary consolidation of materials such as uranium, thorium, zirconium, niobium, titanium, and hafnium. At the present time most of the common materials can be cast, and powder techniques are being used primarily to produce dispersions or to fabricate refractory materials such as carbides, nitrides, borides, and oxides. Also, process refinements are being developed to lower costs.

In this review some of the applications of powder metallurgy to reactor-materials fabrication are reviewed. Special emphasis is given to the new techniques (some of which have not yet been adopted by the industry as a whole). Techniques discussed are powder preparation, powder rolling, vibratory compaction, plasma spraying, hot isostatic compaction, explosive compaction, electrodeposition, and procedures for producing idealized dispersions.

## Processing Techniques

### Powder Preparation

Many modifications of standard grinding, shotting, and chemical-reaction techniques have been utilized to improve the quality of powders for reactor components. However, much of the significant new work has centered around the desire to produce spherical fuel or control-material particles. Hedger and Hall[1] have de-

*Research Associate, Advanced Materials Development Division, Battelle Memorial Institute.

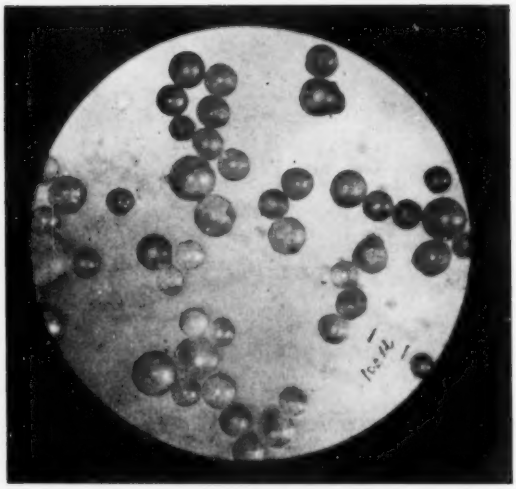

Fig. 1 $Al_2O_3$ particles produced in an induction-coupled argon plasma.[2]

scribed the use of an induction-coupled plasma to produce spherical powders. With the intense heat generated by the plasma, it is possible to spheroidize refractory materials as well as metals. Spherical $Al_2O_3$ produced with this technique by Alexander and Jackson[2] is shown in Fig. 1. Workers at Vitro[3] developed a technique for producing spherical UC by using a consumable electrode of $UO_2$ mixed with graphite to produce a high-intensity arc. As the molten UC forms at the tip of the anode, droplets are blown off and are condensed by an inert-gas stream. This type of powder is shown in Fig. 2. A modification of this process has been developed by Holmgren et al.[4] for the production of high-purity submicron powders of tungsten, molybdenum, niobium, $WO_3$, $MoO_3$, MgO, $SiO_2$, $Al_2O_3$, $ThO_2$, $ZrO_2$, $TiO_2$, $Nb_2O_5$, $Fe_3O_4$, aluminum, and titanium. In general, they were able to produce powders of 99% purity and less than 10 $\mu$ in diameter.

Many of the early efforts to produce spherical fuel particles were conducted at Knolls, and most commercial methods for making spherical $UO_2$ are modifications of the Knolls technique of abrading green-pressed $UO_2$ particles to a rounded shape and sintering. Muccigrosso et al.[5] have described methods used at Knolls to produce spherical $B_4C$. Four methods are described: (1) resistance hot-press method, (2) graphite-tube furnace method, (3) mechanical abrasion method, and (4) plasma-spray method. In the first method, one part of angular particles of $B_4C$ is blended with three parts of graphite powder, held in a hot press 15 min at 2300°C, and cooled in place. The surface tension is sufficient to spheroidize the $B_4C$. The graphite-tube furnace method is similar. A mixture of $B_4C$ and graphite is heated in the furnace for ½ hr at 2350°C, the temperature is raised to 2450°C for 5 min, and the sample is pushed into the furnace cold zone. The mechanical abrasion method consists of grinding the particles to a smooth shape in an air mill. The plasma-spray method consists of feeding sintered $B_4C$ rods into a plasma jet, which melts the $B_4C$ into droplets that quench into spheres as they are carried out of the high-temperature region.

The technique of suspending the carbide particles in graphite and heating to a temperature where melting occurs or where there is sufficient surface tension to cause spheroidization has also been used at General Atomic[6] to produce spherical $UC_2$ powder.

One of the potentially most useful powder developments involves the production of coated and composite powders. Ceramic, metal, and intermetallics are coated by chemical vapor deposition, vapor coating, or chemical coating techniques. These processes will be described in some detail in a future *Reactor Materials* feature article. Table 1 lists some composite powders that have been produced. Possible applications of the coated particles are virtually

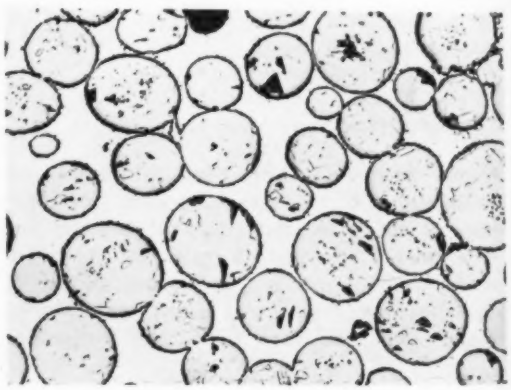

Fig. 2 Spherical UC prepared by arc melting a $UO_2$-carbon electrode in a flowing argon atmosphere.[3] Magnification, 250×.

Table 1 COMPOSITE POWDERS

| Fabrication procedure | Powder | Producer |
|---|---|---|
| Vapor deposition in fluidized bed | Carbon-coated uranium | Battelle |
| | Carbon-coated UC | Battelle |
| | Carbon-coated $UC_2$ | Battelle |
| | Tungsten-coated molybdenum | Battelle |
| | Tungsten-coated $UO_2$ | Battelle |
| | Niobium-coated $UO_2$ | Battelle |
| | BeO-coated $UO_2$ | Battelle |
| | $Al_2O_3$-coated $UO_2$ | Battelle |
| | MgO-coated $UO_2$ | Battelle |
| | Carbon-coated $UO_2$ | Battelle |
| | $ZrO_2$-coated $UO_2$ | Battelle |
| Coating with oxide powder and reducing to metal | Nickel-coated $UO_2$ | Martin-Nuclear |
| | Stainless-steel-coated $UO_2$ | Martin-Nuclear |
| | Tungsten-coated $UO_2$ | Martin-Nuclear |
| | Molybdenum-coated $UO_2$ | Martin-Nuclear |
| Electroless nickel plating | Nickel-coated $UO_2$ | Martin-Nuclear |
| Coprecipitation | $UO_2$-ZrO mixed oxide | Bettis |
| | Nickel-coated tin | Sherrit-Gordon |
| | Nickel-coated copper | Sherrit-Gordon |
| | Nickel-coated chromium | Sherrit-Gordon |
| | Nickel-coated aluminum | Sherrit-Gordon |
| | Nickel-coated $Al_2O_3$ | Sherrit-Gordon |
| | Nickel-coated $Cr_2O_3$ | Sherrit-Gordon |
| | Cobalt-coated WC | Sherrit-Gordon |
| | Nickel-coated graphite | Sherrit-Gordon |
| | Nickel-coated $TiB_2$ | Sherrit-Gordon |

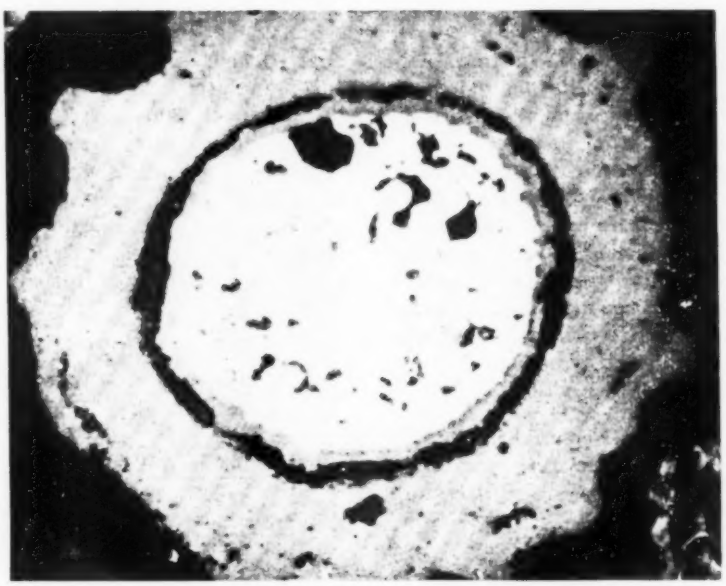

Fig. 3 Typical undamaged $Al_2O_3$-coated $UO_2$ particle after irradiation to 4 to 5% burnup.[7] Coating was applied in six steps, and the fourth layer was inadvertently deposited in a porous condition. This porous layer appears as a dark 6-$\mu$ ring around an inner ring of dense $Al_2O_3$. The majority of undamaged coated particles were found near the center of the irradiated S&P ball. (Unpublished data.) Magnification, 500×.

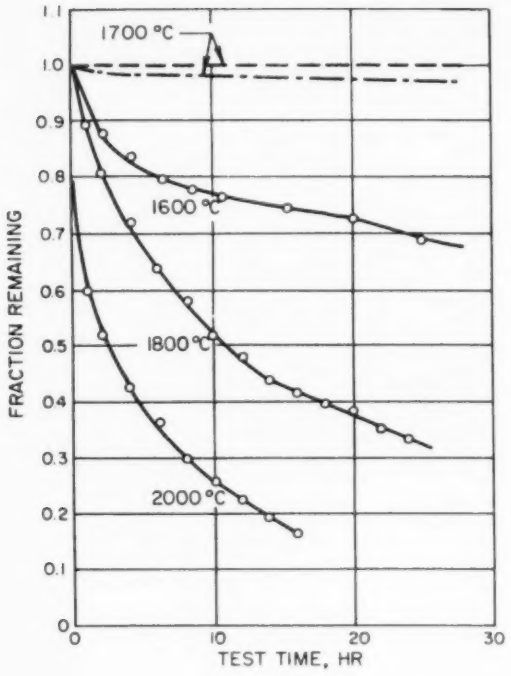


Fig. 4 Release of $Xe^{133}$ from compacts with coated and uncoated fuel particles at indicated test temperatures.[7] – – –, compact with coated fuel particles (25-$\mu$ coating from $C_2H_2$ at 1400°C). — —, coated fuel particles (60-$\mu$ coating from $CH_4$ at 1400°C). ○, compact with uncoated fuel particles.

unlimited, and only a few have been investigated. Each individual coated fuel particle can serve as a miniature fuel element since each particle is coated with a fission-product-retaining cladding. Figure 3 is a photomicrograph[7] of such a particle after irradiation.[7] The xenon retention of coated uranium-thorium carbide fuel particles is illustrated in Fig. 4.

Another use[8] for the coated particles is the preparation of cermets (Fig. 5). The coated particle permits the formation of a dense structure with a continuous metallic phase in a system where the metal does not wet the ceramic. Coatings may also be used as a diffusion barrier to prevent solid-state reactions between the particle and the metal matrix. For example, niobium-coated $UO_2$ has been proposed for use in aluminum matrices to prevent the aluminum-$UO_2$ reaction.[9] Coated particles offer the possibility of "tailoring" composite structures to the desired physical or mechanical properties, as illustrated by the fact that molybdenum–80 vol.% $UO_2$ cermets have a thermal conductivity[10a] greater than that of $UO_2$ by a factor of 8.

### Powder Rolling

Direct rolling of metal powders can be utilized to produce thin strips of any desired length. In principle, it is possible to insert metal powder into a pair of rolls that compact it into a strip strong enough to be transferred to a sintering furnace. If necessary it can be rolled and sintered again to obtain desired properties. Variables that affect the properties of the rolled strip are (1) diameter and pressure of the rolls, (2) shape and size of the powder particles, and (3) rate at which the powder is fed into the rolls.

Extensive use of powder rolling has been carried out by Martin-Nuclear[11] for the production of tubular fuel elements. This process consists of the following steps: (1) a $UO_2$–stainless-steel powder mixture is rolled to a green strip, sintered, cold reduced, annealed,

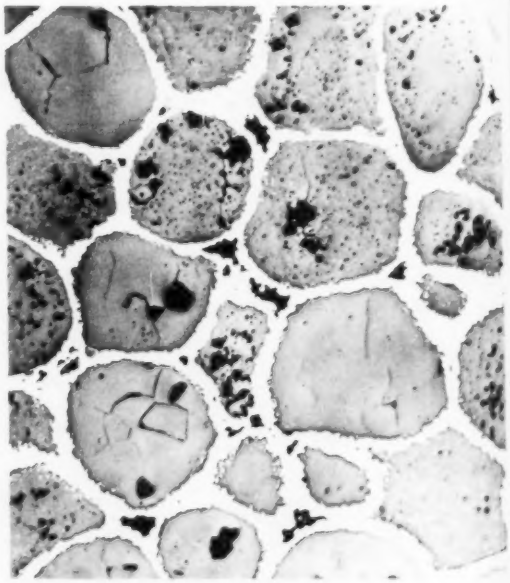

Fig. 5 Cermet irradiation specimen of 80 vol.% $UO_2$–niobium.[8] The −100 + 200-mesh $UO_2$ was coated with niobium by vapor deposition. The coated powder was then green pressed and isostatically pressed in a niobium can for 3 hr at 2300°F under a pressure of 10,000 psi. Magnification, 250×.

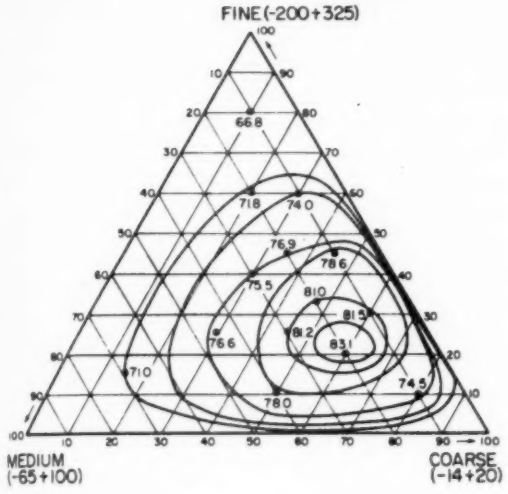


Fig. 6 $UO_2$ densities after vibrational compaction of various particle-size compositions.[14]

and formed into a tube; (2) the core is fitted between two stainless-steel tubes that serve as cladding; (3) the end is swaged, and the tube is drawn down to a tight fit between core and cladding; and (4) the tube is annealed to provide a diffusion bond between core and cladding. Recently, Martin[12] has added gas-pressure bonding as a final step to ensure core-to-cladding bond integrity.

### *Vibratory Compaction*

Packing of tubes with loose powder and vibrating to increase the packed density has been utilized for some time in atomic energy applications. For example, in 1955 The Norton Company reported[13] packing boron carbide to densities of about 76% of the theoretical density by vibration alone. However, in the last three years the development of new equipment and better control over powder shape and size has allowed researchers to develop techniques for packing loose powders to densities on the order of 90% of the theoretical density.

The process has been developed primarily for loading tubes with $UO_2$ or $UO_2$-bearing fuel materials. Two types of vibrational equipment are used: (1) the pneumatic vibrator, in which the vibrational energy is derived from a shock wave created by the impact of an air-driven piston on the housing and (2) the electrodynamic shaker, which produces vibrational energy by means of a high-power audioamplifier driving an electromechanical transducer.

Most of the workers in the field have utilized crushed and fused $UO_2$ in their studies. Some of the advantages of this powder are: it can be obtained in a wide range of particle sizes, and it has a high density, a low surface activity, and a low surface-to-volume ratio.

Particles of $UO_2$ are irregular in shape, and the packing density cannot be treated by the mathematical relation derived for the packing of spheres. However, the initial particle-size distribution has a great effect on the vibration-packed density, and several workers have at-

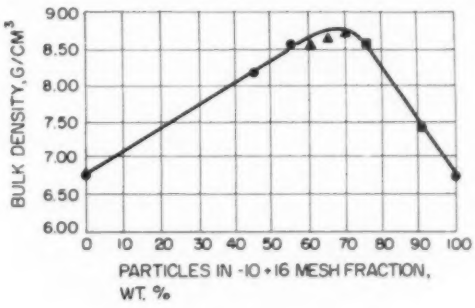


Fig. 7 Effect of particle-size distribution on the vibrated density of binary mixtures (−10 +16 and −200 mesh).[15a] ●, single vibration run, ▲, average of two vibration runs, ■, average of three vibration runs.

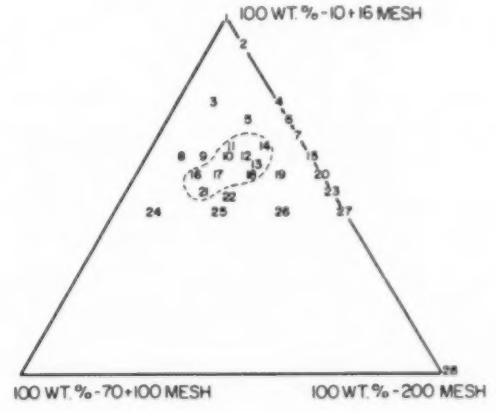


Fig. 8 Effect of particle-size distribution on vibrated density of ternary mixtures.[15a] Broken line encloses approximate area where density exceeds 88% of theoretical density. Numbers indicate individual experiments.

tempted to establish the most favorable particle-size distribution. Early work initiated at Hanford[14] resulted in the chart shown in Fig. 6. Ernst and Beatty[15a] at Oak Ridge have studied the effect of particle-size distribution in two-fraction and three-fraction mixtures. Their results for the two-fraction mixtures are shown in Fig. 7, and those for the three-fraction mixtures in Fig. 8. A maximum density of 87.5% of theoretical was obtained for the two-fraction blend, and densities of 90% of theoretical were obtained with three-fraction blends of a $ThO_2$–3.4 wt.% $UO_2$-mixed oxide. DeHollander[15b] studied three-fraction blends at Vallecitos, and he came to the conclusion that the maximum $UO_2$ density could be attained by using coarse, medium, and fine fractions separated by at least six sieve sizes, and a composition of about 60% coarse, 20% medium, and 20% fine. He obtained a maximum density of 88.5% of theoretical.

Workers at Hanford have used this process extensively. Hauth[15c] has reported the fabrication of 8-ft-long fuel rods by vibratory techniques.

Table 2 ESTIMATES OF CURRENT COSTS OF PELLETIZED AND VIBRATORY-PACKED $UO_2$ FUELS[15b]

| | Pelletized | Vibratory packed |
|---|---|---|
| Labor: | | |
| Fuel loading (density, %)(dia., in.) | (95)(0.369) | (90)(0.350) |
| Pellet weighing, inspection, and loading, man-hours | 0.20 | |
| Powder processing, man-hours | | 0.10 |
| Powder batching, man-hours | | 0.05 |
| Powder loading and compaction, man-hours | | 0.15 |
| End-cap welding, man-hours | | |
| Fuel-rod inspection, man-hours | | |
| Subtotal; man-hours per fuel rod | 0.20 | 0.30 |
| Number of rods per core | 25,450 | 34,433 |
| Typical scrap allowance, % of loading | 1 | 1 |
| Total number of rods required | 25,700 | 34,780 |
| Total man-hours for core loading | 5,140 | 9,834 |
| Total for labor (at $9/hr), $ | 46,260 | 88,506 |
| Materials: | | |
| Fuel | | |
| Quantity, lb (% overage) | 134,740(2) | 132,758(0.5) |
| Cost per pound, $ | 1,000 | 4.50 |
| Subtotal for fuel, $ | 1,347,400 | 597,411 |
| Tubing | | |
| Quality, ft | 257,000 | 347,800 |
| Cost per foot, $ | 1.50 | 1.50 |
| Subtotal for tubing, $ | 385,500 | 521,700 |
| End-cap cost | | |
| Conversion of excess $UO_2$ to $U_3O_8$: | | |
| Excess $UO_2$, lb | 2,642 | 660 |
| Conversion cost, $/lb | 2.00 | 2.00 |
| Subtotal of conversion costs, $ | 5,284 | 1,320 |
| Fuel charge difference, $ | | 310,000 |
| Summary: | | |
| Labor, $ | 46,260 | 88,506 |
| Materials, $ | 1,732,900 | 1,118,111 |
| Conversion, $ | 5,284 | 1,320 |
| Fuel charge difference, $ | | 310,000 |
| Totals, $ | 1,784,444 | 1,517,937 |
| Difference, $ | 266,507 | |

One of the major reasons for investigating vibratory compaction is the desire to produce fuel elements at a lower cost. Some cost estimates made by Murtha and Chernock[15d] are shown in Table 2. Although the current costs show only about a 15% decrease in cost by the use of vibratory methods at the present time, the authors expect the savings to increase to about 30% as fabrication techniques are improved.

Several authors have considered the use of vibratory techniques that are followed by swaging[15e,15f] or hot isostatic pressing.[16] When these techniques are used, final $UO_2$ densities on the order of 94 to 99% of theoretical can be obtained.

### Plasma-Arc Spraying

To date no extensive use has been made of plasma-arc spraying for reactor materials. However, because of the potential use of this spraying for application of coating, production of complex materials, and production of unusual shapes as well as large shapes, some mention should be made of plasma-arc-sprayed materials.

Virtually any material that can be obtained in powder form can be plasma-arc sprayed. The basic process consists in spraying the powder through a hollow electrode into the gas plasma (usually argon) where it is rapidly heated above the melting point and blown onto the surface of the component being prepared. There are many process variables, most of which must be worked out individually for each new component or material. Mash et al.[17] have considered the large number of variables (listed in Table 3) and have attempted to describe conditions for the highest deposition efficiencies for several materials. Several materials are compared in Table 4, and the optimum conditions for spraying these materials are shown in Table 5.

Singleton et al.[18] investigated tungsten fabrication by plasma-arc spraying and obtained tungsten with the properties shown in Table 6. Comparison of the high-temperature tensile strength of arc-sprayed tungsten with that of commercial material is shown in Fig. 9.

Stetson and Hauck[19] have experimented with techniques for spraying toxic and oxidizable materials. They used a dry-box-enclosed plasma gun and an elaborate filtering system. Properties of the materials that they plasma sprayed are shown in Table 7. The adherence was determined by bonding two plasma-sprayed surfaces with Eastman 910 adhesive and pulling in tension.

Table 3 CLASSIFICATION OF PLASMA-SPRAY VARIABLES AND PERTINENT COATING PROPERTIES[17]

| |
|---|
| Process variables by category: |
| Plasma |
| Power input |
| Type of arc gas |
| Flow of arc gas |
| Plasma-torch geometry |
| Powder |
| Composition |
| Physical properties |
| Method of manufacture |
| Powder size |
| Particle-size distribution |
| Powder feed |
| Type of powder feed system |
| Rate of powder addition to carrier gas |
| Type of carrier gas |
| Flow of carrier gas |
| Angle of powder entry into plasma |
| Location of powder entry port |
| Spraying procedure |
| Torch-to-work distance |
| Traverse rate |
| Angle of torch with work |
| Cover gas |
| Spraying atmosphere |
| Substrate |
| Composition |
| Surface-preparation method |
| Surface roughness |
| Temperature |
| Coating properties or characteristics evaluated: |
| Density |
| Microstructure |
| Adherence |
| Deposition efficiency and rate |
| X-ray diffraction analysis of crystal structure |
| Chemical composition |

The major disadvantage of plasma-arc spraying is the relatively low density of the product, which necessitates either using the material in the porous condition or putting it through an additional densification process. Also, some difficulty may be encountered if the material has a high vapor pressure.

### Hot Isostatic Compaction

Among hot-compaction processes, hot isostatic pressing is the most versatile. This process has permitted the production of massive components of high-density high-purity

carbides, nitrides, borides, silicides, intermetallics, and metals. Paprocki et al.[20] have studied both the self-bonding of solid components and the compaction of various powders in the gas-pressure-bonding autoclaves (Fig. 10). Powders are contained in evacuated cans and are isostatically pressed at pressures to 10,000 psi and temperatures to 3000°F. Autoclaves that have capacities of 50,000 psi at 5500°F have been designed and are being tested.[21]

As illustrated in Fig. 11, the pressures available in the autoclave permit densification of refractory metals at low enough temperatures to retain a fine grain structure. The same behavior is observed for ceramics. Keller et al.[10b] have discussed the densification of UC and UN bodies by hot isostatic compaction. They reported densities greater than 95% of theoretical and good control of composition and impurities. As shown in Fig. 5 and as discussed by Cunningham,[10a] this technique has been utilized to produce high-density, idealized structures of $UO_2$ cermets containing 80 vol.% $UO_2$. With such structures appreciable improvements in such properties as thermal conductivity (Fig. 12) have been noted.

Extensive studies have been performed by Paprocki and coworkers[22] and by Sheinhartz and Fugardi[23] to utilize gas pressure for simultaneous bonding and densification of $UO_2$ fuel elements. As reported by Porembka and Boyer[15g] (see Table 8), densities up to 99.5% of theoretical can be achieved by these techniques.

Table 4 COMPARISON OF TYPICAL MATERIALS FOR PLASMA-SPRAY APPLICATIONS[17]

| Material | Diffusivity, $cm^2/sec$ | $C_p(T_{m.p.}-T_1)$, cal/g | $d_{max}$,* $\mu$ | Calculated relative ease of plasma spraying† |
|---|---|---|---|---|
| $ZrO_2$ | 0.005 | 430 | 26 | 5 |
| $UO_2$ | 0.025 | 214 | 58 | 4 |
| TiC | 0.04 | 645 | 72 | 3 |
| TaC | 0.09 | 115 | 110 | 1 |
| ZrC | 0.05 | 525 | 82 | 3 |
| TiN | 0.07 | 556 | 96 | 2 |
| $B_4C$ | 0.06 | 109 | 90 | 2 |
| Stainless steel, type 4340 | 0.08 | 195 | 104 | 1 |
| Stainless steel, type 304 | 0.05 | 226 | 82 | 3 |
| Tungsten | 0.63 | 111 | 280 | 1 |

*Calculated maximum particle diameter for reaching a center temperature of 0.9 melting point in 100 $\mu$sec residence time in a plasma jet.

†Based on $d_{max}$. Indicates degree of control necessary for satisfactory coatings. Group 1 materials can be sprayed under a wide range of conditions, whereas Group 5 requires a relatively narrow range.

Table 5 SUMMARY OF THE CONDITIONS DETERMINED FOR THE HIGHEST DEPOSITION EFFICIENCIES[17]

| | Material | | | | | |
|---|---|---|---|---|---|---|
| | $ZrO_2$ | $UO_2$ | TiC | ZrC | TaC | Steel |
| Power input, kw | >20* | >20* | >19.5* | 16 | >21* | 10 |
| Arc-gas flow, cfh | 60 | 60 | 25 | 30 | 30 | 40 |
| Powder feed rate, g/min | <10 | 30 | <12 | 12 | <15 | <9 |
| Powder gas flow, cfh | 5 | 6 | 5 | 6 | 6 | 7 |
| Spray distance, in. | 4 | 4 | 3.5 | 2 | 3 | 3–5 |
| Traverse rate, in./min | 70 | 50 | 72 | 40 | 72 | 45 |
| Cover-gas type | None | None | He | He | He | He |
| Cover-gas flow, cfh | | | 250 | 250 | >160 | 160 |
| Powder size, $\mu$ | 43–74 | 43–74 | 12–43 | 12–43 | 12–43 | 43–74 |

*Limit of equipment.

Table 6 ROOM-TEMPERATURE PROPERTIES OF TUNGSTEN[18]

| | Arc sprayed | Arc sprayed and sintered | Cold pressed and sintered |
|---|---|---|---|
| Density, % of theoretical | 86 | 93 | 93 |
| Microstructure | Lamellar | Equiaxed fine grain | Equiaxed fine grain |
| Hardness, DPH | 250 | 300 | 300 |
| Ultimate tensile strength,* psi | 22,000 | 70,000 | 60,000 |
| Forgeability | Poor | Good | Good |

*Ring crush test.

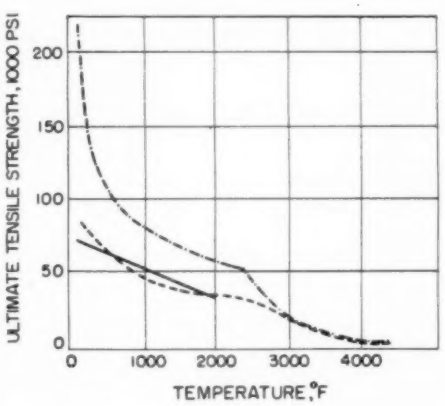


Fig. 9 Tensile properties of tungsten.[18] ——, recrystallized arc sprayed. - - - -, recrystallized commercial. -.-.-, wrought commercial (stress relieved).

Paprocki et al.[24] have also reported on the densification and bonding of solid hydride moderator materials, such as delta-phase zirconium hydride.

### *High-Energy-Rate Compaction*

The density of powder compacts is usually dependent upon the pressure at which they are compacted. When conventional presses are used, the green-pressed density is related to the ductility (i.e., the more ductile powders can be compacted to a high density). Recent developments in the field of high-energy-rate-release systems have permitted the compaction of metals, ceramics, and intermetallics to very near the theoretical density. The high energy can be released by detonation of explosives, sudden release of electrical energy, or the sudden release of stored hydraulic pressure. Generated pressures may be very high. For example, shock waves from explosives may produce pressures on the order of 4 to 12 million psi in a metal-powder compact.

Thus for powder compaction the use of explosives appears to have great potential. Two general types of systems are used with explosives: (1) the contact system and (2) the standoff system. In the contact system an explosive sheet, such as Composition C-3, is wrapped around a can containing metal powder, and detonation deforms the can and compacts the powder. In the standoff system the explosive is removed some distance from the powder and may, as an example, be used to drive a die

Table 7 PROPERTIES OF PLASMA-SPRAYED MATERIAL[19]

| Coating | Substrate | Power level, kw-hr/cu ft | Spray distance, in. | Density, % of theoretical | Adherence, psi | Impact, ft-lb |
|---|---|---|---|---|---|---|
| Be | Steel | 0.2 | 1 | 89.6 | 3005* | |
| Be | Steel | 0.2 | 2 | | 2420† | |
| Be | Steel | 0.2 | 3 | | 1790† | |
| BeO | Be | 0.35 | 1.5 | | 310‡ | |
| TiC | Be | 0.24 | 2 | 89 | 960‡ | >12§ |
| TiC | Be | 0.36 | 3 | 91 | 910‡ | >12* |
| TaC | Be | 0.24 | 2 | 91 | 920‡ | >12§ |
| TaC | Be | 0.36 | 3 | 91 | 1020‡ | >12* |
| ZrC | Be | 0.36 | 3 | 80 | | |
| TiN | Be | 0.43 | 3 | | | |

*Adhesive failure. ‡Cohesive failure.
†Bond failure. §Substrate failure.

punch. These techniques and possible applications were discussed in detail in a paper by Pearson.[25a] Since explosives do not usually require the use of expensive equipment, these methods offer considerable potential for compaction of unusual materials and large shapes.

The compaction of aluminum, copper, iron, and tungsten-titanium (granular powder obtained by a sodium-reduction process) was discussed by Montgomery and Thomas,[26] who reported the data shown in Table 9. With their techniques they produced cylinders as large as $4\frac{1}{2}$ in. in diameter and up to 20 in. long.

Data on a wide variety of metals and dispersions[25b] are given in Table 10, and these data show that ceramics, intermetallics, graphite, and complex structures can be explosively compacted to a high density. The effectiveness of explosive compacting[27] is illustrated in Fig. 13 which shows the high density of explosively compacted tungsten compared with that of normal green-pressed material.

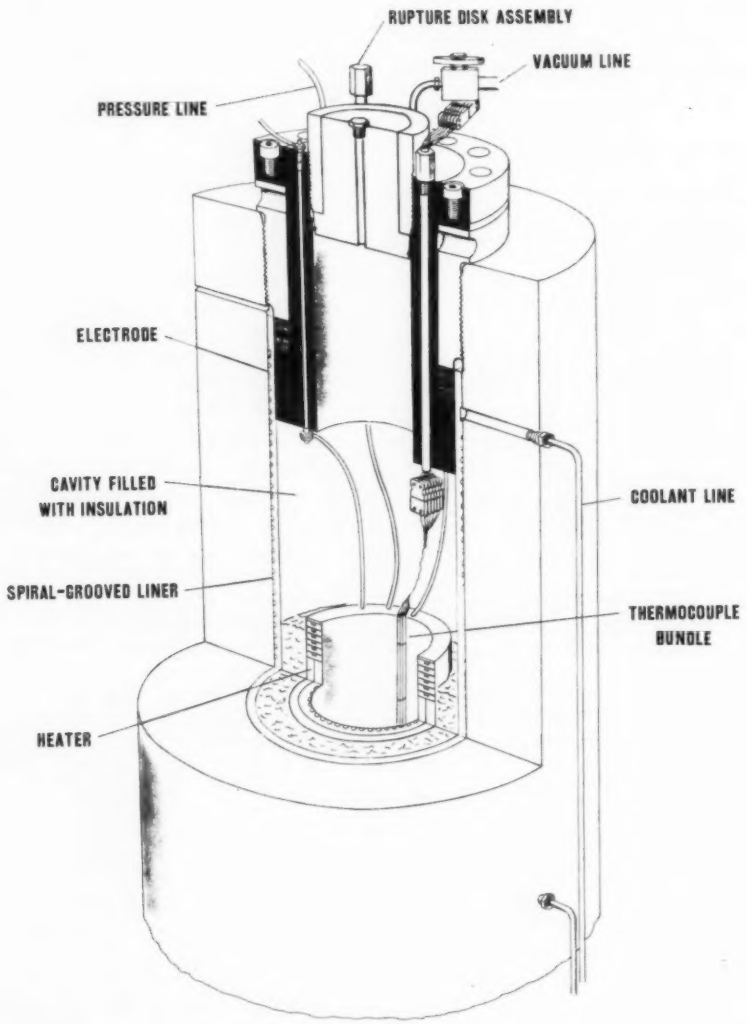


Fig. 10 Sectional view of cold-wall high-pressure autoclave.[20]

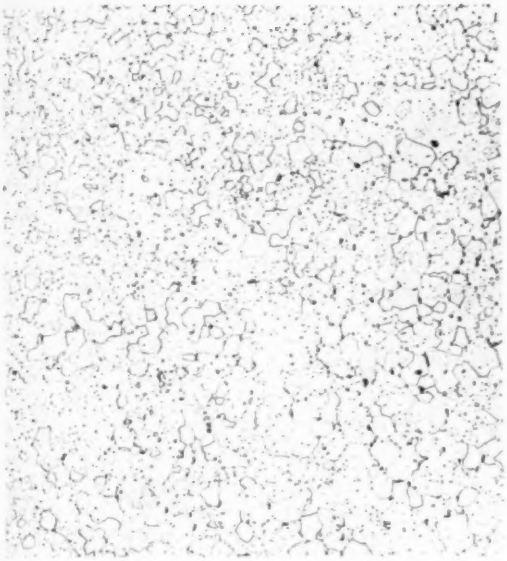

(*a*) Example of densification of molybdenum powder. Gas-pressure bonded at 2600°F and 10,000 psi for 3 hr. Magnification, 100×.

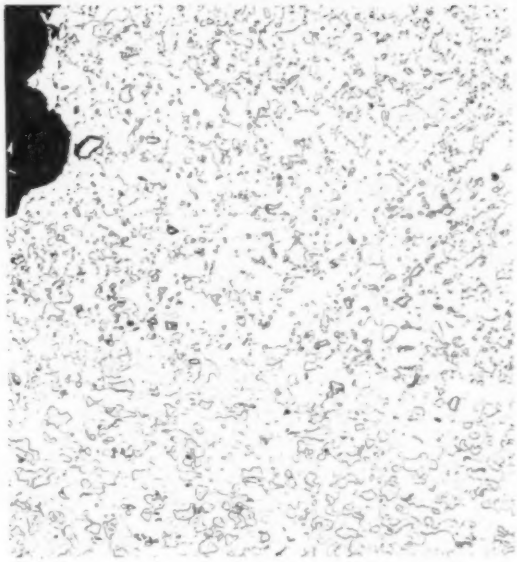

(*b*) Example of densification of columbium powder. Gas-pressure bonded at 2300°F and 10,000 psi for 3 hr. Magnification, 100×.

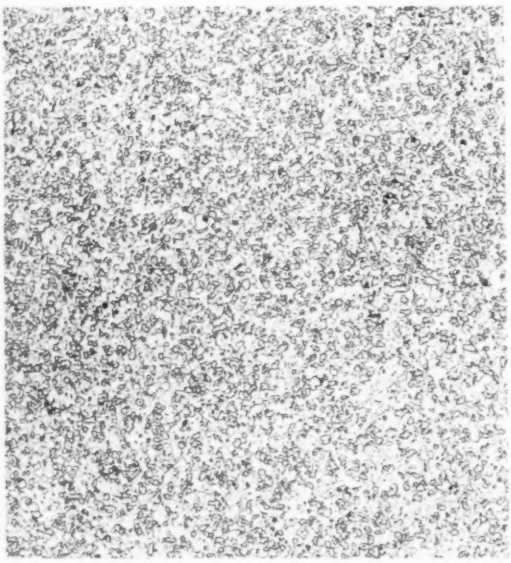

(*c*) Example of densification of tungsten powder. Gas-pressure bonded at 2500°F and 10,000 psi for 3 hr. Magnification, 100×.

(*d*) Example of densification of rhenium powder. Gas-pressure bonded at 2600°F and 10,000 psi for 3 hr. Magnification, 100×.

Fig. 11 Hot isostatically pressed refractory metals.[20]

Workers at Hanford[28] have utilized a high-velocity hydraulic system (Dynapak) for producing high-density $UO_2$. They used modified Bridgeman anvils to generate pressures on the order of 500,000 psi. It was found that fused $UO_2$ increased the plasticity and achievable density. Densities around 99.5% of theoretical were obtained for −200-mesh fused $UO_2$ compacted at 1200°C and 500,000 psi, and a density of 99% of theoretical was obtained for sintered and crushed −200-mesh $UO_2$ compacted under similar conditions.

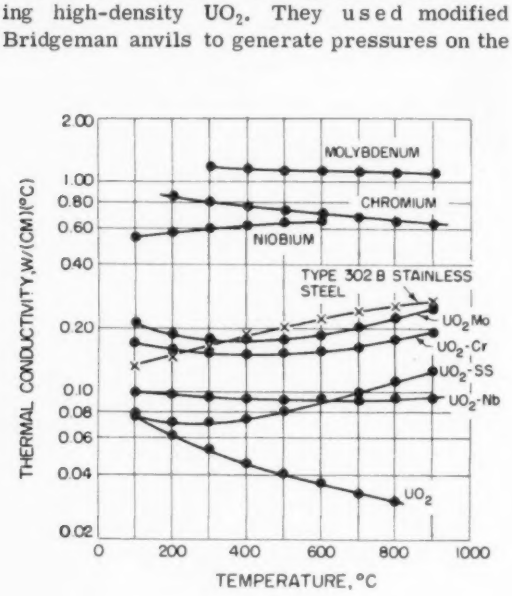


Fig. 12 Thermal conductivity vs. temperature for 80 vol.% $UO_2$ cermets and their matrix metals.[10a]

### *Electrodeposition*

The process of electroplating, although not new, is relatively new insofar as the production of fuel-material or control-material dispersions is concerned. Workers at Vallecitos[29] obtained as a commercial product a dispersion of $B_4C$ in nickel. The dispersion was produced by CEM Division, Platecraft of America Inc., by plating nickel onto a stainless-steel base and then continuing to plate nickel from a bath containing dispersed $B_4C$. Up to 30 vol.% of the dispersed phase can be achieved in plated thicknesses up to ¼ in. on each side of the base plate.

Another electrodeposition technique that offers considerable potential is electrophoretic deposition. In this process powder particles

Table 8 DENSITIES OF PRESSURE-BONDED URANIUM DIOXIDE[15g]

| Description of oxide | Range of initial density, % of theoretical: Pressed at 40 to 50 tsi | Range of initial density, % of theoretical: Tamp packed | Range of bonded densities,* % of theoretical | Structure† |
|---|---|---|---|---|
| Mallinckrodt ceramic | 54.8–58.3 | | 96.7–98.5 | High density with little apparent porosity |
| | | 19.0–20.0 | 98.5–99.5 | |
| Mallinckrodt and NUMEC high fired | 72.7–76.1 | | 90.3–95.8 | Little grain growth; particles not well bonded |
| Mallinckrodt special dense | 75.6–80.3 | | 83.1–93.1 | Oxide particles remained porous; point bonding |
| | | 54.9–63.4 | 85.7–89.6 | |
| Spencer fused | 77.2–85 | | 82.5–94.9 | Point bonding; bridging effect in structure |
| | | 53.8–69.4 | 83.5–88.9 | |
| Fused and ceramic mixture: | | | | |
| 25% ceramic | 72.0–83.5 | | 92:2–96.7 | Occasional bridging of particles |
| 40% ceramic | 74.5 | | 97.8 | Low porosity, well bonded |
| 50% ceramic | 67.0–72.0 | | 99.0–99.5 | Low porosity, well bonded |
| 75% ceramic | 63.0–67.1 | | 99.0–99.5 | Low porosity, well bonded |
| Fused and high-fired mixture: | | | | |
| 25% high fired | 78.5–86.8 | | 88.9 | Little or no bonding |
| High-fired and ceramic mixture: | | | | |
| 25% ceramic | 68.5–71.4 | | 92.9–95.0 | Well bonded, apparent high porosity |

*Samples bonded at 2100 to 2300°F for 3 hr at 10,000 psi.
†Comments based on metallographic observation.

are dispersed in a liquid and caused to acquire an electric charge. When an electric field is applied, the particles can then be forced to move to the component face. Workers at Vitro[30] have described techniques for depositing metals, carbides, cermets, oxides, and oxide-carbide mixtures. Zein (a corn protein material) is mixed with an isopropanol-nitromethane mixture and used as an activator–binder in the dispersions. After electrodeposition the materials may be hydrostatically pressed and sintered, or sintered directly.

Guttierrez et al.[31] have discussed the use of electrophoretic deposition as a coating technique. They used the procedure to produce adherent coatings of B, Dy, Zr, Au, Nb, Mo, W, Re, $Nb_3Sn$, $ZrH_2$, ThC, UC, NpC, PuC, (ZrU)C, $UWC_2$, $UO_2$, $UMoC_2$, $Ta_2O_5$, and W-$UO_2$ and Mo-$UO_2$ composites. They give detailed data for effect of time, current, and voltage on the rate of deposition of niobium powder and also discuss techniques for preparing the powder suspensions. The maximum deposition rate was obtained at about 800 volts and a current density of about 0.3 ma/cm$^2$. The optimum powder particle size was found to be about 6 $\mu$, although powder of 20-$\mu$ size could be plated. Coarse powders (> 25-$\mu$ diameter) gave uneven deposits. Isopropyl alcohol and nitromethane were used as suspending media.

### *Idealized Dispersions*

In principle, dispersion fuels offer the potential of confining radiation damage to small localized areas; thus large volumes of the structural or matrix material are relatively un-

Table 9 COMPACTING OF METAL POWDERS BY DETONATING EXPLOSIVES[26]

(Container for Metal Powder: 17.5 × 5.5 cm in Diameter; 100% of Metal Powders Passed 69 SB Sieve)

| Weight of explosive, g | Metal powder | Bulk density of metal powder, g/cm$^3$ | Weight of metal powder, g | Weight of metal powders: weight of explosive | Av. dia. of compacted mass, cm | Density of solid metal, g/cm$^3$ | Av. density of compacted mass | |
|---|---|---|---|---|---|---|---|---|
| | | | | | | | g/cm$^3$ | % of theoretical density |
| 60.3 | Tungsten-titanium | 1.53 | 675 | 11.2 | 3.5 | 4.5 | 4.0 | 88.9 |
| 59.9 | Aluminum | 1.29 | 575 | 9.6 | 3.8 | 2.7 | 2.7 | 100 |
| 130.5 | Copper | 5.25 | 2154 | 16.5 | 4.2 | 8.9 | 8.45 | 95 |
| 130.1 | Iron | 2.5 | 1080 | 8.3 | 3.2 | 7.9 | 7.65 | 96.8 |

Table 10 DATA ON EXPLOSIVE COMPACTION OF METAL POWDERS[25b]

| Metal powder | Particle size | Initial density,* % of theoretical | Ratio of powder to explosive, g/g | Final density,† % of theoretical |
|---|---|---|---|---|
| Tungsten | 100 mesh | 44.5 | 1.833 | 97.0 |
| Haynes Stellite 25 | −325 mesh | 45.5 | 0.754 | 94.6 |
| Haynes Stellite 31 | −180 mesh | 36.8 | 0.550 | 96.4 |
| Zircaloy-2 | 150 mesh | 27.2 | 0.378 | 97.0 |
| Beryllium | −200 mesh | 31.7 | 0.155 | 96.0 |
| 70 vol.% 347 S.S.–30 vol.% $UO_2$ | −325-mesh S.S. and 100-mesh $UO_2$ | 53.0 | 14.800 | 94.4 |
| 97 vol.% Ta–3 vol.% $ThO_2$ | −325 mesh | 50.4 | 2.110 | 97.0 |
| 80 vol.% $MoSi_2$–20 vol.% $ZrB_2$ | −325 mesh | 46.0 | 0.741 | 95.3 |
| 20 vol.% $ZrB_2$–80 vol.% $MoSi_2$ | −325 mesh | 56.8 | 0.844 | 95.6 |
| Beryllia | −325 mesh | 68.3 | 0.679 | 96.0 |
| 70 vol.% W–30 vol.% $UO_2$ | 100 mesh | 30.3 | 1.168 | 96.8 |
| Reactor-grade graphite | −325 mesh | 31.8 | 0.272 | 93.5 |
| $MoSi_2$ | −325 mesh | 36.8 | 0.750 | 98.1 |

*Calculated density.
†Density determined by pycnometer methods.

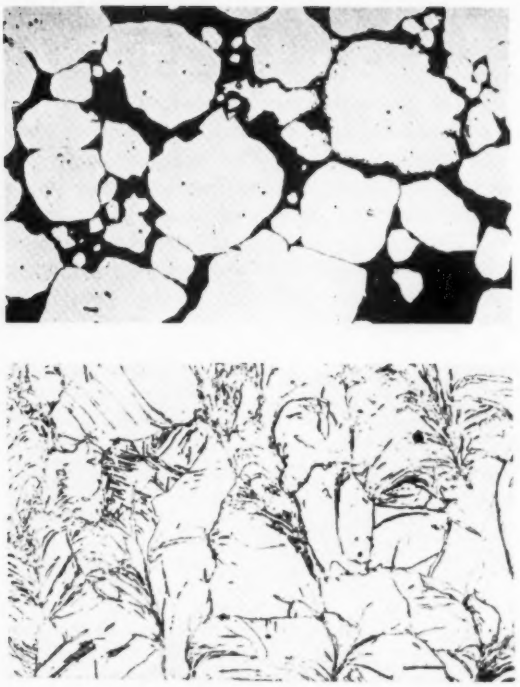

Fig. 13 Tungsten powder compacted by conventional and high-energy techniques. The specimen in the top photomicrograph (250×) was compacted on a conventional press at a pressure of 50 tsi, which resulted in a density of about 65% of theoretical. Explosively compacted powder from the same lot created the specimen below. The density of the latter is above 97% of theoretical.[27]

damaged. In general, good resistance to radiation damage has been observed (see Fig. 14). In this chart Keller[32] has plotted the results of a large number of irradiation tests conducted at various laboratories and on specimens fabricated by several different methods. Dispersions used in most of the tests were far from ideal,[33] and probably the structure shown in Fig. 15 could be considered typical. Yet it is obvious that even without ideal dispersions good resistance to radiation damage can be obtained.

The Second Edition of *Reactor Handbook*[33] contains an excellent discussion of problems relating to fabrication and properties of metal-base dispersion fuels covering the technology through 1959. This discussion indicates that the major effort to improve the dispersions was directed toward ways of minimizing the breakup of the fuel particles due to fabrication and methods of dispersing and maintaining the particles in a random location. These aims were not achieved until spherical fuel particles became available on a commercial basis. As previously mentioned, early development of spherical $UO_2$ was conducted at Knolls, and in 1958 spherical $UO_2$ became available from commercial sources. Figure 16 is a photomicrograph of a $UO_2$–stainless-steel dispersion[34] made with this commercial spherical powder. The improvement over the structure shown in Fig. 15 is obvious.

In a perfectly random dispersion a finite number of fuel particles will touch one another (many pairs and a few groups of three or more particles). Therefore an ideal dispersion should be an ordered arrangement of fuel particles spaced the greatest possible distance apart. As described in a recent report by Smalley et al.,[35] techniques developed for ceramic fuel elements resulted in ideal dispersions of the type shown in Fig. 17. For this work the process of aggregating fine particles (known as pelletizing) was adapted to produce pellets that consisted of $UO_2$ shot coated with $Al_2O_3$. The fabrication study was a part of a basic AEC study on coated-fuel particles, and therefore the pellet-seed particles were $UO_2$ that had been coated with $Al_2O_3$ by vapor deposition. However, pelletizing techniques can be adapted to bare fuel particles or to metal-matrix dispersions.

For coating with $Al_2O_3$, a slip of $Al_2O_3$ fine powder, Carbowax 4000, Goulac, water, and ethanol was intermittently sprayed into a rotating drum that contained the coated fuel particles. The starting materials and the pelletized fuel particles are illustrated in Fig. 18. Similar techniques were used to pelletize graphite-matrix bodies. To produce the dispersions the pellets are pressed and sintered in a normal manner.

When large amounts of a binder are objectionable, two techniques first utilized by Paprocki and coworkers offer considerable improvement. In the first technique, developed for roll-clad $UO_2$–stainless-steel dispersions[36] and high-loading $UO_2$ cermets,[10a] the $UO_2$ is coated with an easy-to-remove binder, such as camphor, and then tumbled with fine metal powder moistened with alcohol. Structures of the type shown in Fig. 16 but somewhat improved are obtained. In the second technique,

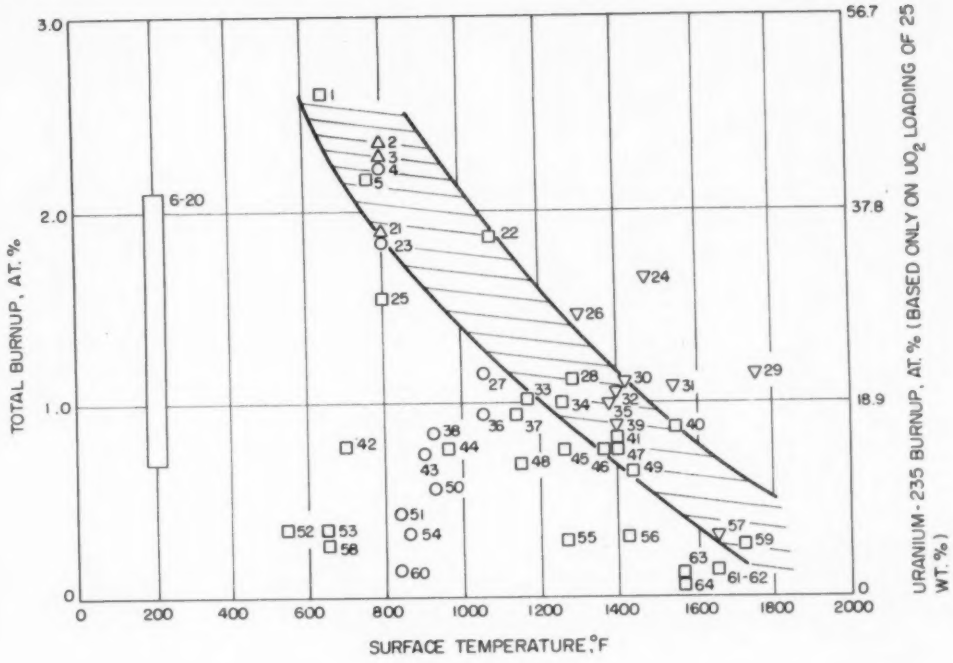


Fig. 14 Burnup characteristics[32] of stainless-steel–$UO_2$ dispersions (15 to 30 wt.% $UO_2$). Plate specimens: ∇, failures; □, no failures. Pin specimens: △, failures; ○, no failures.

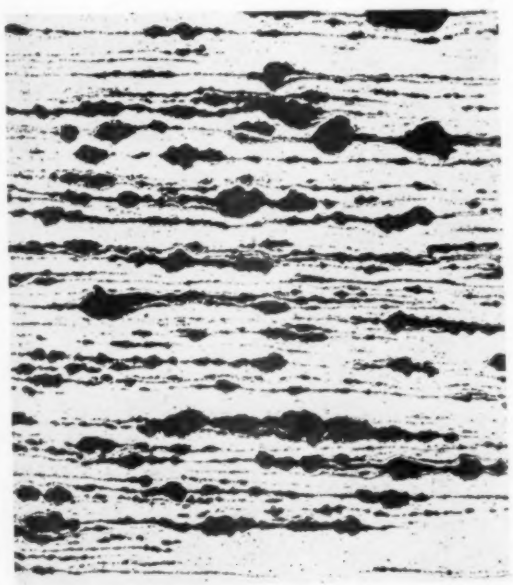

Fig. 15 As-polished 25 wt.% $UO_2$ dispersed in type 318 stainless steel.[33] Magnification, 100×.

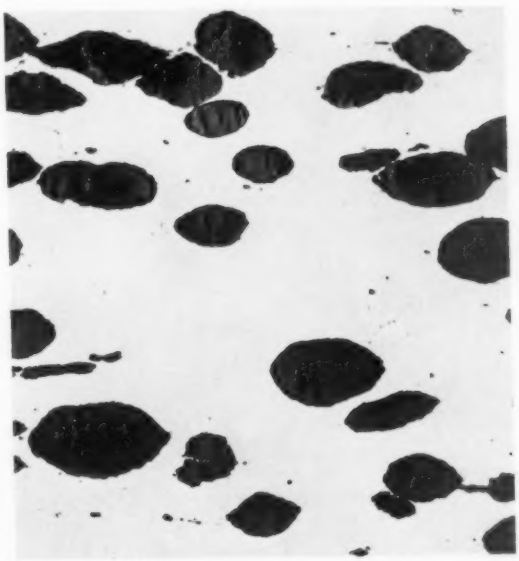

Fig. 16 As-polished structure of 25 wt.% $UO_2$–elemental matrix fuel elements[34] produced with spherical $UO_2$. Magnification, 100×.

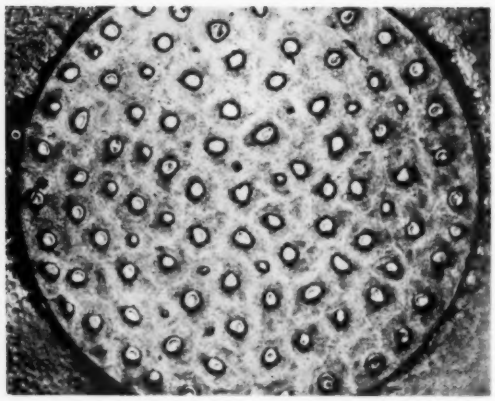

Fig. 17 Dispersion of coated-particle fuel in graphite-matrix body prepared from pelletized fuel.

$UO_2$ particles coated with metal by the vapor-deposition process are hot pressed to produce a high-density uniform structure of the type illustrated in Fig. 5.

## Future Developments

Two of the processes discussed are likely to expand into extensive production processes in the very near future. Vibratory compaction, particularly when followed by swaging or hot isostatic pressing, offers considerable promise. Hot isostatic pressing is extremely versatile and has already been shown to be capable of producing material at rates that compare favorably with more conventional fabrication processes.

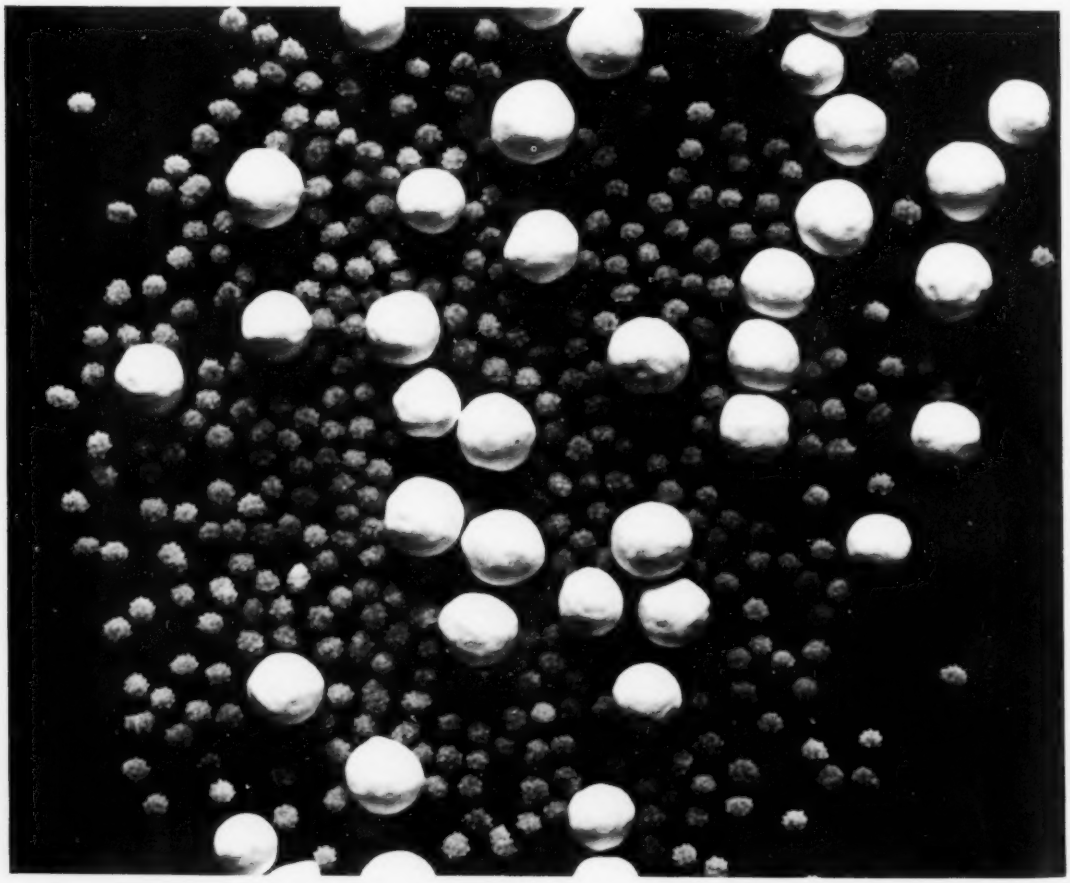

Fig. 18 $Al_2O_3$-coated $UO_2$ particles and oxide-pelletized product.[35] Magnification, 15×.

In view of modern demands for components to withstand higher and higher temperatures, it is expected that fabrication development of nitrides, borides, mixed carbides, and complex structures, such as cermets, wire-reinforced and fiber-reinforced structures, and tungsten-bearing structures will continue. In addition, fabrication of solid moderators will be important for the development of compact reactors. Coated particles will begin to be used extensively to produce ideal dispersions and compatible systems.

In general, powder techniques are expected to prove useful primarily in the creation of materials with unique properties and to a lesser extent in producing more economical materials and high-temperature materials for which cast structures do not have suitable properties.

## References


1. H. J. Hedger and A. R. Hall, Preliminary Observations on the Use of the Induction Coupled Plasma Torch for the Preparation of Spherical Powder, *Powder Met.*, No. 8: 65 (1961).
2. C. A. Alexander, personal communication, September 1962.
3. J. O. Gibson, personal communication, 1960.
4. J. D. Holmgren et al., Development of Submicron Powder Manufacturing Method. Final Technical Engineering Report, Report ASD-TR-62-7-884, Beryllium Corp., August 1962.
5. A. T. Muccigrosso, H. E. Dumas, and G. L. Ploetz, Knolls Atomic Power Laboratory, June 1960. (Unpublished)
6. W. V. Goeddel, General Atomic Div., General Dynamics Corp., PyC-Coated Carbide Fuel Particles and their Use in Graphite-Matrix Fuel Compacts, presented at USAEC Symposium on Ceramic-Matrix Fuels Containing Coated Particles, Battelle Memorial Institute, Columbus, Ohio, Nov. 5–6, 1962. (proceedings to be published)
7. *Reactor Core Materials*, 4(4): 8 (November 1961) and *Reactor Materials*, 5(1): 11 (February 1962).
8. G. W. Cunningham, unpublished data.
9. G. W. Cunningham and S. J. Paprocki, A New Concept for Aluminum Base Fuel Elements, paper presented at Research Reactor Fuel Element Conference, Sept. 17–19, 1962, Gatlinburg, Tennessee, USAEC Report TID-7642, Oak Ridge National Laboratory.
10. Powder Metallurgy in the Nuclear Age, *Fourth Plansee Seminar Proceedings*, Metallwerk Plansee, AG., Reutte/Tirol, Austria, 1962:
    *a.* G. W. Cummingham et al., Cermet Fuel Elements.
    *b.* D. L. Keller et al., Powder Metallurgy of Uranium Carbide and Uranium Nitride.
11. Martin Co., Zero Power Test Manufacturing Report, USAEC Report MND-MPR-1580, December 1958.
12. Martin Co., PM-1 Nuclear Power Plant Program. 9th Quarterly Progress Report, March 1 to May 31, 1961, USAEC Report MND-M-1820, July 10, 1961.
13. *A Handbook on Boron Carbide, Elemental Boron, and Other Stable, Boron-Rich Materials*, The Norton Company, Worcester, Mass., 1955.
14. *Reactor Core Materials*, 4(3): 54 (1961) (taken from classified USAEC Report HW-62656).
15. Symposium on Powder Packed Uranium Dioxide Fuel Elements, November 30–December 1, 1961, USAEC Report CEND-153:
    *a.* W. S. Ernst, Jr., and R. L. Beatty, Vibratory-Compaction Studies at the Oak Ridge National Laboratory, Paper II-D.
    *b.* W. R. DeHollander, Particle Size Relationships in the Packing of $UO_2$, Paper II-E.
    *c.* J. J. Hauth, Fabrication Techniques for Packed-Powder Fuel Elements, Paper I-C.
    *d.* B. E. Murtha and W. P. Chernock, Economics of Powder-Packed Fuel Elements, Paper I-B.
    *e.* E. J. Veil and R. H. Gale, Fabrication of $UO_2$ Fuel Elements by the "Vileswage" Process, Paper III-D.
    *f.* R. L. Eichinger, Vibratory and Swage Compaction of Small Diameter Stainless Steel Clad Fuel Rods, Paper III-E.
    *g.* S. W. Porembka and C. B. Boyer, Consolidation of Uranium Dioxide by Gas-Pressure Bonding, Paper V-E.
16. R. W. Dayton and R. F. Dickerson, Progress Relating to Civilian Applications During July 1962, USAEC Report BMI-1589(Del.), Battelle Memorial Institute, Aug. 1, 1962.
17. D. R. Mash et al., Process Variables in Plasma-Jet Spraying, *J. Metals*, 13: 473 (1961).
18. R. H. Singleton et al., Tungsten Fabrication by Arc Spraying, *J. Metals*, 13: 483 (1961).
19. A. R. Stetson and C. A. Hauck, Plasma Spraying Techniques for Toxic and Oxidizable Materials, *J. Metals*, 13: 479 (1961).
20. S. J. Paprocki, E. S. Hodge, and P. J. Gripshover, Gas-Pressure Bonding, Report DMIC-159, Battelle Memorial Institute, Defense Metals Information Center, Sept. 25, 1961.
21. E. S. Hodge, personal communication, September 1962.
22. S. J. Paprocki (Ed.), Progress on the Use of Gas-Pressure Bonding for Fabricating Low-Cost Ceramic, Cermet, and Dispersion Fuels, USAEC Report BMI-1555, Battelle Memorial Institute, Nov. 24, 1961.
23. I. Sheinhartz and J. Fugardi, Ceramic Fuel Elements Made by Hot Isostatic Pressing, USAEC

Report SCNC-311, Sylvania-Corning Nuclear Corp., September 1960.

24. S. J. Paprocki et al., Cladding of Delta Phase Zirconium Hydride, Symposium on Metallic Moderator and Cladding Material, AIME Nuclear Metallurgy, Vol. VIII, IMD Special Report Serial No. 10, 1960.
25. Creative Manufacturing Seminars, 1960–1961, American Society of Tool and Manufacturing Engineers, Detroit:
    *a.* J. Pearson, The Explosive Compaction of Powders, Paper SP-60-158.
    *b.* S. J. Paprocki et al., Explosive Compaction of Powder Materials, Paper SP-62-29.
26. W. T. Montgomery and H. Thomas, The Compacting of Metal Powders by Explosives, *Powder Met.*, No. 6: 125 (1960).
27. G. W. Cunningham, Powder Metallurgy—The State of the Art, *Battelle Technical Review*, p. 3, August 1962.
28. *Reactor Materials*, 5(3): 73 (1962) (taken from classified USAEC Report HW-70355).
29. W. C. Ballowe, A. N. Holden, W. J. Ozeroff, H. E. Williamson, and B. Weidenbaum, Status Report on Control Rod Materials Research and Development Program, USAEC Report GEAP-3355-2, General Electric Co., Vallecitos Atomic Laboratory, Nov. 14, 1960.
30. A. C. Werner and R. J. Abelson, Preparation of Protective Coatings by Electrophoretic Methods, Report WADC-TR-58-11, Vitro Corporation of America, Nov. 30, 1957.
31. C. P. Guttierrez et al., Electrophoretic Deposition–A Versatile Coating Method, *J. Electrochem. Soc.*, 109: 923 (1962).
32. D. L. Keller, Predicting Burnup of Stainless Steel-$UO_2$ Cermet Fuels, *Nucleonics*, 19(6): 45 (June 1961).
33. D. L. Keller, Dispersion Fuels, in *Reactor Handbook* (2d ed.), Vol. I, Chap. 13, Interscience Publishers Inc., New York, 1960.
34. S. J. Paprocki, D. L. Keller, and G. W. Cunningham, The Effect of Fabrication Variables on the Structure and Properties of $UO_2$–Stainless Steel Dispersion Fuel Plates, USAEC Report BMI-1322, Battelle Memorial Institute, Feb. 18, 1959.
35. A. K. Smalley, M. C. Brockway, and W. H. Duckworth, Improved Techniques for Dispersing Coated Fuel Particles in Ceramic Bodies, USAEC Report BMI-1579, Battelle Memorial Institute, May 22, 1962.
36. S. J. Paprocki, D. L. Keller, G. W. Cunningham, and A. K. Foulds, Incorporation of a Boron Burnable Poison and Spherical $UO_2$ in SM-2 Stainless-Matrix Fuel Plates, USAEC Report BMI-1527, Battelle Memorial Institute, July 6, 1961.

Section

I

Reactor Materials

# Fuel and Fertile Materials

## Uranium Metal and Alloys

### Unalloyed Uranium

Investigators at Argonne[1] have determined the heat content of uranium and uranium-fissium alloys as functions of temperature. Concomitantly, heat of transformation and heat of fusion were found. Figure I-1 presents the data for uranium in graphical form.

Arrhenius plots for the diffusion of chromium, manganese, and cobalt in gamma uranium were also determined, and they are given in Fig. I-2.

When uranium with preferred orientation is heat-treated at low beta-phase temperatures and cooled in air, grain coarsening proceeds at a more rapid rate than the rate of change of preferred orientation. Quenching in water from the beta temperature increases the rate of loss of preferred orientation and refines the grain size.

To account for these effects it is postulated[2] that (1) the transformation from the highly oriented alpha phase to the beta phase is incomplete in short times at low beta-phase temperatures and (2) during cooling the residual alpha grains serve as centers for retransformation to an oriented, large-grained alpha phase. Quenching increases nucleation from the beta phase, and it results in a structure that is finer grained and more randomly oriented.

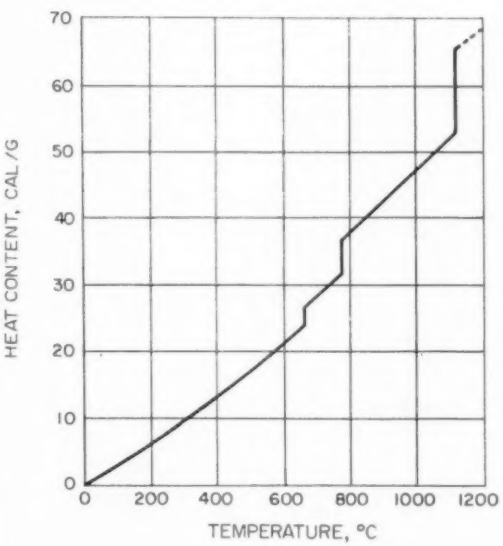


Fig. I-1 Heat content of uranium.[1]

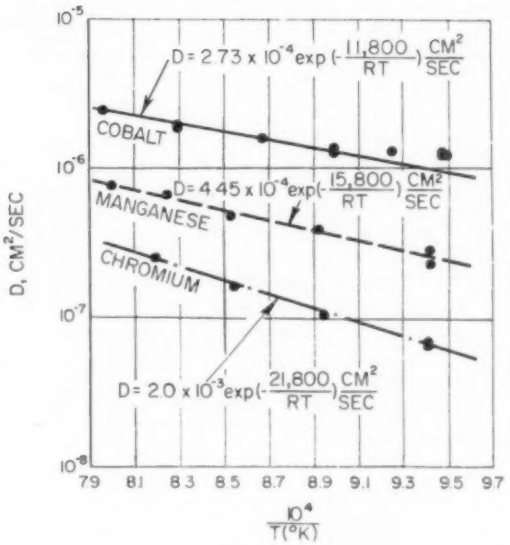


Fig. I-2 Arrhenius plots for the diffusion of chromium, manganese, and cobalt in gamma uranium.[1]

The activation energies of the creep of polycrystalline uranium were determined by the French[3] by study of the variation of the velocity of deformation and temperature. The constant value obtained above 580°C suggests that the uranium creep in this temperature region is controlled by a displacement mechanism for dislocation whose heat of activation is that of self-diffusion.

The French[4] have briefly reviewed the most recent concepts on boundary migration in alpha uranium. In the present study of factors involved in the migration of grain boundaries in alpha uranium, the important role played by various crystallographic mechanisms in the change from the worked state to the recrystallized state is emphasized. The relation between the various deformation modes of the uranium monocrystal and the boundary migration of recrystallized crystals is first analyzed. The interfacial energy of the twin boundaries and the boundary-migration factor of recrystallization grains are discussed. The migration of grain boundaries in uranium by secondary recrystallization is considered. Some orientation relations between the deformed matrix and the

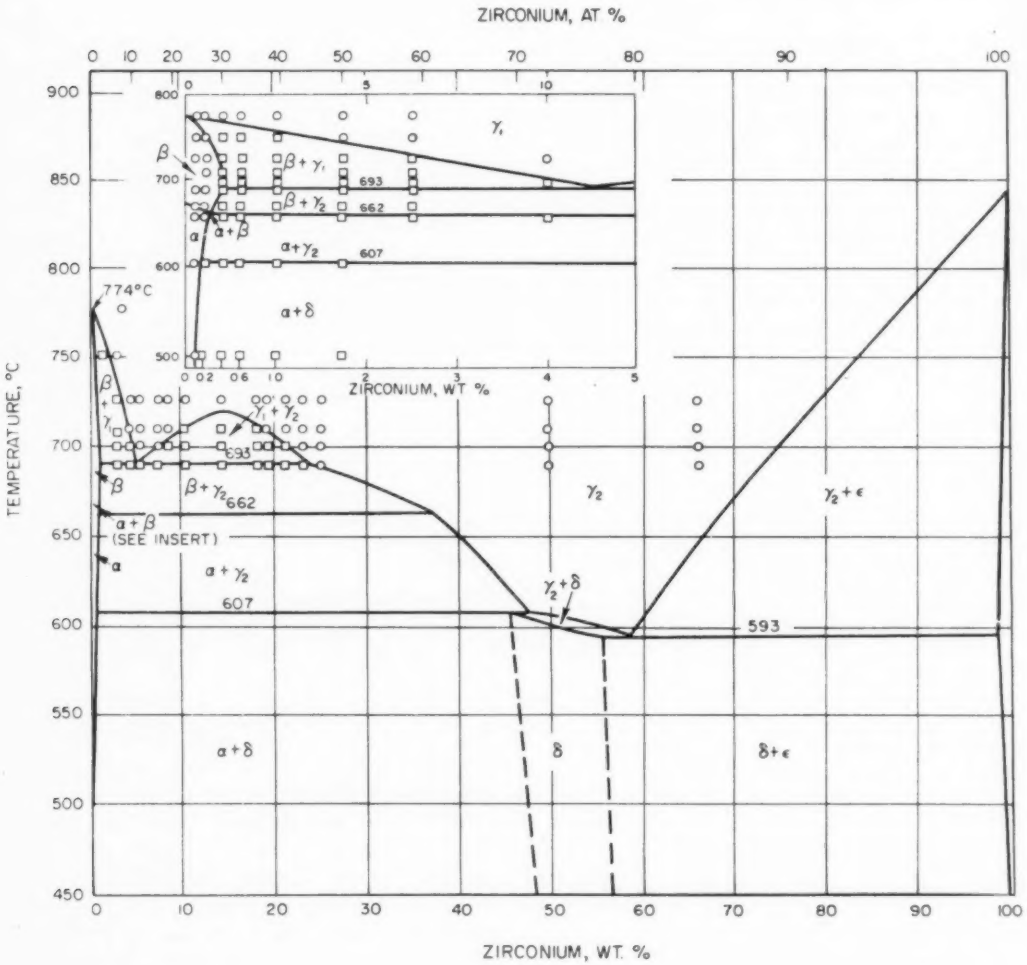


Fig. I-3 Equilibrium phase diagram of uranium-zirconium alloy system.[1] □, two-phase microstructures. ○, single-phase microstructures.

Table I-1 EFFECTS OF IRRADIATION ON UNCLAD SPECIMENS OF INJECTION-CAST URANIUM-FISSION ALLOYS[1]

| Specimen | Composition (balance U), wt.% | Analyzed burnup, at.% | Surface temp., °C | Center temp., °C | Length change, % | Dia. change, % | Density decrease, % | Weight change, mg | % volume change/ at.% burnup | Comments |
|---|---|---|---|---|---|---|---|---|---|---|
| CP-7-4 | 3.3 Fs–1.7 Zr | 1.3 | 355 | 390 | 2.7 | 4.4 | 12.8 | 24 | 11 | Good condition |
| CP-7-1 | 3.7 Fs | 1.5 | 380 | 420 | 5.2 | 10.1 | 19.1 | 17 | 16 | Good condition |
| CP-7-5 | 5 Fs | 1.4 | 355 | 390 | 1.6 | 2.7 | 4.6 | 16 | 3 | Slight swelling at top of specimen |
| CP-7-3 | 5 Fs | 1.5 | 380 | 420 | 2.4 | 4.3 | 9.4 | 22 | 7 | Good condition |
| CP-9-5 | 5 Fs | 5.1 | 680 | 760 | | | 57.6 | 74 | 26 | Uniform swelling over entire length |
| CP-9-3 | 5 Fs | 4.9 | 710 | 790 | | | 62.5 | 34 | 33 | Warped; bumpy surface |
| CP-9-1 | 5 Fs | 4.9 | 710 | 790 | | | 45.5 | | 17 | Severe swelling at center of specimen |
| CP-8-5 | 5 Fs | 5.2 | 600 | 670 | | | 64.7 | | 35 | Distorted and oxidized; broke into four pieces on removal from holder |
| CP-8-3 | 5 Fs | 5.6 | 600 | 670 | | | 60.5 | | 27 | Both ends distorted; taper from both ends to the center of specimen |
| CP-8-4 | 5 Fs | 5.2 | 610 | 680 | | | 56.2 | | 25 | Autoradiograph of specimen still in capsule showed item to be swollen but intact; specimen caught fire in cave, burning away upper third of pin |
| CP-7-2 | 5 Fs–2.5 Zr | 1.4 | 380 | 420 | 3.6 | 8.3 | 12.7 | 20 | 10 | Good condition |
| CP-9-6 | 5 Fs–2.5 Zr | 4.8 | 680 | 760 | | | 53.2 | 138 | 24 | Swollen; slight taper from top to bottom of specimen |
| CP-9-4 | 5 Fs–2.5 Zr | 4.8 | 680 | 760 | | | 51.9 | | 23 | Upper half very distorted |
| CP-9-2 | 5 Fs–2.5 Zr | 4.7 | 710 | 790 | | | 52.4 | 25 | 24 | Uniform swelling; bent at a 25° angle |
| CP-8-6 | 5 Fs–2.5 Zr | 4.9 | 600 | 670 | | | 56.8 | | 27 | Upper half distorted; taper to the bottom of specimen |
| CP-8-2 | 5 Fs–2.5 Zr | 5.3 | 610 | 680 | | | 59.8 | | 28 | Autoradiograph showed large bump on side of specimen; it is feared that this portion also ignited and burned away during capsule opening |
| CP-8-1 | 5 Fs–2.5 Zr | 5.3 | 610 | 680 | | | 60.3 | | 29 | Specimen slumped to a shape resembling a boot |
| CP-7-6 | 10 Fs–5 Zr | 1.0 | 355 | 390 | | | 8.6 | | 9 | Specimen separated into two pieces while handling |

crystal of recrystallization are shown to support the Beck theory of "selective growth," generalized to the case of uranium.

Crack initiation and propagation in uranium at elevated temperatures were studied by investigators at Battelle.[5] Tensile specimens prepared from high-carbon uranium were tested at various temperatures from 20 to 450°C *in vacuo* at a strain rate of 0.0005 in./(in.)(min). The material exhibited a secondary minimum in ductility of 14.5% at 300°C. Metallographic examination of the specimens after testing failed to reveal any evidence of grain-boundary cracking. The mode of fracture in all cases appeared to be carbide rupturing, an increase in void volume due to carbide parting, and, ultimately, rupture of the specimen. Dynamic-modulus data obtained at temperatures up to 1200°F gave no indication of a drastic rate of change in this elastic property.

Papers presented at the Institute of Metals Symposium on Uranium and Graphite, 1962, include "The Evaluation of Creep Tests on Alpha-Uranium Under Isothermal and Thermal Cycling Conditions,"[6a] "The Effect of Neutron Irradiation and Thermal Cycling on Permanent Deformation in Uranium Under Load,"[6b] and "The Swelling of Alpha-Uranium Under Neutron Irradiation to 0.7 at.% Burnup."[6c]

(M. S. Farkas)

## Alpha-Phase Uranium Alloys

The uranium-rich end of the uranium-zirconium alloy system has been reinvestigated by Argonne.[7] The results are shown in Fig. I-3.

Du Pont[8] has reported the irradiation results obtained on a tubular uranium–2 wt.% zirconium element with the following dimensions: 2-in. outside diameter, $1\frac{1}{2}$-in. inside diameter, 44-in. length, and 0.015-in. cladding thickness. This element was irradiated in the Vallecitos Boiling-Water Reactor (VBWR) to a burnup of 1280 Mwd/ton (peak). During irradiation the element had a maximum cladding-surface temperature of 300°C, a maximum cladding-core

Table I-2 IRRADIATION DATA ON TYPE 304 STAINLESS-STEEL-CLAD SODIUM-BONDED U-Fs AND U-Fs-Zr FUEL ALLOYS[1]

| Rod | Composition,* wt.% Fs | Zr | Max fuel temp., °C | Max jacket surface temp., °C | Max heat flux,† Btu/(hr)(sq ft) | Burnup, at.% | Weight change, mg | % volume increase/at.% burnup |
|---|---|---|---|---|---|---|---|---|
| ET3-1 | 5 | | 440 | 420 | 430,000 | 0.88 | −25.2 | 0.30 |
| ET3-2 | 5 | | 440 | 420 | 430,000 | 0.88 | −12.3 | 0.30 |
| ET3-3 | 5 | | 440 | 420 | 430,000 | 0.88 | −7.4 | 0.40 |
| ET3-4 | 5 | | 440 | 420 | 430,000 | 0.88 | 4.8 | 0.30 |
| ET3-5 | 5 | | 440 | 420 | 430,000 | 0.88 | 0.4 | 0.30 |
| ET3-6 | 5 | | 440 | 420 | 430,000 | 0.88 | 1.3 | 0.30 |
| ET1-4 | 5 | | 580 | 550 | 590,000 | 0.58 | −6.4 | 0.43 |
| ET1-5 | 5 | | 580 | 550 | 590,000 | 0.58 | −25.5 | |
| ET1-6 | 5 | | 580 | 550 | 600,000 | 0.58 | −25.0 | |
| ET2-2 | 5 | 2.5 | 590 | 560 | 600,000 | 1.5 | −10.7 | 0.17 |
| ET2-4 | 5 | 2.5 | 590 | 560 | 590,000 | 1.5 | −28.9 | 0.17 |
| ET2-5 | 5 | 2.5 | 590 | 560 | 600,000 | 1.5 | −16.0 | 0.23 |
| ET2-6 | 5 | 2.5 | 540 | 510 | 540,000 | 1.4 | 4.2 | 0.19 |
| ET2-7 | 5 | 2.5 | 540 | 510 | 540,000 | 1.4 | −13.3 | 0.19 |
| ET2-8 | 5 | 2.5 | 540 | 510 | 540,000 | 1.4 | −12.8 | 0.19 |
| ET2A-1 | 5 | 2.5 | 460 | 430 | 450,000 | 0.82‡ | 346.6 | |
| ET2A-8 | 5 | 2.5 | 460 | 430 | 450,000 | 0.82‡ | 9.4 | |
| ET2A-9 | 5 | 2.5 | 460 | 430 | 450,000 | 0.82‡ | −7.8 | |
| ET2A-10 | 5 | 2.5 | 360 | 340 | 340,000 | 0.69 | −9.6 | |
| ET2A-11 | 5 | 2.5 | 360 | 340 | 340,000 | 0.69 | −2.8 | |
| ET2A-14 | 5 | 2.5 | 360 | 340 | 340,000 | 0.69 | 8.5 | 0.39 |
| ET2A-2 | 5 | 2.5 | 400 | 380 | 390,000 | 0.36 | −2.1 | 0.72 |
| ET2A-5 | 5 | 2.5 | 400 | 380 | 390,000 | 0.36 | −6.7 | |
| ET2A-13 | 5 | 2.5 | 400 | 380 | 390,000 | 0.36 | −20.6 | |

*Balance is uranium.
†Based on the outer surface of the jacketed assembly.
‡Burnup estimated, no flux monitors available.

interface temperature of 345°C, and a maximum core temperature of 433°C. It underwent approximately 65 power cycles of amplitude greater than 50% of full power.

Dimensional and volume-displacement measurements made during shutdowns at 150, 890, and 1280 Mwd/ton burnup (peak) revealed that the rate of volume change below 890 Mwd/ton was 6 or 7% increase per atomic percent burnup, whereas the rate of change between 890 and 1280 Mwd/ton was three times this amount. The 1280 Mwd/ton measurements indicate a strain in the outside cladding of 0.7%. The inside cladding dimensions changed a relatively small amount, and there was no significant change in length and bow of the element.

If the higher rate of volume change observed between 890 and 1280 Mwd/ton were to continue, the element life would be limited to about 2200 Mwd/ton (peak), assuming 2% tolerable strain. If the overall swelling rate were to prevail, the useful life of the element on the above basis would be limited to about 3800 Mwd/ton (peak). Savannah River irradiations under somewhat different conditions suggest that the swelling rate decreases at a burnup above that achieved in the VBWR irradiation. A concurrent irradiation of an unalloyed uranium element under conditions similar to those of the VBWR test demonstrated significantly better dimensional stability.

Irradiation experiments on uranium-fissium alloys were conducted by Argonne.[1] The Experimental Breeder Reactor No. 2 core 1 reference alloy, uranium–5 wt.% fissium, was found to swell appreciably in the temperature range between 670 and 750°C for burnups of 0.5 to 1.0 at.%. The results are given in Table I-1.

Uranium-fissium alloys jacketed with 9 mils of type 304 stainless steel and bonded with a 6-mil annulus of sodium were irradiated. The results are given in Table I-2. The data indicate excellent stability in the temperature range from 360 to 590°C and with a bulk volume increase of less than 1% volume change per atomic percent burnup. (M. S. Farkas)

## Gamma-Phase Uranium Alloys

Irradiation results for a series of uranium-molybdenum alloy specimens have been reported by Argonne.[1] The results are summarized in Table I-3.

Table I-3 RADIATION-INDUCED SWELLING IN URANIUM-MOLYBDENUM ALLOYS[1]

| Composition, wt.% | Burnup, at.% | Average temp., °C | | % volume change/ at.% burnup |
|---|---|---|---|---|
| | | Surface | Center | |
| U–11 Mo | 0.14 | 605 | 650 | 1.32 |
| U–11 Mo | 0.12 | 605 | 650 | 2.70 |
| U–11 Mo | 0.37 | 625 | 665 | 2.35 |
| U–14 Mo | 0.33 | 500 | 540 | 3.00 |

Argonne has also investigated a uranium–17 at.% niobium alloy for evidence of tetragonal-phase formation at this composition. The results supported the British observation that the tetragonal structure is metastable and is obtained on quenching. However, it appears that this tetragonal structure is obtained more often than would be indicated by the British work.

A report by the Russians[9] on gamma-phase decomposition has been published. X-ray diffraction studies of uranium-molybdenum alloys indicate that gamma decomposition proceeds by the formation of $U_2Mo$ (delta phase) regions which are ordered to a considerable degree and which are coherently bound to the prior gamma solution on the (0 0 1) planes. In uranium-niobium and uranium-niobium-zirconium alloys, gamma is found to decompose at low temperatures and low niobium compositions by the homogeneous formation of numerous, highly dispersed particles of alpha uranium. At higher temperatures and higher niobium concentrations, transformation is heterogeneous, proceeding by the growth of a limited number of nucleation centers. (A. A. Bauer)

## Epsilon-Phase Uranium Alloys

The electrical resistivity and specific heat of $U_3Si$ (uranium–3.8 wt.% silicon), as measured by Atomics International,[10] increased from 56 μohm-cm at 0°C to 75 μohm-cm at 750°C. The specific heat of $U_3Si$ is given by the equation

$$C_p = 3.16 \times 10^{-6}\, T + 0.0412 \text{ cal/(g)(°C)}$$

from 50 to 430°C.

A Swedish literature survey containing 123 abstracts pertaining to uranium-silicon alloys as nuclear fuel materials has been issued.[11] No evaluation is presented, and data are not

included. American reports and papers form the major basis for the survey.

(A. A. Bauer)

# Plutonium

## Plutonium Metal and Alloys

*Aluminum-Plutonium Alloys.* Chalk River[12] reports the finding of two new polymorphic forms of $PuAl_3$: (1) rhombohedral and (2) cubic. Rhombohedral crystals can be transformed from hexagonal crystals by cycling the alloy through the peritectic temperature. The cubic allotrope forms at 1210°C from hexagonal $PuAl_3$, and it has been preserved by quenching in water from temperatures as high as 1395°C. Cubic $PuAl_3$ allotrope is isostructural with cubic $UAl_3$, and it has a room-temperature lattice constant of $a_0 = 4.259 \pm 0.001$ A.

Solid solubility of plutonium in aluminum at the eutectic temperature of 650°C has been found to be $0.05 \pm 0.02$ wt.% plutonium.

The effects of ternary alloying and spheroidization on the corrosion of aluminum-plutonium alloys in static water and steam are being investigated. Results of recent tests are shown in Table I-4.

*Uranium-Plutonium-Fissium Alloys.* Argonne[13] has reported the effects of irradiation on various uranium-plutonium-fissium alloys. The results tabulated in Tables I-5 and I-6 indicate that the reference fuel alloy, uranium–20 wt.% plutonium–10 wt.% fissium, begins to swell catastrophically at temperatures above 370°C. Minor variations in fissium and zirconium content did not appreciably alter the irradiation characteristics. However, when the plutonium content was reduced to 10 wt.%, the swelling behavior of the alloy was significantly improved. Also, a uranium–20 wt.% plutonium–5 wt.% molybdenum alloy was less dimensionally stable than the uranium-plutonium-fissium alloys investigated. Irradiation data for uranium–20 wt.% plutonium–10 wt.% fissium alloy specimens clad in vanadium, niobium–1 wt.% zirconium, and type 304 stainless steel and irradiated to about 0.8 at.% burnup at 650 to 700°C indicate that swelling can be restrained by a strong cladding.[1]

The thermal conductivities[14] for several uranium-plutonium-fissium alloys are listed in Table I-7. The fissium in these alloys was high in zirconium (2.8 wt.%).

*Molten Plutonium Fuels.* Under corresponding environmental conditions, Los Alamos[15] has found that cerium-cobalt-plutonium alloys containing at least up to 6 g of plutonium per cubic centimeter are less corrosive to tantalum containers than the plutonium-iron alloy being employed in the Los Alamos Molten Plutonium Reactor Experiment. Tantalum capsules containing 1, 2, 3, 4, and 5 g of plutonium

Table I-4 TWENTY-HOUR CORROSION TESTS IN STATIC WATER AND STEAM ON CAST AND HEAT-TREATED BINARY AND TERNARY ALUMINUM-PLUTONIUM ALLOYS[12]

| Alloy composition (balance Al), wt.% | Alloy condition | Depth of corrosion,* mils | | | | | | |
|---|---|---|---|---|---|---|---|---|
| | | Water temp., °C | | | | Steam temp., °C | | |
| | | 280 | 340 | 360 | 380 | 300 | 340 | 360 |
| 5 Pu | As-cast | ~4 | >125 | >125 | | | | |
| | Spherical, 610°C, 20 hr | >125 | | | | >125 | | |
| 20 Pu | As-cast | | 0.6 | 0.5 | >125 | | | |
| | Spherical, 610°C, 20 hr | | >125 | >125 | | | >125 | |
| 5 Pu–15 U | As-cast | | 0.4 | 0.7 | 0.9 | | | |
| | Spherical, 610°C, 20 hr | | | 0.7 | 0.4 | | | |
| 5 Pu–15 Si | As-cast | | 0.5 | 0.6 | 0.7 | | | |
| | Spherical, 530°C, 20 hr | | | 0.6 | >125 | | 0.6 | 1.0 |
| 5 Pu–1 Ni | As-cast | | 0.3 | 0.4 | 0.4 | | | |
| | Spherical, 610°C, 20 hr | | | 0.3 | 0.4 | | | 0.8 |
| 5 Pu–4 Cu | As-cast | | 0.5 | 0.8 | 2.3 | | | |
| | Spherical, 500°C, 20 hr | | | 0.3 | 0.4 | | | 0.3 |
| 5 Pu–1 Cu | As-cast | | | 0.6 | 0.7 | | | |
| | Spherical, 500°C, 20 hr | | | | >125 | | | |

*Tests were carried out on 0.25-in.-diameter specimens. A corrosion depth of $>125 \times 10^{-3}$ in. signifies complete failure.

Table I-5 EFFECT OF IRRADIATION ON URANIUM–20 WT.% PLUTONIUM–10 WT.% FISSIUM FUEL ALLOY[13]

| Specimen | Maximum fuel temp., °C | | Burnup, at.% | Length change, % | Diameter change, % | Density decrease, % | Weight change, mg | % volume change†/ at.% burnup | Postirradiation appearance |
|---|---|---|---|---|---|---|---|---|---|
| | Center | Surface | | | | | | | |
| ANL-36-2-2‡ | 240 | 230 | 1.0 | 1.0 | 0.5 | 1.86 | −65.7 | 3.9 | Surface slightly roughened |
| ANL-36-7-2§ | 290 | 270 | 1.2 | 1.1 | 0.3 | 3.21 | −0.9 | 2.8 | Good |
| ANL-36-4-2 | 310 | 290 | 1.4 | 3.0 | 1.5 | 8.83 | −9.1 | 6.9 | Good |
| ANL-36-4-3¶ | 310 | 290 | 1.4 | 1.0 | 0.7 | 3.70 | −40.5 | 2.7 | Very good |
| EA-3 | 320 | 240 | 2.3 | ** | 7–17 | 36.2 | −1.9 | 24 | Broken in two pieces |
| ANL-36-6-2 | 330 | 310 | 1.4 | 3.2 | 2.3 | 10.0 | −6.0 | 7.9 | Surface slightly roughened |
| ANL-36-3-2 | 370 | 350 | 1.2 | 3.8 | 32 | 37.7 | 122.9 | 50 | Top swollen and oxidized |
| ANL-36-5-2 | 370 | 350 | 1.2 | 16 | 23 | 37.4 | 109.5 | 50 | Bent 15°, top swollen |
| ANL-36-5-3¶ | 370 | 350 | 1.2 | 14 | 11 | 28.9 | 41.1 | 34 | Top swollen |
| ANL-36-9-1 | 370 | 350 | 1.7 | 1.8 | 4.3 | 9.82 | −26.9 | 6.4 | Surface slightly roughened |
| ANL-36-9-3 | 370 | 350 | 1.7 | 3.2 | 1.9 | 11.9 | −101.8 | 7.9 | Good |
| ANL-36-10-3 | 390 | 370 | 1.8 | 8.3 | 2.4 | 28.4 | 66.8 | 22 | Bent 14°, surface roughened, radial cracks near top |
| ANL-36-11-1 | 440 | 420 | 1.3 | 22 | 54 | 43.5 | 173.7 | 59 | Bent 27°, swollen and cracked, oxidized looking |
| ANL-36-8-3 | 470 | 440 | 1.3 | 18 | 32 | 47.4 | 156.3 | 69 | Swollen, longitudinally cracked, top offset from bottom |
| EA-1 | 510 | 370 | 3.0 | ** | 20–26 | 39.4 | −1.4 | 22 | Bent 29°, top porous, cracked and oxidized |
| EA-5 | 610 | 440 | 2.6 | 22 | 21–28 | 41.3 | 0.1 | 27 | Bent 22°, top porous and oxidized |
| EA-4 | 650 | 470 | 2.0 | 18–23 | 10–23 | 39.1 | 0.1 | 32 | Broken in two pieces and bent |
| EA-6 | 730 | 520 | 3.3 | 15 | 14–47 | 38.7 | 0.1 | 19 | Bent 20°, top is cup shaped |
| EA-2 | 800 | 530 | 2.7 | −2.6 | 19–56 | ** | ** | ** | Bent 15°, top is slumped and porous |
| EA-7 | 810 | 580 | 2.8 | ** | 99 | ** | ** | ** | Unable to remove specimen from capsule |

*Specimens are injection-cast except where otherwise indicated.

†Volume change obtained from the relation $(V_{initial} - V_{final})/V_{initial} = 1 - (\rho_{initial}/\rho_{final})$ and assuming no weight change ($V$ = volume and $\rho$ = density).

‡Injection-cast and annealed for 24 hr at 500°C.

§Pour-cast and thermally cycled between 50 and 500°C.

¶Pour-cast, extruded, and thermally cycled between 50 and 500°C.

**Unable to obtain measurements because of the condition of the specimen.

Table I-6 EFFECT OF IRRADIATION ON OTHER URANIUM-PLUTONIUM ALLOYS[13]

| Specimen* | Composition (balance U), wt.% | Burnup, at.% | Maximum temp., °C | | Length change, % | Diameter change, % | Density decrease, % | Weight change, mg | % volume change†/ at.% burnup | Postirradiation appearance |
|---|---|---|---|---|---|---|---|---|---|---|
| | | | Center | Surface | | | | | | |
| ANL-36-2-1 | 10 Pu–10 Fs | 1.0 | 250 | 240 | 0 | 0.7 | 1.85 | −0.4 | 2.0 | Excellent |
| ANL-36-3-1 | 10 Pu–10 Fs | 1.1 | 370 | 350 | 1.7 | 1.6 | 4.95 | −0.5 | 4.7 | Good |
| ANL-36-4-1 | 20 Pu–7 Fs–3 Zr | 1.4 | 310 | 290 | −1.2 | 2.6 | 8.81 | −12.2 | 6.9 | Good |
| ANL-36-5-1 | 20 Pu–7 Fs–3 Zr | 1.2 | 370 | 350 | 5.7 | 9.9 | 26.0 | −5.1 | 30 | Top began to swell |
| ANL-36-6-1 | 20 Pu–10.5 Fs–4.5 Zr | 1.4 | 330 | 310 | 3.7 | 3.0 | 11.8 | −3.1 | 9.5 | Good |
| ANL-36-7-1 | 20 Pu–10.5 Fs–4.5 Zr | 1.1 | 290 | 270 | 1.1 | 2.2 | 6.75 | −1.4 | 6.5 | Good |
| ANL-36-6-3 | 20 Pu–15 Fs | 1.4 | 330 | 310 | 5.9 | 4.6 | 16.4 | 21.2 | 15 | Top distorted with longitudinal cracks |
| ANL-36-7-3 | 20 Pu–15 Fs | 1.1 | 290 | 270 | 6.1 | 18 | 17.1 | 39.1 | 20 | Bent 15°, top end swollen and split open |
| ANL-36-9-2 | 20 Pu–5 Fs‡ | 1.7 | 370 | 360 | 3.4 | 5.3 | 20.8 | −0.5 | 16 | Top swollen |
| ANL-36-11-2 | 20 Pu–5 Fs‡ | 1.3 | 440 | 420 | 18 | 56 | 57.2 | 234.6 | 105 | Bent 18°, top swollen, cracked, porous, and oxidized |
| ANL-36-10-1 | 20 Pu–5.4 Fs–3.6 Mo§ | 1.8 | 390 | 370 | 16 | 12 | 25.5 | 5.3 | 19 | Bent 13°, top distorted |
| ANL-36-10-2 | 20 Pu–5.4 Fs–3.6 Mo‡ | 1.8 | 390 | 370 | 9.3 | 3.8 | 21.7 | 13.4 | 16 | Top swollen |
| ANL-36-11-3 | 20 Pu–5.4 Fs–3.6 Mo‡ | 1.3 | 440 | 420 | 19 | 30 | 46.2 | 82.5 | 66 | Bent 23°, top swollen, cracked, porous, and oxidized |
| ANL-36-8-1 | 20 Pu–5 Mo§ | 1.4 | 470 | 440 | 23 | 34 | ¶ | ¶ | ¶ | Entire specimen distorted and full of cracks |
| ANL-36-8-2 | 20 Pu–5 Mo‡ | 1.4 | 470 | 440 | 29 | 48 | ¶ | ¶ | ¶ | Entire specimen distorted and full of cracks |
| ANL-36-2-3 | 25 Pu–10 Fs | 1.1 | 260 | 240 | 1.2 | −0.3 | 3.06 | −52.9 | 2.8 | Top half distorted |
| ANL-36-3-3 | 25 Pu–10 Fs | 1.2 | 370 | 350 | 21 | 34 | 33.4 | 87.4 | 42 | Bent 30°, top swollen and began to crack |

*Specimens are injection-cast except where otherwise indicated

†Volume change obtained from the relation $(V_{initial} - V_{final})/V_{initial} = 1 - (\rho_{initial}/\rho_{final})$ and assuming no weight change ($V$ = volume and $\rho$ = density).

‡Pour-cast, extruded, and thermally cycled prior to irradiation.

§Pour-cast and thermally cycled prior to irradiation.

¶Specimen ignited and burned to oxide before measurements could be obtained.

per cubic centimeter have withstood 1000 hr at 750°C, 2000 hr at 850°C, and 700 hr at 750°C. The plutonium–2.5 wt.% iron alloy would have penetrated the capsules in less than 200 hr at 750°C. In tests with alloys containing 4, 5.7, 7.6, 9.5, 11, 13, and 15 g of plutonium per cubic centimeter, the capsules containing more than 7.6 g of plutonium per cubic centimeter showed leakage after 200 hr at 750°C. Capsules containing fuel with 4 and 5.7 g of plutonium per cubic centimeter have gone 400 hr at 750°C and 1000 hr at 850°C without leakage. In tests of the same alloys in high-purity electron-beam-melted tantalum capsules annealed 1 hr at 1450°C, no leakage has been experienced after 700 hr at 625°C followed by 700 hr at 700°C.

Table I-7 THERMAL CONDUCTIVITY OF URANIUM-PLUTONIUM-FISSIUM (HIGH ZIRCONIUM) ALLOYS[14]

| Temp., °C | Thermal conductivity, cal/(sec)(cm)(°C), for indicated alloy | | | |
|---|---|---|---|---|
| | U–10 wt.% Pu–10 wt.% Fs | U–20 wt.% Pu–10 wt.% Fs | U–20 wt.% Pu–15 wt.% Fs | U–40 wt.% Pu–10 wt.% Fs |
| 100 | 0.043* | 0.044* | 0.040* | 0.029* |
| 200 | 0.046 | 0.047 | 0.043 | 0.034 |
| 300 | 0.051 | 0.051 | 0.048 | 0.040 |
| 400 | 0.057 | 0.056 | 0.053 | 0.045 |
| 500 | 0.063 | 0.062 | 0.060 | 0.051 |
| 600 | 0.070 | 0.069 | 0.067 | 0.057* |
| 700 | 0.077 | 0.077 | 0.074 | 0.062* |
| 800 | 0.084* | 0.086* | 0.080* | |

*Extrapolated values.

Coefficients of linear thermal expansion of cerium-cobalt-plutonium alloys are listed in Table I-8. These data are in contrast with United Kingdom data which indicate that a cerium–25 at.% cobalt–14 at.% plutonium alloy has a negative coefficient of linear thermal expansion ($-25 \times 10^{-6}$/°C).

Results of initial survey experiments of container materials for a molten uranium–4.5 at.% plutonium–20.4 at.% manganese alloy are presented in Table I-9.

(V. W. Storhok)

## Plutonium Compounds

Investigators at Hanford[16] have attempted unsuccessfully to synthesize PuS by reacting $PuH_3$ with $H_2S$ at 500°C, followed by a 1-hr homogenization at 1500°C. Owing to air leakage into the system, the primary product was $PuO_2$.

The same laboratory has measured the thermal expansion of $PuO_2$ to 1620°C. The expansion is uniform to 1275°C. At this temperature an abrupt change in the slope of $\Delta a/a_0$ is observed.[17] This inflection is attributed to oxygen volatility. Hanford has also prepared single-phase PuN by hydriding alpha plutonium and heating it in nitrogen for 2 hr at 600°C. Defected PuC has been determined to have a structure of four plutonium atoms per unit cell, whereas the number of carbon atoms decreases to 3.2 per unit cell at 39.8 at.% carbon. A solubility of plutonium in hypostoichiometric PuC is reported.

The British[18,19] continue investigation of phase equilibria in the $UO_2$-$PuO_2$ system. Sintering behavior varies markedly with composition and sintering atmosphere. The best density was obtained after calcining at 800°C, ball milling for 10 to 20 hr, and sintering in wet hydrogen at 1500°C for 12 to 14 hr. In working with $PuO_2$-$UO_2$ solid solutions sintered at 1200°C in argon and reduced in hydrogen at 1350°C, Chalk River[12] has found that −400-mesh $PuO_2$ has a density-reducing effect. Coarser $PuO_2$ appears to have a slight grain-refining effect.

Table I-8 THERMAL EXPANSION OF CERIUM-COBALT-PLUTONIUM ALLOYS[15]

| Alloy composition (balance Ce), at.% | Coefficient of linear thermal expansion, $10^{-6}$/°C |
|---|---|
| 25 Co–15 Pu | 27 |
| 25 Co–25 Pu | 23 |
| 25 Co–35 Pu | 27 |
| 25 Co–45 Pu | 10.5 |

Subsequent annealing at 1200°C in argon did not affect the density.

Data for the vapor pressure of $PuO_2$ in air, argon, and oxygen between 1450 and 1775°C have been reported.[20] Included are values of $\Delta H^\circ_{298}$ for vaporization and the standard free energy of formation of gaseous $PuO_2$.

United Nuclear[21,22] reports little effect of time and temperature on densification of $(U_{0.8}Pu_{0.2})C_{0.95}$ in the range 1550 to 1850°C. Optimum sintering temperature was found to be 1925°C. Synthesis is accomplished by heating mixtures of $UO_2$, $PuO_2$, and carbon for 6 hr at 1625°C. The addition of 0.12 wt.% nickel increased the density from 92.4 to 96.8% of theoretical.

Plutonium carbide has been prepared on a kilogram-production basis at Argonne[23] with no composition difficulties. Compatibility studies[1] show reaction zones of 20-$\mu$ width between tantalum and PuC after 260 hr at 1000°C. Stainless steel reacts more extensively under the same conditions. The widths of the reaction zones are dictated by the composition of the PuC. The same authors[1] have published an extensive study of the 400, 570, and 635°C isotherms in the uranium-plutonium-carbon ternary phase diagram.

The wet agglomeration of $PuO_2$ gives bodies with densities in the neighborhood of 5.1 g/cm³. These bodies were sintered to 10.4 g/cm³ after 2 hr at 1550°C in air.[24] Little success has been attained at Nuclear Materials & Equipment Corp. (NUMEC) with plasma spraying to produce spherical particles of $PuO_2$-$UO_2$ solid solutions.[25] (W. M. Pardue)

Table I-9 EXPOSURE OF TEST CONTAINERS[15] TO URANIUM–4.5 AT.% PLUTONIUM–20.4 AT.% MANGANESE FUEL AT 900°C FOR 2 HR

| Test container | Observations |
|---|---|
| Yttrium (1100 ppm O; 70 ppm C; 35 ppm $H_2$; 30 ppm $N_2$) | Not more than 1 mil of solution attack anywhere; no intergranular attack |
| Scandium | Complete intergranular attack of 40-mil wall; some solution attack |
| Calcium oxide ($10^3$–$10^4$ ppm Mg; 100–1000 ppm Si, Fe, Al) | Slight reaction layer; 10 ppm Ca present in fuel; metallography showed no attack |
| Yttria | Slight, if any, reaction layer; metallography showed very little penetration by fuel; less than 5 ppm in Y fuel |
| Cerium sulfide, $CeS_{0.99}$ (1000 ppm Si; 100 ppm Mg, Ca)* | Wetted; no attack observed by metallography or visually; 80 ppm Ce and 10 ppm S in fuel |
| Beryllia, 2.90 g/cm³ 99+% (3000 ppm Al; 500 ppm Ca) | Slight, if any, reaction layer; metallography showed microcracks or intergranular penetration up to 1 mil deep; 10 ppm Be in fuel |
| Magnesia ($10^3$–$10^4$ ppm Si; 2000 ppm Ca; 500 ppm Fe; 200 ppm Ni; 100 ppm Mn) | Very slight reaction layer; up to 3 mils of intergranular attack; 10 ppm Mg in fuel |
| 98 wt.% $Al_2O_3$ + 2 wt.% $Y_2O_3$ ($10^3$–$10^4$ ppm W; 5000 ppm Si; 1000 ppm Ca; 100–1000 ppm Zr; 200 ppm Fe) | Definite reaction layer between fuel and container; up to 2 mils of pitting attack; 250 ppm Al and less than 5 ppm Y produced in fuel |

*Fuel was 74.1 at.% uranium, 4.9 at.% plutonium, and 21.0 at.% manganese in this case.

# Thorium

Investigators at Ames[26] report that the thorium-tantalum system is a simple eutectic type. The eutectic occurs at 1565 ± 10°C and 4.0 ± 0.5 wt.% tantalum. A eutectoid reaction is associated with the thorium alpha-beta transformation. No evidence of intermetallic compounds was found. Solubility of tantalum in thorium at 1565°C is about 0.4 wt.%, and

Table I-10 IRRADIATION DATA FOR CAST URANIUM-THORIUM ALLOYS[1]

| Thorium, wt.% | 10 | 15 | 20 | 25 |
|---|---|---|---|---|
| Burnup, at.% | 4.5 | 4.9 | 4.9 | 5.1 |
| Irradiation temp., °C | 700 | 700 | 700 | 700 |
| % volume change/ at.% burnup | 1.6 | 2.1 | 2.4 | 3.6 |

below 1340°C it is less than 0.2 wt.%. Solubility of thorium in tantalum is less than 0.2 wt.% at 1565°C.

The thorium-vanadium system has a eutectic at 1435 ± 10°C at 5 ± 0.5 wt.% vanadium. The alpha-beta transformation in thorium is lowered by vanadium, and the resulting eutectoid is at 1345 ± 10°C and less than 0.1 wt.% vanadium. Solubility of vanadium in thorium is less than 0.4 wt.% at 1435°C and about 0.05 wt.% at 1345°C. Solubility of thorium in vanadium is less than 0.4 wt.% at 1390°C, and it decreases with decreasing temperature.

Irradiation data,[1] as shown in Table I-10, indicate that (1) uranium-thorium alloys do not swell catastrophically when irradiated at tem-

Table I-11 CUMULATIVE VOLUME INCREASE[14] IN IRRADIATED THORIUM-URANIUM ALLOY SPECIMENS AFTER ANNEALING FOR 100 HR

| Specimen | Composition, wt.% | Total atom burnup, at.% | Annealing temp., °C | % volume change */ at.% burnup |
|---|---|---|---|---|
| ANL-42-7-1 | Th–10 U | 4.0 | 550 | 0.2 |
| | | | 600 | 1.0 |
| | | | 650 | 1.9 |
| | | | 700 | 2.0 |
| | | | 725 | 2.6 |
| | | | 750 | 2.7 |
| | | | 775 | 3.7 |
| ANL-42-1-2 | Th–15 U | 4.5 | 550 | 0.3 |
| | | | 600 | 0.6 |
| | | | 650 | 0.7 |
| | | | 700 | 0.9 |
| | | | 725 | 1.6 |
| | | | 750 | 1.7 |
| | | | 775 | 1.9 |
| ANL-42-1-3 | Th–20 U | 4.5 | 550 | 0.2 |
| | | | 600 | 0.7 |
| | | | 650 | 1.5 |
| | | | 700 | 1.5 |
| | | | 725 | 2.5 |
| | | | 750 | 3.2 |
| | | | 775 | 3.0 |
| ANL-42-5-4 | Th–25 U | 4.2 | 550 | 0.4 |
| | | | 600 | 1.5 |
| | | | 650 | 2.1 |
| | | | 700 | 1.8 |
| | | | 725 | 2.8 |
| | | | 750 | 2.7 |
| | | | 775 | 3.2 |

*The volume change is based on the assumption of no weight change and was calculated from the expression: % volume change = $[(\rho_i/\rho_f)-1] \times 100$, where $\rho_i$ and $\rho_f$ are the initial and final densities, respectively.

Table I-12 THERMAL CONDUCTIVITY OF (9 Th : 1 U) COMPOUNDS[28]

| Temp., °C | Thermal conductivity, cal/(sec)(cm)(°C) | | | | |
|---|---|---|---|---|---|
| | (9 Th : 1 U)C | (9 Th : 1 U)$C_2$ | (9 Th : 1 U)$B_4$ | $UO_2$ | Thorium |
| 200 | 0.0308 | 0.0483 | 0.0652 | 0.019 | 0.093 |
| 400 | 0.0342 | 0.0528 | 0.0731 | 0.014 | 0.100 |
| 600 | 0.0375 | 0.0566 | 0.0810 | 0.011 | 0.106 |
| 800 | 0.0411 | 0.0607 | 0.0891 | 0.009 | |
| 900 | 0.0426 | 0.0629 | 0.0932 | | |
| 950 | | 0.0637 | | | |
| 1000 | 0.0442 | | | | |

peratures of 700°C and (2) swelling increases only slightly with increasing thorium content.

Since the irradiation temperatures were calculated, some doubt existed as to the validity of the irradiation data. Accordingly, Argonne[14] has performed postirradiation annealing experiments with these alloys. The results, listed in Table I-11, show no catastrophic swelling even after 100 hr at 775°C. These data confirm the irradiation experiments.

Rocky Flats[27] has investigated methods for canning thorium which would allow it to be rolled without creating a health-physics problem. The most suitable technique was found to be a hot dip in aluminum at 800°C.

Investigators at Battelle[28] have measured the thermal conductivities of (9 Th:1 U)C, (9 Th:1 U)$C_2$, and (9 Th:1 U)$B_4$. The results, along with comparative values for $UO_2$ and thorium, are listed in Table I-12.

(V. W. Storhok)

## Dispersion Fuels

Figure I-4 shows Young's modulus for type 347 stainless steel and for type 347 stainless steel–20 vol.% $UO_2$ as functions of temperature.[29] It is interesting to note that the 20 vol.% cermet has a modulus of 80% of that of type 347 stainless steel. Figure I-5 shows the tensile properties of the 20 vol.% $UO_2$–type 347 stainless-steel bare plate, transverse to the rolling direction.

At Phillips Petroleum Co.[30] tensile testing has been completed on 94 specimens of irradiated sample fuel plates. Fuel cores were composed of uranium-aluminum alloys, $UO_2$-aluminum cermets, and $U_3O_8$-aluminum cermets. The cladding materials used were 1100, 6061, APM 257, X8001, X8003, and 5052 aluminum alloys. The most significant effect was loss of ductility. At low thermal-neutron dosages (about $2 \times 10^{20}$ neutrons/cm$^2$) the maximum elongation was 4.5%; at $20 \times 10^{20}$ neutrons/cm$^2$ the maximum was 1%; and at $26 \times 10^{20}$ neutrons/cm$^2$ the elongation was zero.

A series of annealing studies of irradiated aluminum–$U_3O_8$ (39 wt.%) dispersion coupons has been initiated by Argonne.[1] The specimen coupons had between 0.0005 and 0.003 in. of aluminum cladding on two faces and none on the edges. A salt bath was used for the annealing study. The data indicated that the

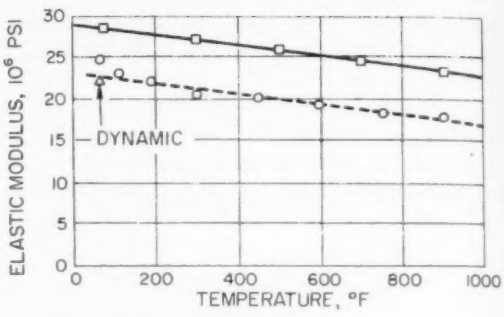


Fig. I-4 Comparison of modulus of type 347 stainless steel and $UO_2$-dispersed stainless steel.[29] ○, type 347 stainless steel–$UO_2$. □, type 347 stainless steel. — —, 80% of elastic modulus for type 347 stainless steel.

aluminum–$U_3O_8$ (39 wt.%) dispersions had excellent resistance to swelling for burnups equal to or less than $1.35 \times 10^{20}$ fissions/cm$^3$ and at temperatures up to 500°C.

Oak Ridge has irradiated prototype fuel elements containing 63 wt.% $U_3O_8$–aluminum dispersions clad with 1100 aluminum.[29] Two fuel plates having maximum $U^{235}$ fission burnups of approximately 57 at.% were heat-treated for 24 hr in 100°F increments from 400 to 1000°F and measured for dimensional stability. Powder samples of the irradiated $U_3O_8$ (63 wt.%)–aluminum dispersions, plus some $UAl_3$ and $UC_2$ dispersions in aluminum, were examined at Battelle by X-ray diffraction to identify the reaction products observed after irradiation. Although $UAl_3$ was identified as a reaction product in the irradiated $U_3O_8$-aluminum specimen, no volume increase was observed. This

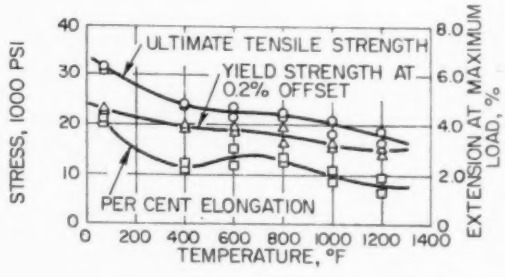


Fig. I-5 Tensile properties of 20 vol.% $UO_2$–type 347 stainless-steel bare plate transverse to rolling direction; annealed at 1150°C for 1 hr in hydrogen and then furnace cooled.[29]

is significant because this formation in previous studies was always accompanied by a volume increase. There were indications that the $UAl_3$ had undergone an order-disorder transformation as a result of irradiation. Similar dimensional stability was reported by Phillips[34] for a $UO_2$-aluminum dispersion that had been heat-treated for 65 hr at 600°C.

The conceptual High-Flux Isotope Reactor target design requires a dispersion of $Pu^{242}$, $Am^{243}$, and $Cm^{244}$ oxides in an aluminum matrix. Rare-earth oxides, which have characteristics similar to the actinide oxides, are being satisfactorily blended with aluminum powder of −325-mesh size in a specially designed blending hopper containing small aluminum rods that act as a blending aid. Mixtures containing 10, 15, 20, and 25 vol.% oxides were blended with the aluminum powder and were cold pressed to give satisfactory dispersions.[29]

Los Alamos[31] has been conducting a sintering study of tungsten-$UO_2$ by use of additions of nickel and $TiO_2$. This study indicated that higher densities (95 to 98% of theoretical) can be obtained in the tungsten-$UO_2$ dispersions through the additions of nickel and $TiO_2$. The nickel is the most successful additive below 1400°C sintering temperature, and $TiO_2$ appears to be the best at 1700°C. When both nickel and $TiO_2$ are added, the densification rate is increased when sintering is done at 1700°C in hydrogen. It was also reported that the sintering atmosphere was as important as the selection of additive. For instance, the hydrogen atmosphere was shown to be superior to vacuum, unless the vacuum-sintered material was first preheated in hydrogen at elevated temperatures. (D. L. Keller)

# Coated-Particle Fuel Materials

## Preparation and Fabrication

*Oxide-Base Fuel.* Further results on the evaluation of nickel-coated and stainless-steel-coated $UO_2$ were reported by Martin-Nuclear.[32] The coating is first deposited on the oxide substrate and is then heat-treated in a hydrogen atmosphere. Details of the coating process were not described. Figure I-6 is a photomicrograph of the stainless-steel-coated particles. The main problem was the maintenance of uniformity and continuity of the coating over the entire fuel-particle surface. Variations are being made in the preparation cycle in attempts to produce more uniform metal coatings. Porosity is of secondary concern since the product can be densified during later fabrication. When such a fuel is used, it is believed that an ideal distribution of $UO_2$ in a stainless-steel matrix can be achieved, and the method is reported to offer promise as an economical processing procedure.

A fairly comprehensive review[33] of the fundamentals of vapor deposition was published recently, and specific applications to coated fuel particles were reviewed[34,35] by Battelle and by NUMEC (Ref. 34). The NUMEC equipment[36] for coating fuel particles with metallic coatings using reactions involving hydrogen reduction of volatile metal halides is shown in Figs. I-7 and I-8. NUMEC recommends the use of vibration to maintain the particles in suspension while they are being coated. Battelle has generally employed fluidized-bed equipment. Figure I-9 is a sketch of one of Battelle's 2-in. fluidized-bed reactors, constructed of stainless steel, and Fig. I-10 is a rotating-basket unit for coating pellets with chromium. Figure I-11 is a diagram of a Vycor unit which employs the fluidized-bed principle and which has been used extensively for the preparation of oxide coatings. The oxide coatings are usually prepared by the hydrolysis of volatile metal halides.

The preparation of high-quality beryllia coatings on $UO_2$ particles was reported by Battelle this quarter.[28,37,38] One coating, 60 $\mu$ thick, which was dense and transparent, was deposited at 1400°C by the steam hydrolysis of $BeCl_2$ on 127-$\mu$ $UO_2$. This coating had a Knoop hardness number (KHN) in the range of 1080 to 1300, which is essentially the same for single-crystal BeO. The coated particles had an average crushing strength of 875 g, and in the standard leach test they lost 10 ppm of $UO_2$. After heating the particles in air at a temperature of 1100°C for 20 hr, the leach test showed that only 10 ppm of the $UO_2$ was attacked. Heat-treatment of a neutron-activated sample yielded a total $Xe^{133}$ release of 0.10 ppm at temperatures up to 1300°C. On the basis of these preliminary tests, this material is being irradiated at low temperatures in the Battelle Research Reactor. Thin beryllia coat-

ings are also being deposited as a fission-recoil-absorbing interlayer before overcoating with $Al_2O_3$ or pyrolytic carbon (PyC).

Studies on $Al_2O_3$ coatings at Battelle have generally followed three avenues of approach to circumvent the problem of coating failure at low temperature during irradiation and at high temperatures during oxide-matrix fabrication. Under irradiation at intermediate temperatures (500 to 1100°C), the $Al_2O_3$ coatings, of course, showed good fission-product retentivities. One approach to the low-temperature failure problem is to permit a void to develop between the coating and the $UO_2$ substrate. Porous $UO_2$ has been coated with $Al_2O_3$, and it is hoped that subsequent sintering of the porous substrate may develop such a void. A composite coating on $UO_2$ of a 20-$\mu$ BeO fission-product-trapping layer, a 5-$\mu$ PyC separation layer, and a 40-$\mu$ $Al_2O_3$ overcoating seal was prepared and will be irradiated if out-of-pile tests continue to indicate satisfactory coating quality.

Magnesia coatings have been prepared at temperatures of 800, 1100, and 1400°C at Battelle.[28,37,38] The coatings prepared at the higher temperatures appeared to be dense and void-free. The hardnesses were slightly less than that of fused MgO. The differential between the thermal expansions of $UO_2$ and MgO caused the coatings to crack, but this problem was essentially overcome by the use of porous $UO_2$ or the incorporation of a void in the particle. Recent investigations indicate that oxygen diffusion through the vapor-deposited MgO is the major cause of the susceptibility of the particle to oxidation at 1100°C.

Efforts are being continued to prepare carbon coatings that are resistant to radiation damage. Composite coatings consisting of inner layers of BeO, $Al_2O_3$, and laminar carbon and alternating layers of high-density and low-density carbon have been prepared to protect the outer carbon coating from recoil damage and crack propagation. Also, a porous $Al_2O_3$

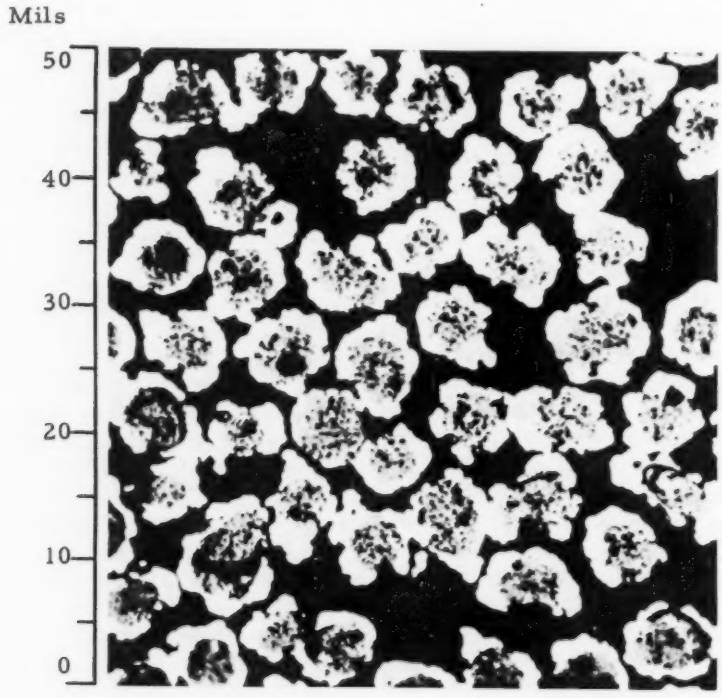


Fig. I-6 Stainless-steel-coated spherical $UO_2$ prepared by Martin-Nuclear.[32] Original magnification, 75×.

interlayer was deposited on $UO_2$ and then overcoated with PyC. This material was subsequently heat-treated to densify the $Al_2O_3$ and to develop a void that might accommodate fuel and/or coating distortion. Although a void was developed by this procedure, the integrity of the coating was reduced by the heat-treatment. A number of these carbon-overcoated materials are now being irradiated.

A patent related to present vapor-deposition studies on oxide coatings was recently awarded to National Distillers & Chemical Corp. on a process for separating hafnium-free zirconium from the mixed tetrahalide vapors.[39] The zirconium was found to be at least partially separated from the mixed halides by reaction with an oxygen-containing gas in the temperature range from 500 to 1250°C in a fluidized bed of zirconia particles.

Two reports issued recently by Battelle summarize their studies on the preparation of oxide bodies from coated-particle fuels by use of pressure-bonding techniques and pelletizing processes. The pressure-bonding method involves vibrationally compacting $Al_2O_3$-coated fuel particles into metallic tubes and then isostatically hot pressing.[40] The alumina coatings were relatively thin, i.e., 5 to 10 $\mu$ of $Al_2O_3$, because of a requirement that the weight percent of $UO_2$ in the fuel bodies be high. In some cases small additions of chromium powder were employed for improved oxidation resistance. Although densified cores declad by acid leaching failed relatively rapidly in 650 and 820°C air, some improvement in resistance was provided by the chromium. Defected clad fuel pins containing dense cores of coated particles showed greater resistance to oxidation at 820 and 950°C than did defected fuel pins with solid $UO_2$ cores.

The pelletizing process provides a technique whereby coated particles prepared by vapor deposition are overcoated with a pelletized coating of the matrix material.[41] The spherical pellets are compacted and then heat-treated. In oxide-base matrices, a burnout layer can be incorporated into the pellet to allow room for matrix shrinkage on sintering and to provide a void surrounding each particle. This void serves as a barrier to prevent a matrix crack from propagating into a particle coating and also as a reservoir to contain the volume expansion associated with any oxidation of $UO_2$ to $U_3O_8$. The advantages of the pelletized product include (1) an ideal geometric dispersion of fuel, (2) protection to the vapor-deposited coatings during subsequent fabrication, (3) uniform fuel content, and (4) a ceramic element whose surfaces are free of fuel particles. Figure 18 of the feature article in this issue is a photograph of coated particles prepared by vapor deposition, both before and after overcoating

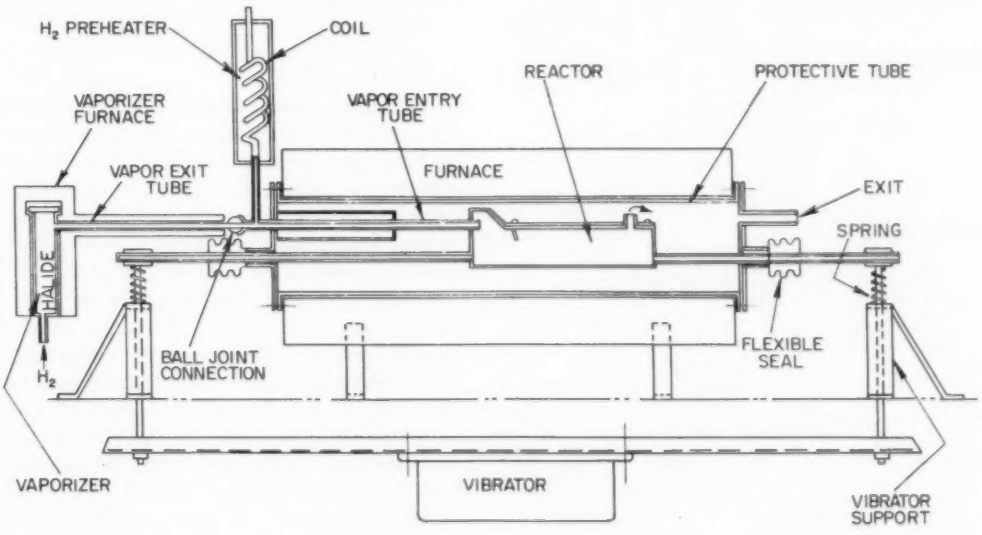


Fig. 1-7 Vibrating-chamber apparatus used by NUMEC for applying metallic films.[36]

with pelletized oxide-matrix material. The fractured surface of an $Al_2O_3$-matrix body prepared from pelletized fuel is shown in Fig. I-12.

Laboratory studies on the reprocessing of graphite-base fuel elements containing coated particles were reviewed by Oak Ridge.[42] Potential processes for recovering uranium and thorium from irradiated elements include (1) grinding followed by acid leaching and (2) burnup and subsequent dissolution of the oxide ash.

*Carbide-Base Fuel.* The laboratory equipment used by General Atomic in coating uranium-thorium dicarbide particles is shown in Fig. I-13. It consists of a mullite reactor, and it employs the fluidized-bed technique to suspend the particles in turbulent motion during coating[43] at temperatures up to about 1400°C. For temperatures above 1400°C, Battelle employs an inductively heated graphite reactor (Fig. I-14) that also utilizes the fluidized-bed technique.[34] It has been operated at temperatures up to about 2000°C. The first patent concerning a ceramic-coated nuclear particle was recently awarded in England to the United Kingdom Atomic Energy Authority in the name of R. A. U. Huddle. The invention relates to a process for preparing a PyC coating on carbide fuel particles, and a rotating cylindrical vessel was used in the first reduction to practice.[44]

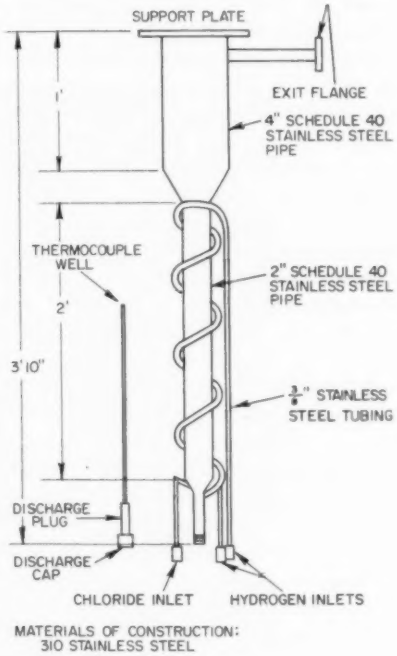


Fig. I-9 Fluidized-bed apparatus used at Battelle for coating particles with niobium films.[35]

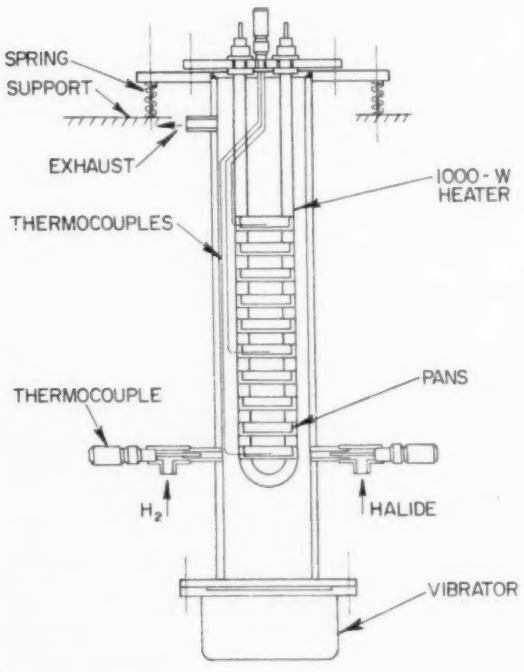


Fig. I-8 Vibrating-multipan apparatus used by NUMEC for applying metallic coatings.[36]

Recent studies at General Atomic have shown that thermodynamically it should not be possible to use nitrogen as a carrier gas for coating carbide particles because the carbide would tend to be converted to the nitride.[45] However, it was recommended that, if the use of nitrogen should prove to be sufficiently attractive economically, it might be desirable to determine the kinetics of the nitriding reactions and to see if thin, impermeable carbon coatings could be produced to protect the carbide from attack. General Atomic[46] is also checking the possibility that the use of zirconium-uranium carbide fuel particles might minimize fuel migration in compacts containing coated particles. In general, it appeared that this type of particle was stable (retained coating integrity) for several hours at 2300 and 2500°C. Pre-

liminary results from an investigation of the susceptibility of carbon coatings on fuel particles to acid electrolysis after irradiation were also revealed by General Atomic.[46] It was demonstrated that acid electrolysis did not affect unirradiated coatings, but similar

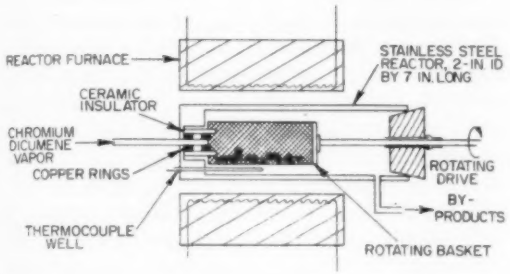


Fig. I-10 Rotating-basket apparatus used at Battelle for coating pellets with chromium films.[35]

studies on irradiated coatings have not been completed.

National Carbon has recently summarized its studies during 1959 and 1960 on the preparation of graphite-matrix fuel elements containing coated particles.[47] Techniques to achieve uniform dispersions of particles in the element, investigations of fuel migration in high-temperature processing and under anisothermal conditions, and methods of testing the integrity of coatings on fueled graphite were reported. Property data obtained at Battelle[28] on graphite-matrix bodies prepared from graphite-pelletized fuel are reported in Table I-13. Although $Al_2O_3$-coated $UO_2$ particles were employed in the preparation of the group of specimens designated PG-6 and BeO-coated $UO_2$ particles in the group designated PG-7, similar results could presumably be obtained with coated carbide fuels.

Oak Ridge has announced that Osterreichische Studiengesellschaft für Atom-Energie, a subcontractor for the Dragon Project, and NUMEC have submitted samples of PyC-coated carbide particles for evaluation and possible irradiation.[48] Studies at Oak Ridge are also continuing on the compatibility of coated particles with Santowax R, high-pressure water, molten fluorides, and water vapor, and the diffusion of uranium in PyC.

A summary of high-temperature stability studies at Oak Ridge with PyC-coated carbide particles has been prepared.[29] It was found that metallic fission products had considerably higher release rates than xenon, iodine, and tellurium at temperatures of 1400°C and above. All the coatings studied were of small crystal size. The laminar coatings showed evidence of a strained lattice.

One of the more interesting evaluation techniques for coated particles developed this quarter was the use of low-voltage radiography by Oak Ridge.[49,50] Examples of the structural information that can be obtained using this technique are shown in Fig. I-15. Coating contamination, the presence of unfueled or doublet particles, and the migration of uranium into the coating can be readily detected. In one experiment, two samples of carbon-coated carbide particles were heat-treated at 1600°C for 95 hr. The major difference between the two samples selected was that the Minnesota Mining & Manufacturing Co. (3M) material had a laminar coating and the High Temperature Materials, Inc. (HTM) sample had a columnar coating. After being heat-treated, the particles were placed directly on a sheet of film and were subjected to 10-kv

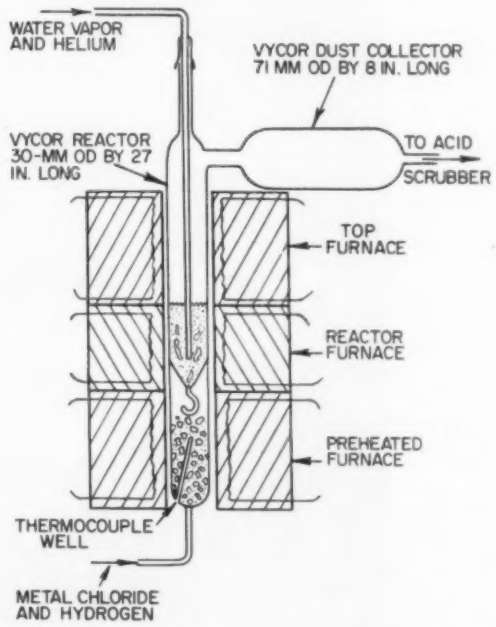
WATER VAPOR AND HELIUM
VYCOR DUST COLLECTOR 71 MM OD BY 8 IN. LONG
VYCOR REACTOR 30-MM OD BY 27 IN. LONG
TO ACID SCRUBBER
TOP FURNACE
REACTOR FURNACE
PREHEATED FURNACE
THERMOCOUPLE WELL
METAL CHLORIDE AND HYDROGEN

Fig. I-11 Fluidized-bed apparatus used at Battelle for coating particles with oxide films.[35]

X rays. Duplicate exposures were made on as-received particles for comparison. Significant uranium migration was found to have occurred in both laminar and columnar coatings. The penetration by uranium was nonuniform in both types of coatings. Further, it was very rapid in some areas of some particle coatings and undetectable in others. This observation suggests that the migration occurs along defects originally present in the coating.

Oak Ridge[51] has also made additional studies on reprocessing of carbon-coated carbide particles. Electrodissolver experiments were conducted with PyC-coated $UC_2$-$ThC_2$ fuel particles in both a direct-contact anode dissolver and a U-shaped "series" dissolver. Under the conditions investigated ($HNO_3$ concentration, 4*M* to 10*M*; current density, 1 to 10 amp/cm$^2$; temperature, 25 to 80°C), uranium and thorium recoveries were less than 0.2%. It was concluded on the basis of these experiments that electrolytic methods were not adaptable to the reprocessing of graphite-base reactor fuels containing carbon-coated particles.

## Irradiation and Evaluation of Coated-Particle Fuels

*Oxide-Base Fuel.* A large amount of data is now becoming available on the irradiation performance of coated-particle fuels. Most of the results on static capsules were reviewed during the last quarter, and similar information is presented in Table I-14 for sweep-capsule experiments. This is a summary of data obtained by both Oak Ridge[48] and Battelle.[28]

Battelle pointed out that alumina coatings on $UO_2$ generally fail very rapidly at low temperatures,[28,37,38] the time for failure being perhaps less than 1 hr. The temperature below which rapid failure occurs seems to be about 500°C. Above this temperature and at tem-

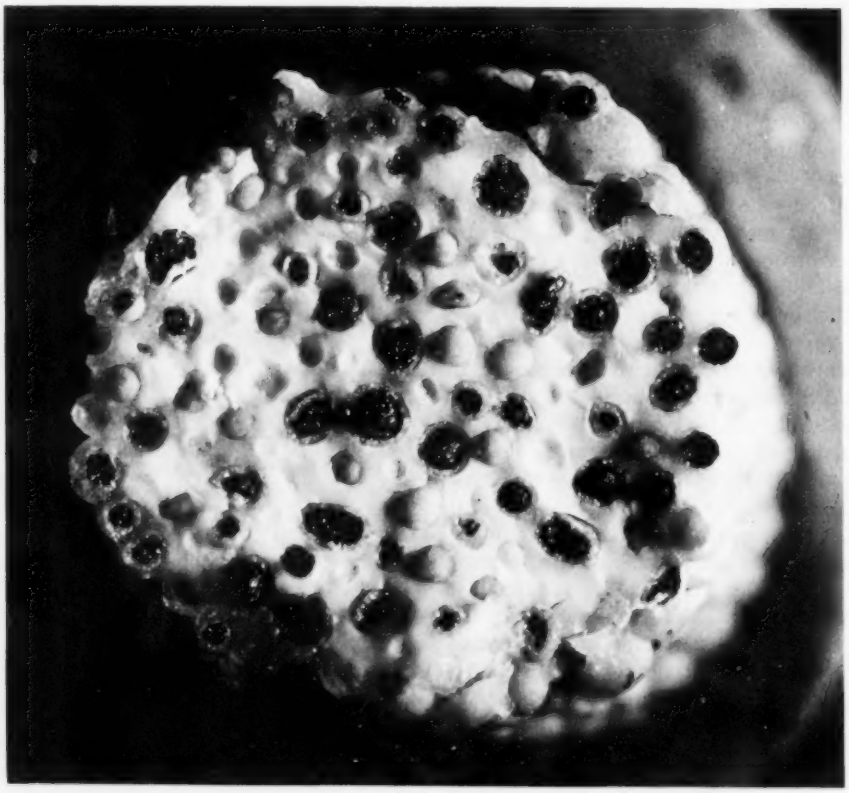

Fig. I-12 Fractured surface of $Al_2O_3$-matrix body prepared from pelletized fuel.[41]

peratures as high as about 1100°C, the oxide-coated fuel has good fission-product retentivity with $R/B$ values of about $10^{-6}$ at a burnup of about 1% uranium. Although the $R/B$ values for low-temperature irradiations are also frequently in this range, the mobility of the fission products is considerably reduced at the lower temperatures, and complete failure of the coating does not necessarily result in the release of significant amounts of fission gases in the sweep stream. However, if particles with cracked coatings were subsequently heated to elevated temperatures, presumably relatively large amounts of fission gas would be released unless the coatings resealed themselves. This resealing seems unlikely but not impossible. Matrix support is apparently not a major factor in the performance of the coated oxide-base fuel. No significant information is available as yet on the effect of coating thickness or fuel diameter.

In one experiment (capsule CIP-10) a fuel consisting of an inner layer of PyC under the $Al_2O_3$ coating was studied. Although the initial results seemed quite promising at temperatures of 1050°C ($R/B = 10^{-7}$), the coating began to break down, and the final values were rather disappointing ($R/B = 10^{-4}$). Another oxide fuel that was fairly extensively tested in capsule CIP-8 was a PyC coating deposited on $UO_2$ at a temperature of 1600°C. However, its behavior followed a pattern similar to that of the $Al_2O_3$ coating with the carbon inner layer.

*Carbide-Base Fuel.* The Oak Ridge data[28] shown in Table I-14 for the B9-8 capsule are especially interesting[48] because of the relatively low levels of fission-product release ($R/B = 10^{-5}$) at burnups of up to 20 at.% of the uranium and at temperatures in the range of 800 to 950°C. This capsule contains coated particles of the duplex type, supplied by National Carbon Company (NCC), and it has been under irradiation for 41 days at 820°C and an additional 15 days at 930°C. During the first six days of irradiation, the fission-gas-release rate was below the detectable amount. On the seventh day the release rate increased, and it reached an equilibrium level after a few days. This equilibrium rate, as given in Table I-14, remained essentially constant during the balance of the period at 820°C. The sudden bursts of activity that were characteristic of similar capsules containing both laminar and columnar types of particles were not observed during this period.

An additional burnup of 5.5% of the uranium was achieved in the 15 days at 930°C.

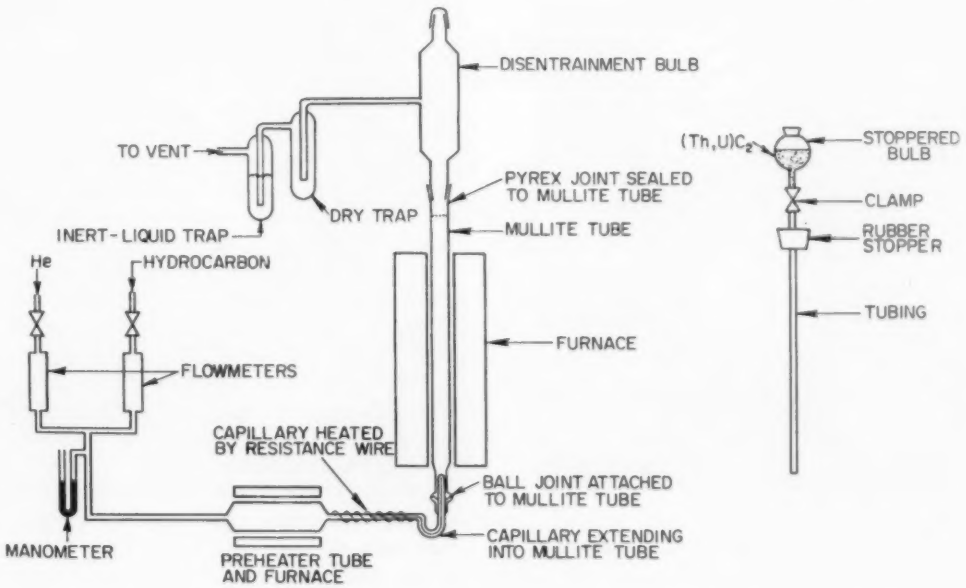


Fig. I-13 Fluidized-bed apparatus used by General Atomic for applying carbon coatings.[43]

During the first 10 days of this irradiation period, the average release of the krypton isotopes increased about 10%, $Xe^{135}$ increased 17%, and $Xe^{133}$ increased 20% above the average release rates at 820°C. After this period the bursts of activity began to appear and become more frequent, and the fission-gas-release rates increased by a factor of 4. In the case of $Xe^{133}$, the rate increased by a factor of 10 over the average for the first 10 days at 930°C. The bursts were attributed to the rupture of the coatings on individual particles.

Oak Ridge has also attempted to correlate the in-pile performance of carbon-coated carbide particles with measurable out-of-pile properties on the basis of static-capsule experiments.[52] The $R/B$ ratio for $Kr^{88}$ and the number of cracked coatings resulting from irradiation were plotted against several independent variables. Both of these indicators of in-pile performance showed a dependence on minimum particle crushing load and on the minimum thickness of the PyC coating (determined by microradiograph measurements). When $R/B$ was plotted against the average crushing load, the dependence was less apparent. This was interpreted to mean that the performance of a given lot of particles was more dependent on the properties of the weakest particles than on the load-carrying ability of an average particle. A similar interpretation was thought to apply to the correlation of performance with particle-coating thickness.

In spite of these relations, Oak Ridge indicated that it was possible that the performance of the particles was primarily dependent upon the structure of the coating.[52] Three of the lots tested represented the laminar, columnar, and duplex types of coatings and yielded $R/B$ values and percentages of cracked coatings that decreased in the same order. A fourth lot of particles, HTM-2, which also had the columnar coating structure, gave poorer performance than any of the other three lots. These particles had somewhat thinner coatings, however, which were therefore weaker, and it was suggested that this circumstance may have

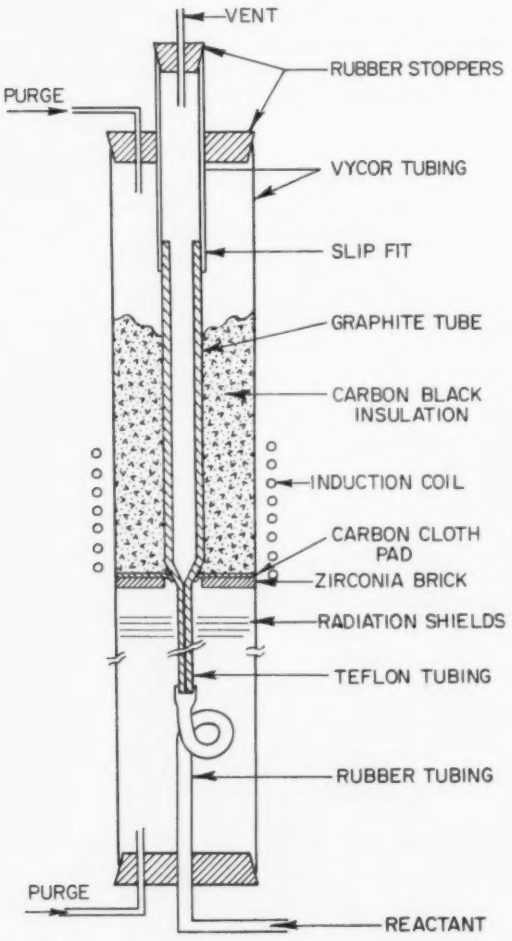


Fig. I-14 Induction-heated fluidized-bed apparatus used by Battelle for applying carbon coatings.[34]

Table I-13 NOMINAL PROPERTY DATA OF SPECIMENS FORMED FROM MATRIX-PELLETIZED FUELS[28]

| | Group PG-6 | Group PG-7 |
|---|---|---|
| Fuel loading: | | |
| $UO_2$, wt.% | 8.7 | 10.2 |
| Coated fuel, vol.% | 10.6 | 12.5 |
| Density, g/cm³: | | |
| Composite | 2.16 | 2.10 |
| Matrix (calculated) | 1.81 | 1.80 |
| Strength,* psi: | | |
| Tensile (WG)† | 2,500 | 2,250 |
| Crushing (AG) | 12,000 | 11,300 |
| $Xe^{133}$ release ratio,‡ ppm | 0.19–228 | 0.26–0.76 |

*Tensile strength was measured by diametral loading of 0.25-in.-diameter by 0.2-in.-long cylinders. Crushing strength was measured on 0.25-in.-diameter by 0.24-in.-long cylinders.

†WG and AG refer to orientations with the grain and against the grain, relative to the graphite orientations that would normally be produced in molding.

‡The ratio of xenon released to that present when specimens were heated to 1150°C for 1 hr following neutron activation.

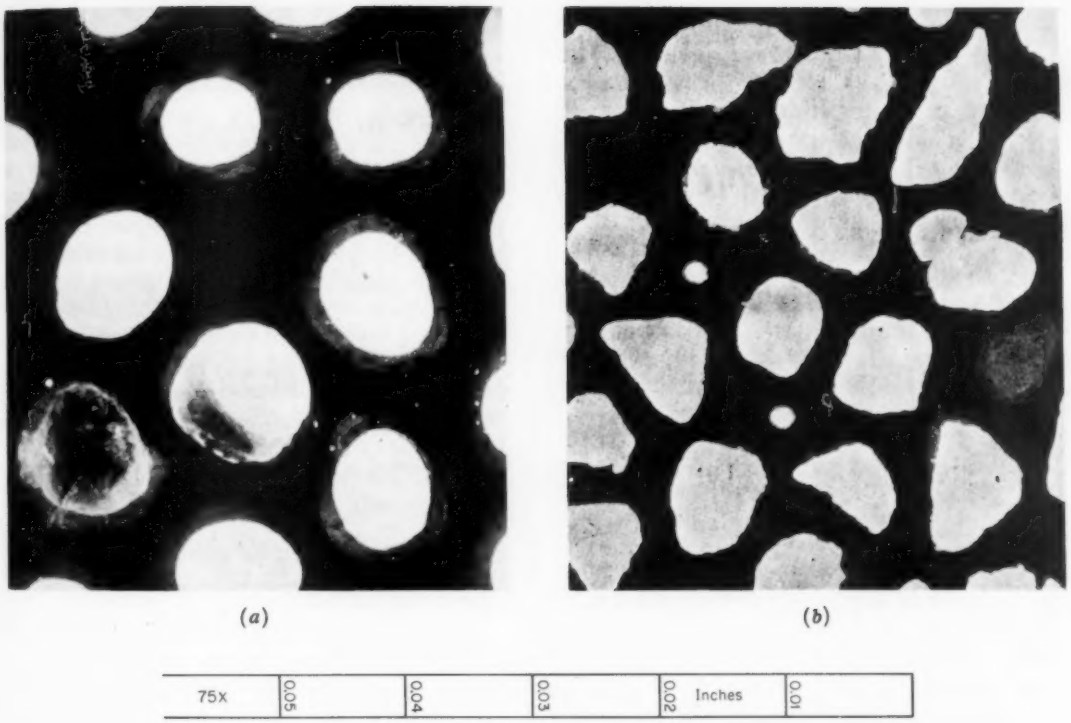


Fig. I-15 Microradiographs of carbon-coated carbide particles which show (*a*) surface contamination, (*b*) presence of unfueled particles, (*c*) presence of doubled particles, and (*d*) uranium diffusion.[50]

Table I-14 SUMMARY OF FISSION-GAS-RELEASE DATA FROM COATED-PARTICLE FUELS IN SWEEP-GAS EXPERIMENTS[28,48]

| Specimen | | | | Irradiation capsule | Nominal irradiation temp., °C | Estimated burnup (at.% U) | R/B | | |
|---|---|---|---|---|---|---|---|---|---|
| Lot | Fuel | Coating* | Matrix | | | | $Kr^{85m}$, $Kr^{87}$ and $Kr^{88}$† | $Xe^{135}$ | $Xe^{133}$ |
| BMI-4E | 127-μ $UO_2$ | 42-μ $Al_2O_3$ | Graphite | BMI-CFP-5 | 1070 | 0.1 | $4 \times 10^{-6}$ | $1 \times 10^{-6}$ | $5 \times 10^{-6}$ |
| | | | | | 1070 | 0.8 | $3 \times 10^{-6}$ | $4 \times 10^{-6}$ | $2 \times 10^{-6}$ |
| BMI-715A | 127-μ $UO_2$ | 42-μ $Al_2O_3$ | None | BMI-CFP-7 | 100 | 0.0 | | $3 \times 10^{-4}$ | $2 \times 10^{-4}$ |
| | | | | | 100 | 1.5 | $4 \times 10^{-5}$ | $4 \times 10^{-5}$ | $2 \times 10^{-4}$ |
| | | | | | 100 | 2.7 | $3 \times 10^{-5}$ | $3 \times 10^{-5}$ | $8 \times 10^{-5}$ |
| BMI-715A | 127-μ $UO_2$ | 42-μ $Al_2O_3$ | None | BMI-CFP-9 | 815 | 0.1 | $4 \times 10^{-9}$ | $4 \times 10^{-9}$ | $4 \times 10^{-9}$ |
| | | | | | 645 | 0.3 | $4 \times 10^{-9}$ | $4 \times 10^{-9}$ | $4 \times 10^{-9}$ |
| | | | | | 470 | 0.5 | $3 \times 10^{-6}$ | $2 \times 10^{-6}$ | $1 \times 10^{-4}$ |
| | | | | | 295 | 1.3 | $3 \times 10^{-5}$ | $1 \times 10^{-4}$ | $3 \times 10^{-4}$ |
| | | | | | 815 | 1.9 | $4 \times 10^{-5}$ | $6 \times 10^{-5}$ | $3 \times 10^{-4}$ |
| BMI-715A-HT | 127-μ $UO_2$ | 42-μ $Al_2O_3$ | None | BMI-CFP-11 | 100 | 0.0 | | | $1 \times 10^{-4}$ |
| BMI-725D | 127-μ $UO_2$ | 56-μ $Al_2O_3$ | Graphite | BMI-CFP-6 | 1070 | 0.1 | $8 \times 10^{-8}$ | $6 \times 10^{-9}$ | $5 \times 10^{-9}$ |
| | | | | | 1070 – 440 | 0.6 | $3 \times 10^{-6}$ | $2 \times 10^{-7}$ | $1 \times 10^{-6}$ |
| | | | | | 750 | 3.4 | $5 \times 10^{-7}$ | $1 \times 10^{-6}$ | $3 \times 10^{-6}$ |
| BMI-736B | 127-μ $UO_2$ | 14-μ PyC | Graphite | BMI-CFP-10 | 1050 | 0.1 | $3 \times 10^{-8}$ | $2 \times 10^{-8}$ | $6 \times 10^{-8}$ |
| | | 29-μ $Al_2O_3$ | | | 800 | 1.3 | $8 \times 10^{-6}$ | $2 \times 10^{-5}$ | $4 \times 10^{-4}$ |
| BMI-1010A | 127-μ $UO_2$ | 66-μ laminar PyC | Graphite | BMI-CFP-8 | 1050 | 0.1 | $3 \times 10^{-8}$ | $4 \times 10^{-8}$ | $5 \times 10^{-8}$ |
| | | | | | 1050 | 1.1 | $2 \times 10^{-5}$ | $1 \times 10^{-5}$ | $4 \times 10^{-5}$ |
| | | | | | 850 | 4.4 | $3 \times 10^{-5}$ | $5 \times 10^{-5}$ | $3 \times 10^{-4}$ |
| 3M-101-U | 200-μ $UC_2$ | None | None | ORNL-Cl-8 | 820 | 4.3 | $1 \times 10^{-2}$‡ | $7 \times 10^{-2}$‡ | $1 \times 10^{-2}$‡ |
| 3M-SP-2 | 200-μ $UC_2$ | 90-μ laminar PyC | None | ORNL-Cl-7 | 820 | 15 | $3 \times 10^{-4}$‡ | $5 \times 10^{-4}$‡ | $2 \times 10^{-4}$‡ |
| HTM-1 | 200-μ $UC_2$ | 80-μ columnar PyC | None | ORNL-B9-7 | 820 | 8 | $4 \times 10^{-5}$‡ | $3 \times 10^{-4}$‡ | $6 \times 10^{-5}$‡ |
| NCC-AD | 200-μ $UC_2$ | 20-μ laminar PyC | None | ORNL-B9-8 | 820 | 14 | $1 \times 10^{-5}$‡ | $3 \times 10^{-5}$‡ | $1 \times 10^{-5}$‡ |
| | | 80-μ columnar PyC | | | 930 | 20 | $3 \times 10^{-5}$‡ | $3 \times 10^{-4}$‡ | $4 \times 10^{-5}$‡ |
| BMI-918A | 200-μ $UC_2$ | 55-μ columnar PyC | Graphite | BMI-CFP-2R | 1070 | 0.2 | $1 \times 10^{-8}$ | $2 \times 10^{-8}$ | $3 \times 10^{-8}$ |
| | | | | | 1070 | 2.5 | $2 \times 10^{-4}$ | $1 \times 10^{-4}$ | $3 \times 10^{-3}$ |
| | | | | | 1070 | 0.7 | $5 \times 10^{-3}$ | $5 \times 10^{-4}$ | $5 \times 10^{-3}$ |
| BMI-918A | 200-μ $UC_2$ | 55-μ columnar PyC | None | BMI-CFP-9 | 815 | 0.1 | $3 \times 10^{-9}$ | $3 \times 10^{-9}$ | $3 \times 10^{-9}$ |
| | | | | | 645 | 0.8 | $9 \times 10^{-5}$ | $6 \times 10^{-5}$ | $4 \times 10^{-4}$ |

*Coatings are listed in order of preparation in the case of multiple coatings.
†Data are an average of the release fraction of the three krypton isotopes.
‡Average values for the irradiation period at the temperatures listed.

masked the dependence on the structure of the coating. Only a marginal relation was found when the results of neutron-activation testing ($Xe^{133}$ release) were plotted against particle-surface area contamination ($\alpha$ count). All other attempts to correlate performance with a particular property failed to show any relation.

Microradiographic techniques were also used by Oak Ridge for examination of 3M particles after irradiation.[53] It was found that fuel migration through 30 to 50% of the PyC coatings was most pronounced in particles that otherwise appeared to be sound. The migrating fuel assumed a ringlike concentration gradient around the original fuel particle. A microradiograph of a sample of the unirradiated fuel showed only superficial fuel migration into the coating.

(J. H. Oxley)

# Refractory Fuel and Fertile Materials

## Properties and Behavior of Uranium Oxide Fuels

Measurements of the specific volume of $UO_2$ just below and above the melting point were performed at Hanford.[54] The results of these measurements,[55] along with earlier specific-volume data from Stanford[56] covering the temperature range from 1200 to about 2800°K, are summarized in Fig. I-16. The volume change during melting was 9.6%. The densities of the solid and liquid phases at the melting point (2790°C) were 9.67 and 8.50 g/cm$^3$, respectively. At 3100°C the density of the liquid was 8.50 g/cm$^3$.

At Oak Ridge the radial-heat-flow method[29] was used to measure thermal conductivity at temperatures ranging from 27 to 875°C. The material was $UO_2$, pressed and sintered to 93.4% of theoretical density. The results, along with the British[57] results obtained by the same method, are shown in Fig. I-17. The results from the first heating with a specimen can be represented within ±1% by $K = \rho/[6.5647 + 0.02033T]$, where $\rho$ is the ratio of the measured bulk density to the theoretical density, $K$ is the thermal conductivity in watts/(cm)(°C), and $T$ is the temperature in °K. Measurements at 600°C after the specimen was cooled from 875°C were the same as those from the first heating. The value of $K$ found at 223°C, however, was 5.4% higher than the value determined initially. It is thought that these changes were caused by a slight loss of oxygen from the specimen which occurred during the course of the experiment. The oxygen-to-uranium ratio dropped from 2.012 to 2.006. Above 600°C, the thermal-conductivity values for a second heating on the same specimen were within 1% of those obtained on the first heating. The second-heating results followed the equation $K = \rho/[5.1295 + 0.02157T]$ to within 1%. The variation in the thermal conductivity with oxygen-to-uranium ratio appears to be less sensitive at temperatures above 600°C. Possibly the discrepancies between the thermal conductivities reported for $UO_2$ in the literature can be ascribed to oxygen-concentration differences. Thermal-conductivity measurements were conducted in Italy[58] for Euratom on swaged $UO_2$ with densities of 78, 85, and 90% of theoretical. The thermal conductivities of the 90% dense swaged $UO_2$ were approximately 30% lower at 150°C than for sintered pellets of the same density. With increasing temperature, the thermal conductivity of the swaged $UO_2$ diminished at a slower rate than that of the sintered material. At 500°C, the swaged material had a 20% higher thermal conductivity.

Rothwell[59] has detected the formation of elemental uranium in $UO_2$ heated at temperatures in excess of 1800°C. The uranium is observed as small inclusions dispersed throughout the $UO_2$. Above 1800°C, $UO_2$ exposed to an atmosphere containing a very low partial pressure of oxygen is assumed to lose oxygen to give a substoichiometric phase $UO_{2-y}$, with the value of $y$ increasing with increasing temperature. Similar observations have also been made by Colombo and Frigerio.[60]

A phase diagram recently reported by Bettis[61] for the $UO_2$-$ZrO_2$ system is presented in Fig. I-18. In the temperature range from 2300 to 2550°C, a continuous face-centered cubic solid solution exists from pure $UO_2$ to pure $ZrO_2$. This confirms the third (cubic) polymorphic form of pure $ZrO_2$ in addition to the tetragonal and monoclinic phases that are stable at successively lower temperatures. A high-temperature two-phase region, previously unreported, exists in the $ZrO_2$-rich region above 1600°C. The single-phase compositions quenched from high temperatures, which result in cubic or

tetragonal structures without an intervening two-phase region, are explained by a diffusionless transformation that occurs when cooling compositions of 55 mole % or less.

General Electric[62] has reported that the addition of $Cr_2O_3$ to $UO_2$ prevents the deleterious reaction between $UO_2$ and aluminum in an iron-chromium-aluminum-yttrium alloy which shows considerable promise as a cladding material because of its resistance to high-temperature oxidation. The $Cr_2O_3$-$UO_2$-$O_2$ system has been investigated.[63] Between 1200 and 1600°C, three phases were identified: (1) $Cr_2O_3$, (2) $U_3O_8$, and (3) a mixed-oxide phase that had orthorhombic symmetry and the lattice constants $a_0 = 4.868$ A, $b_0 = 5.048$ A, and $c_0 = 11.785$ A. The $CrUO_4$ phase was observed to volatilize at elevated temperatures, probably dissociating into $UO_3$ and $CrO_3$.

The creep-in-bend characteristics of $Y_2O_3$-$UO_2$ solid solutions containing 0.5 and 1 wt.% $Y_2O_3$ have been studied[64] in both the fully reduced and the oxidized conditions at 940°C under a maximum fiber stress of 5000 psi. The fully reduced material did not deform plastically; however, $Y_2O_3$ additions to $UO_{2.18-2.20}$ reduced its plasticity. Hill[65] investigated the volatility behavior of $UO_2$-$La_2O_3$ solid solutions heated at 1675°C for periods varying from 25 to 310 hr. Specimens with more than 60 mole % $LaO_{1.5}$ showed very slight weight losses.

Uranium dioxide and bivalent metal oxides were reacted at Battelle[66] under a pressure of 60,000 atm at temperatures ranging from 900 to 1200°C. A $CaU_3O_9$ compound with $Cu_3Au$ type ordering of uranium and calcium ions was produced. This is the first time that this type of ordering has been reported in a mixed-oxide system. Solid solutions of MgO and ZnO in the $UO_2$ fluorite structure with lattice parameters as low as $a_0 = 5.24$ A were observed in samples reacted at high pressure. $MgUO_4$ and $ZnUO_4$ were also synthesized at high pressure. Some solubility of MgO in $UO_2$ was noted at

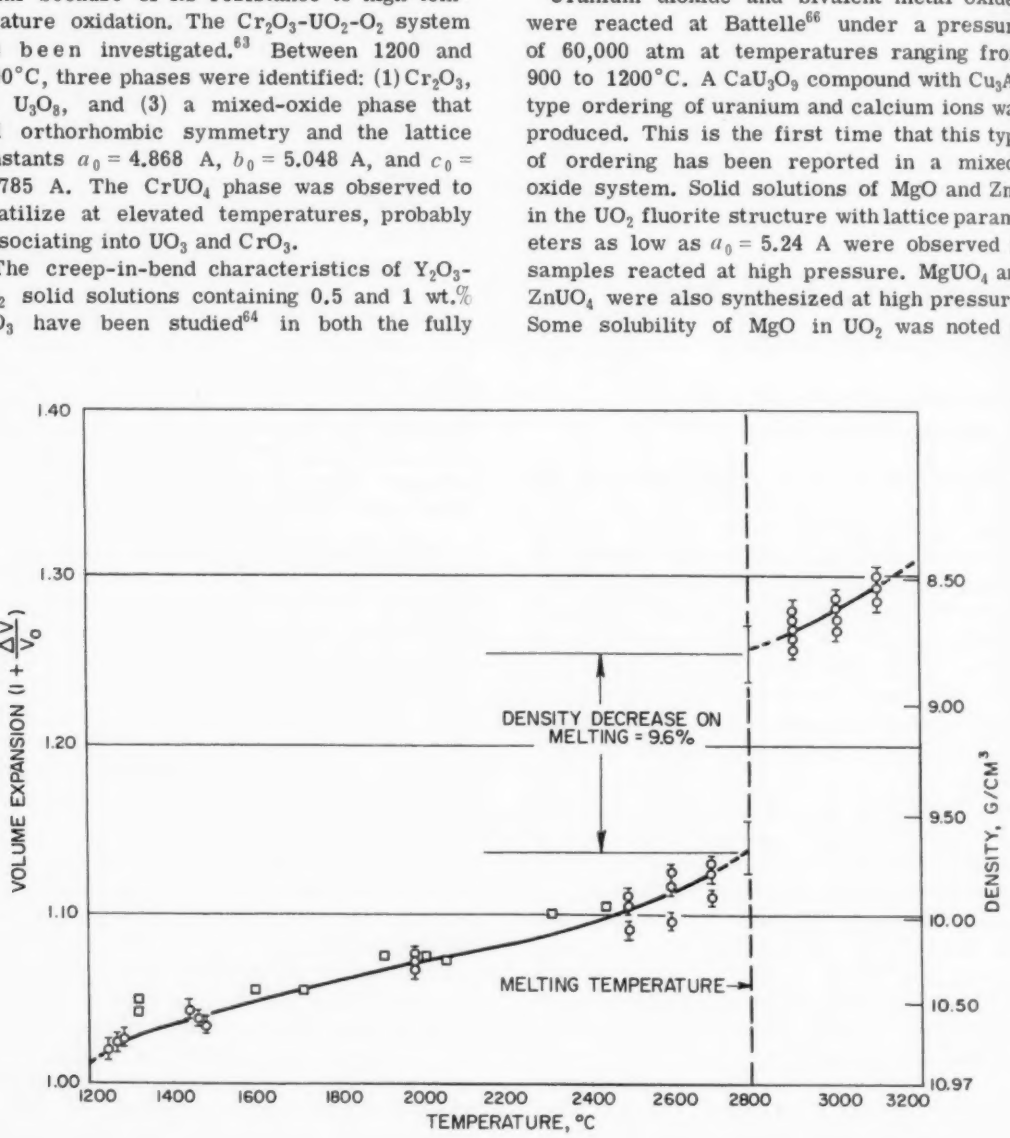


Fig. I-16 Thermal expansion of uranium dioxide. ○, Hanford data,[55] single crystals; □, Stanford data,[56] large-grained compacts.

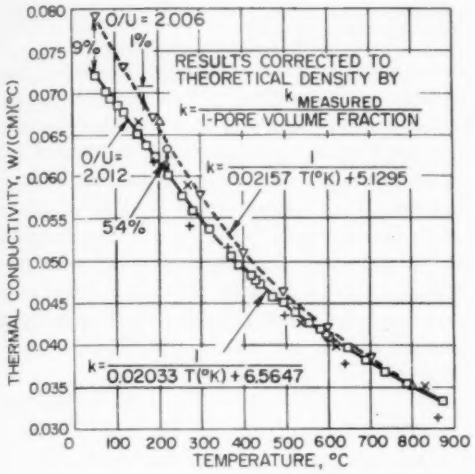


Fig. I-17 The effect of temperature and stoichiometry on the thermal conductivity of $UO_{2+x}$ pressed and sintered to 93.4% of theoretical density.[29] Godfrey and McElroy data:[29] □, first heating; ○, first cooling; ▽, second heating; △, second cooling. Howard and Gulvin data:[67] ×, specimen 3; +, specimen 4.

atmospheric pressure. The solubility of ZnO in $UO_2$ with the formation $ZnUO_4$ occurred only at high pressure. No reaction between $UO_2$ and NiO was observed at atmospheric pressure. Also, no solid solutions of NiO in $UO_2$ were observed at high pressure; however, $NiUO_4$ formed at high pressure.

Tests at Chalk River[67] showed that rapid failures of defected Zircaloy-clad $UO_2$ fuel elements can be caused by about 500 ppm fluoride impurity in the $UO_2$.

Investigators at Argonne[68] have studied the kinetics of the reduction of $UO_2$, $UO_{2.2}$, $UO_{2.4}$, and $U_3O_8$ by hydrogen and CO under static conditions at pressures of about 1 mm Hg. Over the temperature range from 590 to 950°C, reduction by both gases was controlled by a surface process that followed the rate expression

$$\frac{dP}{dt} = -P_n K_0 \exp(-E/RT)$$

The exponent $n$ was unity for hydrogen and two-thirds for CO. $E$, the activation energy, was independent of the reducing gas. $E$ did depend, however, on the structure of the oxide. For $U_3O_8$, $E$ was about 25 kcal/gram mole. For the three other compositions, $E$ was about 10 kcal/gram mole.

Solid-fission-product diffusion in $UO_2$ is being investigated at Oak Ridge.[29] Penetration curves for the diffusion of $Nb^{97}$ in sintered polycrystalline and single-crystal $UO_2$ are presented in Fig. I-19. The characteristics of the penetration curve for the sintered $UO_2$, which had a density of 97% of theoretical, typify the results obtained with sintered material over the temperature range from 1400 to 1950°C. This curve seems to indicate that diffusion did not occur entirely in lattice diffusion. After the results for the nonvolume-diffusion contribution were corrected, a diffusion coefficient of $3.4 \times 10^{-11}$ $cm^2/sec$ was calculated for $Nb^{97}$ diffusion in $UO_2$ at 1445°C. For the single-crystal $UO_2$, the penetration curve shown in Fig. I-19 is linear for depths greater than

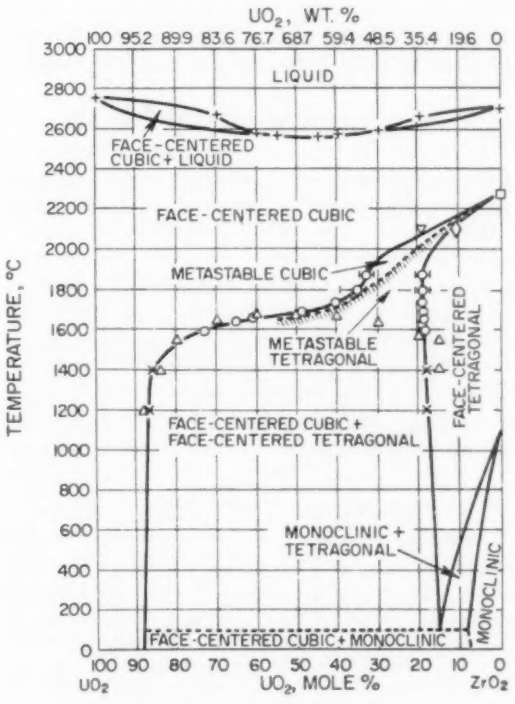


Fig. I-18 $UO_2$-$ZrO_2$ phase diagram.[61] ○, data points derived from metallography. ×, data points derived from X-ray diffraction. +, liquidus points of Wisnyi, KAPL. △, data points of Voronov. □, $ZrO_2$ face-centered cubic to face-centered tetragonal transformation. ▽, transformed cubic. ◇, untransformed tetragonal.

5 $\mu$. The high concentration next to the surface is attributed to the slow rate of cation interchange between $Nb_2O_3$ and $UO_2$. The diffusion coefficient determined for the single-crystal material at 1505°C is $1.46 \times 10^{-10}$ cm²/sec. For comparison, the diffusion coefficient for the self-diffusion of $U^{235}$ in $UO_2$ at 1505°C is $6.5 \times 10^{-15}$ cm²/sec (Ref. 69), and for $Xe^{133}$ in $UO_2$ is $5 \times 10^{-14}$ cm²/sec (Ref. 70). These diffusion coefficients indicate that a sizable difference would be expected between the release rates of different fission products from ceramic fuels. Schmitz and Lindner[71] have measured the diffusion of $Y^{91}$, $Pm^{147}$, and $Zr^{95}$ in sintered $UO_2$ at temperatures from 1120 to 1450°C. The results, which are summarized in Tables I-15 and I-16, indicate that the diffusion coefficients and activation energies are comparable with values observed for the fission gases. The activation energies were found to increase with ion radius and ion charge. Lindner and Schmitz[72] also measured $U^{233}$ self-diffusion in $UO_2$. Over the temperature range 1300 to 1600°C, diffusion followed the relation

$$D = 0.23 \exp(-104.6 \text{ kcal}/RT) \text{ cm}^2/\text{sec}$$

for measurements conducted under helium. Other measurements using argon resulted in an activation energy of only 52 kcal/gram mole from 900 to 1200°C.

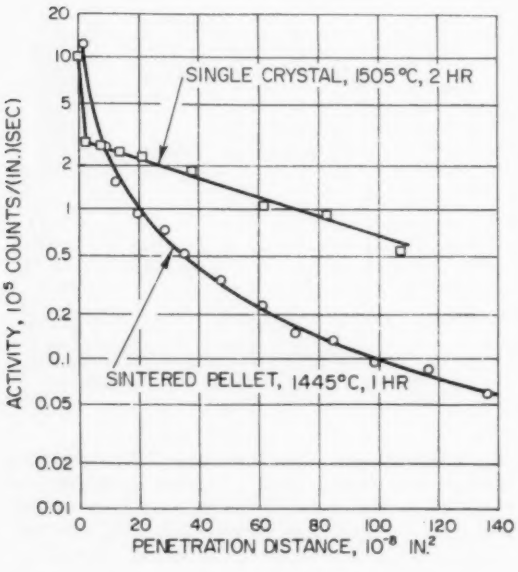


Fig. I-19 Diffusion of $Nb^{97}$ in $UO_2$ (Ref. 29).

Work with irradiated $UO_2$ at Hanford[73] has revealed an extensive relocation of fission fragments from the point at which their kinetic energy of fission is completely dissipated and a relocation of plutonium from its site of formation. This phenomenon is characterized by a depletion of $Zr^{95}$-$Nb^{95}$, $Cs^{137}$, $Ru^{106}$, $Ce^{144}$, and plutonium in the high-density, large columnar grains. It is thought this is a result of a vapor-phase process, which forms the large columnar grains and transports vaporized impurities toward the center of the fuel.

(R. H. Barnes)

## Properties of Uranium Carbides and Nitrides and of Thorium Compounds

Marnoch of Atomics International[74] has made photomicrographs of a series of uranium-carbon alloys containing from 4.2 to over 6.1 wt.% carbon to assist in analysis of alloys in this system. With the aid of these photographs and the accompanying descriptions, it should be possible to obtain accurate analyses by microstructural inspection of uranium-carbon alloys, particularly those near UC.

Henney and Hill of Harwell report[75] that $U_2C_3$ is stable in the presence of carbon up to 1600°C and at oxygen impurity levels of 100 to 200 ppm. This temperature is more than 100°C higher than the stability limit found at other laboratories. Data obtained by Henney and Hill suggest that at least 7000 ppm oxygen are soluble in tetragonal $UC_2$ and that this phase is stabilized by the presence of oxygen. It is stated that $U_2C_3$ will form from $UC_2$ only at lattice parameters corresponding to oxygen contents less than 2000 ppm.

Compatibility studies at Atomics International[76] have produced the following results: After 380 hr at 2000°F, two samples of hypostoichiometric UC formed a liquid in contact with stainless steel. After 1000 hr at 1600°F, a 0.5-mil layer of ZrC was found between a uranium–5.2 wt.% carbon alloy and a high-strength zirconium alloy (zirconium–1¼ wt.% aluminum–1 wt.% tin–1 wt.% molybdenum). After 400 hr at 1600°F, a 0.15-mil layer of $Nb_2C$ or NbO was found between uranium–5.2 wt.% carbon alloy and niobium–1 wt.% zirconium alloy.

The properties of ThC and $ThC_2$ are presented in considerable detail[77] by Kempter and Krikorian of Los Alamos. The diamond pyramid hardness (DPH) of the ThC is 850, the resistivity is 25 $\mu$ohm-cm, and the lattice parameter is 5.346 A. The DPH of $ThC_2$ is 600, the resistivity is 30 $\mu$ohm-cm, and the lattice parameters are $a = 10.555$ A, $b = 8.233$ A, and $c = 4.201$ A.

The electronic work function of uranium carbide of undetermined composition was measured by Hopkins.[78] By use of a tungsten reference electrode, a work function of 3.97 ev was obtained for uranium carbide deposited on tantalum carbide.

The linear-thermal-expansion coefficients of various samples of uranium-carbon alloys prepared by several techniques have been determined by Kalish and Crane of United Nuclear Corporation.[79] For the temperature range 20 to 1000°C, typical values obtained on cast samples are 11.0 $\mu$in./(in.)(°C) for uranium–4.7 wt.% carbon alloy and 11.5 $\mu$in./(in.)(°C) for uranium–5.3 wt.% carbon alloy.

Included in a paper[80] by Ivanov and Alekseyeva, which also contains constitutional data originally reported at the 1958 Geneva conference, is a statement that hardness in the UC-ZrC system increases from 850 kg/mm$^2$ at UC to 2130 kg/mm$^2$ at UC–90 mole % ZrC and then decreases to 1920 kg/mm$^2$ at ZrC.

Atomics International[76] has irradiated a sample of uranium–4.8 to 5.0 wt.% carbon alloy in a nickel cladding to a burnup of 16,600 Mwd/ton. At a peak surface temperature of 1220°F and a peak central temperature of 2050°F, the sample released 0.18% of its fission gas, and it showed a maximum diameter increase of 5%.

Lambert and Bradbury of Harwell[75] have irradiated two arc-melted samples of UC–10 wt.% PuC in stainless-steel claddings to burnups of about 19,000 and 22,800 Mwd/ton. At central core temperatures of 600 and 700°C, the samples released 0.026 and 0.001% of their xenon, respectively. The authors gave no explanation for this large difference nor for the lower release at 700°C. No dimensional changes were detected.

Oak Ridge[50] has completed the analysis of six samples of UC that failed during irradiation at central core temperatures ranging from 2000 to 2260°F. These tantalum-clad samples sustained burnups ranging from 0.15 to 0.62 at.% of the uranium, and they released from 5 to 30% of their $Kr^{85}$. Metallographic sections disclosed that a severe reaction had occurred between the UC and the tantalum. Uranium metal was found in the UC and on the inner surface of the thermocouple cavity. Uranium metal and $Ta_2C$, as well as tantalum metal and UC, were identified in the samples by X-ray techniques.

Strasser and Taylor[21] have irradiated 94%-dense uranium carbide pellets in stainless-steel or niobium claddings to burnups of 18,500 Mwd/metric ton. At an average central core temperature of 760°C, a diameter increase

Table I-15 DIFFUSION COEFFICIENTS[71] FOR FISSION-PRODUCT DIFFUSION IN $UO_2$

| $Y^{91}$ | | $Pm^{147}$ | | $Zr^{95}$ | |
|---|---|---|---|---|---|
| Temp., °C | Diffusion coefficient, cm$^2$/sec | Temp., °C | Diffusion coefficient, cm$^2$/sec | Temp., °C | Diffusion coefficient, cm$^2$/sec |
| 1150 | $4.7 \times 10^{-15}$ | 1120 | $3.6 \times 10^{-15}$ | 1120 | $3.1 \times 10^{-15}$ |
| 1200 | $1.03 \times 10^{-14}$ | 1200 | $8.9 \times 10^{-15}$ | 1200 | $1.07 \times 10^{-14}$ |
| 1315 | $2.49 \times 10^{-14}$ | 1298 | $3.94 \times 10^{-14}$ | 1305 | $3.42 \times 10^{-14}$ |
| 1420 | $8.15 \times 10^{-14}$ | 1419 | $1.22 \times 10^{-13}$ | 1410 | $1.32 \times 10^{-13}$ |
| 1450 | $7.74 \times 10^{-14}$ | | | | |

Table I-16 ACTIVATION ENERGIES[71] FOR FISSION-PRODUCT DIFFUSION IN $UO_2$

| Ion | Ionic radius, A | $D_0$, cm$^2$/sec | Activation energy, kcal/gram mole |
|---|---|---|---|
| $Y^{+3}$ | 0.88 | $6.8 \times 10^{-3}$ | 46.4 ± 2.3 |
| $Pm^{+3}$ | 0.98 | $3.5 \times 10^{-4}$ | 56.8 ± 1.8 |
| $Zr^{+4}$ | 0.77 | $1.6 \times 10^{-4}$ | 59.2 ± 1.2 |
| $U^{+4}$ | 0.93 | 0.23 | 104.6 ± 7.0 |

corresponding to a 1.4% volume increase was detected, and 0.4% of the fission gas generated was collected from one sample. The stainless-steel claddings showed a slight increase in carbon content. No reaction was observed between the niobium and the UC.

A series of studies[81a,81b,82] of the effects of radiation damage upon the physical properties of UC and UN and of the recovery of these properties in thermal annealing has been performed. These studies are consistent only in that all find that damage is recovered in two stages: (1) between 100 and 200°C and (2) between 500 and 700°C.

Accary and Marchal[83] have performed studies on the grain growth of powder compacts of UN (similar to their previous studies of grain growth in UC) by heat-treating the compacts for various lengths of time at temperatures from 1200 to 2200°C. They indicate that grain growth in powder compacts of UN occurs in three stages having activation energies of 26, 30, and 35 kcal/mole.

The effect of molybdenum fibers upon the physical, mechanical, and chemical properties of thoria has been the subject of an investigation by Baskin and Handwerk.[84] Thoria reinforced with 5 to 20 wt.% molybdenum fiber shows improved thermal-shock resistance, higher thermal conductivity, and superior resistance to damage by irradiation. Compressive strength, modulus of rupture, and Young's modulus are substantially reduced by additions of molybdenum to thoria. The oxidation resistance of the cermets is directly related to their density; but regardless of density the cermets are severely attacked in air at temperatures above 1000°C. (W. Chubb)

## Fabrication of Uranium Carbide and Nitride Fuels

There is a continuing trend on the part of many investigators to sinter refractory uranium compounds in the presence of a liquid phase, inasmuch as there are practical limitations to the solid-state sintering of these compounds into fully dense products. It is to be expected that both the characterization of the products and the understanding of the mechanisms involved in such multiphase processes will be much more difficult than in the inherently simpler single-phase processes. It goes without saying that to be useful a liquid-phase sintering agent must not only perform its function of speeding the sintering process at relatively low fabrication temperatures but must also be either completely removed or combined in such a manner that the high-temperature properties of the fuel are not impaired.

Researchers at Carborundum have recently reported[85] the results of microprobe analyses on two UC specimens to which 0.1 wt.% nickel had been added as a sintering aid. In a specimen sintered for 4 hr at 1525°C, all the nickel was found in solid solution with the UC. A second phase, apparently promoted by the nickel, was tentatively identified as $U_2C_3$. In a specimen that was annealed in a vacuum for 1 hr at 1850°C, about half of the nickel was still found homogeneously in solution with the UC. Two other phases, a "light" phase and a gray phase, were tentatively identified as $UO_2$ (or $UC_2$) and $U_3O_8$, respectively; no nickel was present in the solution in either phase. Concentrations in excess of 40 to 50 wt.% nickel were detected at the interfaces of the white, gray, and matrix phases. These researchers indicate that these nickel-enriched areas were smaller than the size of the electron beam (1 to 2 $\mu$) and point out the possibility that there may even be more nickel than was actually detected.

On the basis of the above observations, the Carborundum workers conclude that annealing in vacuum at 1850°C promotes diffusion of nickel to grain boundaries, with probable subsequent evaporation. They find no evidence to indicate that low-melting nickel alloys or compounds are formed which would be detrimental to the performance of the material as a high-temperature fuel.

It may be possible, however, that, because of the very small amount of nickel (0.1 wt.%) added initially, the 40 to 50 wt.% nickel phase that appeared in the annealed specimen could escape detection as the "$UNi_3$" intermetallic compound that, as pointed out in the August 1962 issue of *Reactor Materials*, was observed on the UC-nickel tie line by University of Sheffield workers. It was also mentioned in the same review that Union Carbide observed a phase developing with a particular crystallographic habit in a UC specimen to which considerably more nickel (0.5 wt.%) had been added. The 40 to 50 wt.% nickel composition does correspond to complex compounds that

have been reported intermediate between $UNi_2$ and $UNi_5$ in the uranium-nickel system.[86]

Further developments with this liquid-phase sintering technique will be watched with great interest. (E. O. Speidel)

# Basic Studies of Irradiation Effects on Fuel Materials

## Metallic Fuels

In a continuing investigation of uranium-molybdenum alloys, the transformation kinetics of the gamma phase are being reexamined by Atomics International.[76] In uranium–16 wt.% molybdenum a metastable alpha-uranium phase appears during the gamma-gamma′ transformation. The amount of alpha increases with decreasing transformation temperature. On the basis of recent irradiation results, gamma-phase reversion is postulated to occur in alloys containing 1 to 4 wt.% molybdenum.

A brief theoretical study[76] has failed to provide a mechanism that could account for the continuous nature of fission-fragment tracks.

Rogers and Adam[87] have measured, over a considerable range of neutron doses, the number of atoms ejected from the surface of uranium metal by fission fragments leaving its surface. The results indicate that the rate at which uranium is returned, by ejection from the collector, to the parent uranium surface becomes equal to the rate of evaporation from that surface when the collected layer is about 0.0001 as thick as the range of fission fragments in uranium. Both the present and previously published experiments, when interpreted on this basis, indicate that the number of atoms ejected per escaping fission fragment is of the order of 2000. The exact nature of the surface in all the experiments reviewed did not appear to cause a significant change in this number. This interpretation is believed to be quite different from that given in previously published work.

The effect of deliberate additions of atoms widely different in size from uranium atoms on subsequent xenon release during irradiation is being studied at Atomics International.[88] These experiments are designed to test the hypothesis that such additions will reduce swelling in uranium by trapping fission-gas atoms. Beryllium additions had no effect on release at 630°C, but cerium and vanadium additions almost eliminated gas release. Yttrium additions gave uncertain results.

A theory of the swelling of fissile material has been developed by Agranovich and Mikhlin[89] on the basis of a simplified model, and special consideration is given to the processes occurring before swelling. The pores are assumed to be evenly distributed, spherical, and of equal radius, and should begin to grow only when the elastic limit is reached as a consequence of fission-fragment (gas) diffusion. This moment is considered as the beginning of swelling.

Argonne[1] has correlated swelling and bubble formation in pure uranium with phase transformations. Swelling is greatest in gamma and least in beta. Pits, approximately 100 A in diameter, were visible before irradiation. After irradiation, cathodic etching produced shallow depressions, about 600 A in diameter, surrounding the original pits. This suggests that fission gas is attracted to dislocations. The presence of grain boundaries greatly facilitates the growth of bubbles, which indicates that vacancy migration to areas of high gas concentration occurs, and bubbles precipitate to relieve lattice strain.

The strain tensor has been employed by Morris[90] to describe dimensional change of an alpha-uranium single crystal after irradiation. It is pointed out that the ratio of the length in an arbitrary direction before and after irradiation depends on crystal shape. This dependence has been solved for a spherical crystal.

## Irradiation Effects in Ceramic Fuels

Hanford[91] has measured the physical properties of irradiated $UO_2$ as a function of exposure. Some of the properties measured were thermal conductivity, fission-product segregation, and melting point. The most important effect on these properties was correlated with columnar grain growth above 1800°C. Harwell[19] has found the lattice parameter of a set of isostructural uranium compounds to vary as

$$a_\phi = a_0 \left[1 - \exp\left(-\alpha\,\phi\right)\right]$$

where $a_\phi$ is the lattice parameter after a thermal-neutron dose $\phi$. From the experimental evaluation of alpha, approximately $4\times$

$10^5$ atoms are affected per fission (somewhat lower than previous values).

Rothwell[92] has found that the release of $Kr^{85}$ from uranium dioxide is more rapid at annealing temperatures of 1800°C or above than extrapolations of lower temperature data would indicate. The release occurs in three stages: (1) an initial burst, (2) steady-state release, and (3) a cooling burst starting at about 1450°C. Factors important in determining the high release are substoichiometry of the oxide at high temperature and segregation of gas bubbles to grain boundaries. Chalk River[12] has shown that irradiation exposures in excess of $10^{15}$ fissions/cm$^3$ resulted in a reduced fractional release of fission xenon from $UO_2$ during postirradiation annealing at 1400°C. The lower releases are consistent with an immobilization of xenon on irradiation-induced traps rather than with a change in the diffusion coefficient.

In-pile release rates of xenon and krypton isotopes from a fuel element are given as a function of half-life by General Atomic.[45] An equation for the calculation of the effective permeability (square centimeters per second) of an isotope penetrating a fuel-element sleeve is given as a function of the experimental-system parameters.

The diffusivity of $Kr^{85}$ in $ThO_2$ was reported by Matzke[93] from postirradiation annealing of powders as

$$D_0 = 9.6 \pm 0.2 \text{ cm}^2/\text{sec}; Q = 32.2 \pm 0.8 \text{ kcal/mole}$$

These values are in substantial agreement with previous work on $Xe^{133}$ in $ThO_2$ by the same authors. (F. R. Winslow and F. A. Rough)

## References


1. Argonne National Laboratory, Metallurgy Division Annual Report for 1961, USAEC Report ANL-6516, 1961.
2. W. R. McDonell, Kinetics of Structural Changes During Beta Transformation of Uranium, *Nucl. Sci. Eng.*, 12(3): 325–336 (March 1962).
3. J. P. André and P. Tacombe, Activation Energies for the Creep of Polycrystalline Uranium (in French), *Compt. Rend.*, 254: 2159–2161 (Mar. 19, 1962).
4. D. Calaris et al., Factors in the Migration of Grain Boundaries in Alpha Uranium, in *4e Colloque de Métallurgie Propriétés des Joints de Grains*, pp. 53–70, Centre d'Études Nucléaires, Saclay, France, and Presses Universitaires de France, 1961.
5. N. E. Daniel, F. R. Shober, E. L. Foster, Jr., and R. F. Dickerson, Crack Initiation and Propagation in Uranium at Elevated Temperatures, USAEC Report BMI-X-10011, Battelle Memorial Institute, Aug. 1, 1962.
6. Papers presented at Institute of Metals Symposium on Uranium and Graphite, London, 1962:
   *a*. L. R. T. Gardner and W. N. Miller, The Evaluation of Creep Tests on Alpha-Uranium Under Isothermal and Thermal Cycling Conditions, Paper No. 4.
   *b*. R. G. Anderson and J. F. W. Bishop, The Effect of Neutron Irradiation and Thermal Cycling on Permanent Deformation in Uranium Under Load, Paper No. 3.
   *c*. R. G. Bellamy, The Swelling of Alpha-Uranium Under Neutron Irradiation to 0.7 At.% Burnup, Paper No. 8.
7. S. T. Zegler, The Uranium-Rich End of the Uranium-Zirconium System, USAEC Report ANL-6055, Argonne National Laboratory, February 1962.
8. H. C. Quigley, Irradiation of a U–2 At.% Zr Fuel Tube in the VBWR, USAEC Report DP-709, E. I. du Pont de Nemours & Co., April 1962.
9. O. S. Ivanov and Yu. S. Virgilev, The Decomposition of the Gamma-Uranium Base Solid Solutions as Revealed by X-ray Investigators, *J. Nucl. Mater.*, 6(2): 199–202 (July 1962).
10. J. A. Cape and R. E. Taylor, Thermal Properties of Refractory Materials, Report WADD-TR-60-581 (Pt. II), Atomics International, July 1961.
11. W. Uhlmann, Silicon-Uranium Systems as Nuclear Fuel, A Literature Survey, Swedish Report VDIT-53, February 1962.
12. J. R. MacEwan and W. H. Stevens, Xenon Diffusion in $UO_2$: Some Complicating Factors, paper presented at the 15th Pacific Coast Regional Meeting of the American Ceramic Society, Seattle, Oct. 17–19, 1962.
13. J. A. Horak, J. H. Kittel, and R. J. Dunworth, The Effects of Irradiation on Uranium-Plutonium-Fissium Fuel Alloys, USAEC Report ANL-6429, Argonne National Laboratory, July 1962.
14. Argonne National Laboratory, Reactor Development Program Progress Report, July 1962, USAEC Report ANL-6597, Aug. 15, 1962.
15. Los Alamos Scientific Laboratory, Quarterly Status Report on LAMPRE Program for Period Ending May 20, 1962, USAEC Report LAMS-2720, June 1962.
16. Hanford Atomic Products Operation, Reactor and Fuels Research and Development Operation Monthly Report, July 1962, USAEC Report HW-74522A, Aug. 15, 1962. (Classified)

47. National Carbon Company, Graphite-Matrix Nuclear Fuel Elements, Summary Report – Phase II, for Period Nov. 1, 1959 – Oct. 31, 1960.
48. Oak Ridge National Laboratory, Coated Particle Fuel Element Development Activity Letter for the Period May 15 to July 15, 1962, USAEC Report CF-62-8-59, Aug. 22, 1962.
49. Oak Ridge National Laboratory, July 10, 1962. (Unpublished)
50. Oak Ridge National Laboratory, Gas-Cooled Reactor Program Quarterly Progress Report for Period Ending March 31, 1962, USAEC Report ORNL-3302, July 16, 1962.
51. A. H. Kibbey and L. M. Ferris, U-Th Recovery From Pyrolytic Carbon-Coated Carbide Fuel Particles by Electrolysis in Nitric Acid, USAEC Report ORNL-TM-384, Oak Ridge National Laboratory, Sept. 26, 1962.
52. Oak Ridge National Laboratory, Oct. 10, 1962. (Unpublished)
53. Oak Ridge National Laboratory, Sept. 11, 1962. (Unpublished)
54. Hanford Atomic Products Operation, Fuels Development Operation, Quarterly Progress Report, April – June 1962, USAEC Report HW-74377, July 20, 1962. (Classified)
55. J. A. Christensen, Hanford Atomic Products Operation, private communication, Jan. 8, 1963.
56. F. A. Halden, H. C. Wohlers, and R. H. Reinhart, Thermal Expansion of Uranium Dioxide, USAEC Report TID-5722, Apr. 15, 1959.
57. V. C. Howard and T. F. Gulvin, Thermal Conductivity Determinations on Uranium Dioxide by a Radial Flow Method, British Report IG-Report-51, Nov. 17, 1960.
58. Swaging of Uranium Dioxide. Quarterly Report No. 3, USAEC Report EURAEC-61, Apr. 30, 1961.
59. E. Rothwell, High Temperature Substoichiometry in Uranium Dioxide, *J. Nucl. Mater.*, 6(2): 229 – 236 (July 1962).
60. R. Colombo and G. Frigerio, On the Occurrence of Uranium Metal Particles in Fused $UO_2$, *J. Nucl. Mater.*, 5(2): 259 – 261 (February 1962).
61. I. Cohen and B. E. Schaner, A Metallographic and X-Ray Study of the $UO_2$-$ZrO_2$ System, USAEC Report WAPD-253, Westinghouse Electric Corp., Bettis Atomic Power Laboratory, June 1962.
62. General Electric Co., Flight Propulsion Laboratory Dept., High-Temperature Materials Program Progress Report No. 15, Part A, USAEC Report GEMP-15A, Sept. 14, 1962.
63. J. Felton et al., The System $Cr_2O_3$-$UO_2$-$O_2$, paper presented at 64th Annual Meeting of the American Ceramic Society, April 30 – May 2, 1962, New York, New York.
64. G. Christie and J. Williams, The Effect of Small Additions of Yttria on the Plasticity of Uranium Oxides at 940°C, *J. Nucl. Mater.*, 5: 1 – 4 (January 1962).
65. D. C. Hill, Volatility Behavior of Urania-Lanthana Solid Solutions, *J. Am. Ceram. Soc.*, 45: 143 (March 1962).
66. A. P. Young and C. M. Schwartz, Reactions Between Uranium Oxide and Bivalent Metal Oxides at 60,000 Atm, USAEC Report BMI-1585, Battelle Memorial Institute, July 10, 1962.
67. M. J. F. Notley, R. D. MacDonald, G. W. Parry, and G. M. Allison, The Irradiation of Defected Zircaloy-2 Clad $UO_2$ Fuel Elements Containing Fluoride Impurities (Irradiation Test X-204), Canadian Report CRFD-1067, January 1962.
68. M. Volpe and S. Mihailovich, Kinetics of the Reduction of Uranium Oxides by Carbon Monoxide and by Hydrogen, USAEC Report ANL-6475, Argonne National Laboratory, July 1962.
69. A. B. Auskern and J. Belle, Uranium Ion Self-Diffusion in $UO_2$, *J. Nucl. Mater.*, 3(3): 311 (March/April 1961).
70. A. H. Booth and G. T. Rymer, Determination of the Diffusion Constant of Fission Xenon in $UO_2$ Crystals and Sintered Compacts, Canadian Report CRDC-720 (AECL-692), August 1958.
71. F. Schmitz and R. Lindner, Diffusion in Tri- and Tetra-Valent Fission Product Ions in $UO_2$, *Z. Naturforsch.*, 16a: 1096 – 1097 (October 1961).
72. R. Lindner and F. Schmitz, Diffusion of Uranium-233 in Uranium Dioxide, *Z. Naturforsch.*, 16a: 1373 – 1378 (December 1961).
73. S. Goldsmith and P. F. Ashbrook (Eds.), Research and Development Programs Executed for the Division of Reactor Development Quarterly Progress Report, January – March 1962, USAEC Report HW-73915, Hanford Atomic Products Operation, Aug. 1, 1962.
74. K. Marnoch, Metallographic Analysis of Weight Percent Carbon in Uranium Carbide, USAEC Report NAA-SR-Memo-6819, Atomics International, Oct. 20, 1961.
75. J. M. Simmons, USAEC, private communication from P. Murray, AERE, Harwell.
76. Atomics International, AEC Unclassified Programs Quarterly Technical Progress Report, January – March 1962, USAEC Report NAA-SR-7333, June 1962.
77. C. P. Kempter and N. H. Krikorian, Some Properties of ThC and $ThC_2$, *J. Less-Common Metals*, 4: 244 – 251 (1962).
78. B. J. Hopkins, Work Function of Uranium Carbide, *Nature*, 193: 668 – 669 (Feb. 17, 1962).
79. United Nuclear Corp., Fuel Cycle Development Program, Quarterly Progress Report, April 1 to June 30, 1962, USAEC Report UNC-5033, Aug. 31, 1962.
80. O. S. Ivanov and Z. M. Alekseyeva, Investigating the Structure of Alloys in the Systems UC-ZrC, UC-ThC, and ThC-ZrC, in *Structures of Alloys of Certain Systems With Thorium and Uranium* (in Russian), Academy of Sciences of the USSR, Institute of Metallurgy, Gosatomizdat, Moscow, 1961.

17. Hanford Atomic Products Operation, Reactor and Fuels Research and Development Operation Monthly Report, June 1962, USAEC Report HW-74153A, July 15, 1962. (Classified)
18. L. E. Russell and N. H. Brett, Observations on Phase Equilibria and Sintering Behaviour in the $PuO_2$-$UO_2$ System, *J. Nucl. Mater.*, 5(2): 216 (February 1962).
19. United Kingdom Atomic Energy Authority, 1961. (Unpublished)
20. S. J. Paprocki, D. L. Keller, C. A. Alexander, and W. M. Pardue, The Volatility of $PuO_2$ in Nonreducing Atmospheres, USAEC Report BMI-1591, Battelle Memorial Institute, Aug. 16, 1962.
21. A. Strasser and K. Taylor, Carbide Fuel Development, Progress Report, January 1, 1962, to March 31, 1962, USAEC Report UNC-5013, United Nuclear Corp. and Carborundum Co., May 28, 1962.
22. A. Strasser and K. Taylor, Carbide Fuel Development, Progress Report, April 1, 1962, to June 30, 1962, USAEC Report UNC-5030, United Nuclear Corp. and Carborundum Co., Aug. 10, 1962.
23. Argonne National Laboratory, Reactor Development Program Progress Report, May 1962, USAEC Report ANL-6573, June 15, 1962.
24. Nuclear Materials & Equipment Corp., Development of Plutonium-Bearing Materials, Progress Report for Period January 1 Through March 31, 1962, USAEC Report NUMEC-P-100, April 1962.
25. K. H. Puechl, Development of Plutonium-Bearing Fuel Materials, Monthly Progress Letter for Month of July 1962, USAEC Report NUMEC-P-44, Nuclear Materials & Equipment Corp., Aug. 5, 1962.
26. Ames Laboratory, Annual Summary Research Report in Metallurgy, July 1960–June 1961, USAEC Report IS-351, December 1961.
27. R. C. Bailie, Thorium Canning Methods, USAEC Report RFP-268, Dow Chemical Co., June 20, 1962.
28. R. W. Dayton and R. F. Dickerson, Progress Relating to Civilian Applications During August 1962, USAEC Report BMI-1593, Battelle Memorial Institute, Sept. 1, 1962. (Classified)
29. Oak Ridge National Laboratory, Metals and Ceramics Division Annual Progress Report for Period Ending May 31, 1962, USAEC Report ORNL-3313, Aug. 16, 1962.
30. Phillips Petroleum Co., Materials Testing Reactor–Engineering Test Reactor Technical Branches Quarterly Report, January 1–March 31, 1962, USAEC Report IDO-16781, June 15, 1962.
31. W. H. Lenz and P. D. Mundinger, High Density W-$UO_2$ by Activated Sintering, USAEC Report LAMS-2716, Los Alamos Scientific Laboratory, May 1962.
32. Martin Co., Nuclear Div., PM Research and Development Program, 4th Quarterly Progress Report, January 1, 1962, to March 31, 1962, USAEC Report MND-MD-2560-4, August 1962.
33. Battelle Memorial Institute, Defense Metals Information Center, Chemical Vapor Deposition, Report DMIC-170, June 1962.
34. Oak Ridge National Laboratory, Nuclear Reactor Chemistry. Second Conference, Gatlinburg, Tennessee, October 10–12, 1961, USAEC Report TID-7622, July 1962.
35. J. H. Oxley et al., Microminiaturized Fuel Elements by Vapor-Deposition Techniques, *Ind. Eng. Chem., Process Design Develop.*, 1(2): 102–107 (June 1962).
36. Nuclear Materials & Equipment Corp., Final Report [on Corrosion and Radiation Damage Resistant Fuel Material], USAEC Report NYO-9187, September 1960.
37. R. W. Dayton and R. F. Dickerson, Progress Relating to Civilian Applications During June 1962, USAEC Report BMI-1583, Battelle Memorial Institute, July 1, 1962. (Classified)
38. R. W. Dayton and R. F. Dickerson, Progress Relating to Civilian Applications During July 1962, USAEC Report BMI-1589, Battelle Memorial Institute, Aug. 1, 1962. (Classified)
39. L. Berl, Process for the Separation of Zirconium and Hafnium Values, U. S. Patent 3,012,850, Dec. 12, 1962.
40. S. J. Paprocki, D. L. Keller, and W. M. Pardue, Study of Experimental Fuel Bodies Made from Alumina-Coated $UO_2$ Particles, USAEC Report BMI-1586, Battelle Memorial Institute, July 16, 1962.
41. A. K. Smalley, M. C. Brockway, and W. H. Duckworth, Improved Techniques for Dispersing Coated Fuel Particles in Ceramic Bodies, USAEC Report BMI-1579, Battelle Memorial Institute, May 22, 1962.
42. L. M. Ferris, Chemical Processing of Coated Particle Fuels, USAEC Report ORNL-TM-193, Oak Ridge National Laboratory, Apr. 3, 1962.
43. C. S. Luby, Apparatus and Procedure for Coating Thorium-Uranium Carbides with Carbon at 1000 1400°C, USAEC Report GA-2241, General Atomic Div., General Dynamics Corp., May 25, 1961.
44. R. A. U. Huddle, Improvements in or Relating to Nuclear Fuel Materials, British Patent 878,927, Oct. 4, 1961.
45. General Atomic Div., General Dynamics Corp., 40-MW(E) Prototype High-Temperature Gas-Cooled Reactor Research and Development Program, Quarterly Progress Report for the Period Ending June 30, 1962, USAEC Report GA-3396 (Prelim).
46. W. V. Goeddel (Ed.), Coated Fuel Particle Newsletter, May–July 1962, USAEC Report GAMD-2646 (Pt. 9), General Atomic Div., General Dynamics Corp., August 1962.

81. Papers presented at IAEA Symposium on Radiation Damage in Solids and Reactor Materials, Venice, Italy, May 7–11, 1962:
   *a.* B. R. T. Frost et al., Irradiation Effects in Fissile Oxides and Carbides at Low and High Burnup Levels.
   *b.* B. G. Childs, The Low Temperature Irradiation Behavior of Cast Uranium Carbide.
82. M. D. Rogers and J. Adam, Radiation Damage and Its Thermal Recovery in Uranium Monocarbide and Uranium Mononitride, British Report AERE-R-4046, June 1962.
83. A. Accary and M. Marchal, Behavior of UN Under Heat Treatment, *Mem. Sci. Rev. Met.*, 59: 57–70 (January 1962).
84. Y. Baskin and J. H. Handwerk, Thoria and Thoria-Urania Reinforced by Metal Fibers, USAEC Report ANL-6529, Argonne National Laboratory, June 1962.
85. A. Strasser and K. Taylor, Carbide Fuel Development, Progress Report, September 15, 1961, to December 31, 1961, USAEC Report UNC-5003, United Nuclear Corp. and Carborundum Co., Feb. 9, 1962.
86. J. D. Grogan and R. J. Pleasance, A Survey of the Uranium-Nickel System, *J. Inst. Metals.*, 82: 141–147 (1953–1954).
87. M. D. Rogers and J. Adam, Ejection of Atoms From Uranium by Fission Fragments, *J. Nucl. Mater.*, 6(2): 182–189 (July 1962).
88. J. W. Savage, Monthly Progress Report on Mechanisms of Fuel Swelling, Fission Effects in Metal Fuel, Report 62AT4251, Atomics International, May 1962.
89. V. M. Agranovich and E. Ya. Mikhlin, Theory of Swelling of Porous Materials (in Russian), *At. Energ. (USSR)*, 12(5): 385–391 (1962).
90. P. R. Morris, Irradiation Growth in Alpha-Uranium Single Crystals, *J. Appl. Phys.*, 33: 1611–1612 (April 1962).
91. W. E. Roake, Irradiation Alteration of Uranium Dioxide, USAEC Report HW-73072, Hanford Atomic Products Operation, March 1962.
92. E. Rothwell, The Release of Kr-85 From Irradiated Uranium Dioxide on Postirradiation Annealing, *J. Nucl. Mater.*, 5(2): 241–249 (February 1962).
93. H. Matzke, Diffusion of Kr-85 in $ThO_2$, *Z. Naturforsch.*, 16a(11): 1255–1257 (November 1961).

Section

II

Reactor Materials

# Moderator Materials

## Graphite

Graphite degassing experiments at Oak Ridge[1] have shown that the gas composition and volume release from boronated graphite were much different than those for unboronated graphite in the 1600 to 1800°C range. A 5 wt.% boron sample was heated stepwise at 1000, 1400, 1600, and 1800°C. It behaved normally at 1000°C, releasing mostly hydrogen (91%), and at 1400°C, releasing mostly CO (84%). At 1600°C, however, it released 96% nitrogen, and at 1800°C it released 98% nitrogen. This resulted in a total evolution of 451 $cm^3$ of gas (STP)/100 $cm^3$ of graphite, and the gas was 91% nitrogen, 6% hydrogen, and 3% CO. A possible explanation for the very large total volume and nitrogen concentrations is that the graphite contains boron nitride, as well as boron carbide, and that nitrogen is produced as follows:

$$4BN_2 + C \rightarrow B_4C + 4N_2$$

In a continuing study on the effect of graphite variables on irradiation behavior, Hanford reports interesting preliminary data.[2] A raw-coke filler graphite with an accumulated exposure of 6900 Mwd/adjacent ton at approximately 600°C has shown parallel growth of 0.001%, and transverse growth of 0.006%. This is the first time that growth in all directions has been observed in hot test-hole irradiations of equivalent exposure. Also, low-level exposure of hot-worked graphites appears promising. Grade ZT-4130 has shown no net perpendicular contraction after 3120 Mwd/adjacent ton; CSF graphite, in comparison, has displayed at least 0.05% contraction for the same exposure.

Oxidation rates for the graphite–water-vapor reaction under gamma irradiation in a $Co^{60}$ facility are reported for a range of water-vapor partial pressures in helium.[3] A solid cylinder of TSX graphite (approximately 8.3 g) was used. Table II-1 summarizes the results.

Table II-1 OXIDATION OF TSX GRAPHITE IRRADIATED IN MOIST HELIUM[3]

| Water-vapor concentration, ppm | Oxidation rate, $10^{-7}$ g/(g)(hr) | |
|---|---|---|
| | 600°C | 700°C |
| 50 | 2.18 | 6.17 |
| 90 | | 7.12 |
| 155 | 5.29 | 8.90 |
| 300 | 5.42 | 10.13 |

At a given temperature, the pressure dependence of the rate can be represented by an equation of the form

$$R = R_L\,(1 - e^{-kp})$$

where $R_L$ is the limiting value to the rate; $p$ is the partial pressure of water vapor; and $k$ is the constant. The limiting values of oxidation rate at 600 and 700°C are about $5.5 \times 10^{-7}$ and $10.5 \times 10^{-7}$ g/(g)(hr), respectively.

It has long been recognized that the temperature dependence of the dimensions of a polycrystalline graphite aggregate must be a function of several factors: first, the thermal expansion of the crystal lattice, which is markedly anisotropic, and, second, the degree of preferred orientation of the crystals, which depends on the structure of the original coke particles and on the type of manufacturing process. These two factors are insufficient to account for the thermal-expansion behavior of most artificial graphites since they would require considerably larger expansion than is observed in practice. A third factor, the accommodation of crystalline expansion, must

therefore be invoked. British investigators[4] have reported analysis of crystal orientation and the thermal-expansion behavior of two blocks of British Reactor Grade A graphite. This has shown that accommodation of the thermal expansion is associated with the crystallographic $c$-axis, some 37% of the $c$-expansion contributing to that of the bulk. This result is confirmed by analysis of the thermal-expansion behavior of several different types of reactor graphite and of a pressed natural graphite. It is shown that the thermal-expansion behavior of polycrystalline graphite may be characterized by two basic parameters: (1) a measure of the effective contribution of lattice $c$-expansion to that of the bulk material and (2) a measure of the preferred orientation of the crystals. These parameters may be derived from measurements of the linear thermal-expansion coefficients at 400°C in directions parallel and perpendicular to that of extrusion or pressing. Accommodation of thermal expansion in reactor graphite is attributed to the presence of transcrystalline cleavage cracks, observed by electron microscopy of replicas. These cracks exist in parallel arrays, with individual crack lengths up to approximately 10 $\mu$, mean width approximately 250 A, and mean periodicity of approximately two cracks per micron. Their estimated volume agrees well with that of the closed porosity, 4.3%, relative to the volume of crystalline material, derived from density measurements by X-ray diffraction and helium displacement. The cracks are believed to have been initiated during cooling from the graphitization temperature, approximately 2700°C, and are thought to have formed in order to relieve internal stresses generated by interaction between the restraining effect of strong, intercrystalline C–C bonds and anisotropic contraction of the crystal lattice. Evidence is given that the marked increase in thermal expansion observed in the course of neutron irradiation of reactor graphite at 200°C is associated with the closing of cleavage microcracks.

A very useful bibliography on graphite has been published.[5] The compilation contains 958 selected references to reports and published literature. The references pertain primarily to reactor-grade graphite, although information on the manufacture and uses of graphite in other fields is included. The references, which were selected from *Nuclear Science Abstracts*, cover the period 1948 through mid-1961. Subject, author, and availability indexes are provided.

(M. C. Brockway)

# Beryllium Metal and Alloys

## Beryllium Casting

The Beryllium Corp. reported[6] the successful development of a thermal-casting technique to control center-line shrinkage in cast beryllium ingots. Fast, controlled cooling rates produced sound fine-grained 3-in.-diameter ingots. Although small additions of germanium, zirconium, or lanthanum appeared to refine the grain somewhat, this effect was relatively small when compared to fast cooling. No inoculant tried produced effective grain refinement, but low-frequency mechanical vibration during solidification did help to break up the cast structure. The fine-grained ingots could be fabricated by extrusion or rolling. Fabrication refined the cast columnar grain structure and improved the mechanical properties by several orders of magnitude. Even so, the mechanical strength of the cast and wrought beryllium was lower than that of specimens produced by powder-metallurgy methods.

## Beryllium Fabrication

Creep forming, chem milling, brazing, and various machining operations have been developed[7] which produce desired shapes from beryllium sheet stock and from honeycomb structures. The preferred method of joining beryllium-faced honeycomb panels to other structural units is to braze lugs of readily weldable material to the beryllium and then weld these lugs to the mating unit.

Recent feasibility studies[8] have demonstrated the practicability of back-extruding large closed-end tubular parts as well as a large part consisting of a truncated-cone section attached to a closed-end cylinder. Preliminary indications are that parts made by this technique will be considerably less costly than similar parts made by machining from hot-pressed and sintered beryllium. These mechanical properties of the back-extruded beryllium are considerably better also.

Beryllium sheets that were 64 in. long, 16 in. wide, and 0.020 in. thick were formed into segments. These segments were spliced together to form a complete ring. Forming gave a noticeable, but unexplained, increase in ductility. The segments were joined by brazing with Easy-Flo 3. In pressure tests,[9] two of these beryllium cylinders failed at 34.5 and 28.5 psi, respectively (0.020-in. magnesium cylinders failed at 6.05, 5.43, and 6.2 psi; 0.020-in. titanium cylinders failed at 14.55 and 17.00 psi).

Jahnle[10] concluded that, although cross-rolled beryllium sheet can be resistance spot welded, this joining method should be used mainly for positioning. Preheating and postheating reduced the tendency of the spot-welded beryllium to crack by reducing the residual stresses during cooling. The cast-nugget grain size was dependent on base-metal grain size; hence fine-grained sheets should be chosen for this welding method. Electrode sticking is reduced by improved surface finish. Bending must be eliminated or reduced through proper design if the beryllium weldments are to show adequate strength.

Beryllium sheet under $\frac{1}{4}$ in. thick can now be satisfactorily fusion welded by the tungsten–inert-gas arc method. MacPherson and Beaver[11] recommend the use of beryllium welding wire for sheets thicker than 0.040 in. The parts to be welded are pickled in a nitric-hydrofluoric acid bath prior to welding and then fixtured carefully. For automatic welding of beryllium up to 0.125 in. thick, stainless steel sprayed with a 0.005-in.-thick aluminum oxide coating is recommended as the backup material. A solid aluminum oxide block is preferred for thicker weldments. The cleanest welds are made with alternating current. The arc atmosphere generally used is a 50-50 mixture of argon and helium. The welding amperage must be kept low, which results in a slow welding speed. Postheat-treatment at Brush Beryllium has been standardized at 825°C for 30 min.

Argon–arc-fusion welding and pressure welding were found[12] to be more satisfactory methods of putting end caps on beryllium fuel tubes for burst tests than brazing or electron-beam welding. Warm-extruded beryllium rod showed greater response to heat-treatment and much more consistent properties than hot-extruded rod. Burst tests on Brush warm-extruded tubing indicated better and more consistent welding results than were obtained with Pechiney hot-extruded tubing. Moreover, the Brush warm-extruded tubing did not show the undesirable tendency of the several other types of tubes examined to develop a radial alignment of basal planes.

## Analysis of Beryllium

In the course of experiments to evaluate distilled beryllium, Gelles[13] found that it was necessary to develop an analytical technique for the determination of small amounts of tantalum in beryllium. By means of a liquid-extraction technique followed by photometric determination of tantalum as tantalum phenylfluorone, a method was developed with a minimum detection limit of 2 ppm.

Pemsler et al.[14] estimated that the solubility of nitrogen in beryllium is about 60 ppm at 1000°C. This value appears to be temperature independent. The solubility of hydrogen in beryllium is believed to be very small. Measurements of the growth characteristics of hydrogen bubbles formed in beryllium by proton bombardment indicate a value for the diffusion coefficient of hydrogen in beryllium of $9 \times 10^{-10}$ $cm^2/sec$ at 850°C.

Design and operating factors of an apparatus for the vacuum-fusion determination of oxygen in beryllium were investigated thoroughly by Everett and Thompson.[15] They described a method that has been used without difficulty for beryllium samples with oxygen contents ranging from 0.1 to 3.0 wt.%. It is believed that the lower limit of usefulness of this method could be extended to 0.01 wt.%.

Rooksby and Green[16] found two intermetallic compounds, not yet fully identified, during an analytical study of a series of specimens of beryllium metal. They discuss various techniques for the identification and quantitative determination of phases in metals, with special reference to beryllium.

According to Eberle and Lerner,[17] a new 8-quinolinol extraction of tin from uranium, beryllium, thorium, zirconium, steels, and other materials, combined with a spectrophotometric procedure, permits the rapid and accurate determination of tin in these metals. Molybdenum accompanies the tin, but since extraction of tin requires the presence of a halide, separation and determination of these two ele-

ments can be performed by controlling the halide concentration.

The U. S. Navy has instituted a new program at Battelle to develop analytical techniques for the determination of minute quantities of selected elements, especially oxygen, in beryllium.[18] The data in Table II-2 show typical analyses of the better commercial and research grades of beryllium that have been produced recently.

Splettstosser[19] made radiographic technique studies on 0.06- to 6-in. samples of beryllium. Control of the effects of the amount of radiation energy, focus-film distance, and applied voltage gave radiographic sensitivity equivalent to that of magnesium or aluminum.

An essentially electrolytic process for polishing beryllium metallographic specimens, using a modified "Disa Electropol" apparatus, has been described by Dingle and Moore.[20] The total time required for preparation of a specimen with this apparatus is approximately 1 hr, and it requires complete attention of the operator for only 15 min. This compares to 2 to 3 hr by conventional processes.

## Physical Metallurgy of Beryllium

Wolff et al.[21] investigated the role of impurities in commercial beryllium prepared from powders. Diverse aging treatments caused the ultimate tensile strength to vary from 52,000 to 95,000 psi and the ductility to vary from less than 1 to 14%. No significant changes in yield strength were noted, and no textural changes occurred. Properties between room temperature and 400°C increased with decreasing cooling rate from the solutionizing temperature (1100°C for 1 hr). X-ray studies showed a precipitate after aging which had a face-centered cubic structure with a lattice constant of 6.07 A and a preferred orientation with respect to the beryllium matrix.

Barnaby[22] discussed the stress concentration below a tilt boundary that ends within a crystal and gives rise to basal cleavage in a hexagonal metal. If an obstacle to the gliding motion of a tilt boundary restricts its movement, part of the boundary may glide on and leave the other part behind; this creates a stress concentration sufficient to overcome the cohesive forces between basal planes in a hexagonal metal. Splitting of the boundary may be aided by the pressure of glide dislocations behind the boundary. Barnaby also discusses surface tilts and basal slips in the model of a Stroh crack [Stroh, *Phil. Mag.*, 3: 597 (1958)], which is shown in perspective.

X-ray diffraction analysis was made by Amonenko et al.[23] on the texture of beryllium precipitates obtained by condensation in a vacuum of beryllium vapor from high-purity beryllium onto texturized rolled sheets of molybdenum, tantalum, zirconium, nickel, titanium, copper, iron, and amorphous material. Except on molybdenum and nickel, all the deposits, which varied from 150 to 500 $\mu$ thick, had an axial texture [0 0 1] perpendicular to the base. On molybdenum sheet with a (1 0 0) [0 1 1] texture, the beryllium sheet had a (1 0 2) [2 $\bar{1}$ $\bar{1}$] texture that was very excellent, whereas on nickel with a (1 1 0) [1 1 2] texture, the precipitate was a slightly less excellent (1 0 0) [0 0 1]; i.e., the (1 0 0) of the beryllium crystals lies in the precipitation plane, whereas the hexagonal axis corresponds with the rolling direction of the nickel sheet.

At Electro-Optical Systems, Inc., laboratories, no significant change of structure followed ultrarapid quenching of alloys of beryllium with aluminum, silicon, nickel, or copper. In four other systems, beryllium-hydrogen, beryllium-oxygen, beryllium-scandium, and beryllium-zinc, the experiments on ultrarapid quenching could not be carried out.[24]

Taylor and Moore[25] studied the fractures of vacuum-cast electrolytic-flake beryllium and two beryllium-iron alloys after extrusion at 1050°C. Each alloy was tested in the as-extruded condition and after heat-treatments designed to overage the material with respect to its iron content. They came to the following conclusions:

1. Brittle transcrystalline failure within the range 20 to 200°C is probably initiated by the Stroh split-bend-plane mechanism and is unaffected by overaging anneals. Between 200 and 400°C, further deformation modes become operative which relieve the split-bend-plane mechanism. The temperature at this level is not high enough to cause precipitation hardening. Between 400 and 600°C, grain-boundary failure, which leads to a falloff in ductility, becomes increasingly important. Suitable overaging anneals replace this intergranular fracture by a fibrous mixture of transcrystalline and bound-

Table II-2 SEVERAL BERYLLIUM METALS AND THEIR ANALYSES[18]

| Type of material | Method of analysis used | Analysis, wt.% | | | | | | | | | | | | | | Material source |
|---|---|---|---|---|---|---|---|---|---|---|---|---|---|---|---|---|
| | | Metallics | | | | | | | | | | Nonmetallics | | | | |
| | | Fe | Ni | Mn | Cr | Ca | Co | Mg | Pb | Si | Al | $N_2$ | C | H | $O_2$ | |
| Vacuum distilled | Emission spectrograph for metallics* | 15 | <7 | <6 | 7 | <10 | <4 | <10 | <2 | <20 | <20 | | 10 | | 250 | Battelle preparation using QMV beryllium as starting material |
| QMV chunk, vacuum melted | Emission spectrograph for metallics* | 100 | 10 | 15 | 30 | 10 | <15 | 100 | 20 | 30 | 300 | <15 | 280 | 16 | 250 | Obtained from Brush Beryllium |
| Berylco five-pass ingot, zone refined and vacuum cast: | | | | | | | | | | | | | | | | |
| First end to freeze | Spark-source mass spectrograph† | 250 | 300 | 1 | <1 | <30 | 1 | <1 | | <30 | 3 | <15 | 240 | 10 (as BeH) | 450 (plus about 7 as $Be_2O$) | Franklin Institute material |
| Last end to freeze | Spark-source mass spectrograph† | 620 | 130 | 24 | | <30 | 1 | <1 | | <60 | 105 | | 530 | | 780 (plus about 10 as $Be_2O$) | Franklin Institute material |
| Pechiney powder rod | Spark-source mass spectrograph† | 390 | 110 | 60 | 25 | <130 | 1 | 50 | | 250 | 1800 | <40 | 800 | 7 (as BeH) | 1070 (plus about 7 as $Be_2O$) | |
| Ultrahigh purity, vacuum distilled | Colorimetric-chemical for metallics | 5 | 2 | 5 | 1 | | | | | 12 | 20 | 5 | 10 | | 300 (estimated upper limit) | Nuclear Metals, Inc. |

*Battelle analysis.
†Bell & Howell Research analyses.

ary failure; thus increased elongation values result.

2. In the alloys studied, twinning did not appear to make an important contribution to tensile deformation.

3. Additions of iron as the as-extruded material extend the brittle transcrystalline fracture normally associated with room temperature to higher temperatures; thus an overall decrease in ductility is produced.

Sumner[26] found that the failure of fuel elements with beryllium cans in contact with the fuel takes place on cooling by the propagation of a helical crack following the $(11\bar{2}0)$ planes of the highly textured tube. The biaxial nature of the strain field produces the helical form of the crack. Sufficient ductility is possessed by lower textured material, particularly hot-vacuum-pressed powder, to withstand the thermal-contraction strains experienced by the fuel elements.

Tensile tests on warm-extruded Brush N-50-B and Brush S-200-B beryllium tubes in the as-received state (stress relieved by the supplier at 800°C) showed reductions in area of 4.5 and 36% at room temperature and 400°C, respectively. Yield stresses[27] at room temperature and 400°C for the N-50-B are 40,000 and 23,500 psi, and for the S-200-B, 52,000 and 32,800 psi. No improvement in room-temperature ductility of either material resulted from a heat-treatment of 1100°C for 1 hr followed by cooling at 4°C per minute. At 500°C, the N-50-B material showed 1000-hr rupture lives at 4000 (as received) and 11,200 psi (slowly cooled). The S-200-B materials tested at 500°C showed 10- and 100-hr lives (as received) at 16,200 and 12,400 psi, whereas the values[27] for the slowly cooled material were 24,900 and 17,200 psi.

The shear strengths of tungsten–inert-gas arc-welded end closures in beryllium tubes were determined at Oak Ridge[1] by pushing the end cap out of the tube by shearing the weld. The results at room temperature and at 600°C are summarized in Table II-3.

Table II-3 RESULTS OF ROOM-TEMPERATURE AND ELEVATED-TEMPERATURE SHEAR TESTS ON END-CAP WELDS IN BERYLLIUM TUBES[1]

| Tube fabrication method | Ultimate shear strength, psi | |
|---|---|---|
| | At room temp. | At 600°C |
| Machined from hot-pressed rod: | | |
| Low carbon content | 25,700 | 10,100 |
| High carbon content | 27,700 | 10,600 |
| Machined from hot-extruded rod | 24,400 | 16,200 |
| Machined from warm-extruded rod | 26,000 | 10,800 |
| Warm extruded to size | 22,300 | 9,500 |
| Hot impact extruded to size | 24,400 | 11,700 |
| Hot extruded to size | 21,700 | 12,900 |
| Extruded to size | 20,900 | 10,300 |

In other tests at Oak Ridge, a simulated fuel element consisting of hollow $UO_2$ pellets clad with finned beryllium tubing was fabricated and thermally cycled out-of-pile to failure. The experiment was designed to determine the number of cycles required for failure of the beryllium-clad element under the most disadvantageous conditions. The element was cycled between 482 and 1202°F for 112 cycles with an as-assembled diametral gap of 0.001 in. The following observations were recorded:

1. No permanent axial deformation of the beryllium cladding occurred during thermal cycling.

2. The capsule fractured circumferentially on the 67th thermal cycle.

3. An axial crack was located in the beryllium between two fins. The maximum tangential strain in the beryllium due to the differential expansion between the $UO_2$ and the beryllium should have been 0.7%.

4. The average grain size in the beryllium after the test was ASTM-6. The abnormal grain growth at the inner surface of the tubing increased the grain size to ASTM-3 to a depth of 0.005 to 0.01 in. in the micrograph shown in the reference. The tubing was reamed on the inner surface prior to testing to permit insertion of the $UO_2$ pellets. Similar grain growth has been observed in other beryllium tubes that were reamed.

## Corrosion and Irradiation Behavior of Beryllium

The corrosion resistance of beryllium is greatly affected by the purity of the metal. Some of the impurities in commercial beryllium reduce its resistance to corrosion. Steele[28] found that, in a standard humidity test, vacuum-deposited coatings of silicon monoxide on beryllium disks or sheet afforded complete protection to the beryllium. Beryllium sheet, coated with zirconium metal that had been (acci-

dentally?) overheated, forming blue beryllium nitride, also appeared to resist corrosion completely in this test.

Laboratory tests have shown that the corrosion of beryllium is much more pronounced in tap water than in steam condensate, distilled water, or demineralized water. Schmitt[29] notes that the addition of as little as 5 ppm of chloride ion to distilled water stimulates the corrosive attack on beryllium, but the addition of fluoride salts to tap water inhibits corrosion. Anodized beryllium is much more resistant to corrosion in tap water or distilled water than is normal QMV beryllium.

Beryllium exposed to $CO_2$ at temperatures above 600°C is subject to a pitting type of corrosion. Corrosion rate is very dependent on the pressure of the $CO_2$ gas, and it becomes catastrophic at higher pressures and temperatures. Raine and Robinson report[30] that additions of calcium metal to beryllium in amounts greater than 0.15 wt.% result in an alloy with markedly increased resistance to corrosion by $CO_2$. A beryllium–0.4 wt.% calcium alloy was found to be completely free of pitting type corrosion in the temperature range of 600 to 800°C in $CO_2$ at 6.8 atm and at 20.5 atm. Strangely, the corrosion resistance was higher at the higher gas pressure. After 8000 hr at 700°C in $CO_2$, the oxide film thickness was not measurable, and it had the appearance of a temper color only. These results, found at Associated Electrical Industries Ltd., Manchester, England, have been partially confirmed[31] at Oak Ridge.

Frye and Cunningham[31] found that the effects of irradiation on the stress-rupture life of warm-extruded beryllium tubing are only about half as severe as in tubing produced by hot pressing or hot extrusion. An exposure of $2 \times 10^{20}$ nvt decreased the stress-rupture life of the hot-pressed or hot-extruded beryllium by 20% and that of the warm-extruded beryllium by 10%.

The effects of irradiation on beryllium exposed to between $1 \times 10^{20}$ and $6 \times 10^{20}$ nvt (>1 Mev) at temperatures between 50 and 780°C were reported by Weir.[33] Stress-rupture experiments on beryllium tubes were made at 600°C in neutron fluxes of $3 \times 10^{13}$ and $9 \times 10^{13}$ nv (>1 Mev). Several specimens were stressed when the test reactor had attained full-power level, whereas others were held at 600°C until an exposure of $3 \times 10^{20}$ nvt was attained; then the specimens were stressed to rupture in 100 hr. The results indicate that a slight hardening occurs on irradiation or postirradiation annealing at temperatures below 600°C. Beryllium swells 3% at 700°C on exposure to $3.6 \times 10^{20}$ nvt; no swelling occurs at lower temperatures. The onset of swelling appears to be associated with migration of small cavities to large nuclei, perhaps inclusions in the beryllium. The stress-rupture properties at 600°C are reduced as a function of exposure.

(W. Hodge)

## Beryllium Oxide

The Literature Research Group at Aerospace Corp.[33] has published an annotated bibliography of beryllium oxide ceramics. The bibliography, which consists of 283 entries, covers the period from 1955 to 1961. Emphasis is given to the chemical, physical, and mechanical properties of ceramic bodies and to preparation of BeO powders and fabrication of BeO bodies. Attention also is given to intermetallic compounds and alloys of beryllium and to toxicity and handling precautions for beryllium materials.

University of Cincinnati investigators[34] have completed a comprehensive survey and have published a guide for those responsible for protecting the health of persons working with beryllium and its compounds. The report covers the history of the beryllium disease, and it describes the syndromes of both chronic and acute phases. Hygienic standards and tolerances are given, as well as recommended environmental control procedures. Sampling and analysis, housekeeping, personal hygiene, and a proposed medical program are discussed. Also, illustrations of ventilation controls are included.

Work is continuing at Atomics International[35] on the growth of single BeO crystals. Investigators there report that minor additions of bismuth, silicon, phosphorus, arsenic, strontium, antimony, or tellurium atoms to a lithium molybdate flux are beneficial to the quality of BeO crystals grown in the flux. The characteristic crystal pattern is governed by the particular additive employed. The maximum satisfactory growth rate of crystals in the molybdate flux is about ½ mm per day under steady-state conditions. Nearly perfect crystals measuring up to 1 cm in major dimensions have been prepared, and they are being used to study neutron-

irradiation effects and fission-product diffusion in BeO.

Mechanical-property measurements on hot-pressed BeO ceramics also are continuing at Atomics International. Investigators report that BeO bodies containing 1 wt.% MgO retain flexural strength up to 1000°C, but they lose strength rapidly at higher temperatures. Pure BeO bodies, on the other hand, appear to lose strength more slowly and uniformly up to 1600°C. In studies on the effects of strain rate on strength, no apparent differences were observed in the behavior of pure BeO and BeO–1 wt.% MgO bodies. At room temperature, increased strain rate led to increased strength values. High-density (99.5% of theoretical) specimens exhibited this effect less than specimens whose densities were 98% of theoretical. At 77°K, measured strengths were 15 to 25% greater than those at room temperature, and the strain-rate effect was greatly reduced.

Atomics International investigators also have reported some electrical-property measurements of hot-pressed BeO ceramics. Measurements at 220 Mc showed the dielectric constant to increase from 7.1 at room temperature to 9.9 at 2500°F. The loss tangent at the same frequency remained constant at 0.0003 between room temperature and 1900°F, but it rose to 0.0065 at 2500°F. At 9375 Mc, the dielectric constant ranged from 7.3 to 9.2 at room temperature and 2500°F, respectively. The loss tangents increased from 0.005 to 0.0014 over the same temperature range.

Russian investigators[37] have reported studies of the reaction

$$BeO + \tfrac{3}{2}C \text{ (graphite)} \rightleftharpoons \tfrac{1}{2}Be_2C_3 + CO(g)$$

at 1800 to 2000°K and $10^{-4}$ mm Hg. They derived the following relation for temperature dependence of the equilibrium constant of the reaction

$$\log K_{eq} = (9.021 \pm 0.092) - \frac{(20{,}712 \pm 222)}{T}$$

Continued studies on foamed BeO ceramics have been reported by General Electric workers.[37] Specimens whose density was 0.98 g/cm$^3$ and whose pore diameters ranged from 0.01 to 0.02 cm, were subjected to thermal gradients of up to 810°C across a 1.6-cm thickness. The maximum hot-face temperature was 1580°C. Specimens held in various thermal gradients and at various hot-face temperatures for unspecified periods of time showed no changes in dimensions or weights. Thermal conductivities calculated for thermal-gradient data showed them to vary from 0.0013 to 0.0024 cal/(cm)(sec)(°C) between 600 and 1450°C. These data may be compared with the conductivity of BeO corrected to theoretical density. For approximately the same temperature range, the calculated conductivities for nonporous BeO are 0.112 and 0.0391 cal/(cm)(sec)(°C) at 600 and 1400°C, respectively.[38]

Table II-4 EFFECT OF NEUTRON EXPOSURE[39] ON STRENGTH OF BeO

| Fast flux, nvt | $\Delta a/a$, % | $\Delta c/c$, % | Compressive strength at 20°C, metric tons/cm$^2$ |
|---|---|---|---|
| None | 0 | 0 | 20 |
| $2.5 \times 10^{19}$ | 0.011 | 0.095 | 15.3 |
| $6.0 \times 10^{19}$ | 0.036 | 0.310 | 4.5 |
| $9.0 \times 10^{19}$ | 0.037 | 0.520 | 1.4 |
| $2.0 \times 10^{20}$ | 0.100 | Not measurable | Powder |

The modulus of rupture of the foamed BeO was not sensitive to temperature up to 1480°C, and it was in the range of 450 psi. The pieces could readily be clamped and machined with conventional diamond tooling.

French investigators[39] have described the effects of fast-neutron irradiation at less than 100°C on the lattice parameters and compressive strength of sintered, unfueled BeO. The specimen densities were in the range 2.97 to 3.0 g/cm$^3$; the purity was not specified. Table II-4 summarizes the conditions and results of the experiment.

The rapid deterioration of strength with increasing exposure was attributed to the disparity between $\Delta c/c$ and $\Delta a/a$. Intergranular regions in the specimens were particularly disturbed, as evidenced by wide grain boundaries in the irradiated bodies. The author concluded that the irradiation temperature, in

this experiment very low, had a predominant influence on the behavior of BeO during irradiation.

Another experiment described by the same author dealt with the irradiation of sintered MgO specimens. The specimens were of two densities: 83 and 95% of theoretical. They were irradiated to $2.2 \times 10^{20}$ nvt (fast) at 400°C. This exposure caused an increase in the MgO lattice parameter of from $4.2115 \pm 0.0008$ A to $4.2150 \pm 0.0008$ A. The crushing strength of the less dense specimens was substantially unaffected by irradiation. However, the crushing strength of the more dense MgO was increased from about 5 to about 10 metric tons/cm$^2$ by irradiation. It would be expected that the combination of higher irradiation temperature and the isotropic crystal lattice of the MgO would lead to a higher degree of irradiation stability than that observed in the BeO described above. However, the observed increase in the strength of dense MgO on irradiation is difficult to explain. In any case, the results of this experiment suggest that closer examination of MgO as a potential reactor material might be rewarding. (A. K. Smalley)

# Solid Hydrides

A bibliography containing 94 references, principally on the hydrides of zirconium, yttrium, and titanium, has been compiled by Pratt & Whitney.[40] This listing includes most of the literature published on these compounds from 1955 to 1959.

## Zirconium Hydride

A summary of the technology involved in the use of zirconium hydride as a moderator material has been published by General Electric.[41] The properties of the material are outlined, together with the method of preparation of moderator sections and techniques for cladding. The zirconium hydride can be used at temperatures up to 1200°F without cladding, and up to 1500°F when clad.

The brittle behavior of zirconium hydride of low hydrogen content has been studied at Argonne.[42] As an introductory step, the habit planes of hydride precipitates in the zirconium were ascertained. They were found to be mostly {100} planes. Tensile-test studies showed that (1) slip occurs at lower resolved shear stress than any mode of twinning; (2) of the twinning systems, only {111} can be considered important deformation modes; and (3) fractures do not occur before considerable deformation has been observed, and they are not of the cleavage type.

The solubility of hydrogen in alpha zirconium and in Zircaloys has been reported by Ostberg.[43] The values differ only slightly from those of previous investigators, and the differences can be accounted for on the basis of oxygen content of the metals used. However, he observed that cold-working the zirconium gave a significant increase in the solubility limit for hydrogen. The exact amount of increase was not stated.

## Yttrium Hydride

The tensile properties of hydrided yttrium were measured at Iowa State.[44] The maximum tensile strength occurs when the metal contains 700 ppm hydrogen. There is a continuous increase in yield strength and a decrease in ductility as the hydrogen content increases, as shown in Table II-5.

Table II-5 TENSILE PROPERTIES OF YTTRIUM-HYDROGEN ALLOYS[44]

| Hydrogen, ppm | Tensile strength, psi | Yield strength, psi | Uniform elongation, % |
|---|---|---|---|
| 100 | 28,500 | 6,000 | 15 |
| 150 | 28,500 | 7,000 | 14.5 |
| 350 | 43,000 | 12,000 | 13 |
| 700 | 49,700 | 12,300 | 16.5 |
| 900 | 47,800 | 18,300 | 11 |
| 1100 | 21,000 | 20,300 | 0.5 |

## Lithium Hydride

The physical properties of lithium hydride are summarized in a publication by General Electric.[45] The density values reported range from 0.775 g/cm$^3$ at room temperature to 0.690 g/cm$^3$ at 688°C. In the molten state, the density decreases gradually to a value of 0.496 g/cm$^3$ at 945°C. The best value of the melting point is given as $686 \pm 2$°C. The heat of fusion is $5519 \pm 25$ cal/mole. Extensive tables listing heat capacity, thermal conductivity, and linear coefficient of expansion as a function of temperature are presented also.

The corrosive effects[46] of lithium hydride, lithium metal, and mixtures of the two upon various structural metals were investigated at TAPCO. The metals studied included iron, nickel, and cobalt-base alloys, some refractory-base alloys, plus molybdenum and titanium. Sealed metal capsules containing the corrosive material were used as test specimens. The tests were conducted in air, argon, and hydrogen up to 3000 hr and at either 1500 or 1600°F or cycled between 1165 and 1600°F. All materials other than AISI 1010 steel and molybdenum metal suffered attack greater than 5 mils in 10,000 hr when subjected to the mixture. For lithium hydride alone, five materials were sufficiently resistant to be considered as containers: (1) type 347 stainless steel, (2) Haynes Alloy No. 25, (3) molybdenum, (4) molybdenum–0.5 wt.% titanium, and (5) type 316 stainless steel.

### Alloy Hydrides

The crystal structure of $NiZrH_3$ has been determined by Korst.[47] Cell constants for the hydride phase are $a = 3.53 \pm 0.01$ A, $b = 10.48 \pm 0.02$ A, and $c = 4.30 \pm 0.01$ A. These values indicate that the structure of this compound is an expanded version of that of the parent compound NiZr. (H. H. Krause)

## References


1. Oak Ridge National Laboratory, Gas-Cooled Reactor Program Quarterly Progress Report for Period Ending March 31, 1962, USAEC Report ORNL-3302, July 16, 1962.
2. F. W. Albaugh, Reactor and Fuels Research and Development Operation Monthly Report, June 1962, USAEC Report HW-74153-A, Hanford Atomic Products Operation, July 15, 1962. (Classified)
3. Hanford Atomic Products Operation, March 1962. (Unpublished)
4. A. L. Sutton and V. C. Howard, The Role of Porosity in the Accommodation of Thermal Expansion in Graphite, British Report TRG-Report-171, Apr. 4, 1962.
5. T. F. Davis (Comp.), Graphite, A Selected Bibliography, USAEC Report TID-3314, February 1962.
6. J. P. Denny and B. H. Hessler, Beryllium Casting, Final Report, Report ASD-TDR-62-390, Beryllium Corp., March 1962.
7. J. N. Krusos, A. S. Kjelby, J. Borosic, and T. J. Byrne, Beryllium Composite Structures. Volume II. Materials and Processes, Report ASD-TR-61-706(Vol.II), Aeronca Manufacturing Corp., January 1962.
8. M. E. Tatman, Processing Beryllium–Physical Characteristics of the Material; Machining and Forming Procedures, *Aircraft Production*, 23: 466–470 (December 1961).
9. E. H. Nickell and R. F. Crawford, Structural Shell Optimization Studies — Final Report. Volume 2, Optimization of Stiffened Cylindrical Shells Subjected to Uniform External Hydrostatic Pressure, Report AD-267624, Lockheed Aircraft Corp., Missiles and Space Div., June 30, 1961.
10. H. A. Jahnle, Resistance Spot Welding Beryllium, *Welding J. (N. Y.)*, 41: 331–336 (April 1962).
11. B. M. MacPherson and W. W. Beaver, How to Fusion Weld Beryllium, *Welding J. (N. Y.)*, 41: 327–330 (April 1962).
12. W. D. Bennett, Annual Report on Beryllium Research, 1961, Canadian Report CW-R&DL-24, February 1962.
13. S. H. Gelles, Beryllium Research and Development Program, Quarterly Progress Report to Aeronautical Systems Division for the Period January 1, 1962–March 31, 1962, Report NMI-9519, Nuclear Metals, Inc., June 25, 1962.
14. J. Pemsler, R. W. Anderson, and E. J. Rapperport, Solubility and Diffusion of Gases in Beryllium, Report NMI-9815, Nuclear Metals, Inc., Mar. 14, 1962.
15. M. R. Everett and G. E. Thompson, A Study of the Determination of Oxygen in Beryllium by Vacuum Fusion, *Analyst*, 87(1036): 515–529 (July 1962).
16. H. P. Rooksby and I. R. Green, The Identification and Determination of Foreign Phases and Constituents in Metals, with Special Reference to Beryllium, *Analyst*, 87(1036): 539–547 (July 1962).
17. A. R. Eberle and M. W. Lerner, Determination of Tin and Molybdenum in Nuclear Reactor and Other Materials, *Anal. Chem.*, 34(6): 627–632 (May 1962).
18. W. M. Henry, Development of Analytical Techniques for the Determination of Minute Quantities of Selected Elements in Beryllium, Interim Report No. 1, Battelle Memorial Institute, Aug. 10, 1962.
19. H. R. Splettstosser, Radiography of Beryllium, *Nondestructive Testing*, 20(2): 98–102 (March–April 1962).
20. J. H. Dingle and A. Moore, A Rapid Electrolytic Method for the Preparation of Metallographic Surfaces on Fabricated Beryllium, *J. Inst. Metals*, 90: 270–271 (March 1962).
21. A. K. Wolff, S. H. Gelles, and L. R. Aronin, Impurity Effects in Commercially Pure Beryllium Prepared From Powder, USAEC Report NMI-TJ-40(Rev.), Nuclear Metals Inc., Sept. 11, 1961.
22. J. T. Barnaby, Microcracks in Beryllium, *J. Inst. Metals*, 90: 271–272 (March 1962).
23. V. M. Amonenko et al., Oriented Growth of Beryllium Precipitates on Textured and Isotropic

Bases, *Phys. Metals Metallog.*, 12(1): 64–67 (1961).

24. Electro-Optical Systems, Inc., Investigation of the Effect of Ultra-Rapid Quenching on Metallic Systems, Including Beryllium Alloys, Report ASD-TDR-62-181, June 1962.
25. W. Taylor and A. Moore, Tensile Fracture Characteristics of Extruded Ingot Beryllium and Beryllium–Iron Alloys, British Report AWRE-0-42/62, August 1962.
26. G. Sumner, The Brittleness of Extruded Beryllium Tubes, British Report TRG-308, 1962.
27. Atomic Energy of Canada, Ltd., 1962. (Unpublished)
28. J. R. Steele, Beryllium Corrosion, *Materials Protection*, 1(7): 59–62 (July 1962).
29. C. R. Schmitt, Miscellaneous Beryllium Corrosion Studies, USAEC Report Y-1397, Union Carbide Nuclear Co., Y-12 Plant, May 16, 1962. (Classified)
30. T. Raine and J. A. Robinson, The Corrosion of Beryllium and Alloys of Beryllium with Calcium in Carbon Dioxide, *J. Nucl. Mater.*, 5(3) 341–343 (1962).
31. Oak Ridge National Laboratory, Metals and Ceramics Division Annual Progress Report for Period Ending May 31, 1962, USAEC Report ORNL-3313, Aug. 16, 1962.
32. J. R. Weir, The Effect of High Temperature Reactor Irradiation on Some Physical and Mechanical Properties of Beryllium, Preprint No. 28 of paper presented at the Institute of Metals Conference on the Metallurgy of Beryllium, London, October 16–18, 1961.
33. T. Cheron (Comp.), Beryllium Oxide. A Literature Survey, Report AD-269729, Aerospace Corp., Sept. 1, 1961.
34. J. Cholak, R. A. Kehoe, L. H. Miller, F. Princi, and L. J. Schafer, Toxicity of Beryllium, Final Technical Engineering Report, Report ASD-TR-62-7-665, University of Cincinnati, Kettering Laboratory, April 1962.
35. Atomics International, AEC Unclassified Programs Quarterly Technical Progress Report, January–March 1962, USAEC Report NAA-SR-7333.
36. F. Sh. Muratov and A. V. Novoselova, The Problem of Reaction Equilibrium of the Carbon Reduction of Beryllium Oxide, *Doklady Akad. Nauk SSSR*, 143(3): 599–602 (1962).
37. General Electric Co., Flight Propulsion Laboratory Dept., High-Temperature Materials Program, Progress Report No. 13, Part A, USAEC Report GEMP-13A, July 31, 1962.
38. W. D. Kingery et al., *J. Am. Ceram. Soc.*, 37(2): 107–110 (February 1954).
39. J. Elston, Behavior of Neutron-Irradiation Sintered Beryllium Oxide, USAEC Translation AEC-tr-5140 (translated from French Report DM/1182), 1962.
40. E. A. Cernak (Comp.), Hydrides of Titanium, Yttrium, and Zirconium, USAEC Report CNLM-2370-2, Pratt & Whitney Aircraft Div., United Aircraft Corp., Apr. 28, 1960.
41. R. G. Cook, M. B. Goldstein, C. W. Moon, and W. Z. Prickett, Gas-Cooled High-Temperature Nuclear Reactor Design Technology. 4. Cellular Metallic Fuel Reactors, USAEC Report APEX-800(Pt. B), General Electric Co., Flight Propulsion Laboratory Dept., June 30, 1962.
42. Argonne National Laboratory, Metallurgy Division Annual Report for 1961, USAEC Report ANL-6516.
43. G. Ostberg, Determination of Hydride Solubility in Alpha Phase Zirconium, Zircaloy-2, and Zircaloy-4, *J. Nucl. Mater.*, 5: 208–215 (February 1962).
44. Ames Laboratory, Annual Summary Research Report in Metallurgy, July 1960–June 1961, USAEC Report IS-351, December 1961.
45. F. H. Welch, Lithium Hydride Properties, USAEC Report DC-61-3-73, General Electric Co., Aircraft Nuclear Propulsion Dept., Mar. 14, 1961.
46. E. J. Vargo and D. B. Cooper, An Investigation of the Corrosion Resistance of Metallic Materials to Molten Lithium Hydride at Cyclic Elevated Temperatures, USAEC Report NP-11952, TAPCO Div., Thompson Ramo Wooldridge, Inc., Feb. 14, 1962.
47. W. L. Korst, The Crystal Structure of $NiZrH_3$, *J. Phys. Chem.*, 66: 370–372 (February 1962).

Section

# III

Reactor Materials

# Nuclear Poisons

## Metallic Poisons

Irradiation testing of 1 wt.% boron–austenitic stainless-steel alloys to depletions as high as 98% of the $B^{10}$ and at temperatures up to 530°F have been carried out at Westinghouse.[1] These tests have shown the behavior of these alloys to be consistent with the model of irradiation damage in $B^{10}$-containing iron-base alloys. This model attributes irradiation damage to embrittlement of the matrix, which is caused by the transmutation products from $B^{10}$, and also to formation of microcracks within the embrittled matrix. The microcracks are caused by boron-particle swelling owing to helium and lithium formation. These effects cause a linear solid-volume swelling rate of 0.33% volume per $10^{20}$ depletions of $B^{10}$ per cubic centimeter in the alloy core. No apparent difference in swelling rates was found in specimens whose claddings had been purposely defected and which were in contact with water.

Phase diagrams of hafnium-vanadium and hafnium-iridium have been completed by the Bureau of Mines.[2] These are shown in Figs. III-1 and III-2. (M. Kangilaski)

## Dispersion Control Materials

Workers at Oak Ridge[3] have continued to investigate europium oxide for use in $Eu_2O_3$–stainless-steel dispersions. They have concluded that swelling and erratic sintering behavior are due to adsorption and reaction of $CO_2$ and $H_2O$ to form a europium hydroxycarbonate. The undesirable phase can be removed, and the monoclinic single-phase structure can be produced by heat-treatment at 1350°C in a pressure of $10^{-5}$ torr. Europium oxide compacts were found to be severely attacked in 100°C water within 5 hr, regardless of processing history.

Irradiation of $Eu_2O_3$–stainless-steel dispersions containing 20, 30, or 40 wt.% $Eu_2O_3$ produced no evidence of dimensional or structural changes after exposures of $2.9 \times 10^{21}$ nvt (unperturbed) at 170°F in the Materials Testing Reactor. As shown in Table III-1, irradiation did not affect the aqueous corrosion resistance, although the 30 and 40 wt.% $Eu_2O_3$ specimens

Table III-1 CORROSION RESISTANCE OF $Eu_2O_3$–STAINLESS-STEEL DISPERSIONS IN WATER AT 570°F AND 1200-PSI PRESSURE[1]

| Specimen number | Integrated unperturbed dose, nvt ($\times 10^{20}$) | Results of postirradiation corrosion exposures | |
|---|---|---|---|
| | | Weight gain, % | Thickness gain, % |
| | 20 wt.% $Eu_2O_3$ | | |
| 2A*–control | | 0.03 | 0 |
| 2B*–control | | 0.04 | 0.91 |
| 39-1 | 7.0 | 0.01 | 0.84 |
| 39-2 | 12.1 | 0.05 | 2.50 |
| | 30 wt.% $Eu_2O_3$ | | |
| 3A–control | | 0.002 | 0 |
| 3B–control | | 0.01 | 0.02 |
| 39-5 | 7.6 | 0.42 | 13.3 |
| 39-6 | 14.6 | 0.62 | 15.4 |
| 39-7 | 27.9 | 0.71 | 11.3 |
| | 40 wt.% $Eu_2O_3$ | | |
| 4A–control | | 2.35 | 25.5 |
| 4B–control | | 1.53 | 27.3 |
| 39-9 | 7.2 | 0.24 | 34.0 |
| 39-10 | 14.8 | 1.58 | 30.5 |
| 39-11 | 28.7 | 1.51 | 31.3 |

*A specimens were in cold laboratory; B specimens were run simultaneously with irradiated specimens in hot cell.

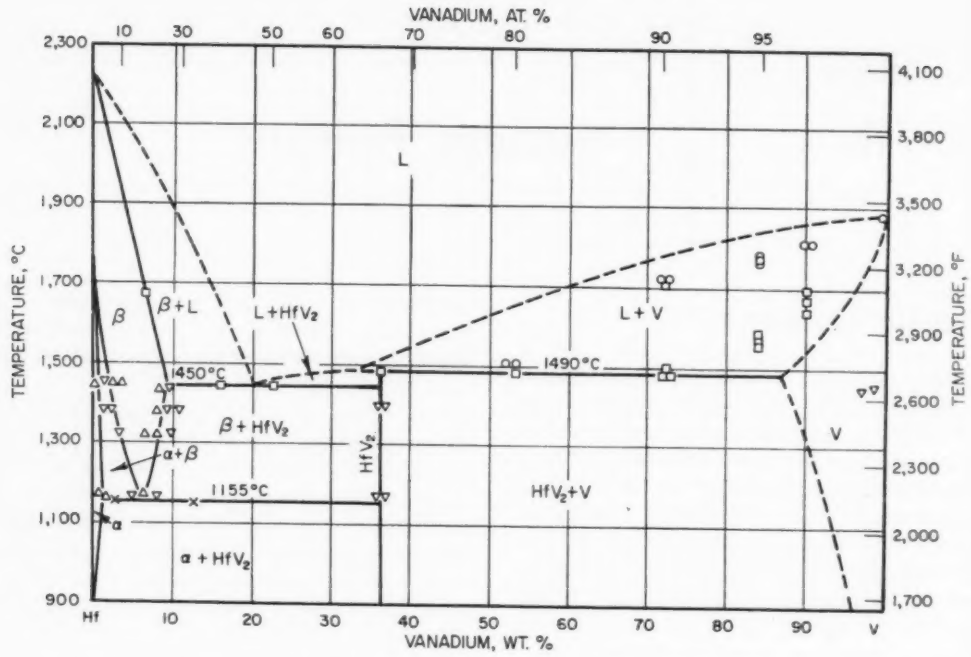


Fig. III-1 Hafnium-vanadium phase diagram.[2] ○, liquidus. □, solidus. △, single phase. ▽, two phase. ×, differential thermal analysis.

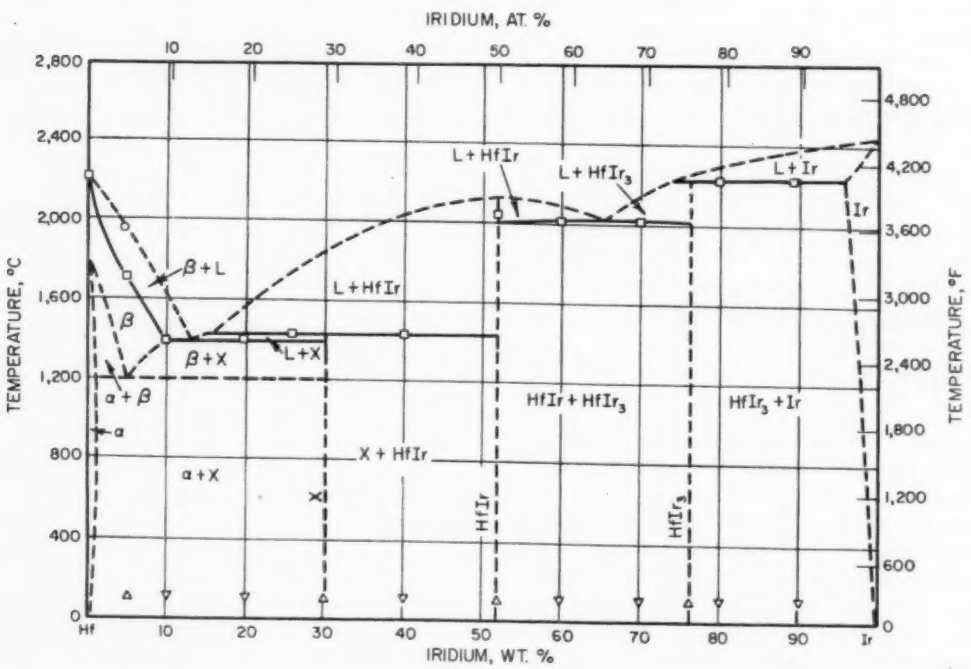


Fig. III-2 Hafnium-iridium phase diagram.[2] ○, liquidus. □, solidus. △, single phase. ▽, two phase.

swelled appreciably when briefly exposed to 570°F water.

Aerojet[4] has reported work on the evaluation of $Eu_2O_3$–stainless-steel dispersions for burnable poisons. A small quantity of unclad 5.8 wt.% $Eu_2O_3$–stainless-steel foil, fabricated at Battelle, was evaluated by boiling in distilled water to measure $Eu_2O_3$ loss to see if any reaction occurred. Several specimens were Kanigen-nickel plated in an effort to inhibit the europium loss observed in unplated specimens. After four weeks of exposure, no europium loss could be detected in the plated specimens.

General Electric[5] has continued study of europium sesquioxide and has reported the data shown in Table III-2 on five oxide phases and a hydroxide phase. Techniques for producing the newly reported phases are also described. The EuO phase is produced by reacting $Eu_2O_3$ and europium metal at 1000°C and by heating to 1450°C to remove excess europium. The orange Ortho I phase is produced by heating $Eu_2O_3$ in flowing hydrogen at 1420 to 1650°C. The Ortho II phase is produced by heating $Eu_2O_3$ to 2460°C in dry hydrogen for 5 min. The europium hydroxide [$Eu(OH)_3$] was prepared by reacting europium metal with water at room temperature. In studies on the stability of $Dy_2O_3$, $Sm_2O_3$, $Gd_2O_3$, and $Eu_2O_3$ in hydrogen, little change in weight and no change in structure occurred for the $Dy_2O_3$, $Sm_2O_3$, and $Gd_2O_3$ after 200 hr at 1650°C in dry hydrogen, but, under the same conditions, $Eu_2O_3$ lost 73.09% in weight and changed to the Ortho II structure.

Roberts and Barnes[6] have studied swelling in irradiated boron–steel control rods. A 4 wt.% boron–steel tube was irradiated for 30 months at 300°C (1460 Mwd/metric ton). No metallographic change was detected until segments were heated to 800°C; small bubbles (300 to 600 A) then appeared in the $Fe_2B$ particles. At 900°C, the overall volume increased approximately 5%, six bubbles were increased in size, and some bubbles appeared in the iron within recoil range of the $Fe_2B$ phase boundary. At 1000°C, the phase boundaries contained large irregular bubbles, which were the main cause of the overall volume increase (approximately 30% in 24 hr at 1050°C).

The British[7] are investigating other boron control materials. They irradiated samples of 8 wt.% $B_4C$ in stainless steel (clad and unclad), 10 wt.% $B_4C$ in copper clad with stainless steel, 3 wt.% boron in titanium (unclad), 3 wt.% boron in stainless steel (unclad), 1 wt.% $B^{10}$ in stainless steel (unclad), and 8 and 11 wt.% ferroboron (unclad) at exposures up to $3 \times 10^{21}$ neutrons/cm$^3$. The largest density change (−12.2%) was observed for the 1 wt.% $B^{10}$–stainless-steel rod, and the next largest changes (−7.2 to −11.9%) were observed for the ferroboron alloys and the unclad 8 wt.% $B_4C$–stainless-steel structures. Comparatively small density changes were observed for clad 8 wt.% $B_4C$–stainless steel (−1.94 to −5.1%), 10 wt.% $B_4C$–copper dispersions (−2.5 to −3.2%), and 3 wt.% boron in titanium (−4.5 to −5.4%), but direct

Table III-2 CRYSTALLOGRAPHIC DATA FOR EUROPIUM-OXYGEN COMPOUNDS[5]

| Phase | Color* | Crystal structure | Lattice parameters | X-ray density† | Optical properties |
|---|---|---|---|---|---|
| Monoclinic $Eu_2O_3$ | White | Monoclinic | $a$ = 14.042 A; $b$ = 3.638 A; $c$ = 8.746 A; and $\beta$ = 100° 0.7′ | 7.99 | Biaxial negative; $N_x$ = 2.07; and $N_z$ = 2.10 |
| Cubic $Eu_2O_3$ | White | Body-centered cubic | $a$ = 10.869 A | 7.283 | |
| EuO | Black-brown | Face-centered cubic | $a$ = 5.142 A | 8.207 | Opaque |
| Ortho I | Orange | Orthorhombic | $a$ = 5.63 A; $b$ = 7.08 A; and $c$ = 9.71 A | | Biaxial positive; $N_x$ = 1.92; and $N_z$ = 1.93 |
| Ortho II | Black | Orthorhombic | $a$ = 3.50 A; $b$ = 12.01 A; and $c$ = 10.07 A | | N's near 2.10 |
| $Eu(OH)_3$ | White | Hexagonal | $a$ = 6.35 A and $c$ = 3.67 A | | |

*Color of bulk material.
†Density calculated from lattice parameters.

comparisons cannot be made since irradiation temperatures varied from 125 to 325°C.

Keil and Hanks[8] have reported on the technique used to fabricate boral control rods for the KIWI reactors. They blended 80 wt.% aluminum and 20 wt.% $B^{10}$, hot pressed the mixture in large billets (15 in. by 4.5 in. by 0.4 in.), canned the billets in aluminum, and hot rolled at 800°C to a 0.070-in. thickness. They then removed the can and reduced the billets bare to a 0.050-in. thickness at 400°C and formed them to a $1\frac{7}{8}$-in. radius at 250 to 300°C.

Martin[9] has procured or fabricated specimens of $B_4C$ dispersed in $Al_2O_3$, $ZrB_2$ in Zircaloy-2, and $B_4C$–Zircaloy-2 dispersions that will be irradiated at pellet surface temperatures of about 500°C and examined in the Battelle hot cells. The $B_4C$–$Al_2O_3$ dispersions are hot pressed, and the Zircaloy dispersions are hot extruded.

Secrist[10] is studying the lithium-boron-carbon system. A lithium-carbon phase ($Li_2C_2$) was formed in lithium-carbon mixtures quenched from temperatures between 350 and 700°C. A lithium-boron phase ($B_{12}Li$) was reported to exist. In mixtures of $B_4C$ in lithium reacted at 600 and 700°C, both lithium boride and lithium carbide formed.

Spedding and Daane[11] have edited a book on rare earths. In addition to data on occurrence and preparation of rare-earth metals and alloys, there are discussions on the properties and applications of these materials. Some nuclear applications as control materials are discussed, and there are some data on the hydrides.

(G. W. Cunningham)

## References


1. R. G. Gray, W. Yeniscavich, and L. R. Lynam, Irradiation Behavior of Austenitic Stainless-Steel Burnable Poisons, USAEC Report WAPD-262, Westinghouse Electric Corp., Bettis Atomic Power Lab., August 1962.
2. Bureau of Mines, Metallurgical Quarterly Progress Report No. 15 for the Period of April 1, 1962, Through June 30, 1962, USAEC Report USBM-U-952.
3. Oak Ridge National Laboratory, Metals and Ceramics Division Annual Progress Report for Period Ending May 31, 1962, USAEC Report ORNL-3313, Aug. 16, 1952.
4. Aerojet-General Nucleonics, Army Gas-Cooled Reactor Systems Program. Semiannual Progress Report, January 1 Through June 30, 1962, USAEC Report IDO-28590, Aug. 17, 1962.
5. General Electric Co., Flight Propulsion Laboratory Dept., High-Temperature Materials Program. Progress Report No. 13, Part A, USAEC Report GEMP-13A, July 31, 1962.
6. E. Roberts and R. S. Barnes, An Investigation of Swelling in an Irradiated Boron–Steel Control Rod, British Report AERE-R-4021, April 1962.
7. United Kingdom Atomic Energy Authority, 1961. (Unpublished)
8. R. W. Keil and G. S. Hanks, Fabrication of Boral Control Plates for KIWI Reactors, USAEC Report LA-2737, Los Alamos Scientific Laboratory, Sept. 20, 1962.
9. C. Eicheldinger, PM Research and Development Program 4th Quarterly Progress Report, January 1, 1962, to March 31, 1962, USAEC Report MND-MD-2560-4, Martin Co., August 1962.
10. Knolls Atomic Power Laboratory, Reactor Technology Report No. 20—Metallurgy, USAEC Report KAPL-2000-17, March 1962.
11. F. H. Spedding and A. H. Daane (Eds.), *The Rare Earths*, John Wiley & Sons Inc., New York, 1961.

Section

IV

Reactor Materials

# Cladding and Structural Materials

## Corrosion

### Zirconium Corrosion

*Radiation Effects.* Oak Ridge has found that the corrosion resistance of zirconium alloys in in-pile circulating uranyl sulfate solutions is improved by excess additions of sulfuric acid.[1] It is believed that the excess acid reduces uranium sorption in the oxide film on the zirconium surface, with a consequent reduction in local intensity of fission recoils. The latter has been found to influence markedly the corrosion behavior of zirconium alloys under these conditions.

Harwell has reported[2a] effects of radiation on the corrosion of Zircaloy-2 in steam. Gamma radiation was found to produce a small increase in the rate of growth of thin (interference color) films at 400°C, but it had no effect on the thicker oxide films of interest in reactor technology. On the other hand, fast-neutron fluxes of greater than $10^{11}$ neutrons/(cm$^2$)(sec) decreased the time to transition and increased the posttransition oxidation rate [by a factor of about 8 at 340°C and $10^{13}$ neutrons/(cm$^2$)(sec)]. The fraction of corrosion-produced hydrogen which was absorbed by Zircaloy-2 was not greatly affected by irradiation, although the total amount absorbed increased under those conditions where irradiation increased the oxidation rate.

*Water and Steam.* Saclay has reported on the effects of alkaline solutions on the corrosion behavior of Zircaloy-2 and Zircaloy-4 in high-temperature water.[2b] Experiments conducted at 360°C indicated "critical thresholds" where corrosion increased at concentrations above 2 g of LiOH per liter or 12 g of NaOH per liter. No critical threshold was observed for solutions containing up to 28 g of KOH or $NH_4OH$ per liter. Severe crevice corrosion and hydriding occurred in Zircaloy crevice specimens exposed to solutions containing more than 0.024 g (*p*H 11) of LiOH per liter and more than 8 g of NaOH per liter. No crevice effects were noted in the KOH and $NH_4OH$ solutions studied. It was believed that the solution in the crevices became concentrated by the depletion of water as it reacted with the zirconium to form $ZrO_2$ and hydrogen.

Corrosion results for zirconium–2.5 wt.% niobium in water, air, and $CO_2$ have recently been summarized by Chalk River.[2c,3] The alloy was found to have acceptable resistance to 325°C water, but it was not as good as Zircaloy-2. Its resistance to air and $CO_2$ at 300 to 500°C was less favorable. Additions of tin or iron and chromium to the alloy did not improve its corrosion resistance. Additions of copper improved its resistance in water and steam to some extent and its resistance to air and $CO_2$ to a greater extent. Thermal flux of 3 to $7 \times 10^{13}$ neutrons/(cm$^2$)(sec) had little or no effect on oxidation and hydriding in high-temperature water. Heat-treatment studies suggested that the amount of niobium in solution in the alloy controlled the rate of oxidation and hydriding and that concentration, size, and distribution of second phase were of little importance.

Italian scientists[2d] have studied the corrosion behavior of Zircaloy-2 in flowing wet steam at 200 to 300°C. Corrosion rates were found to increase with increasing specific mass-flow rate in the range investigated, 295 to 553 g/cm$^2$.

Boric acid has been found to improve markedly the corrosion behavior of zirconium crystal bar in 500°C, 1000-psi steam tests conducted at Harwell.[4] Greater than 0.03 g of $H_3BO_3$ per gram of steam resulted in corrosion rates of 30 mg/dm$^2$ after a 24-hr exposure,

as compared with 5400 mg/dm$^2$ with no $H_3BO_3$. Weight gains after 70 days were about 120 mg/dm$^2$ in the $H_3BO_3$-inhibited steam. Boric acid had much less effect on Zircaloy-2; it reduced the corrosion rate by one-half. It had no effect on the corrosion rate of zirconium–0.5 wt.% copper–0.5 wt.% tungsten alloy. Alloying with boron was less effective in improving corrosion behavior than adding $H_3BO_3$ to the steam.

Harwell[5] has recently summarized its corrosion studies in 400 and 500°C steam. An alloy-development program has shown that certain alloys containing copper, copper-tungsten, iron, chromium, chromium-nickel, or chromium-iron were most resistant, whereas those containing silver, copper-molybdenum, copper-niobium, gold, chromium-vanadium, chromium-vanadium-nickel, iron-tungsten, or chromium-vanadium-iron-tungsten-nickel were least resistant. Alloys containing nickel, copper, cobalt, or chromium showed an increased percentage of hydrogen pickup after transition (like Zircaloy-2), whereas unalloyed zirconium, binary iron alloys, and 0.5 wt.% copper–0.5 wt.% tungsten alloy did not. Mechanism studies have led to the following conclusions: (1) it is the residual amount of the added element throughout the oxide film which is responsible for improved properties and (2) intermetallic precipitates are irrelevant, except so far as they ensure that all parts of the oxide receive the appropriate addition.

*Oxidation.* Work performed at Vallecitos[2e] on zirconium oxide has revealed a grain-boundary network of oxygen-saturated alpha zirconium after hot pressing. Oxidation of the as-pressed oxides resulted in preferential oxidation of the metallic phase and intergranular shattering of the oxide. Since metallic zirconium has been reported in $ZrO_2$ that has been cooled after heating above the eutectoid temperature, the Vallecitos scientist speculates that transition in the water and steam corrosion of zirconium may be related to impurity elements that drastically lower the eutectoid temperature of the oxide. Metallic zirconium might be formed upon cooling from the corrosion temperature, and its oxidation upon subsequent exposure could cause cracking of the oxide film.

A technique has been developed by Westinghouse[6] as an alternative method to the autoclave test for obtaining protective oxide films on zirconium alloys. Exposure to dry oxygen at 2 psig and 750°F resulted in lower hydrogen pickup, simpler test procedures, and less cost as compared with conventional steam-autoclave testing.

General Nuclear has completed a study[7] of the long-term corrosion behavior of zirconium alloys in $CO_2$ at 800 to 1292°F and 15 to 500 psi. Binary additions of copper, cerium, beryllium, antimony, vanadium, nickel, lead, barium, molybdenum, manganese, palladium, or chromium improved the corrosion resistance of zirconium. Binary additions of titanium, yttrium, niobium, or tellurium had a deleterious effect. When the $CO_2$ pressure was increased, the corrosion of poor alloys increased, but it had no effect on the better alloys. The 0.5 wt.% copper–0.5 wt.% molybdenum ternary alloy had the best overall corrosion resistance; it exhibited very little attack (about 150 mg/dm$^2$) after 17,000 hr at 800°F, moderately heavy attack (about 1000 mg/dm$^2$) after 18,000 hr at 1050°F, and heavy attack (about 1200 mg/dm$^2$) after 5500 hr at 1150°F.

*Hydriding.* Westinghouse[8] has conducted in-reactor water-corrosion studies with intentionally defected Zircaloy-2-clad $UO_2$-core fuel elements. It was found that heavy hydriding occurred only in the presence of a defect, and it occurred very rapidly, in a matter of hours. Since the corrosion process was too slow to account for the rapid pickup, it was believed that the radiolytic decomposition of the water offered the best hypothesis for the source of hydrogen. (W. E. Berry)

## Aluminum Corrosion

Argonne[9] has found evidence that indicates different corrosion mechanisms for low-silicon aluminum-nickel alloys in 260 and 360°C water. One-half to two-thirds of the oxide film was removed from specimens previously exposed to 260°C water, and the specimens were then returned to 260°C water. An increase in the amount of corrosion was noted, which suggests that a significant thickness of the corrosion film was involved in determining the corrosion rate. Similar experiments conducted earlier in 350°C water had shown no increase in corrosion after grinding and upon reexposure, which indicated that the rate-determining barrier was close to the metal-oxide interface.

An aluminum–1 wt.% rhodium alloy has exhibited the lowest corrosion rates ever obtained in 290°C water at Argonne. Metallographic and polarization characteristics of this alloy are being examined for clues as to its superior corrosion resistance at 290°C.

A 270-day corrosion test of aluminum-powder products in refreshed distilled water at 290°C has recently been completed.[10] Of 15 extrusions tested, 10 exhibited penetrations of 0.002 to 0.003 in. These had been prepared for aluminum–1 wt.% nickel–0.5 wt.% iron–0.1 wt.% titanium or aluminum–1 wt.% nickel–0.1 wt.% titanium powders to which had been added 3 to 8 wt.% $AlPO_4$, $SiO_2$, ZrC, and SiC. The five extrusions that failed prior to 270 days contained various percentages of $Al_2O_3$ and a 10 wt.% ZrC matrix and were extruded at a lower temperature.

Hanford[11] has studied the effect of molybdic acid, $H_2MoO_4$, additions at *p*H 4.5 on the 300°C water-corrosion behavior of X-8001 aluminum. The $H_2MoO_4$ produced results similar to those for *p*H 4.5 $HNO_3$, but neither acid was as effective as *p*H 4.5 $H_3PO_4$ in reducing corrosion behavior. Equilibrium corrosion rates with $H_2MoO_4$ were 0.34 mil/month, and with $H_3PO_4$ they were 0.27 mil/month.

An engineering viewpoint of the stress-corrosion cracking of aluminum and aluminum alloys has recently been presented by Alcoa scientists.[12] The articles indicate that most wrought high-strength aluminum alloys are susceptible to stress-corrosion cracking to some degree, depending upon temper, product, and section size, as well as magnitude and direction of stress. Tabular data are presented for laboratory tests which indicate maximum stress levels at which failures did not occur as related to alloy, temper, and product (plate, bar, extrusion, or forging). Methods of avoiding stress-corrosion cracking are also discussed.

(W. E. Berry)

## Stainless-Steel Corrosion

Oak Ridge[2f] has summarized the results of oxidation, carburization, and decarburization reactions of type 304 stainless steel with $CO_2$ and $CO$-$CO_2$ atmospheres and at temperatures between 425 and 982°C. Oxidation rates were found to be governed by the type of oxide formed and by the temperature. When $Fe_3O_4$ was the major surface-reaction product, the oxidation rate was also dependent on $CO_2$ pressure and the ratio of $CO_2$ to CO. Carburization and decarburization occurred simultaneously in a complicated manner that was dependent upon the carburizing potential $(CO)^2/CO_2$ of the gas, the temperature, and the type of oxide formed on the metal surface.

Harwell[13] has also reported on the oxidation of stainless steel (20 wt.% chromium–25 wt.% nickel, niobium stabilized) in $CO_2$ at 76 mm pressure and 600 to 800°C. Weight gain after 300 hr at 750°C was 70 $\mu g/cm^2$, and the oxidation rate was 0.08 $\mu g/(cm^2)(hr)$. The major oxidation reaction was associated with the generation of CO. A second possible reaction involved carbon deposition during the first few hours of oxidation. It is believed that this carbon first diffused into the steel where a carbon gradient was set up. A small fraction then slowly diffused out again through the oxide film and reacted with $CO_2$ at the gas/oxide interface. The carbon originally in the steel was believed to remain immobilized, and only the deposited carbon behaved in this manner.

The scaling behavior of superheater-tube alloys has been reported[14] by Babcock & Wilcox Co. Ferritic steels containing up to 9 wt.% chromium exhibited heavier scales after a 12-month exposure at 1100 to 1200°F than did austenitic alloys exposed 18 months at 1200 to 1500°F. Steam appeared to be no more corrosive than air at the temperatures investigated. All alloys except type 310 stainless steel, Inconel, and Incoloy displayed a tendency for flaking and exfoliating, which increased with temperature and time. Of the austenitic materials, these three alloys had the thinnest scales, 17-14 CuMo and 15-15 N (CrNi) had the thickest scales, and the 18-8 type stainless steels and 16-25-6 had scales of intermediate thickness.

Du Pont[15] has studied the stress-corrosion behavior of 17-4 PH stainless steel in 240°C $D_2O$ at *p*H 10.5 (adjusted with LiOH). Notched and unnotched stressed specimens were exposed to the liquid vapor. Only the notched specimens that were given a final 900°F aging treatment were cracked after a 3900-hr exposure. Other heat-treatments investigated were: solution treated, aged at 1100°F, and cold worked prior to aging at 900°F or 1100°F.

Vallecitos[16] has conducted laboratory experiments to determine the cause of transgranular

and intergranular failures that occurred in a type 304 stainless-steel-clad fuel element in the Vallecitos Boiling-Water Reactor superheated-steam loop. The failure was attributed to heavy-metal chloride deposition and occasional "wet" conditions. These resulted in transgranular stress-corrosion cracking at temperatures below 1000°F and in intergranular attack from heavy-metal chlorides (particularly $CuCl_2$ and $FeCl_3$) at higher temperatures where the stainless steel was sensitized.

American[17] and Russian[18] scientists have recently reported on the effects of time and temperature on the nature of grain-boundary carbide precipitates and the susceptibility to intergranular corrosion during sensitization of austenitic stainless steels. Long-time (up to 1500 hr) heat-treatments by the Americans at about 1050 to 1200°F produced sheets of connected small particles, whereas at higher temperatures (above 1350°F) the carbides occurred as isolated dendritic particles. Exposure to the Strauss corrosion test produced maximum etching in those specimens sensitized at the higher temperature where the precipitate was a maximum. However, bend tests after corrosion revealed considerable ductility in specimens treated at the higher temperatures and extreme brittleness with cracking, and often complete disintegration, in those treated at low temperatures. (W. E. Berry)

## Corrosion of Base-Metal Alloys and Yttrium

*Aqueous Corrosion.* The Martin Co. has summarized four years of study on alloys for service in pressurized-water reactors.[19] Tests were carried out in simulated primary and secondary waters in tilting autoclaves, miniature heat exchangers, model boilers, and superheaters. Of the alloys tested, Inconel possessed superior overall corrosion resistance; Monel and nickel pitted somewhat; type 430 stainless steel, carbon steel, and Croloy 16-1 pitted severely when oxygen was present; and type 347 stainless steel exhibited stress-corrosion cracking in the presence of chlorides and oxygen.

The corrosion behavior of carbon steels and other steels in simulated boiling-water-reactor environments has been reported[20] by Vallecitos. Corrosion rates of steels containing up to 5 wt.% chromium averaged less than 10 mg/(dm$^2$)(month) after a 5289-hr exposure to water and steam at 546°F (steam contained 10 to 20 ppm oxygen and 1 to 2 ppm hydrogen). However, steels containing up to 5 wt.% chromium were found to pit and rust during reactor shutdown when the water was near room temperature and had access to air. A stressed specimen of type 431 martensitic stainless steel cracked in the high-temperature steam-water environment, but no cracking occurred with ferritic stainless steels, austenitic stainless steels, or the alloys containing up to 5 wt.% chromium.

Hanford[21] has investigated the effect of heat-treatment on the corrosion behavior of A-212 carbon steel in flowing 290°C water adjusted to *p*H 10 with LiOH. Stress relieving at 700°F, annealing at 1192 or 1450°F, normalizing at 1650°F, or cold working had no effect on corrosion rates. The penetration rate was 0.15 mil/year after a 2700-hr exposure, and crud ($Fe_3O_4$) release rate became linear at 0.41 mg/(dm$^2$)(day) after a 500-hr exposure.

Mellon Institute[22] has reported on the stress corrosion of high-strength steels and alloys in artificial environments of 1 mole NaCl, $NaNO_3$, $Na_2SO_4$, $(NaPO_3)_2$, or $Na_2S$. All martensitic alloys showed a susceptibility to stress-corrosion cracking in varying degrees. Precipitation-hardening alloys showed less susceptibility or none at all. In the $\mu$-bend tests, decarburizing the metal surface reduced the failure rate by several orders of magnitude, whereas alloying with uranium decreased the failure rate by one order of magnitude. Organic coatings were not too effective in inhibiting cracking.

*Gaseous Corrosion.* In experiments reported by Aerojet-General,[23] which are related to the ML-1 reactor turbine, several alloys have been found to be resistant to gaseous environments. Inconel, Inconel 713C, Incoloy 901, N-155 (Multimet alloy), and type 347 stainless steel exhibited negligible corrosion after a 5000-hr exposure to 1300°F air, nitrogen, or 99.5 vol.% nitrogen–0.5 vol.% oxygen. Type 304 stainless steel showed negligible corrosion after a 5000-hr exposure to these same gases at 900°F (maximum anticipated temperature for type 304 stainless steel).

Results of continuing tests in static air at 1300°C, conducted by General Electric,[24] have indicated that iron–25 wt.% chromium–4 wt.% aluminum alloys containing 1 wt.% thorium or 1 wt.% yttrium are more oxidation resistant

than any other known heat-resistant alloy. Penetrations after a 1000-hr exposure were less than 0.001 in.

Tests of 24-hr duration at Ames[25] on the air oxidation of high-purity yttrium in the temperature range of 500 to 950°C produces weight gains of 5 to 12 mg/cm$^2$. Long-term tests of up to 448 hr revealed that specimens formed a semiprotective oxide film on the surface, and weight gains leveled off after a few hours at temperatures between 500 and 800°C. Above 800°C the specimens were completely oxidized after several hundred hours. Except for fluorine, binary additions ranging up to 0.5 wt.% of the impurity elements normally found in yttrium had no effect on oxidation behavior.

Australian scientists have reported[26] additional information on the corrosion of chromium steels in $CO_2$. The corrosion of 1 wt.% chromium–0.5 wt.% molybdenum and of 2.25 wt.% chromium–1 wt.% molybdenum alloys was measured at 450 to 500°C, and that of a 12 wt.% chromium–1 wt.% nickel alloy was measured at 600 to 725°C. Weight gains obtained were dependent on temperature, and they varied little with gas pressure, water content of gas, or surface treatment of the metal. After a 1000-hr exposure under semistatic conditions, the weight gains varied from 1.7 to 5.2 mg/cm$^2$ for the low-chromium alloys and from 0.05 to 0.47 mg/cm$^2$ for the 12 wt.% chromium alloy.

Windscale has published a tabular reference[27] on compatibility of materials with $CO_2$ in the temperature range of 350 to 700°C. Data are also included for behavior of materials paired with beryllium, Magnox, magnesium, uranium, and other materials.

*Atmospheric Corrosion.* The effect of induced radioactivity on the atmospheric corrosion behavior of Armco iron and steel has been reported by Russian scientists.[28] Samples were subjected to $0.87 \times 10^{13}$ neutrons/(cm$^2$)(sec) and then exposed to an atmosphere of 100% relative humidity. Corrosion rates of the irradiated samples were many times greater than those of unirradiated samples (178 times greater for Armco iron and 107 times greater for carbon steel after a 30-day exposure). The rate of corrosion was directly proportional to the specific activity induced. It is believed that lattice defects caused by the radiation accelerated cathodic corrosion. (F. W. Fink)

## Corrosion of Uncoated Refractory Metals

*Aqueous Corrosion.* Studies of the corrosion of selected niobium-base materials in various aqueous media[29] showed that niobium exhibits excellent resistance to corrosion in most media, approximating the behavior of its sister element, tantalum. However, alloying to substantially improve strength or oxidation resistance of niobium at elevated temperatures (D-31, niobium–10 titanium–10 molybdenum, for example) results in pronounced degradation of the ability of niobium to resist aqueous corrosion.

The Russians report that the resistance of molybdenum to corrosion by aqua regia or nitric-oxalic acid solutions at room temperature can be improved by alloying with tungsten.[30] In aqua regia, an alloy containing 20 at.% tungsten is required to achieve improved performance, whereas in the nitric-oxalic acid solution, 50 at.% tungsten is required. The improved performance is attributed to the formation of a thin (0.1 to 0.2 $\mu$) tungsten-rich surface layer.

*Oxidation.* Investigations at Research Chemicals Div., Nuclear Corp. of America, of rare-earth-metal additions to niobium and its alloys[31] showed no significant improvement in 1000°C oxidation behavior which was attributable to the rare-earth additions.

Studies at General Electric[32] were directed toward development of niobium-titanium-aluminum alloys with auxiliary additions of chromium or silicon for use as oxidation-resistant coating materials. These alloys, whose compositions generally resulted in the (Nb,Ti)Al structure, exhibited excellent low-temperature (650 to 815°C) behavior but were less attractive at temperatures in excess of 1095°C, judged by weight-change data.

The oxidation behavior of tungsten was the subject of investigations recently completed at Ohio State University.[33] The subject was treated to ascertain:

1. Thermodynamic and phase equilibria in the tungsten-oxygen system.
2. Kinetics of oxidation of tungsten at low pressures.
3. Volatilization of oxides as affected by water vapor.

Thermodynamic studies indicated that $WO_3$ is unstable at temperatures above 725°C, $W_{18}O_{49}$ is unstable at temperatures below 585°C, $W_{20}O_{58}$

is unstable at temperatures below 485°C, and $WO_2$ and $WO_3$ phases are stable to very high temperatures. Reduction in the partial pressure of oxygen decreases both the parabolic and linear constants of the oxidation process and also increases the thickness of the blue oxide phase ($W_{18}O_{49}$ or $W_{20}O_{58}$ ?). Volatilization rates in general increase linearly with water-vapor partial pressure and also increase with temperature in accordance with the Arrhenius relation. The compound $WO_3$ is the most volatile species, followed by $W_{18}O_{49}$ and then $WO_2$.

A General Electric patent[34] describes the improvement in resistance of chromium to oxidation and nitrogenation at high temperatures by alloying with from 0.5 to 6 wt.% of rare-earth elements. (E. S. Bartlett)

## Corrosion of Coated Refractory Metals

Recent developments of major significance in the field of coatings for refractory metals[35] include announcement of Chromalloy's W3 coating for molybdenum alloys. This coating displayed an average life of 812 hr at 1370°C or 268 hr at 1480°C in air over the molybdenum–0.5 titanium substrate. Low-pressure failure of $MoSi_2$ coating at reentry temperatures (1370 to 1650°C), wherein the temperature for a 30-min coating life is reduced by some 165 to 275°C, has been attributed to $SiO_2$ instability and SiO volatilization under the low-pressure conditions defined at Lockheed.

Investigations at Borolite[36] demonstrated that $MoSi_2$ and $WSi_2$, attractive coating materials for molybdenum and tungsten, respectively, reacted readily with carbon. The presence of carbon, in either solid or gaseous form, resulted in serious deterioration of the disilicides.

In studies at General Electric,[32] modified aluminide coatings for niobium were found to be permeable to nitrogen at 1370°C. After exposure to air for 25 hr, the niobium substrate increased from 160 to 756 ppm nitrogen. Furthermore, coatings in the niobium-titanium-aluminum systems exhibit excessive diffusional instability with niobium substrate. Diffusion depletion of the coating (20 mils in 10 hr at 1370°C) resulted in the loss of oxidation resistance of the coating material. Moderate efforts on aluminide coatings modified with silver or tin showed retained liquid phase at elevated temperatures, which may act beneficially to buffer thermal-shock effects.

(E. S. Bartlett)

## Corrosion by Liquid Metals and Fused Salts

A program at Argonne to provide lightweight mercury-resistant alloys is continuing. Nitrided titanium alloys have shown promise, and, in a recent test series, samples of the following alloys, nitrided and in the as-polished condition, were exposed for 14 days to 1000°F mercury and mercury vapor: titanium–2.5 wt.% aluminum–16 wt.% vanadium, titanium–3 wt.% aluminum–5 wt.% chromium, titanium–7 wt.% aluminum–12 wt.% zirconium, and titanium–8 wt.% molybdenum. In liquid mercury,[37] weight gains of the nitrided specimens ranged from 0.07 to 0.13 mg/cm$^2$, whereas the as-polished specimens lost from 20 to about 80 mg/cm$^2$. In mercury vapor, nitrided-sample weight gains were in the 0.64 to 2.82 mg/cm$^2$ range. Subsequent metallurgical examinations[38] showed:

1. A high degree of mercury-vapor attack for the nitrided titanium–7 wt.% aluminum–12 wt.% zirconium and titanium–3 wt.% aluminum–5 wt.% chromium alloys but little attack by liquid mercury.
2. Little effect either by vapor or liquid on the nitrided titanium–8 wt.% molybdenum alloy. However, considerable recrystallization occurred.
3. Moderate uniform type attack of the nitrided titanium–2.5 wt.% aluminum–16 wt.% vanadium alloy also accompanied by pronounced recrystallization.

Oak Ridge investigators[39] found $CF_4$ in an irradiation capsule above graphite boats containing the molten fluoride salt LiF-$BeF_2$-$ZrF_2$-$ThF_4$-$UF_4$ (69.5–23–5–1–1.5 mole %); this mixture is the reference fuel for the Molten-Salt Reactor. This escape of $CF_4$ is viewed as quite important since it represents a significant chemical change in the fuel. A possible countermeasure is an overpressure of $CF_4$ in the reactor system, but this introduces a question regarding core-materials compatibility. To explore this question, samples of INOR-8 were immersed in fluoride melts and suspended in a CF-vapor zone above the melts. Results indicated that the presence of $CF_4$ did not affect the 600°C resistance of INOR-8 to attack (negligible weight loss and no surface change after a 1000-hr exposure). However, it appeared that some minor effects occurred at 700°C.

DiStefano and Hoffman[40] have summarized corrosion data in refractory-metal–lithium

systems. The work covered dealt primarily with the effect of oxygen on the corrosion process, and it led to several conclusions, some of which have been outlined in past reviews. One such conclusion is that the presence of small quantities of oxygen in either niobium or tantalum can result in rapid corrosion by lithium. The attack of oxygen-containing niobium is characterized by the formation of a corrosion product most often found either in the grain boundaries or along (1 1 0) planes. In addition to lithium penetration, transfer of oxygen in refractory-metal–lithium systems appears to occur according to Nernst's Law of distribution for a solute between two immiscible solvents. (J. H. Stang)

## Metal-Water Reactions

The results of an extensive study of the zirconium-water reaction using the condenser-discharge method were reported recently by Argonne.[41] The reaction was studied with initial metal temperatures from 1100 to 4000°C and with 30- and 60-mil wires in water from room temperature to 315°C (1500-psi vapor pressure). Runs in heated water showed markedly greater reaction. This was explained in terms of a two-step reaction scheme in which the reaction rate is initially controlled by the rate of gaseous diffusion of water vapor toward the hot metal particles and of hydrogen, generated by reaction, away from the particles. At a later time the reaction becomes controlled by the parabolic rate law, which results in rapid cooling of the particles.

A mathematical model of the reaction of molten-metal spheres with water was proposed, and the equations describing the reaction were programmed on an analog computer. The parameters of the parabolic rate law were obtained empirically from the computer solutions and by reference to two previous isothermal studies of the zirconium-water reaction. These are plotted in Fig. IV-1. The following rate law was deduced:

$$w^2 = 33.3 \times 10^6 t \exp(-45{,}500/RT)$$

where $w$ is milligrams of zirconium reacted per square centimeter of surface area and $t$ is time in seconds.

The total extent of reaction of zirconium spheres suddenly brought into contact with water was found to depend primarily on the water temperature and on the sphere diameter. The theoretical curves for this dependence are plotted in Fig. IV-2 along with the curves for reaction to constant depths of metal of 25 $\mu$ and 60 $\mu$. The curve for 25 $\mu$, which corresponds roughly to the results in room-temperature water, was previously proposed by Aerojet for reaction in room-temperature water, whereas that for 60 $\mu$ shows limited agreement with the heated-water curve.

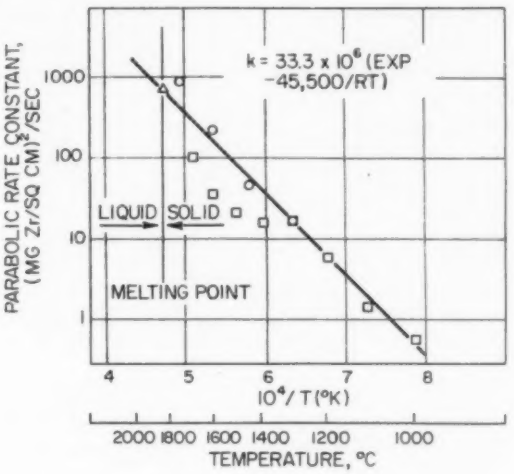


Fig. IV-1 Effect of temperature on the zirconium-water reaction.[41] Δ, condenser-discharge method. ○, Bostrom, WAPD-104 (recalculated). □, Lemmon, BMI-1154 (recalculated).

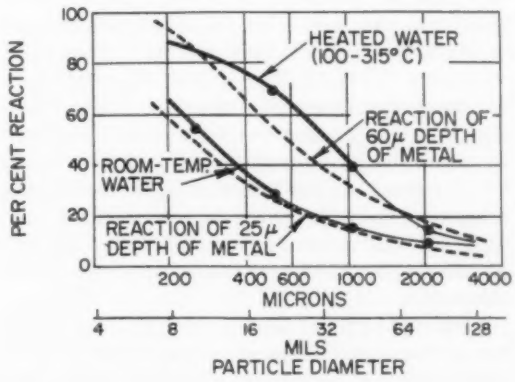


Fig. IV-2 Extent of reaction as a function of particle diameter for molten-zirconium spheres formed in water.[41] Theoretical curves: —— rapid reaction (1 to 5 msec); —— slow reaction.

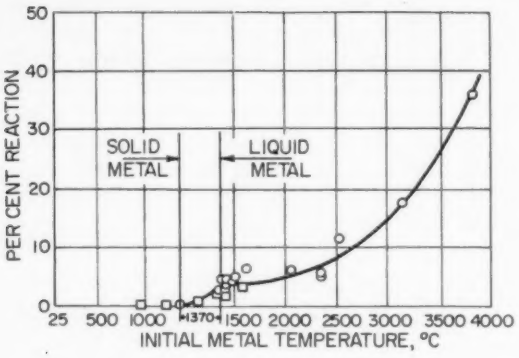


Fig. IV-3 Reaction of type 316 stainless steel with water by the condenser-discharge method.[42] Room-temperature water. ○, 30-mil wires. □, 60-mil wires.

Decreased extent of reaction in room-temperature water was best described on the assumption that in room-temperature water the effective vapor pressure of water (driving diffusion) is one-half the value in heated water. Explosive reactions were found to occur with particles smaller than about 1 mm in heated water and 0.5 mm in room-temperature water. The explosive reactions were due to the ability of the evolving hydrogen to propel the particles through water at high speed. The high-speed motion, which was detected on motion-picture film, had the effect of removing the gaseous diffusion barrier, resulting in very rapid reaction.

The extent and rate of reaction depended on the particle diameter and on the water temperature, and they were relatively independent of the metal temperature so long as the metal was fully melted. This makes it possible to estimate the extent of zirconium-water reaction that would occur during a reactor accident in which the particle sizes of the residue could be estimated. Comparisons were made with the results of meltdown experiments in the Transient Reactor Test Facility (TREAT), and applications to reactor-hazards analysis were discussed.

Additional studies reported by Argonne[42] pertain to the stainless-steel–water reaction. Runs completed to date using the condenser-discharge technique were made in the high-pressure reaction cell. Room-temperature water was used for the runs. Runs were made with 30- and 60-mil wires. Results are shown in Fig. IV-3. It is evident that there is no significant reaction up to the melting point of stainless steel (1370°C). Pressure rises were probably explosive in the very energetic runs reported.

(A. W. Lemmon, Jr.)

# Radiation Effects in Nonfuel Materials

## Defects: Structure and Properties

*Metals.* A note[43] presented by Cleland et al. points out that the lattice defects produced by the action of gamma rays emanating from shielding material should be considered in all reactor irradiation experiments in which shielding against thermal neutrons is employed. At least an order of magnitude more defects were noted for cadmium-shielded experiments than for boron-shielded experiments. This is because cadmium emits energetic gamma rays (over half are between 1 and 5 Mev) upon neutron capture, whereas boron captures neutrons by an $(n, \alpha)$ reaction, and the alphas are essentially stopped in the shield. The amount of damage was inferred from measurements of the Hall coefficient in high-purity *n* type silicon and germanium irradiated at 40°C under the assumption that two carriers are removed per Frenkel pair. Most predictions of damage owing to gamma rays have been based on results from experiments using the $Co^{60}$ gamma rays (1.3 Mev). The experimental results reported here using secondary gammas (up to 5 Mev) more nearly approach theoretical predictions. This improvement in agreement between theory and experiment implies that either the theory becomes more valid as the energy of the incident radiation increases beyond the threshold or else that the defects produced by the relatively more energetic cadmium gamma rays are more resistant to thermal annealing at 40°C.

The changes in residual electrical resistance produced by bombardment with high-energy electrons[44] were measured for a number of metals as a function of electron energy in the range 0.5 to 1.4 Mev. The irradiations were performed at <20°K, and recovery measurements were made up to 300°K. The production curves were analyzed by use of the simple displacement theory, and the following values were found for the average threshold energies: aluminum, 32 ev; gold, >40 ev; silver, 28 ev;

copper, 22 ev; iron, 24 ev; molybdenum, 37 ev; nickel, 24 ev; titanium, 29 ev; and tungsten, >35 ev. Approximate values for the resistivities of Frenkel pairs (in units of microohm-centimeters per atomic percent) were also obtained as follows: aluminum, 3.4; silver, 1.4; copper, 1.3; iron, 12.5; molybdenum, 4.5; nickel, 3.2; and titanium, 42. In the case of aluminum, it was necessary to take secondary-defect production into account, and a number of representative theoretical curves, based on different assumptions concerning the process of secondary-defect production, are included. The behavior of zinc was anomalous in that the added resistivity was not a linear function of electron dose at 20°K. In a second paper,[45] it is shown that there is an empirical correlation between these point-defect resistivities and the normal, high-temperature electrical resistivities of different metals. The threshold energies are discussed, and extrapolations are made to predict values for certain metals whose threshold energies have not yet been measured. The low-temperature (Stage I) recovery of most of the metals studied is shown to be qualitatively similar to that in copper, and the correlation of recovery temperatures with certain bulk properties is discussed. The radiation-damage parameters derived from the electron results are used to compare theory and experiment for irradiations performed with heavy particles. It is shown for neutron irradiations that there is a general tendency for the simple displacement theory to give better agreement with experiment as the atomic weight of the bombarded material increases.

Quenching and annealing experiments[46] on 99.998% pure silver led to the following observations: The energy required to form a lattice vacancy is $1.10 \pm 0.04$ ev. The activation energy required to move a lattice vacancy is $0.83 \pm 0.05$ ev. In specimens quenched from above 600°C, most of the defects observed annealed with an activation energy of $0.57 \pm 0.03$ ev. Pulse heating breaks up the 0.57-ev defect; at least one of the fragments thus produced is a single vacancy having a migration energy of $0.83 \pm 0.05$ ev. It is suggested that the 0.57-ev defect is a divacancy. Pulse heating establishes the binding energy of the 0.57-ev defect to be $0.38 \pm 0.05$ ev. When a quenched specimen is annealed below 0°C, the 0.57-ev defect anneals by second-order kinetics. When a quenched specimen is annealed above 90°C, one observes a fast annealing (approximately first order with energy of motion $0.60 \pm 0.06$ ev), followed by a slow annealing process having an energy of motion of $0.80 \pm 0.1$ ev. It is suggested that above 90°C the 0.57-ev defect does not cluster, but migrates to dislocations. The fact that below 0°C the 0.57-ev defect forms clusters, whereas above 90°C it does not, leads to a binding energy for quadrivacancies of $0.30 \pm 0.08$ ev.

The resistivity of molybdenum wires that were neutron irradiated at liquid-nitrogen temperatures showed recovery peaks at 130 and 440°K, with associated activation energies of $0.40 \pm 0.04$ ev and $1.23 \pm 0.06$ ev, respectively.[47] The activation energy increases linearly with temperatures between 80 and 350°K, where, in a rather discontinuous way, a 0.25-ev higher value is reached, which remains practically constant up to 480°K. It is suggested that the 1.23-ev stage is basically governed by the same processes as the third annealing stage in the face-centered cubic metals. Annealing was continued up to 800°K. Recovery of neutron damage above room temperature in niobium and tantalum was observed[48] at 120°C with an activation energy of $1.22 \pm 0.02$ ev and at 160°C with an activation energy of $1.25 \pm 0.08$ ev, respectively. Similar results were observed in deformed samples, except that the tantalum recovery occurred at 120°C.

Franklin Institute has presented its annual report on studies of the basic mechanisms of the neutron damage in metals.[49] The two principal courses of study for the previous year were: (1) transmission-electron microscopy of thinned-down portions of copper, nickel, and molybdenum in both the strained and the unstrained state and (2) dilatometric measurements of the permanent changes in length of irradiated-copper single crystals after annealing at various temperatures. Study of prismatic dislocation loops observed in irradiated copper but not in irradiated nickel has been continued. By certain treatment, structures that might be small prismatic loops have been observed in irradiated nickel. The dilatometry measurements revealed a density change in copper between 200 and 350°C, which may correspond to changes reported elsewhere in the electrical resistivity and mechanical properties of copper in this temperature range. In other work at Franklin Institute,[50] electron microscopy of thin sections showed that the point defects

in stainless steel tend to form three-dimensional aggregates with no associated stress fields. These anchor "old" dislocations in the material, lead to climb during glide in "new" dislocations, and, by inference, cause other effects in the bulk material.

Bierlein et al. at Hanford have been studying neutron damage in high-purity molybdenum foils with the electron microscope.[51] Also, lattice-parameter increases of the order of 0.023% in as-rolled material were observed with X-ray diffraction.[52] Recovery by annealing of the radiation-produced microhardness was studied. The recovery occurred in a single stage, centered at 1025°C. Two separate processes, one with an activation energy of 2.2 ev and the other with about 4 ev, produced this annealing. The 4-ev process is described as recrystallization. No orders were determined.

Hardening effects produced in copper crystals by 4-Mev electron irradiation were investigated by measuring critical shear stresses.[53] The whole stress-strain curve was raised to higher stresses. The effect is independent of temperature below a dose of about 5 $\mu$a/(hr)(cm$^2$); above this dose the critical shear stress of specimens irradiated at 20°C saturated at 0.5 kg/mm$^2$. Specimens irradiated at −195°C continue to harden and, after 100 $\mu$a/(hr)(cm$^2$), they have a critical shear stress of 1 kg/mm$^2$. Annealing at 20°C of the low-temperature-irradiation specimens produced about a 10% recovery. Annealing of the damage in 20°C irradiated specimens commences at 80°C and continues to 400°C, showing no discrete recovery stages. Thin-film electron-microscopy studies revealed no clustered damage. The absence of the displacement spikes is shown to have a profound effect on these samples, based on a comparison of their damage with that produced in similar samples by neutron irradiation.

Dislocation loops in aluminum formed after bombardment with 38-Mev alpha particles have been studied with transmission-electron microscopy and selected-area diffraction.[54] The loops generally lie on {1 1 0} planes with a [1 1 0] Burgers vector normal to the loop. However, these loops are seen only where the alpha particle comes to rest. Analysis with diffraction-contrast methods indicates that the loops are interstitial loops, as has been previously suggested from their annealing behavior.[55] Piercy and Whitton,[56] in their latest work, have not observed dislocation loops (> 50 A in diameter) in annealed samples of fast-neutron ($4 \times 10^{19}$ neutrons/cm$^2$)-irradiated aluminum. The only samples showing loops were previously deformed aluminum or an aluminum−1.0 wt.% magnesium alloy quenched from 600°C into brine. Bierlein and Mastel,[57] on the other hand, found small dislocation loops in annealed aluminum (600°C for 1 hr) after fast-neutron irradiation ($3 \times 10^{18}$ nvt, $E > 1$ Mev) if the samples had been thinned to 0.005- or 0.003-in.-thick foils before annealing. They suggested that the small loops are prismatic and are due to clustering with subsequent collapse of the vacancies produced by the neutron bombardment. Dislocations that encounter prismatic loops frequently form rings about the loops or, likewise, around other obstacles.

In checking whether or not the recovery of neutron-produced damage in molybdenum at 200°C was due to the annihilation of vacancies by forming clusters resulting in dislocation loops, Kerridge[58] et al. reported that no loops were observed in the electron microscope. The limit of detectability for the loops was of the order of 25 A. The samples were electrolytically thinned foils of molybdenum that had been annealed at 1250°C for 1 hr and irradiated in the British Experimental Pile O at Harwell to a dose of $10^{19}$ nvt at about 40°C. Beevers[59] has succeeded in observing radiation-produced dislocation loops in molybdenum; however, his irradiation damage resulted from bombardment with 38-Mev alpha particles and 85-kev $H^+$ ions. The samples were 99.98% pure sheets, 0.003 in. thick, which had been annealed at 1000°C for 2 hr to produce a grain size of about 2 $\mu$. The first series of samples was irradiated at a rate of $9 \times 10^{12}$ ions/(cm$^2$)(sec) to a dose of $1.5 \times 10^{17}$ $He^{2+}$ ions at about 500°C. The samples were thinned and were observed with transmission-electron microscopy. Loops up to 250 A in diameter were observed. The $H^+$ ion samples were prethinned and irradiated at a rate of $5 \times 10^{14}$ ions/(cm$^2$)(sec) to a dose of $6 \times 10^{18}$ ions at temperatures less than 80°C. The resulting loops had a higher density than the $He^{2+}$ irradiation and are explained because of the higher flux and the lower temperature of bombardment for the $H^+$ ions.

Some of the factors that influence the size of dislocation loops formed in neutron-irradiated metals have been mentioned in a brief

note.[60] The stacking-fault energy and the rate of production of defects are correlated with existing experimental evidence to illustrate two factors that influence dislocation sizes.

Electron irradiations (<1 Mev) of copper[61] indicate that the minimum threshold energy for atom displacement is less than 22 ev. The recovery is more complicated than was anticipated. Atomic displacements created near threshold along directions near the ⟨110⟩ directions are found to be important. Theory confirms this if the displacement energy is taken as 19 ev and the Frenkel resistivity is taken between 2 and 3 μohm-cm per atomic percent of interstitial-vacancy pair. Focusing collisions in aluminum have been studied[62] by observing the ejection of atoms due to 50-kev $A^+$ ion bombardment. Analysis of deposit patterns shows that the energy ejected in the ⟨110⟩ direction is 2.4 times that ejected in the ⟨100⟩ direction and five times that ejected in the ⟨111⟩. Angular deviations are discussed[62] in terms of thermal scattering of collision sequences, and this discussion is extended in a subsequent paper[63] by Nelson et al., which is covered in the subsection on "Theories of Radiation Effects" in this issue of *Reactor Materials*. Similar results of focused-deposit patterns have been shown and discussed for copper.[64]

The continuation of Merkle and Hart's[9] studies of fission-fragment damage in evaporated gold films appears in a recent Argonne report. The work has also been extended to copper and silver. Most of the damage, which appears in the electron microscope as dark loops having some crystallographic orientation, is observed to anneal out between 350 and 400°C. About 25 spots are observed per fission fragment, which agrees with similar observations made in bulk gold.

Fission-fragment damage in thin aluminum foils irradiated at 80°C is shown by electron microscopy to result in both vacancy and interstitial clusters that initially attract their own kind and repel the other.[65] The result is that each type grows almost independently by a process that involves both conservative climb and slip. As they enlarge, slip becomes more important, and nearby loops of the opposite kind on similar slip cylinders slip together, partially canceling one another.

Beryllium swelling of 3% at 700°C was reported[66] after a neutron irradiation of $3.6 \times 10^{20}$ nvt. The swelling is associated with the migration of small cavities to larger nuclei or perhaps inclusions. These cavities are formed as a result of the neutron reactions produced in beryllium and the gas formed thereby. Stress-rupture characteristics are also discussed.

Nuclear particle tracks were observed in fine-grained photosensitive layers in the electron microscope.[67] These layers were prepared by evaporating silver directly on microscope screens (resulting in grains about 100 A in diameter), followed by sensitization with bromine under red light. The final grids were coated with gelatin and dried. Long tracks were rarely seen; the few long tracks observed contained side spurs associated with secondary electrons scattered from the silver.

Cyclic torsional strains at room temperature have been observed to partially recover faults that were produced in a single-crystal iron fiber by neutron irradiation.[68] Young's modulus, hardening, and internal friction were measured. Structural changes as a result of irradiation are ruled out as the cause of the enhanced catalytic activity observed in copper.[69] No alternative is suggested.

Detailed discussions of studies by Muss[70–72] on defects and internal friction in irradiated tungsten have appeared. The work of Ruedl et al.[73] on electron-microscopical studies of fission damage in platinum foils has also been published. As reported before, boundary defocusing was observed.[74]

*Defects in Metal Alloys.* Most of the irradiation studies at Harwell[75] have been reported in earlier Reviews under the specific investigators. One exception is the work of Higgins and Roberts, who are studying defect formation after fission-fragment bombardment in 20 wt.% nickel–20 wt.% chromium niobium-stabilized stainless steel. Defects about 25 A in size were seen after doses of $1.8 \times 10^{14}$ fragments/cm$^2$. An increase in the dose increased the size, until obvious loops were formed similar to those seen in other face-centered cubic metals. An estimated 250 defect pairs per fission were counted. For higher bombardment rates in 93% enriched fuel, 45 defects were observed per fission; however, it is suggested that many defects formed at the higher rates are unobservable.

Radiation hardening, resulting from neutron irradiation, was found to anneal out of zirco-

nium[76] and Zircaloy-2 at 250 to 400°C with an activation energy of about 2.3 ev and at about 200 to 400°C in the case of type 410 stainless steel with an activation energy of 2.4 ev.

Thermal spikes are used to explain the neutron-produced phase transformation observed in tin bronze[77] (copper–8 at.% tin) with the addition of 1 at.% plutonium. The transformation consists in the dissolution of the precipitated intermetallic phase $Cu_3Sn$ in the alpha solid solution. The binary alloy did not show this transformation, even after prolonged exposure to fast neutrons.

Ordering, sensitive to the direction of the magnetic field, is observed in a 50 wt.% iron–nickel alloy under neutron irradiation.[78] The very strong magnetic anisotropy that results is caused by the formation of an FeNi structure of the AuCu type. The critical temperature for the corresponding order-disorder transformation is close to 330°C.

The macroscopic diffusion of zinc in an alloy of 10 wt.% zinc–90 wt.% copper was studied under bombardment with 30-kev neon ions.[79] The samples were electrolytically polished and etched. The neon bombardment produced defects (vacancies plus interstitials) at a calculated rate of 0.048 atomic fraction per second. At 243°C, this resulted in a computed vacancy concentration under steady state of $2.2 \times 10^{-5}$. Under irradiation, the average diffusion coefficient was $1.8 \times 10^{-14}$ cm$^2$/sec, and the average activation energy was 8700 cal/gram mole. The diffusion coefficient showed a square-root dependence on the bombarding flux. These results indicated diffusion under constant production of defects and simultaneous annealing of defects to fixed sinks, plus direct recombination. Without irradiation the average diffusion coefficient was $2.7 \times 10^{-15}$ cm$^2$/sec at 243°C, and the average activation energy was 27,000 cal/gram mole. These low values, compared with those from other experiments, indicated inhomogeneous diffusion along short-circuit paths such as dislocations. Samples that were cold worked by mechanical grinding showed diffusion coefficients a factor of 10 greater. These cold-worked samples, however, exhibited inhibited diffusion during irradiation. The heavy ion bombardment erased the effects of the previous history of the sample. The conclusion is that radiation-enhanced bulk diffusion is observed under heavy ion bombardment.

*Defects in Other Materials.* Effects due to thermal spikes are suggested in explaining the decomposition behavior of several alkali nitrate crystals that had been irradiated with $Po^{210}$ alpha particles.[80] The heavy-particle irradiations produced considerable effects that were not observed after irradiation with gamma rays or X rays. Additional considerations of thermal-spike occurrence have been reported in studies of protein.[81] As the protein is bombarded with fission recoils, the region that is raised to an elevated temperature results in inactive or decomposed protein. Classical heat flow is used to predict the volume so affected. Good agreement is shown for linear energy transfers above $10^3$ Mev/(g)(cm$^2$), whereas a reasonable explanation is proposed for the poorer agreement below this value.

Evidence for the concept of a displacement spike resulting from fission-fragment damage has been seen in the electron microscope in crystals of molybdenum disulfide.[82] Intermittent dark-contrast tracks suggest a discontinuous release of energy by the recoil. The authors point out, however, that the effects produced in such substances are not representative of what happens in other systems where electronic effects are more significant. Bowden and Chadderton[83] have also presented a detailed discussion of high-resolution electron-microscopical techniques that are being used to study individual fission-recoil tracks in various materials.

Fission-fragment tracks have been observed in single-crystal $UO_2$ by diffraction contrast in the electron microscope.[84] The tracks appear as long lines with associated black spots, which are described as dislocation loops formed by the collapse of clusters of point defects. These clusters are about 100 A wide by about 220 A long, and they occur, on the average, every 1200 A along the fission tracks. Tracks in polycrystalline films show regions where material has been evaporated. The difference in behavior is explained in terms of the grain size since it is suggested that the evaporation is caused by excitons, electrons, and phonons reflected at the grain boundaries. Damage produced in lead iodide crystals by uranium fission-fragment penetration appears in the electron microscope as randomly distributed dislocation loops that are inclined to the surface.[85] These loops are formed by the aggregation of highly mobile point defects, and they

have diameters up to about 250 A. No linear regions of damage have been observed.

Fission fragments were observed to initiate a high-temperature phase transformation in synthetic fluor-phlogopite mica.[86] Transmission-electron microscopy revealed selected-area diffraction patterns of platelike structures near the regions where the recoils intersected the surface. These were consistent with the forsterite form of mica that formed at about 800°C. Similar transformations in unirradiated samples never occurred below 890°C. Wittels et al.[87] have published their studies on radiation-induced phase transformations in $ZrO_2$ which were reported previously.[88]

Lattice defects in natural and synthetic quartz crystals were studied by X-ray and transmission-electron-microscopy methods[89] after the samples had been exposed to fast-neutron irradiations ranging from $10^{19}$ to $10^{20}$ nvt. A close correlation was established between the alignment of clusters rich in interstitial silicon atoms as directly observed with the electron microscope and the strain distribution as disclosed by the X rays. Results were interpreted by suggesting that clusters of interstitial atoms were aligned in certain directions relative to the open screw channels of the quartz structure. A large irradiation interaction of clusters occurred which was apparently aided by thermal spikes, and the crystals still exhibited a high degree of crystallinity.

A detailed study of defect clusters formed in graphite by high-flux neutron irradiations at temperatures up to 650°C has been made with the electron microscope.[90] A linear relation exists between cluster radius and irradiation temperature (see Fig. IV-4). Subsequent annealing of the defects is consistent with the hypothesis that the visible defects are all of one kind, probably interstitials. Some observations at the highest temperatures and doses suggest that vacancy clusters may also become identifiable. The effects of irradiation temperature on the stored energy of graphite were reported[91] for irradiations at temperatures up to 300°C. Enthalpy was measured, by means of differential thermal analysis, between ambient temperatures and 800°C. Integration of the energy spectrum furnished the total stored energy. For small doses the energy liberated at a given temperature by the irradiated graphite increased directly with dose. For low-temperature irradiations (30 to 70°C), there

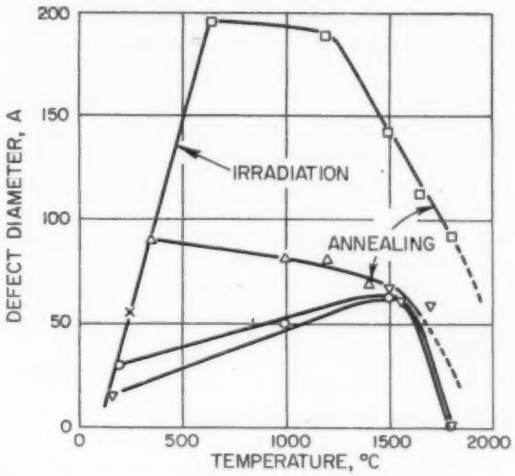


Fig. IV-4 Mean defect diameter as a function of irradiation and annealing temperature of graphite.[90]

is a peak of energy release near 200°C. As the irradiation temperature increases, this energy peak diminishes, and it finally disappears at about 200°C. The results of this study are in agreement with results obtained by other investigators.

Data have been reported[92] which show that there is no marked difference in the magnitude of the $c$-spacing contraction of graphite with increasing neutron doses up to $3.7 \times 10^{20}$ nvt. There is, therefore, still no firm indication that observed changes in the bulk properties of graphites on irradiation are dependent on changes in the crystal expansion coefficient (as has been suggested). Another study[93] suggests that less than 5 atom layers of carbon will be sputtered per year from the recoils resulting from helium-gas atoms (in a gas-cooled reactor) that are driven in the graphite because of collisions with fast neutrons.

The lattice-parameter changes[94] that occur on neutron irradiation of hot-pressed beryllium oxide to integrated fission-neutron doses of $1 \times 10^{19}$ nvt at 75 to 100°C and to doses of 1 to $1.5 \times 10^{20}$ nvt at 500 to 650°C are reported. In agreement with other workers, it is shown that an anisotropic lattice expansion occurs, the expansion in the $c$ direction being greater than the expansion in the $a$ direction. The lattice expansion at irradiation temperatures of 500 to 600°C is almost a factor of 3 smaller than that for equivalent neutron doses at 75 to 100°C. The volume expansion calculated from

X-ray data is shown to agree with the macroscopic volume expansion. The annealing behavior of the lattice-parameter changes is described, and it is shown that temperatures of 1400 to 1500°C are required for complete recovery of the damage to occur. Line-broadening effects are discussed in a qualitative manner, and it is suggested that defect clusters are formed in the basal planes of the hexagonal beryllium oxide lattice.

Bowen et al.[95] have reported on direct evidence for the existence of defect clusters in neutron-irradiated BeO and MgO.

(T. G. Knorr)

### Theories of Radiation Effects

Additional weight has been added to the suggestion that the split-interstitial configuration (two atoms split in the ⟨100⟩ direction about a normal lattice site) is most stable in the noble metals. Johnson and Brown[96] have calculated the energies for seven other configurations, which are found to be less stable. At the University of Illinois, this split interstitial has been used to explain the difference in annealing behavior of electron damage in copper and gold.[97] The split interstitial is shown to have a higher probability of formation in electron-irradiated gold.[98] This analysis is also considered theoretically, and the general concept of interstitials in the noble metals has been discussed.[99] Seeger et al.[100] have also reported on calculations of the interstitial configuration in copper.

Nelson et al. have proposed a theory that begins to explain the effects of surface temperature on the distribution of sputtered material from metal surfaces.[63] Reasonable agreement with experiments is shown. The most important mechanism that might cause scattering of the focused-collision sequence responsible for ejection is concluded to be the lateral displacement of atoms from the focusing line by the thermal motion. In applying this to radiation damage and sputtering, it is implied that such scattering renders mass transport by ⟨110⟩ sequences very inefficient. Furthermore, it is implied that both the rate of defect formation and the spatial distribution of defects should be affected by temperature. Neutron-induced focusing collisions in the graphite-layer planes is found[101] to be possible only in ⟨1120⟩ directions. The smallest diameter of a carbon atom at which focusing can occur is two-thirds of the interatomic distance (1.42 A) in the plane. Indirect focusing is found to be impossible. The threshold energy for focusing is of the order of some tens of electron volts. Calculation of atomic displacements[102] produced by primary knock-on atoms with energies greater than the ionization threshold energy have shown enhancement in specimens of finite geometry relative to the displacement in the semi-infinite systems. The enhancement is relatively large in the case of isotropic neutron scattering in the sample.

Distortion and the accompanying energy change due to a point defect in a crystal are calculated using a Green's-function method.[103] The method permits consideration of the simultaneous relaxation of the position of all atoms in the crystal, and it is based on an expansion of the potential energy of the crystal up to quadratic terms in the displacements of the atoms from their equilibrium positions in the undistorted crystal. Bennemann[104] has derived the wave functions of the conduction electrons in metals that have been redistributed because of interstitials, vacancies, and impurities. The expressions are determined from an integral equation derived from the Hartree-Fock equation. The wave functions take into account the effect of multiple scattering that arises from an ensemble of point defects, and they are used to determine the redistribution of the conduction electrons and the electronic contribution to the interaction energy of point defects. The energy distribution of the primary atoms in copper for 1.5- and 3.7-Mev neutrons and for reactor neutrons was calculated[105] with the spectrum given by Holmes et al. for Channel 12 of the Oak Ridge Graphite Reactor by application of the measured differential cross section for elastic neutron scattering. For the same neutron energies, the numbers of radiation-induced Frenkel defects were determined by the Kinchin and Pease method. The energy distribution in the case of reactor neutrons up to a primary energy of 60 kev can be represented by two simple functions. As the total cross section for the production of primary atoms, the value 5.7 barns was obtained for reactor neutrons, 2.9 barns for 1.5-Mev neutrons, and 2.3 barns for 3.7-Mev neutrons. According to Kinchin and Pease, 75 Frenkel pairs per primary atom should be produced in reactor irradiation, 650 in irra-

diation with 1.5-Mev neutrons, and 640 in irradiation with 3.7-Mev neutrons. The values obtained were compared with the experimental results of Blewitt et al.

Merkle[106] suggests an explanation for the fission tracks observed in thin polycrystalline samples in terms of electronic effects that result from the grain size. Excited electrons are trapped within the grains with energies that can be sufficient to vaporize a small enough grain. Electron micrographs are shown of tracks in gold films which support this theory.

Robinson[107] has presented a short note suggesting that the range of atoms and ions in solids can be inferred from measurements of the sputtering yield of a solid target and of the amount of beam material collected in the target during the irradiation. Complete experimental tests are not yet available.

A note has appeared which suggests that the strains resulting from irradiation-produced creep might not be as large as previously estimated.[108] The proposal states that, in a constant neutron flux, the irradiation-produced defects all flow to dislocations. Each segment of the dislocation will receive, on the average, defects at the same rate. Makin[109] shows that the present theory proposed to account for hardening of crystalline solids by gas bubbles, in terms of semicircular dislocation formation, does not apply when the bubbles are very small ($< 1 \times 10^{-6}$ cm radius). (T. G. Knorr)

## Surveys on Radiation-Induced Defects

*Nuclear Science Abstracts* lists the abstracts[110] of a number of papers that were presented at the IAEA Symposium on Radiation Damage in Solids and Reactor Materials, held in Venice, Italy, May 7–11, 1962. The proceedings are of general interest and are scheduled for publication at some future date. Two of the Russian papers of interest have already been translated.[111,112]

Balluffi et al.[113] have prepared an extensive discussion concerned with the state of knowledge of point defects in face-centered cubic metals. They are specifically interested in deformed material, but their discussion includes formation and annealing studies of radiation-damage specimens. In general, an overall view is presented which results in a good picture of present-day knowledge of defects in these materials.

A survey[114] has been presented which discusses the importance of radiation effects as they contribute to the knowledge of the solid state. Such matters as distinguishing between phenomena involving single mobile defects and phenomena associated with larger damage volumes are considered and are illustrated with examples. A recently published book[115] is concerned with ionization in gases. Sputtering experiments are of particular interest.

Damask[116] has presented a very compact review of the radiation effects in nonfissionable alloys. Such things as destruction of order,

Table IV-1 MECHANICAL PROPERTIES OF ZIRCALOY-2 SPECIMENS[122]

| Mechanical properties | Unirradiated | | | | Irradiated | | |
|---|---|---|---|---|---|---|---|
| | As-received | Welded* | Welded and hydrided | Heat-treated | Welded | Welded and hydrided | Heat-treated |
| Tested at room temperature: | | | | | | | |
| Proportional limit, 1000 psi | 44.4 | 41.0 | 46.5 | 34.8 | 45.1 | 60.1 | 49.8 |
| Yield strength (0.2% offset), 1000 psi | 48.6 | 47.3 | 52.2 | 39.2 | 49.3 | 63.3 | 54.9 |
| Ultimate tensile strength, 1000 psi | 72.0 | 62.7 | 68.4 | 67.1 | 62.3 | 74.7 | 74.8 |
| Elongation, % | 24.4 | 11.9 | 12.0 | 25.3 | 14.3 | 11.9 | 24.2 |
| Uniform elongation, % | 13.3 | 10.2 | 8.4 | 13.4 | 11.4 | 7.7 | 12.0 |
| Tested at 260°C: | | | | | | | |
| Proportional limit, 1000 psi | 19.6 | 22.3 | 22.3 | 20.8 | 29.4 | 28.2 | 26.4 |
| Yield strength (0.2% offset), 1000 psi | 21.3 | 24.8 | 25.0 | 23.9 | 30.9 | 29.4 | 28.2 |
| Ultimate tensile strength, 1000 psi | 35.1 | 37.3 | 36.1 | 44.1 | 39.2 | 38.0 | 43.1 |
| Elongation, % | 41.8 | 21.3 | 21.5 | 35.4 | 18.5 | 23.5 | 29.1 |
| Uniform elongation, % | 13.3 | 12.3 | 11.7 | 13.8 | 9.3 | 11.6 | 8.6 |

*Average of three specimens. All others are average of two specimens at each temperature.

breakup of precipitates, enhanced diffusion, and nucleation of phase changes are discussed.

Clarke[117] has presented a paper concerned with irradiation-produced changes in various ceramic materials. Critical examinations of mechanisms are discussed in the light of observed changes. Primak and Bohmann[118] report on radiation-induced phenomena in ceramics, which include collision phenomena, thermal annealing, radiation annealing, transient effects, chemical effects, and atomic excitation.

Three books[119–121] that contain general discussions concerned with the topics reported here have been published: *ASTM Symposium on Radiation Effects in Refractory Fuel Compounds, Properties of Reactor Materials and the Effects of Radiation Damage*, and *Proceedings of the Fifth International Congress for Electron Microscopy* (Vol. I; see Sections F and G on Radiation Damage). (T. G. Knorr)

## Effects of Radiation on Mechanical Properties

General Electric[24,102] personnel have been studying the radiation-induced property changes in two nickel-base alloys and a stainless steel. The stress-rupture properties and the short-time tensile properties are being determined at elevated temperatures, after irradiation at elevated temperatures, for Hastelloy X, René 41, and A-286 stainless steel. Preliminary data indicate that both Hastelloy X and René 41 show a significant decrease in the 10-hr rupture strength at 870°C after irradiation to approximately $4 \times 10^{19}$ neutrons/cm$^2$ (<1 Mev) at 870°C. The threshold of neutron-induced reduction in a 50-hr rupture life of samples irradiated and tested at 650°C appears lower for A-286 stainless steel than for Hastelloy X. A-286 stainless steel irradiated at 540 and 650°C does not show appreciable change in ultimate tensile and yield strength, although the 10-hr rupture strength at these temperatures is reduced 7 to 24% by irradiation.

At a number of sites, the irradiation effects in zirconium alloys, principally Zircaloy-2 and in some instances Zircaloy-3, are being investigated. Chalk River[122] has studied, as part of an investigation on welded Zircaloy-2, the effect of neutron irradiation on the weld material. The specimens were irradiated in the X-5 loop of the Canadian National Research Experimental Reactor (NRX) to an exposure in the range of 0.3 to $1.9 \times 10^{19}$ neutrons/cm$^2$ (thermal). It was found that the room-temperature yield strength of welded and hydrided material was increased about 20% and that the yield strength of heat-treated material increased about 40% by irradiation. The ultimate tensile strengths were increased slightly after irradiation, whereas the uniform and total elongations remained constant. These changes in properties are shown in Table IV-1. The impact properties also were not altered by irradiation, as shown in Fig. IV-5. The evaluation of spigot welds after irradiation did not indicate any effect of irradiation on the breaking strength of either the autoclaved or the unautoclaved Zircaloy-2 specimen. It was reported that a higher percentage of cup-and-cone fractures occurred in the irradiated samples than in the unirradiated samples.

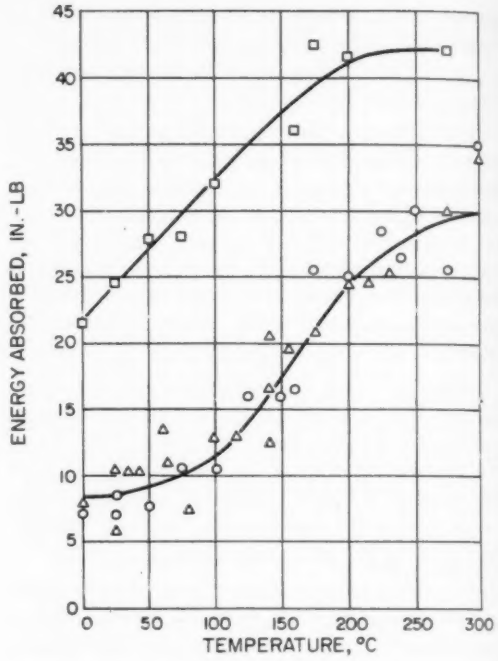


Fig. IV-5 Effect[122] of welding on the impact properties of as-received Zircaloy-2 and of neutron irradiation on the impact properties of welded Zircaloy-2. ○, welded, irradiated; △, welded, unirradiated; □, as received, unirradiated.

Both Zircaloy-2 and Zircaloy-3 have been investigated at Du Pont, Wilmington,[15] and it

Table IV-2 EFFECT OF IRRADIATION[15] ON TENSILE PROPERTIES OF ZIRCALOY-2 AND ZIRCALOY-3

| Test temp.: | 25°C | | 250°C | | 350°C | |
|---|---|---|---|---|---|---|
| Condition: | Unirradiated* | Irradiated† | Unirradiated* | Irradiated† | Unirradiated* | Irradiated† |
| Zircaloy-2, 555 ppm oxygen: | | | | | | |
| Tensile strength, psi | 72,500 | 81,600 | 38,500 | 50,600 | 32,500 | 40,200 |
| Yield strength, psi | 41,000 | 76,000 | 18,500 | 47,000 | 15,500 | 39,800 |
| Total elongation, % | 22.5 | 13.5 | 39.3 | 16.6 | 38.2 | 21.6 |
| Reduction of area, % | 42.5 | 50.0 | 64.1 | 61.5 | 68.8 | 51.4 |
| Zircaloy-2, 1395 ppm oxygen: | | | | | | |
| Tensile strength, psi | 96,000 | 101,000 | 50,500 | 62,300 | 39,000 | 48,700 |
| Yield strength, psi | 66,500 | 92,300 | 38,500 | 55,400 | 21,000 | 44,800 |
| Total elongation, % | 21.0 | 9.5 | 37.0 | 17.1 | 36.8 | 25.8 |
| Reduction of area, % | 37.5 | 38.2 | 59.8 | 56.0 | 64.6 | 53.8 |
| Zircaloy-3, 640 ppm oxygen: | | | | | | |
| Tensile strength, psi | 65,000 | 72,200 | 30,800 | 41,300 | 26,000 | 33,200 |
| Yield strength, psi | 31,300 | 63,500 | 13,000 | 40,400 | 10,500 | 32,500 |
| Total elongation, % | 22.8 | 14.7 | 49.6 | 23.8 | 47.7 | 29.2 |
| Reduction of area, % | 43.0 | 37.0 | 72.0 | 65.6 | 77.0 | 63.5 |
| Zircaloy-3, 1350 ppm oxygen: | | | | | | |
| Tensile strength, psi | 89,500 | 101,000 | 43,000 | 57,000 | 32,500 | 43,200 |
| Yield strength, psi | 53,800 | 91,600 | 21,000 | 52,800 | 15,500 | 40,500 |
| Total elongation, % | 21.2 | 12.2 | 42.6 | 26.2 | 42.6 | 33.7 |
| Reduction of area, % | 39.8 | 34.1 | 65.0 | 55.1 | 71.5 | 64.2 |

*Average data from Harvey Aluminum Co. tests on unirradiated specimens.

†Average data from Savannah River Laboratory tests on irradiated specimens. Irradiation exposure: $5.1 \times 10^{20}$ nvt (fast) at less than 100°C.

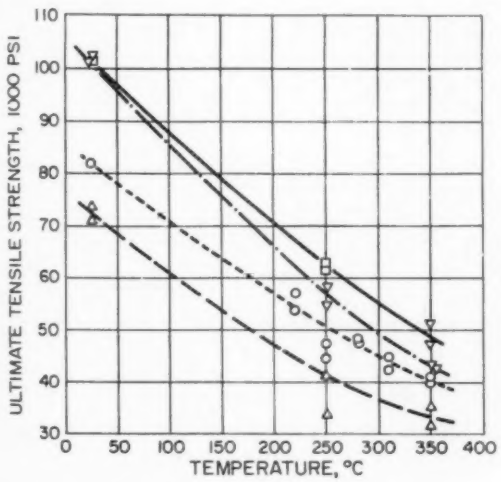


Fig. IV-6 Ultimate tensile strength of irradiated Zircaloy-2 and Zircaloy-3 as a function of temperature.[122] Irradiation exposure, $5.1 \times 10^{20}$ nvt (fast) at less than 100°C. ○----○, Zircaloy-2, 555 ppm oxygen; □ ——— □, Zircaloy-2, 1395 ppm oxygen; Δ – – – Δ, Zircaloy-3, 640 ppm oxygen; ▽ —·— ▽, Zircaloy-3, 1350 ppm oxygen.

was found that the ductility, as indicated by the reduction in area, of both was not appreciably influenced by irradiation. The other properties—ultimate tensile strength, yield strength, and total elongation—were modified by the irradiation. These data are shown in Table IV-2. Figures IV-6 to IV-10 show these irradiation effects graphically, together with the effect of oxygen content.

Hanford[52] also has been studying the effect of irradiation on Zircaloy-2. One of these programs has been directed toward determination of the short-time tensile properties at room and elevated temperatures after irradiation at about 300°C. It was found that the properties of annealed Zircaloy-2 changed only slightly between exposures of $1 \times 10^{19}$ and $1 \times 10^{20}$ neutrons/cm$^2$. A second program has been concerned with in-reactor creep properties of Zircaloy-2 at elevated temperatures. The most recent data indicate that at 310°C the total creep deformation is increased for that specimen in the reactor. It was noted, however, that most of the creep occurred during reactor shutdown. The procedure has been to maintain test temperature during reactor shutdown.

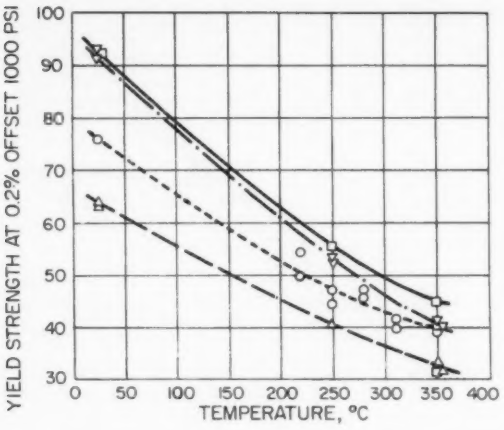


Fig. IV-7 Yield strength of irradiated Zircaloy-2 and Zircaloy-3 as a function of temperature.[122] Irradiation exposure, $5.1 \times 10^{20}$ nvt (fast) at less than 100°C. ○----○, Zircaloy-2, 555 ppm oxygen; □ —— □, Zircaloy-2, 1395 ppm oxygen; Δ — — — Δ, Zircaloy-3, 640 ppm oxygen; ∇ —·— ∇, Zircaloy-3, 1350 ppm oxygen.

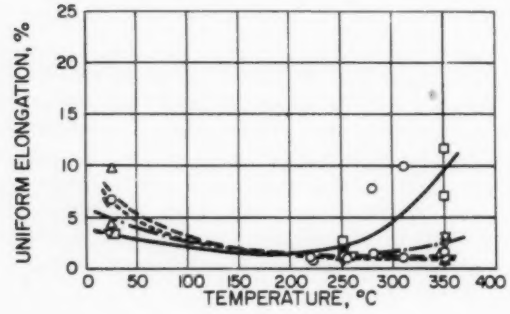


Fig. IV-8 Uniform elongation of irradiated Zircaloy-2 and Zircaloy-3 as a function of temperature.[122] Irradiation exposure, $5.1 \times 10^{20}$ nvt (fast) at less than 100°C. ○----○, Zircaloy-2, 555 ppm oxygen; □ —— □, Zircaloy-2, 1395 ppm oxygen; Δ — — — Δ, Zircaloy-3, 640 ppm oxygen; ∇ —·— ∇, Zircaloy-3, 1350 ppm oxygen.

The Canadians at Chalk River[123] are continuing their studies on the in-reactor creep properties of Zircaloy-2. They have also investigated the tensile properties of a zirconium–2.5 wt.% niobium alloy after irradiation at 360°C in an NRX transformer rod to about $3 \times 10^{19}$ neutrons/cm$^2$ (>500 ev). The control samples were heated at the same temperature for times similar to the irradiation time. The results, shown in Table IV-3, indicate no significant changes in properties after irradiation.

Hanford,[52] in an investigation on pure metals, has shown that the room-temperature tensile properties of ingot iron show drastic changes after an exposure of $2 \times 10^{18}$ neutrons/cm$^2$. Figure IV-11 shows that all uniform elongation is lost after that exposure. (F. R. Shober)

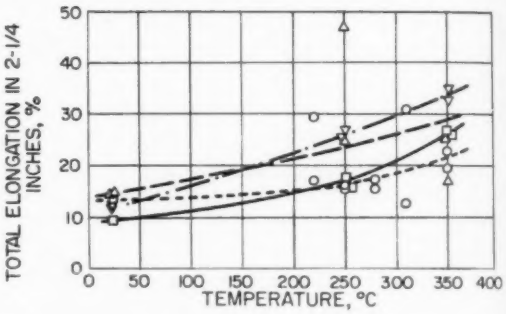


Fig. IV-9 Total elongation of irradiated Zircaloy-2 and Zircaloy-3 as a function of temperature.[122] Irradiation exposure, $5.1 \times 10^{20}$ nvt (fast) at less than 100°C. ○----○, Zircaloy-2, 555 ppm oxygen; □ —— □, Zircaloy-2, 1395 ppm oxygen; Δ — — — Δ, Zircaloy-3, 640 ppm oxygen; ∇ —·— ∇, Zircaloy-3, 1350 ppm oxygen.

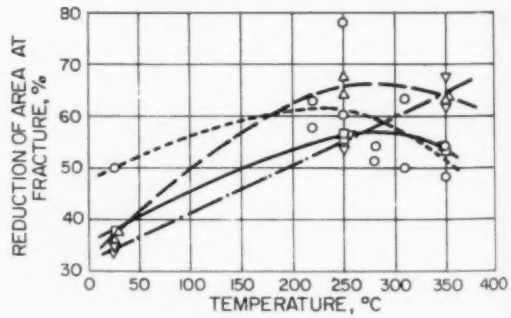


Fig. IV-10 Reduction of area at fracture of irradiated Zircaloy-2 and Zircaloy-3 as a function of temperature.[122] Irradiation exposure, $5.1 \times 10^{20}$ nvt (fast) at less than 100°C. ○----○, Zircaloy-2, 555 ppm oxygen; □ —— □, Zircaloy-2, 1395 ppm oxygen; Δ — — — Δ, Zircaloy-3, 640 ppm oxygen; ∇ —·— ∇, Zircaloy-3, 1350 ppm oxygen.

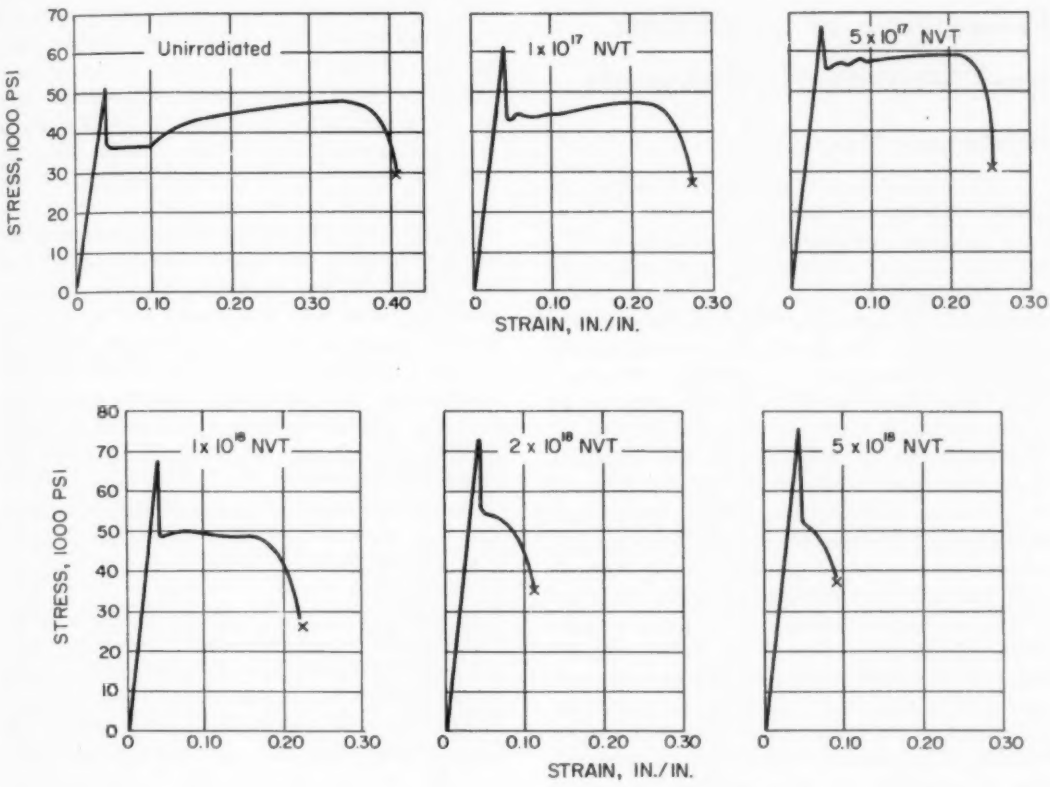


Fig. IV-11 Typical stress-strain curves for irradiated ingot iron.[52]

Table IV-3 EFFECT OF RADIATION AT 360°C ON TENSILE PROPERTIES OF ZIRCONIUM–2.5 WT.% NIOBIUM ALLOY[123]

| | Irradiated | | | Control specimens for this irradiation | | | Previous values for the as-heat-treated condition | | |
|---|---|---|---|---|---|---|---|---|---|
| Test temp., °C | Ultimate tensile strength, 1000 psi | Elongation, % | Reduction of area, % | Ultimate tensile strength, 1000 psi | Elongation, % | Reduction of area, % | Ultimate tensile strength, 1000 psi | Elongation, % | Reduction of area, % |
| RT | 131 | 14.6 | 58 | 128* | 15.7 | 63 | 125 | 12.5 | 63 |
| 300 | 92.6 | 14.3 | 68 | | | | 86† | 14.3 | 75 |
| 360 | 91.3 | 15.6 | 77 | 84.6 | 15.8 | 79 | 83‡ | | |
| 400 | 84.5 | 17.3 | 79 | | | | 76 | 17.0 | 81 |

*Average of two specimens.
†Average of nine specimens.
‡Value expected from results at 350 and 375°C.

# Selected Mechanical Properties of Cladding and Structural Materials

## Miscellaneous Alloys

A literature survey of a number of high-temperature alloys for nuclear superheat applications has been prepared by General Electric.[124] Both mechanical and metallurgical properties are discussed in detail. A number of curves showing mechanical properties vs. temperature are presented. The materials covered include Hastelloy X, Hastelloy N, AISI type 406 stainless steel, Incoloy, Inconel, RA 330, 17-14 CuMo, Discoloy, R-20, and Ni-O-Nel.

The results of tests on type 304 stainless steel, completed by Oak Ridge National Laboratory,[125] indicate that air, CO, $CO_2$, and $N_2$ are strengthening to this alloy. Carburization and nitriding are believed to be primarily responsible for the strengthening of these environments. At 1500°F, oxygen at 1 atm pressure has a deleterious effect on the creep properties, but at 1700°F the creep properties are improved. Creep tests at 1500°F in various argon-oxygen mixtures show that small oxygen concentrations cause pronounced strengthening, with a maximum effect occurring at 10 ppm oxygen. At 1500°F the creep properties appear to be unaffected by hydrogen, but at 1700°F deleterious effects are observed. Tensile tests were used to evaluate the influence of carbon on the rupture ductility of this material. It was found that when the carbon content was increased, a significant reduction in ductility occurred. It was found that copper plating effectively reduced the rate of carburization at 1300°F. The service life of copper films at higher temperatures was seriously limited.

## Strength of Refractory Metals

The tensile properties of electron-beam-melted niobium and a series of niobium-nitrogen alloys containing up to 0.036 wt.% nitrogen were examined by Armour[126] at room temperature over a range of grain sizes. The variation of lower yield stress, $\sigma_{LY}$, with grain size was used to determine the values of $\sigma_0$ and $K$ in a Petch type equation, $\sigma_{LY} = \sigma_0 + Kd^{-\frac{1}{2}}$. Whereas $K$ was not influenced by nitrogen content and was, with one exception, very small, $\sigma_0$ was particularly sensitive to nitrogen content. Some dispersion-hardened structures ($Nb_2N$ as dispersed phase) were studied, and, by use of the Petch equation, a quantitative measure of the contribution of the dispersion to yield strength was made. A Heslop-Petch type analysis was used to measure the Peierls-Nabarro force for the niobium lattice at room temperature.

Begley of Westinghouse[127] presents the results of studies for many binary, ternary, and quaternary alloys. Rhenium, tungsten, and molybdenum additions increased the ductile-to-brittle transition of niobium. One alloy, niobium–10 wt.% tungsten–5 wt.% vanadium–1 wt.% zirconium, had excellent room-temperature ductility and had ultimate tensile strengths of 64,800 and 29,450 psi at 2200 and 2400°F, respectively.

Short-time high-temperature stress-rupture data on several refractory-metal alloys were disclosed by Stauffer.[128] These are summarized in Table IV-4.

A report that deals with the metals niobium, molybdenum, tantalum, and tungsten has been published by the Advisory Group for Aeronautical Research and Development.[129] The report covers physical properties, mechanical properties at various temperatures, and oxidation behavior. In addition, recommendations are made for research and development. The state of knowledge of each metal in regard to phase diagrams, impurities effects, and diffusion couples is presented, along with a bibliography.

A compilation of the tensile properties of tungsten up to 6000°F has been published by the Defense Metals Information Center.[130]

The Russians[131] investigated the hardness and strength of cast and hardened zirconium alloys with tantalum (0 to 100%) and with

Table IV-4 STRESS-RUPTURE DATA ON REFRACTORY-METAL ALLOYS[128]

| Temp., °F | Rupture strength, 1000 psi | | | |
|---|---|---|---|---|
| | SM 278 (Nb-Ta-Mo) | | SM 291 (Nb-Ta-W) | |
| | 10 min | 100 min | 10 min | 100 min |
| 2400 | 12.8 | 10.6 | | |
| 2800 | 9.0 | 7.5 | 9.8* | 7.5* |
| 3000 | 5.4 | | 6.5* | 4.8* |
| 3200 | | | 5.4 | 3.9 |

*Temperature approximate.

niobium (0 to 20%) and also ternary alloys containing up to 18 wt.% tantalum and niobium. The hardness was measured in an argon atmosphere. It was found that a maximum appeared on the composition-hardness and composition-strength curves which can be explained by the transformation of the beta phase into the alpha phase. Alloying zirconium with tantalum and niobium increases the strength and hardness at room and high temperatures. Up to 10 wt.% niobium strengthens zirconium to a greater degree than similar additions of tantalum. (J. A. DeMastry)

# Selected Metallurgical Aspects of Cladding and Structural Materials

## Aluminum Stacking Faults

German investigators[132] have shown that no deformation stacking faults occur in pure aluminum after cold working. In the systems aluminum - magnesium, aluminum - zinc, and aluminum-magnesium-zinc, however, this effect could be detected with small amounts of the alloying elements. The stacking-fault density in the binary systems increases with increasing content of magnesium or zinc. The system aluminum-zinc shows a distinct maximum of the stacking-fault probability. In cold-worked aluminum-copper alloys, no stacking faults could be found.

## Chromium Phase Studies

Russian workers[133] report on a constitutional diagram for the chromium-nickel-niobium system. They constructed a chromium-nickel-$Ni_3Nb$-NbCr quadrangle. A four-phase peritectic equilibrium was found at 1175 ± 5°C, a four-phase eutectic equilibrium was found at 1173 ± 5°C, and a four-phase peritectoid equilibrium was found at 1160 ± 5°C. It was shown that a quasi-binary section, $NbCr_2$-$Ni_3Nb$, appears in the system limited by the chromium-nickel-$Ni_3Nb$-$NbCr_2$ quadrangle. With 5 to 7 wt.% nickel, a beta phase based on low-temperature modifications of $NbCr_2$ was replaced by an epsilon phase of a base of high-temperature $NbCr_2$.

The presence of a transition in pure chromium around 40°C (from 25 to 65°C, depending on the specimen investigated) is reported by California Institute of Technology workers.[134] This transition is evidenced by the anomalous behavior of various physical properties in the vicinity of the transition. The properties investigated include electrical resistivity, Young's modulus, Poisson's ratio, Hall coefficient, and specific heat.

## Refractory-Metal—Oxygen Systems

Investigators at the University of Cincinnati[135] have investigated the system niobium-titanium-zirconium-oxygen at 1500°C. Up to 66.7 at.% oxygen, the system contains nine four-phase regions. Isopleths at 10, 20, 30, 40, 50, and 55 at.% oxygen were constructed.

A thorough investigation of the strengthening of niobium by oxygen has been reported by Rensselaer Polytechnic Institute.[136] The following conclusions have been drawn from this work:

1. The relation between the lattice parameter of solid solutions of oxygen in niobium and the oxygen content is not linear, but the parameter increases at an increasing rate with increasing oxygen content.
2. Elliott's relation concerning the solubility limit of oxygen in niobium is correct at high temperatures but somewhat high at low temperatures.
3. The mechanism of precipitation from solid solutions of oxygen in niobium in the temperature range of 650 to 705°C involves the localized, continuous precipitation of NbO at high-energy points, such as grain-boundary intersections.
4. The rates at which NbO precipitates are quite slow.
5. The precipitate surface reaction, and not diffusion, is the rate-controlling step in the precipitation in the temperature and concentration ranges employed in this work.

## Properties of Refractory Metals

A bibliography of properties of tungsten of interest in the field of nuclear power has been published by Los Alamos.[137]

The results of hardness measurements on a number of refractory-metal alloys being developed by Nuclear Metals[138] are shown in Table IV-5.

Table IV-5 ROOM-TEMPERATURE HARDNESS OF REFRACTORY-METAL ALLOYS[138]

| Re, Hf, or Ru content, at.% | DPH, kg/mm² (1-kg load) | | | | | | |
|---|---|---|---|---|---|---|---|
| | Mo-Re | W-Re | Nb-Re | Ta-Re | W-Hf | W-Ru | Ta-Ru |
| 0 | 188 | 402 | 94 | 150 | | 432 | 138 |
| 2 | | | | | 470 | 583 | |
| 5 | 176 | 377 | 220 | 283 | 655 | 808 | 334 |
| 10 | 206 | 431 | 351 | 430 | 665 | 1148 | 502 |
| 15 | 254 | 510 | 431 | 538 | | 1400 | 622 |
| 20 | 273 | 520 | 482 | 650 | | 1800 | 730 |
| 25 | | 526 | | | | | |
| 30 | 381 | 467 | 546 | 691 | | | 792 |
| 35 | 368 | | | | | | 953 |
| 40 | | | 730 | 653 | | | 1136 |

These results show a significant difference between the effect of rhenium on the hardness of the Group V metals, molybdenum and tungsten, and its effect on the Group VI metals, niobium and tantalum. In the Group V metals, the addition of 5 at.% rhenium produces an insignificant change in hardness, whereas larger additions produce increases, with an apparent peak at 25 to 30 at.% addition. In Group VI metals, the 5 at.% rhenium addition produces increases that continue up to the solubility limit. The effect of rhenium on the hot hardness of tungsten is shown in Table IV-6.

Table IV-6 EFFECT OF RHENIUM ON HOT HARDNESS OF TUNGSTEN[138]

| Rhenium addition, at.% | DPH, kg/mm² (1-kg load) | | |
|---|---|---|---|
| | *RT* | 1100°C | 1200°C |
| 0 | 402 | 63 | 63 |
| 5 | 377 | 136 | 107 |
| 10 | 431 | 204 | 179 |
| 15 | 510 | 179 | 140 |
| 20 | 520 | 175 | 160 |
| 25 | 526 | 194 | 149 |
| 30 | 467 | 202 | 168 |

### Properties of Zirconium Alloys

It has been found on investigating[139] the zirconium-niobium system that, even when 99.9% pure iodide zirconium is used, the oxygen content of the alloys leads to a distinct ternary character of the phase diagram. In this way the monotectoid point of the binary system is extended over a transformation range, which, in the case of alloys made from sponge zirconium, is over 200°C. The maximum solubility of niobium in alpha zirconium is about 2 wt.%, and it is dependent on the purity of the original material. In sponge zirconium the solubility is less. The lattice constants of alpha zirconium are reduced by niobium. It was not possible to establish whether the alpha solid solution could be age hardened.

The United Kingdom Atomic Energy Authority[140] has published a manual for zirconium. This manual is a compilation of the best available unclassified data on the physical, mechanical, and irradiation properties of zirconium and certain of its alloys, particularly Zircaloy-2.

A German investigation[141] on the behavior of zirconium alloys during thermal cycling between 20 and 350°C is reported. Tests were carried out on zirconium–3 wt.% niobium–1 wt.% tin and on Zircaloy-2. It appears from this work that a slight increase in the length of tubes occurs in tube sections annealed at temperatures between 575 and 1000°C. In cold-drawn tubes the thermal cycling results, in the case of both alloys, in contractions of 0.05 to 0.1% at cold-drawing degrees of 20 to 27%, irrespective of the annealing temperature. The contraction is caused by recovery processes, and it is mostly achieved after one heating. However, in the case of other textures (e.g., rolling), texture-conditioned length variations can occur which are not dependent on the number of preceding thermal cycles.

(J. A. DeMastry)

## Diffusion Studies

Sawatzky and Vogt[142] at Chalk River have analyzed the kinetics of the thermal diffusion of hydrogen in Zircaloy-2. By means of mathe-

matical solutions to the appropriate diffusion equations, they have described the kinetics of the process for the various temperatures and concentrations encountered in a heavy-water-moderated reactor. The phase relations and hydrogen redistributions are discussed in detail, and they would be of considerable interest to those concerned with this particular area.

An intensive study and interesting discussion of the self-diffusion of zirconium are presented by Oak Ridge.[143] Chemically pure $Zr^{95}$ was used to determine the self-diffusion coefficients in the body-centered cubic phase of iodide zirconium over the temperature range 900 to 1750°C. Owing to curvature of the Arrhenius plot, the temperature dependence of the diffusion coefficients could not be described by the usual Arrhenius type equation. A comparison with other published results indicates generally good agreement. The Oak Ridge data are described by the following equation:

$$D = 3 \times 10^{-6} \left(\frac{T}{1136}\right)^{15.6} \times \exp\left[-\frac{19{,}600 + 31\,(T - 1136)}{RT}\right] \text{ cm}^2/\text{sec}$$

where the 1136°K corresponds to the alpha-to-beta transition temperature.

The Russians have carried out experiments[144] in which $Nb^{95}$ and $C^{14}$ were used to study the diffusion of niobium and carbon in metallic niobium and some of its carbides. The activation energies that were determined are included in Table IV-7.

Results have been reported for the diffusion of chromium, manganese, and cobalt in gamma uranium. The values for the Arrhenius type equations contained in Table IV-8 were determined by Rothman and Peterson at Argonne.[9]

Table IV-7 ACTIVATION ENERGIES FOR DIFFUSION OF NIOBIUM OR CARBON IN NIOBIUM OR NIOBIUM CARBIDES[144]

| Diffusing element | Diffusion in structure of | Activation energy, kcal/gram atom |
|---|---|---|
| Niobium | Nb | 85 |
| | $NbC_{0.98}$ | 55 |
| Carbon | Nb | 32 |
| | $NbC_{0.98}$ | 32–33 |
| | $NbC_{0.75}$ | 32–33 |
| | $NbC_{0.5}$ | 32–33 |

Table IV-8 VALUES FOR ARRHENIUS TYPE EQUATIONS [$D = D_0$ EXP $(-Q/RT)$ $CM^2/SEC$] FOR DIFFUSION OF CHROMIUM, MANGANESE, AND COBALT IN GAMMA URANIUM[9]

| Element | $D_0$ | $Q$ |
|---|---|---|
| Cobalt | $2.73 \times 10^{-4}$ | 11,800 |
| Manganese | $4.45 \times 10^{-4}$ | 15,800 |
| Chromium | $2.0 \times 10^{-3}$ | 21,800 |

Diffusion coefficients for $Al^{26}$ and $Mn^{54}$ in aluminum have been determined at Oak Ridge[145] for temperatures between 450 and 650°C. The temperature dependences of the coefficients obtained are expressed by the following equations:

$$D \text{ for } Al^{26} = 1.71 \exp(-34{,}000/RT)$$

$$D \text{ for } Mn^{54} = 0.22 \exp(-28{,}800/RT)$$

An interesting review paper on the compatibility of nuclear materials has been published by Hanna[146] of the Australian Atomic Energy Commission. This paper is recommended to the reader who wants a general survey of the types and principles of the solid-state reactions between fuel-element materials. Subjects receiving specific attention in the paper are: (1) the principles of layer growth in diffusion reactions, (2) the diffusion between uranium and aluminum or beryllium, (3) the effect of pressure on diffusion reactions, (4) the reactions between beryllium and oxides of uranium or thorium, (5) the reaction between uranium dioxide and zirconium, and (6) the effects of irradiation on compatibility. It should be noted, however, that the paper should have made use of more current references. For instance, a 1955 report on the $UO_2$-zirconium reaction was used as a reference instead of a more complete 1957 report. Also, information on uranium-aluminum diffusion zones was obtained from a 1957 annual report, but later results on this subject published in subsequent annual reports were not referenced.

(D. C. Carmichael)

# Ceramic Technology

Harwell investigators[147] are continuing their studies of the deformation and fracture of single-crystal MgO. They have found that an

as-cleaved crystal may go through several distinguishable stages of deformation prior to fracture. The fracture mechanism depends on the stage of deformation when fracture occurs. In all cases, fracture occurs when an aggregation of dislocations localizes strain energy near a subcritical crack. This localized energy supplements the energy available from the overall strain field, and so assists fracture. The dislocations may vary in type. For example, they may be slip-band intersections, broadened slip bands, etc.

Arthur D. Little, Inc., has described[148] a program in progress on the thermodynamic and kinetic behavior of the carbides and borides of zirconium and hafnium. Studies are being conducted at temperatures to 3000°K and in atmospheres of $O_2$, $O_2 + H_2O$, $Cl_2$, $F_2$, HF, $H_2$, CO, $NH_3$, and $N_2$. The stated aims of the program are:

1. To provide data leading to tabulation of free-energy functions of the compounds.
2. To identify gaseous species formed by vaporization and to study their interaction with the various atmospheres.
3. To develop thermodynamic data on important gaseous species.
4. To develop kinetic data on the reactions of the compounds with the various atmospheres.

The preparation and characterization of macrocrystalline, high-purity $ZrB_2$ and ZrC are described.

Avco investigators[149] have reported the effects of sodium vapors on various ceramics and glasses. The materials studied were Vycor, pyrex, BN, $Al_2O_3$, BeO, MgO, and pyrolytic graphite. These were exposed to gaseous sodium at 940°C for 15 min. The observers reported complete destruction of Vycor and pyrolytic graphite, extensive reaction with pyrex, and diffusion of sodium into all other test materials.

Studies have been made at Oak Ridge[145] on hot pressing of $ThO_2$. The controlled variables of temperature, time, and pressure ranged from 1000 to 1600°C, 20 to 900 sec, and 0 to 3000 psi, respectively. Bulk densities of the hot-pressed pieces were measured, and the data were analyzed statistically. From this, a relation between the hot-pressing conditions, a material constant, and the hot-pressed density was developed.

In other work at Oak Ridge, the diffusion of thorium in $ThO_2$ is being investigated. A thin layer of $ThO_2$ enriched with $Th^{230}$ was deposited on a normal $ThO_2$ pellet of 97.5% of theoretical density. The composite pellet was heated for various times and at various temperatures. It was then sectioned, and the sections were analyzed for $Th^{230}$ penetration. Diffusion coefficients were calculated, and they ranged from $3 \times 10^{-12}$ to $5 \times 10^{-11}$ for temperatures of 1430 to 2000°K, respectively. The activation energy of thorium diffusion in $ThO_2$ was found to be 37.8 kcal/mole, as compared with 14.7 kcal/mole for oxygen diffusion.

Berard[150] of Iowa State University has prepared an annotated bibliography, together with tabular data, on all phases of diffusion in ceramics. The bibliography, which contains 165 entries, covers oxides, silicates, glasses, borides, carbides, and graphite.

(A. K. Smalley)

## References


1. G. H. Jenks and J. E. Baker, Determination of the Effect of High Excess $H_2SO_4$ Concentrations on the Radiation-Induced Corrosion of Zirconium and Titanium Alloys in 0.17*M* $UO_2SO_4$, USAEC Report ORNL-2943, Oak Ridge National Laboratory, May 1, 1962.
2. Preprints of papers to be published in the Proceedings of the International Atomic Energy Conference on the Corrosion of Reactor Materials, Salzburg, Austria, June 4–9, 1962:
   *a*. R. C. Asher and B. Cox, The Effects of Irradiation on the Oxidation of Zirconium Alloys.
   *b*. H. Coriou et al., The Corrosion of Zircaloy in Various Alkaline Media at High Temperatures.
   *c*. S. B. Dalgaard, Corrosion and Hydriding Behaviour of Some Zr–2.5 Wt.% Nb Alloys in Water, Steam, and Various Gases at High Temperature.
   *d*. A. Bossi et al., Zircaloy-2 and Stainless Steel Corrosion in Flowing Wet Steam.
   *e*. D. L. Douglass, Corrosion Mechanism of Columbium, Zirconium, and Their Alloys: I. Diffusion of Oxygen and Columbium Pentoxide and Zirconium Dioxide.
   *f*. H. Inouye, High-Temperature Reactions of Type 304 Stainless Steel in Low Concentrations of Carbon Dioxide and Carbon Monoxide.
3. S. B. Dalgaard, Corrosion and Hydriding Behaviour of Some Zr–2.5 Wt.% Nb Alloys in Water, Steam, and Various Gases at High Tem-

perature, Canadian Report AECL-1513, May 1962.

4. C. F. Britton and J. N. Wanklyn, Inhibition by Boric Acid of the Oxidation of Zirconium in High Pressure Steam, *J. Nucl. Mater.*, 5: 326–327 (April 1962).
5. J. N. Wanklyn, The Corrosion of Zirconium and Its Alloys in High Temperature Steam, British Report GCM/UK/39, February 1962.
6. E. Landerman and C. J. Kubit, Development of Fabrication Procedures for Construction of Thermal Baffles, Including Preoxidizing of Zircaloy, USAEC Report CVNA-113, Westinghouse Electric Corp., Atomic Power Dept., Sept. 5, 1961.
7. General Nuclear Engineering Corp., An Investigation of Zirconium Alloys for Resistance to Carbon Dioxide Corrosion. Final Report, USAEC Report GNEC-235, June 30, 1962.
8. Westinghouse Electric Corp., Bettis Atomic Power Laboratory, Pressurized Water Reactor (PWR) Project. Technical Progress Report for the Period April 24, 1962, to June 23, 1962, USAEC Report WAPD-MRP-98.
9. Argonne National Laboratory, Metallurgy Division Annual Report for 1961, USAEC Report ANL-6516.
10. Argonne National Laboratory, Reactor Development Program Progress Report, May 1962, USAEC Report ANL-6573, June 15, 1962.
11. S. Goldsmith (Ed.), Research and Development Programs Executed for the Division of Reactor Development, Quarterly Progress Report, October, November, December, 1961, USAEC Report HW-73100, Hanford Atomic Products Operation, May 1, 1962.
12. D. O. Sprowls and R. H. Brown, What Every Engineer Should Know About Stress Corrosion of Aluminum, Part 1, *Metal Progr.*, 81(4): 79–85 (April 1962); Part 2, *Metal Progr.*, 81(5): 77–83, 118–122 (May 1962).
13. W. B. Jepson, J. B. Warburton, B. L. Myatt, and J. E. Antill, United Kingdom Atomic Energy Authority, February 1962. (Unpublished)
14. F. Eberle and C. H. Anderson, Scaling Behavior of Superheater Tube Alloys in ASME High Temperature Steam Research Tests at 1100–1500°F, *J. Eng. Power*, Series A, 84(3): 223–257 (July 1962).
15. R. R. Hood and L. Isakoff, Heavy Water Moderated Power Reactors, Progress Report, May 1962, USAEC Report DP-745, E. I. du Pont de Nemours & Co., June 1962.
16. G. G. Gaul, W. L. Pearl, and M. Siegler, Stress Corrosion of Type 304 Stainless Steel in Simulated Superheat Reactor Environments, USAEC Report GEAP-4025, General Electric Co., Vallecitos Atomic Laboratory, Feb. 26, 1962.
17. R. Stickler and A. Vinckier, Morphology of Grain Boundary Carbides and Its Influence on Intergranular Corrosion of 304 Stainless Steel, *Am. Soc. Metals, Trans. Quart.*, 54(3): 362–380 (September 1961).
18. Kh. I. Cheskis et al., Effect of Prolonged Heating on the Susceptibility of 1 Cr–18 Ni–9 Ti Steel to Intercrystalline Corrosion, *Intercrystalline Corrosion and Corrosion of Metals Under Stress*, I. A. Levin (Ed.), pp. 25–41, 1960; English translation published by Consultants Bureau, New York, 1962.
19. I. C. Mayes and J. McGrew, ANPP Corrosion Program. Final Summary Report, Report MND-E-2727, Martin Co., February 1962.
20. D. C. Vreeland, G. G. Gaul, and W. L. Pearl, Corrosion of Carbon Steels and Other Steels in Simulated Boiling-Water-Reactor Environment, Phase II, Report NP-11552, General Electric Co., Vallecitos Atomic Laboratory; paper presented at 18th Annual Conference of the National Association of Corrosion Engineers, Kansas City, Missouri, Mar. 19–23, 1962.
21. A. P. Larrick, The Corrosion of Stress Relieved, Annealed, Normalized, and Cold-Rolled A212 Carbon Steel in High Temperature Water, USAEC Report HW-68037, Hanford Atomic Products Operation, Feb. 27, 1961.
22. C. J. Owen, Stress Corrosion of High Strength Steels and Alloys; Artificial Environment, Final Report, Report NP-11948, Mellon Institute, 1962.
23. B. E. Farwell and J. S. Brunhouse, Army Gas-Cooled Reactor Systems Program. Effects of Gas Corrosion and Aging on ML-1 Turbine Alloys, USAEC Report IDO-28591, Aerojet-General Nucleonics, August 1962.
24. General Electric Co., Flight Propulsion Laboratory Dept., High-Temperature Materials Program. Progress Report No. 13, Part A, USAEC Report GEMP-13A, July 31, 1962.
25. Ames Laboratory, Annual Summary Research Report in Metallurgy, July 1960–June 1961, USAEC Report IS-351, December 1961.
26. A. Draycott et al., Corrosion of Alloy Steels in Carbon Dioxide, *J. Australian Inst. Metals*, 7: 76–84 (February 1962).
27. A. Thurlbeck, Summarised Compatibility Review of Reactor Materials for $CO_2$-Cooled Graphite-Moderated Reactors, British Report TRG-Report-267, Mar. 15, 1962.
28. V. I. Spitsyn et al., A Study of the Atmospheric Corrosion of Radioactive Samples of "Armco" Steel and of Carbon Steel-2, *Doklady Akad. Nauk SSSR*, 143: 1406–1408 (Apr. 21, 1962).
29. D. L. Macleary, Testing of Columbium and Columbium Alloys, *Corrosion*, 18: 67t–69t (February 1962).
30. N. N. Gratsianskii and N. A. Bogacheva, Investigation of the Corrosion Resistance of Solid Solutions of Mo-W, *Zhur. Fiz. Khim.*, 36: 546–548 (March 1962).
31. C. G. Kirkpatrick, Properties of Yttrium and the Rare Earth Metals, Effect of Minor Addi-

tions to Niobium-Base Alloy on Elevated Temperature Oxidation Resistance, Report WADD-TR-61-123 (Pt. II), Research Chemicals Div., Nuclear Corp. of America, June 1962.

32. R. C. Lever, Metallic Fuel Element Materials, USAEC Report APEX-913, General Electric Co., Flight Propulsion Laboratory Dept., June 20, 1962.
33. J. E. Battles, W. T. Ebihara, W. P. Meuli, M. J. Pool, R. Speiser, J. W. Spritnak, and G. J. St. Pierre, Research on the Oxidation Behavior of Tungsten, Report ARL-62-324, Ohio State University, April 1962.
34. J. A. McGurty and J. F. Collins, Oxidation Resistant Chromium Alloy, U. S. Patent 3,015,559, Jan. 2, 1962.
35. W. A. Gibeaut and J. J. English, DMIC Review—Oxidation-Resistant Coatings for Refractory Metals, DMIC Newsletter, Battelle Memorial Institute, Defense Metals Information Center, Aug. 3, 1962.
36. A. Blum, Furnaces, Supports, and Atmosphere for the Sintering of Some Borides, Nitrides, and Silicides, *Planseeber. Pulvermet.*, 10: 72–77 (1962).
37. Argonne National Laboratory, Reactor Development Program Progress Report, July 1962, USAEC Report ANL-6597, Aug. 15, 1962.
38. Argonne National Laboratory, Reactor Development Program Progress Report, August 1962, USAEC Report ANL-6610, Sept. 15, 1962.
39. Oak Ridge National Laboratory, Oct. 10, 1962. (Unpublished)
40. J. R. DiStefano and E. E. Hoffman, Relation Between Oxygen Distribution and Corrosion in Some Refractory-Metal–Lithium Systems, USAEC Report ORNL-TM-327, Oak Ridge National Laboratory, Oct. 4, 1962.
41. L. Baker, Jr., and L. C. Just, Studies of Metal-Water Reactions at High Temperatures. III. Experimental and Theoretical Studies of the Zirconium-Water Reaction, USAEC Report ANL-6548, Argonne National Laboratory, May 1962.
42. Argonne National Laboratory, Chemical Engineering Division Summary Report (for) January, February, March, 1962, USAEC Report ANL-6543, June 1962.
43. J. W. Cleland et al., Lattice Defect Production in Thermal Neutron Shielded Material, *J. Appl. Phys.*, 33: 2906 (September 1962).
44. P. G. Lucasson and R. M. Walker, Production and Recovery of Electron-Induced Radiation Damage in a Number of Metals, *Phys. Rev.*, 127: 485–500 (July 15, 1962).
45. P. G. Lucasson and R. M. Walker, Variation of Radiation Damage Parameters in Metals, *Phys. Rev.*, 127: 1130–1136 (Aug. 15, 1962).
46. M. Doyama and J. S. Koehler, Quenching and Annealing of Lattice Vacancies in Pure Silver, *Phys. Rev.*, 127: 21–31 (July 1, 1962).
47. J. Nihoul, The Recovery of Radiation Damage in Molybdenum, *Phys. Status solidi*, 2: 308–316 (1962).
48. D. E. Peacock and A. A. Johnson, Point Defects in Niobium, Molybdenum, and Tantalum, *Nature*, 195: 169 (July 14, 1962).
49. Franklin Institute, An Experimental Study Concerning the Basic Mechanism of Radiation Damage. Annual Report, USAEC Report TID-14667, Jan. 16, 1962.
50. H. G. F. Wilsdorf and D. Kuhlmann-Wilsdorf, Dislocation Behavior in Quenched and in Neutron Irradiated Stainless Steel, *J. Nucl. Mater.*, 5: 178–192 (February 1962).
51. Hanford Atomic Products Operation, Fuels Development Operation. Quarterly Progress Report, January–March 1962, USAEC Report HW-72347, Apr. 16, 1962. (Classified)
52. Hanford Atomic Products Operation, Fuels Development Operation. Quarterly Progress Report, April–June 1962, USAEC Report HW-74377, July 20, 1962. (Classified)
53. M. J. Makin and T. H. Blewitt, The Hardening of Copper Single Crystals by Electron Irradiation, *Acta. Met.*, 10: 241–246 (March 1962).
54. D. J. Mazey, R. S. Barnes, and A. Howie, On Interstitial Dislocation Loops in Aluminum Bombarded with Alpha-Particles, British Report AERE-R-4087, June 1962.
55. R. S. Barnes and D. J. Mazey, The Nature of Radiation-Induced Point Defects, *Phil. Mag.*, 5: 1247 (1960).
56. G. R. Piercy and J. C. Whitton, Investigation of Radiation Damage in Pure Aluminum and Aluminum–1 Per Cent Magnesium Alloy by Transmission Electron Microscopy, *J. Inst. Metals*, 90: 386–388 (June 1962).
57. T. K. Bierlein and B. Mastel, Defect Structures Observed in Neutron-Bombarded Aluminum, *J. Appl. Phys.*, 33: 2873 (September 1962).
58. J. F. Kerridge et al., On the Mechanism of Vacancy Annihilation in Neutron Irradiated Molybdenum, *Phil. Mag.*, 7: 1073–1074 (June 1962).
59. C. J. Beevers, Irradiation Damage in Molybdenum after Energetic $H^+$ and $H^{++}$ Ion Bombardment, *Phil. Mag.*, 7: 1061–1064 (June 1962).
60. S. S. Sheinin, Some Factors Influencing Dislocation Loop Size in Neutron Irradiated Metals, *Nature*, 194: 1272–1273 (June 30, 1962).
61. A. Sosin, Energy Dependence of Electron Damage in Copper, *Phys. Rev.*, 126: 1698 (June 1, 1962).
62. R. S. Nelson, M. W. Thompson, B. W. Farmery, and M. J. Hall, Focused Collision Sequences in Aluminum, British Report AERE-R-4014, April 1962.
63. R. S. Nelson, M. W. Thompson, H. Montgomery, B. W. Farmery, and M. J. Hall, The Influence of Thermal Vibration on Focused Collision Sequences, British Report AERE-R-4044, March 1962.

64. R. S. Nelson and M. W. Thompson, Evidence for Focused Recoil Trajectories from a High-Energy Sputtering Experiment with Copper, *Phys. Rev. Letters*, 2: 124–126 (Sept. 1, 1962).
65. K. H. Westmacott, A. C. Roberts, and R. S. Barnes, The Growth of Dislocation Loops During the Irradiation of Aluminium, British Report AERE-R-4096, July 1962.
66. J. R. Weir, The Effect of High-Temperature Reactor Irradiation on Some Physical and Mechanical Properties of Beryllium, Preprint 28, Institute of Metals, London, 1961.
67. W. F. Noyes, Observations of Nuclear Particle Tracks in the Electron Microscope, *Rev. Sci. Instr.*, 33: 878–879 (August 1962).
68. R. Conte et al., Cold Working Recovery of Faults Created in Iron by Irradiation, *Compt. Rend.*, 254: 1023–1025 (Feb. 5, 1962).
69. P. Tetenyi and L. Babernics, The Effect of Irradiation on the Catalytic Properties of Copper, *Doklady Akad. Nauk SSSR*, 143: 616–667 (Mar. 21, 1962).
70. D. R. Muss and J. R. Townsend, Internal Friction and Young's Modulus in Irradiated Tungsten, *J. Appl. Phys.*, 33: 1804–1807 (May 1962).
71. D. R. Muss, Defect Production, Internal Friction, and Young's Modulus in Irradiated Tungsten, *Dissertation Abstr.*, 22: 4059 (May 1962).
72. D. R. Muss and J. R. Townsend, Energy Dependence of Radiation Damage in Tungsten, *J. Appl. Phys.*, 32(2): 189 (1961).
73. E. Ruedl et al., Electron Microscopic Study of Dislocations and Fission Damage in Platinum Foils, *J. Nucl. Mater.*, 6: 46–68 (1962).
74. E. Ruedl, Evidence for Focusing Collisions in Irradiated Platinum, *Phys. Rev. Letters*, 6(10): 530–532 (May 15, 1961).
75. United Kingdom Atomic Energy Authority, 1961. (Unpublished)
76. L. M. Howe, Radiation Damage in Zirconium, Zircaloy-2, and 410 Stainless Steel, Canadian Report AECL-1484, April 1962.
77. S. T. Konobeevskii et al., Effect of Irradiation on Phase Transformation in Cu-Sn and Cu-Sn-Pu Alloys, *J. Nucl. Mater.*, 5: 317–325 (April 1962).
78. J. Pauleve et al., Establishment of an Ordered Fe-Ni Structure by Neutron Irradiation, *Compt. Rend.*, 254: 965–998 (Feb. 5, 1962).
79. R. A. Arndt, Radiation Effects on Diffusion of Zinc in Brass, *Dissertation Abstr.*, 22: 2845 (February 1962).
80. C. J. Hochanadel, Evidence for "Thermal Spikes" in the Alpha-Particle Radiolysis of Nitrate Crystals, *Radiation Research*, 16: 286–302 (March 1962).
81. A. Norman and P. Spiegler, Thermal Spikes in Protein, *J. Appl. Phys.*, 33: 2658 (August 1962).
82. L. T. Chadderton, Experimental Evidence for the Concept of the Displacement Spike, *Nature*, 195: 987–998 (Sept. 8, 1962).
83. F. P. Bowden and L. T. Chadderton, Fission Fragment Damage to Crystal Lattices: Dislocation Formation, *Proc. Roy. Soc. (London)*, 269A: 143–164 (Sept. 11, 1962).
84. A. D. Whapham and M. J. Makin, The Nature of Fission Fragment Tracks in Uranium Dioxide, British Report AERE-R-4066, June 1962.
85. L. T. Chadderton, Dislocation Loops in Fission Fragment Bombarded Lead Iodide, *J. Appl. Phys.*, 33: 3021–3022 (October 1962).
86. P. B. Price and R. M. Walker, Electron Microscope Observations of a Radiation-Nucleated Phase Transformation in Mica, *J. Appl. Phys.*, 33: 2625 (August 1962).
87. M. C. Wittels et al., Radiation Effects in Uranium Doped Zirconia, *J. Nucl. Energy: Pts. A & B*, 16: 237–244 (May 1962).
88. M. C. Wittels and F. A. Sherrill, Fission Fragments Damage in Zirconia, *Phys. Rev. Letters*, 3(4): 176–177 (Aug. 15, 1959).
89. S. Weissmann, T. Imura, K. Nakajima, and S. E. Wisnewski, Lattice Defects of Quartz Induced by Fast Neutron Irradiation, USAEC Report NYO-10444, Rutgers University, September 1962.
90. W. N. Reynolds and P. A. Thrower, Irradiation Damage in Graphite, British Report AERE-R-3979, March 1962.
91. J. Rappeneau, Énergie Emmagasinee par le Graphite Irradie Effets de la Temperature d'Irradiation, *J. Nucl. Mater.*, 6: 107–118 (May/June 1962).
92. B. P. Jackets and D. J. Dyson, Dependence on Temperature of the Interlayer Spacing of Irradiated Graphites, *Nature*, 195: 680–681 (Aug. 18, 1962).
93. E. Creutz and S. Cunningham, Erosion of Graphite by Helium Recoils from Neutron Scattering and by Formation of HeC, USAEC Report GAMD-657, General Atomic Div., General Dynamics Corp., Jan. 22, 1959.
94. B. S. Hickman et al., X-Ray Diffraction Studies of Irradiated Beryllium Oxide, *J. Nucl. Mater.*, 6: 190–198 (July 1962).
95. D. H. Bowen et al., Irradiation Damage Clusters in the Oxides of Beryllium and Magnesium, *J. Nucl. Mater.*, 6: 148–151 (May/June 1962).
96. R. A. Johnson and E. Brown, Point Defects in Copper, *Phys. Rev.*, 127: 446–454 (July 15, 1962).
97. W. Bauer, Low Temperature Annealing Spectrum of Electron-Irradiated Gold and Cadmium, Univ. of Ill. Tech. Report No. 28, USAEC Report TID-16373, June 1962.
98. J. W. DeFord, Interpretation of Annealing Spectra of the Noble Metals, Univ. of Ill. Tech. Report No. 29, USAEC Report TID-16378, June 1962.
99. J. S. Koehler and G. Leibfried, The Interstitial Configurations in the Noble Metals, Univ. of Ill. Tech. Report No. 30, USAEC Report TID-16701, May 1962.

100. A. Seeger et al., Zwischengitteratome in Kubisch-Flächenzentrierten Kristallen, Insbesondere in Kupfer, *J. Phys. Chem. Solids*, 23: 639-658 (1962).
101. M. Balarin, Focusing Conditions for Elastic Atomic Collisions in Graphite, *Phys. Status solidi*, 2(1): 60-72 (1962).
102. General Electric Co., Flight Propulsion Laboratory Dept., High-Temperature Materials Program Progress Report No. 15, Part A, USAEC Report GEMP-15A, Sept. 14, 1962.
103. P. A. Flinn and A. A. Maradudin, Distortion of Crystals by Point Defects, *Ann. Phys. (N. Y.)*, 18: 81-109 (April 1962).
104. K. H. Bennemann, Redistribution of the Conduction Electrons Due to Point Defect Complexes in Metals, Univ. of Ill. Tech. Report No. 33, USAEC Report TID-16660, July 1962.
105. H. Wollenberger, The Energy Distribution of the Primary Atoms in Copper in Irradiation with Fast Monoenergetic and Reactor Neutrons, *Nukleonik*, 4: 25-30 (February 1962).
106. K. L. Merkle, Fission-Fragment Tracks in Metal Oxide Films, *Phys. Rev. Letters*, 9: 150-152 (Aug. 15, 1962).
107. M. T. Robinson, Deduction of Ion Ranges in Solids from Collection Experiments, *Appl. Phys. Letters*, 1: 49-51 (Oct. 1, 1962).
108. D. Mosedale, Influence of Irradiation on Creep, *J. Appl. Phys.*, 33(10): 3142-3143 (October 1962).
109. M. J. Makin, Some Factors Affecting the Hardening Caused by Gas Bubbles, British Report AERE-M-1000, February 1962.
110. *Nucl. Sci. Abstr.*, 16(17): Abstract Nos. 22679-22706 and 22816 (Sept. 15, 1962).
111. N. F. Pravdyuk and A. N. Ivanov, Effects of Neutron Irradiation on the Electric Resistance of Certain Metals, USAEC Translation AEC-tr-5263 (translated from Paper SM-25/87 presented at the IAEA Symposium on Effects of Neutron Emission on the Electric Resistance of Certain Metals, Venice, Italy, May 7-11, 1962).
112. G. P. Saenko, Effects of Neutron Irradiation on the Ordered Alloy $Fe_3Al$, USAEC Translation AEC-tr-5245 (translated from Paper SM-25/86 presented at the IAEA Symposium on Effects of Neutron Emission on the Electric Resistance of Certain Metals, Venice, Italy, May 7-11, 1962).
113. R. W. Balluffi, J. S. Koehler, and R. O. Simmons, Present Knowledge About Point Defects in Deformed Face-Centered Cubic Metals, Univ. of Ill. Tech. Report No. 26, USAEC Report TID-16222, February 1962.
114. S. T. Konobeevskii, Effect of Irradiation as a Material Science Problem, USAEC Translation AEC-tr-5181 (translation of a paper presented at the International Colloquium on the Impact of Science on Materials Technology, San Carlos de Bariloche, April 2-7, 1962).
115. *Ionization Phenomena in Gases*, Vol. I, North-Holland Publishing Co., Amsterdam, 1962.
116. A. C. Damask, Radiation Effects in Nonfissionable Alloys, *Nucleonics*, 20: 43-46 (July 1962).
117. F. J. P. Clarke, The Effects of Reactor Irradiation on Ceramic Materials, *Special Ceramics*, pp. 82-101, Academic Press Inc., New York, 1960.
118. W. Primak and M. Bohmann, Radiation Damage, *Progr. Ceram. Science*, 2: 103-180 (1962).
119. ASTM Symposium on Radiation Effects in Refractory Fuel Compounds, *Am. Soc. Testing Mater., Spec. Tech. Publ.*, 306 (1962).
120. D. J. Littler (Ed.), *Properties of Reactor Materials and the Effects of Radiation Damage*, Butterworth & Co., London, 1962.
121. *Proceedings of the Fifth International Congress for Electron Microscopy*, Philadelphia, Aug. 29 to Sept. 5, 1962, Vol. I, Electron Microscopy, Academic Press Inc., New York, 1962.
122. D. G. Evans, The Effect of Neutron Irradiation on the Mechanical Properties of Welded Zircaloy-2, Canadian Report CRGM-1093, July 1962.
123. Atomic Energy of Canada Ltd., 1962. (Unpublished)
124. C. N. Spalaris, F. A. Comprelli, D. L. Douglass, and M. B. Reynolds, Materials for Nuclear Superheat Applications, USAEC Report GEAP-3875, General Electric Co., Atomic Power Equipment Dept., Jan. 5, 1962.
125. H. E. McCoy, Jr., and D. A. Douglas, Jr., Effect of Environment on the Creep Properties of Type 304 Stainless Steel at Elevated Temperatures, USAEC Report ORNL-2972, Oak Ridge National Laboratory, Sept. 18, 1962.
126. P. R. V. Evans, The Effect of Nitrogen on the Yield Strength of Niobium, *J. Less-Common Metals*, 4: 79-91 (February 1962).
127. R. T. Begley (Ed.), Development of Niobium-Base Alloys, USAEC Report WADC-TR-57-344, Westinghouse Electric Corp., September 1961.
128. E. S. Bartlett and F. F. Schmidt, Review of Recent Developments in the Technology of Columbium and Tantalum, Battelle Memorial Institute, Defense Metals Information Center, Apr. 20, 1962.
129. R. Syre, Niobium, Molybdenum, Tantalum, and Tungsten, A Summary of Their Properties with Recommendations for Research and Development, Report AGARDograph-50, June 11, 1962.
130. J. L. Ratcliff and H. R. Ogden, A Compilation of the Tensile Properties of Tungsten, Report DMIC-Memo-157, Battelle Memorial Institute, Defense Metals Information Center, Sept. 11, 1962.
131. V. S. Yemel'yanov et al., Mechanical Properties of Binary and Ternary Zirconium Alloys with Tantalum and Niobium at Room and High Temperatures, *Ref. Zh., Mashinostroyeniye*, No. 20: 16 (1961).

132. H. J. Seemann and F. Stavenow, X-Ray Study on the Occurrence of Stacking in Various Aluminum Alloys, *Z. Metallk.*, 52: 667–670 (October 1961).

133. V. M. Sveehnikov and V. M. Pan, Diagram of States of Cr-Ni-Nb, *Dopovidi Akad. Nauk Ukr. RSR*, No. 10: 1290–1295 (1961).

134. Jean-Francois Marin, Transitions in Chromium, USAEC Report TID-14740, January 1962.

135. W. C. Wyder and M. Hoch, The System Niobium-Titanium-Zirconium-Oxygen at 1500°C, *Trans. Met. Soc. AIME*, 224: 373–378 (April 1962).

136. F. V. Lenel, L. J. Regitz, and W. R. Hulsizer, The Strengthening of Columbium Alloys by Interstitial Alloying Elements, Report AROD-2530:1, Rensselaer Polytechnic Institute, May 11, 1962.

137. B. J. Thamer (Comp.), Properties of Tungsten of Interest in the Field of Nuclear Power, USAEC Report LAMS-2675, Los Alamos Scientific Lab., Jan. 15, 1962.

138. A. R. Kaufmann, Fundamental and Applied Research and Development in Metallurgy, USAEC Report NMI-2104, Nuclear Metals, Inc., May 4, 1962.

139. H. Richter et al., The Constitution of Zirconium-Niobium Alloys, *J. Less-Common Metals*, 4(3): 252–265 (June 1962).

140. B. J. Seddon (Comp.), Zirconium Data Manual—Properties of Interest in Reactor Design, British Report TRG-Report-108, Sept. 19, 1961.

141. H. Richter, P. Wincierz, and U. Zwicker, Examination of Alloys of Zirconium with Niobium and/or Silicon with a View to their Use as a Cladding Material in Water-Cooled Nuclear Reactors. Technical Report to Part 2: Length Variations in Zirconium Alloys Caused by Thermal Cycling, USAEC Report EURAEC-201, Oct. 10, 1961.

142. A. Sawatzky and E. Vogt, Mathematics of the Thermal Diffusion of Hydrogen in Zircaloy-2, Canadian Report CRT-1049, October 1961.

143. T. S. Lundy and J. I. Federer, Diffusion of $Zr^{95}$ in Body-Centered Cubic Iodide Zirconium, USAEC Report ORNL-3339, Oak Ridge National Laboratory, Sept. 5, 1962.

144. P. V. Gel'd and V. D. Lyubimov, Diffusion of Niobium and Carbon into Niobium and Its Carbides (in Russian), *Izvest. Akad. Nauk SSSR, Otd. Techn. Nauk, Met. i. Toplivo*, No. 6: 119–126 (November–December 1961).

145. Oak Ridge National Laboratory, Metals and Ceramics Division Annual Progress Report for Period Ending May 31, 1962, USAEC Report ORNL-3313, Aug. 16, 1962.

146. G. L. Hanna, Solid-State Reactions Between Nuclear Fuel Materials, *J. Australian Inst. Metals*, 7(1): 1–9 (February 1962).

147. H. B. Tattersall and F. J. P. Clarke, Slip Distribution and Fracture in Magnesium Oxide, British Report AERE-R-4104, July 1962.

148. Arthur D. Little, Inc., Thermodynamic and Kinetic Studies for a Refractory Materials Program, Report ASD-TDR-62-204, Part I, April 1962.

149. M. E. Ihnat, The Reaction of Glasses, Pyrolytic Graphite, and Selected Refractories with Sodium Vapor at Elevated Temperatures, Report RAD-TM-60-44, Avco Corp., April 1960.

150. M. F. Berard, Diffusion in Ceramic Systems. A Selected Bibliography, USAEC Report IS-448, Ames Laboratory, May 1962.

Section

V

Reactor Materials

# Special Fabrication Techniques

## Melting and Casting

The effect of processing variables imposed during the remelting of uranium on the chemistry of uranium ingots has been of considerable interest to National Lead.[1] Recent studies have been directed toward the utilization of pickled extrusion skulls and briquetted-dingot machine turnings for remelt stock. For these investigations a series of 36 charges was vacuum induction melted and cast. An evaluation of the remelt ingots led to the following conclusions:

1. Ingots produced from the extrusion skulls and the briquetted-dingot surface turnings were lower in carbon and higher in both iron and silicon than were the control ingots.

2. The ingot yields from the briquetted materials were low, as expected from fuel material of this type.

3. The core-to-good-core yields were excellent for all materials.

Considerable interest in the utilization of electron-beam melting techniques is evidenced by the variety of materials upon which these techniques are now being employed. The Bureau of Mines[2] is continuing investigations concerning the purification of hafnium and yttrium metal, and both Oak Ridge[3] and the Central Institute for Industrial Research[4] are employing electron-beam melting to produce niobium single crystals.

The hafnium-purification studies at the Bureau of Mines[2] have shown that the impurities are removed in the following sequence: ZrO, AlO, $Al_2O$, iron, magnesium, oxygen, CrO, $CrO_2$, TiO, $TiO_2$, and copper. The magnitude of the change in removal rate was proportional to the energy input and to the duration of the melt. The studies concerned with the purification of yttrium have been less successful to date owing to the affinity of the base metal for the interstitials it contains. However, many of the metals (aluminum, copper, iron, magnesium, and sodium) have been removed to the limit of detection in 2 hr at 9 kw per square inch of sample area.

The electron-beam techniques used in the production of single crystals of niobium[3,4] are simple adaptations of zone-refining techniques. The rate of movement for the floating zone reported by the Norwegians was 1.8 mm/min; the parameters employed at Oak Ridge were not described.

A volume[5] containing numerous articles dealing with the technology of electron-beam melting has recently been published. This should be of interest to all those concerned with electron-beam melting, casting, and heat-treatment.

The Bureau of Mines[2] has continued its studies on the preparation and evaluation of hafnium carbide (2.72 to 11.2 wt.% carbon) and uranium carbide. The maximum melting point of arc-cast hafnium carbide was found to be 50 to 100°C less than the literature value of 3890°C, and the measured density was 96% of theoretical. Stoichiometric cast HfC exhibited a diamond pyramid hardness of approximately 2000 $kg/mm^2$, and it had an electrical resistivity higher than that exhibited by sintered material.

The UC studies at the Bureau of Mines[2] have been concerned with the evaluation of materials for consumable-electrode melting. The preparation of six types of electrodes has been attempted. Two of these types were prepared from commercial uranium carbide: (1) Vitro's fine spherical shot and (2) Spencer's crystalline compaction grade. The other four types were prepared from unreacted materials: (1) $UO_2$ + $U_3O_8$ + carbon, blended and arc welded; (2) ura-

nium sawdust plus carbon; (3) uranium lathe turnings plus carbon; and (4) hollow carbon rods enclosing solid uranium rods.

Attempts to compact the commercial uranium carbides were unsuccessful at pressures up to 20 tsi; however, one button was made from the Vitro stock using a tungsten cathode, and electrodes were prepared from the Spencer material by fusion welding. The button of consolidated Vitro material analyzed 5.6 wt.% carbon, whereas the starting material showed a carbon content of 5.2 wt.% prior to consolidation. Carbon analyses of the melts prepared from the Spencer material showed a variation in carbon content from 2.6 to 4.3 wt.%. It should be noted that the highest carbon content exhibited by the Spencer material is considerably less than that of the stoichiometric UC composition. An explanation for the extremely low and variable carbon content may lie in the oxygen content of the electrodes prior to melting. Since none of the aforementioned methods of UC preparation have proved successful, further work will be confined to a composite type of electrode, and uranium and graphite will be utilized.

A Canadian report[6] of interest concerns the preparation of aluminum-uranium alloys. The techniques employed were used earlier by Saller. Ten batches of $UO_2$ were reduced in aluminum under a cryolite flux to form aluminum–28 wt.% uranium alloys. During this initial reduction, recoveries of up to 98% of the uranium were achieved, and the slag was easily removed from the billets. Upon remelting, homogeneous castings free of internal and surface porosity were obtained. The reported recoveries and densities in the as-cast materials are markedly better than those attained in previous studies of this nature.

The effects of coolant flow rate and crucible wall thickness on the power required to cause failure of the copper crucible during consumable-electrode melting are under continuing study by the Bureau of Mines.[2] No effect of coolant flow rates has been noted, whereas increases in wall thickness to greater than $\frac{5}{16}$ in. greatly decreased the current required to damage the crucible wall. However, it is inferred that wall thicknesses of less than $\frac{3}{8}$ in. are preferable from the standpoint of heat transfer.

(N. E. Daniel)

# Fabrication and Heat-Treatment

The fabrication of uranium by extrusion is being investigated at numerous sites. Canadian investigators have shown the feasibility of gamma-phase extrusion.[7,8] Investigators at Bridgeport Brass[9] are evaluating the capabilities of Dynapak extrusion to form tubes, and they are also investigating the warm extrusion of uranium by conventional techniques. Hanford[10] is utilizing conventional extrusion techniques to evaluate the effects of small additions of zirconium and carbon on the fabricability of uranium.

The Hanford studies[10] are concerned with the effects of additions of up to 2 wt.% zirconium and 40 to 1600 ppm carbon on the extrusion behavior and physical properties of uranium. It has been noted that small additions of zirconium increase the extrusion coefficients rapidly, whereas the increase attributable to carbon is gradual. Excessive carbon in the uranium-zirconium alloys caused the formation of UC, and regardless of the addition the extruded material was always softer than the starting material.

The fabrication of zirconium and its alloys is also being actively investigated at other sites. At Argonne[11] investigators have found that copper plating of Zircaloy-2 will result in the prevention of die seizure and an improved tube surface when reducing tubing from 0.283 in. in outside diameter to 0.119 in. in outside diameter in 12 drawing operations. The Advanced Technology Laboratories[12] has reported the successful extrusion of Zircaloy-2 at temperatures from room temperature to 400°C and with reductions in area of 50, 60, and 80%. The successful fabrication of thin-walled thermal baffles from zirconium alloys is reported by Westinghouse.[13] Cold forming, inert-gas welding, vacuum annealing, and final cold drawing were employed to obtain the desired shape and dimensions. Hanford[14] has been evaluating the effects of up to 2 wt.% cerium additions on properties of Zircaloy-2. No effect on the room-temperature hardness was detected. Buttons with various cerium contents were heated in a salt bath and rolled at 730°C. Edge cracking was noted in the high-cerium alloys.

Nuclear Metals' interest in Zircaloy[15] is more closely related to joining than to fabrication per se. In these studies, metallurgically bonded tubular joints of stainless steel and Zircaloy have been prepared by tandem extrusion. It was found that the mechanical and corrosion properties were limited by the Zircaloy rather than by the interface, and up to 40% cold working of the bond did not prove detrimental to the bond quality.

(N. E. Daniel)

# Cladding

## Cladding by Rolling and Swaging

In the area of densification of $UO_2$ by swage cladding, most of the data reviewed this quarter were reported previously. However, contributions have appeared from several new sources, including European firms working under Euratom auspices.[16–18]

A significant development in the swage-cladding area, reported by Hanford,[19] is the production of 8-ft-long Plutonium Recycle Test Reactor (PRTR) fuel elements with excellent longitudinal dimensional control. By controlling the weight of the cladding tubes within ± 1% prior to swaging, they are able to cold swage tubes to within $^3/_{16}$ in. in length with a 15% reduction in area. With the same processing, a weight variation of ± 4% gave a $^5/_8$-in. variation in length.

Other workers at Hanford reported some success with Zircaloy cladding of plutonium–15 wt.% zirconium by roll bonding. The core material was fabricated to 0.020-in. sheets and was found to be single phase. During assembly, aluminum foil was wrapped around the core inserts to prevent excessive contamination of the Zircaloy cladding. Bonding was accomplished by jacketing the assembly in mild steel and by rolling at 840°C to a total reduction of 93%. The samples were well bonded, as revealed by metallography and ultrasonics. However, as a result of the appearance of a hard second phase, apparently during fabrication, dimensional control of the core was poor. Investigators felt that the second phase was an intermetallic compound, possibly $PuAl_2$, which was produced by reaction of the core with the aluminum barrier.

(H. D. Hanes)

## Pressure Bonding

Hodge et al. published a paper[20] on the general equipment employed in the gas-pressure-bonding process. Gas-pressure-bonding methods are described which utilize autoclaves operating at pressures up to 15,000 psi and at temperatures up to 1100°C, to attain direct densification, cladding, and joining of components. The components are placed in a disposable container in the autoclave and are subjected to gas pressures sufficient to deform the components plastically and bring them into intimate contact for solid-state bonding or to deform powder-metallurgy products sufficiently to cause densification. Nuclear applications of the method are emphasized.

Bettis[21] has been employing the gas-pressure-bonding process to produce fuel elements for the PWR core 2. Fourteen production pressure-bonding runs have been made to date. A total of 764 seed type elements has been made. Nondestructive testing results indicate that all fuel-element dimensions and bond-quality attributes are within specification and design limits. On this basis a reduced nondestructive testing program has been established for in-process control. In this work Bettis has experienced some difficulty with sticking of the Inconel-X platens and the specimens. Preliminary evaluation indicates that more careful control of the graphite-coating process for the platens will eliminate the problem.

Argonne[22] is using a hot-pressing technique to achieve bonding between 0.006-in.-thick plutonium foil and 0.002-in.-thick aluminum cladding. Various bonding aids, such as silicon, germanium, tin, magnesium powder, silver foil, and silver powder, were studied; silicon appeared the most effective in producing good plutonium-to-aluminum bonds. Six assemblies have been successfully made in this fashion.

The Bureau of Mines has demonstrated that niobium and tantalum can be joined by pressure bonding.[23] Low mechanical pressure is utilized at relatively high temperatures to achieve high-strength joints.

(P. J. Gripshover)

## Diffusion Bonding

At General Electric[24] the diffusion bonding between various combinations of niobium-, molybdenum-, nickel-, and cobalt-base alloys, stainless steel, copper, and beryllium is being considered. Experiments thus far have been

conducted using bonding conditions of 2000°F for 4 hr. A niobium-base alloy (F-48) in contact with molybdenum–0.5 wt.% titanium did not reveal much interdiffusion, but in contact with stainless steel (type 316) and with a cobalt-base alloy (L-605) it formed a very hard intermetallic interface. The molybdenum–0.5 wt.% titanium, bonded to the stainless steel, the cobalt-base alloy, and a nickel-base alloy (René 41), also resulted in the formation of hard intermetallics. Additional couples have been bonded at 1800°F for 4 hr to continue the study.

To form diffusion bonds between refractory-metal carbides and tantalum, workers at General Electric[25] heated the components in vacuum at 2700°K for about 15 min under an unspecified (but presumably a low and uniaxial) pressure. Heating and cooling rates were maintained at about 200°C/min in order to minimize thermal stresses. It is reported that successful bonds were obtained between tantalum and NbC, HfC, and $TaC_{0.8}ZrC_{0.2}$. The diffusion bond between tantalum and UC was not considered successful. The authors also studied a brazing technique in which molybdenum or iridium was used as a filler. This was concluded to be more practical than diffusion bonding because the time required at the maximum temperature was only about 1 min for brazing as compared with about 30 min for diffusion bonding. Overlooking the unexplained 15 additional min for the diffusion-bonding time, the authors' evaluation of the quality of the diffusion bonds and the brazed joints does not appear to justify such a conclusion, at least based on the results described. Also, a study of the relation between the applied pressure and the required temperature and time for diffusion bonding would likely help to clarify the relative merits of the two joining methods.

(D. C. Carmichael)

## Coextrusion

Metallurgically bonded tubular joints of types 304L and 347 stainless steel and Zircaloy-2 or Zircaloy-4 and zirconium have been prepared by tandem extrusion by workers at Nuclear Metals.[15] The mechanical and corrosion behavior of these joints is limited by the Zircaloy rather than by the interface. The joints have been cold worked to at least a 40% reduction in area without detriment to the bond quality.

(C. B. Boyer)

## Canning

Vibratory-compaction studies of superheater fuel rods for Pathfinder were initiated by Allis Chalmers[26] because of the simplicity and economy associated with this process. The same fuel and cladding materials were used as for the swage-compaction studies already under study. Initially arc-fused $UO_2$ powders of the same particle-size distribution used by other investigators were used for this study. Fuel rods were vibrated under various conditions. In no case could densities greater than 86% of theoretical be achieved, even though larger values are reported in the literature. It was found that a 10-min vibration time using a $1\frac{1}{4}$-in. pneumatic-piston vibrator was sufficient for maximum density to be obtained. Considerable comminution of the larger particle-size fractions occurred during the compaction operations.

Development of a vibrational-compaction process at Hanford[27] for fabricating plutonium-bearing fuel elements is continuing. Efforts have been concentrated on determining (1) the optimum size distribution of $UO_2$ and $PuO_2$ fuel materials and (2) a method for loading the fuel material into a cladding tube, which will result in a uniform dispersion of $PuO_2$.

Several loading techniques have been used to achieve a uniform dispersion of $PuO_2$. In one technique, –325-mesh $PuO_2$ and –325-mesh $UO_2$ powders were blended, and this mixture was added to the fuel tube along with a coarse $UO_2$ fraction. Another technique involved uniform incremental loadings of –325-mesh $UO_2$ powder, alternated with loadings of coarse $UO_2$ particles. In a third technique a feeder mechanism blended coarse and fine particles just before they were fed into the fuel tube. When the tube was filled, the vibrator was turned on. This procedure was repeated until the tube was fully loaded. For all the above loading techniques, the variation of the fines was a factor of 2 or 3 greater than that obtained in swaged rods.

Hanford[27] has also been concerned with indirect coupling of vibrational forces to fuel-element cladding components for application to remote fabrication of recycled plutonium-bearing fuels. In general, this technique involves applying vibration to the cladding by a beam structure connected to a vibrator. Preliminary results indicate that the coupling arrangement facilitates uniform compaction and has little effect on compaction efficiency.

Construction of such a facility has been completed at Hanford.[19] Vibrational energy is transmitted to the fuel rods through a 15-ft-long steel beam to which the fuel rods are attached. Seven Mark I PRTR fuel elements have been satisfactorily compacted for use in physics experiments. One-step fabrication of a complete fuel element by remote vibrational compaction is being evaluated. A completed Mark II-C nested tubular PRTR element was vibrated at frequencies between 200 and 3600 cps and at accelerations up to 60 g without appreciable damage to the components. Further studies are planned using accelerations up to 100 g to determine whether damage to nested elements will result.

A special loading technique has been developed at Argonne[28] for loading depleted-uranium blanket slugs and plutonium-aluminum fuel slugs so as not to expose the exterior of the Zircaloy-2 jacket or weld area to contamination. A vinyl pouch that has fittings projecting from it serves as a guide for the Zircaloy-2 jacket and permits a leaktight external seal while loading the slugs.

Optimum parameters have been established for NaK filling and bonding of these loaded jackets. Some problems occurred in getting the liquid NaK to flow into the loaded jackets and completely fill the annulus between slugs and jacket. It was found that pressurizing the filling chamber, followed by vibration and evacuation, was most effective in minimizing voids and entrapped gas bubbles in the NaK. The subsequent bonding heat-treatment consists of holding at 425 to 450°C for 4½ hr.

A recent article[29] describes the work of several laboratories concerned with vibration-compacted ceramic fuels. Particular emphasis is placed on the process for fabrication of the nested PRTR fuel element developed at Hanford. A detailed account of the materials used, as well as the process variables considered, is given for the PRTR process.

(E. G. Smith, Jr.)

## Nonelectrolytic Chemical-Plating Techniques

Two state-of-the-art reviews[30,31] of chemical vapor deposition, covering work on chemical transport of materials, the preparation of solid materials in bulk form, overlay coatings, and diffusion coatings, became available during the past quarter.

Chemical transport between a uranium carbide cathode and a platinum anode is under study.[32] An objective of this work is to minimize the vaporization loss from carbide cathodes operating in the temperature range 2100 to 2500°K so that their performance and life can be improved. Chemical additions of hydrogen and halogens in the thermionic cell appear to be potentially helpful for this purpose. Useful dissociation data for the halogens and for the cesium halides are presented in tabular form.

A relatively rigorous theoretical analysis of the vapor transport of solids was published.[33] This analysis should be of interest to those concerned with mass-transfer problems in the field of chemical vapor deposition. An extension was made of the above analysis to indicate the relation between diffusion and the vapor transport of solids.[34]

Chemical vapor deposition of solid materials in bulk form (i.e., in massive deposits rather than in thin coatings) holds much promise as a means of producing refractory-metal and metal-alloy parts and then joining these parts to form structures. The progress of a research program in this area was described.[35]

Relatively pure boron, in the form of rods and filaments, has been prepared by chemical vapor deposition.[36,37] Cylindrical crystalline rods that were 3 mm in diameter and 10 cm long were grown on 6-$\mu$-diameter incandescent tungsten filaments by the reaction of $BBr_3$ and hydrogen. Amorphous boron deposits on 0.5-mil tungsten wire were formed both in batch processes and on a continuous basis. Boron filaments that were 4 mils in diameter and over 700 ft long were produced at the rate of 4 ft/min.

Pyrolytically deposited "alloys" of carbon plus boron have oxidation rates 30% below those of pyrolytic carbon and pyrolytic boron nitride at certain air-flow rates.[38] Such material (trade name: Boron Pyralloy), however, should be considered equivalent to pyrolytic carbon in oxidation resistance.

The processes of chemical vapor deposition are useful in the preparation of refractory oxides. For example, tabular alpha corundum[39] is obtained as the end product of the steam hydrolysis of $AlF_3$. Thermal treatment at temperatures above 800°C is carried out in a bed fluidized by steam and air. The product contains substantial amounts of aluminum oxyfluoride.

An attempt was made to grow $UO_2$ crystals using the reaction

$$UF_4(g) + 2(H_2O)g \rightarrow UO_2(s) + 4HF(g)$$

A dark brown deposit[40] was obtained in a 100-hr run at 1200°C. It was identified as $UO_2$ by X-ray diffraction.

Overlay coatings of 0.5-mil-thick chromium were deposited on uranium carbide pellets by thermal decomposition of chromium dicumene.[41] Mechanically bonded coatings of tungsten were formed[42] on roughened copper, graphite, vanadium, ferrochromium, alumina, silicon nitride, and zircon substrates by hydrogen reduction of $WF_6$ at 550°C. Coatings of $Nb_3Sn$, formed by the hydrogen reduction of mixed chlorides, were deposited on niobium ribbon substrates in a continuous process.[43] In other experiments at the same site, $Nb_3Sn$ coatings were formed on $Al_2O_3$ flat plates and tubes. Also, whiskers of $Nb_3Sn$ that were 8 mm long by 0.1 mm wide were prepared. Pyrolytic graphite coating of refractory boride, carbide, and nitride fibers is under study.[43] Such coated fibers are subsequently subjected to heat-treatment to promote bonding. Carbon and graphite fibers have been coated with the borides, carbides, and nitrides of titanium and zirconium.[44a]

The wide-scale government-supported research effort to develop diffusion type silicide coatings to protect refractory metals and alloys against oxidation at high temperatures was continued. Work reported includes a discussion of the fundamental aspects of the siliconizing of molybdenum[44b] and a description of a process for the deposition of a composite titanium-$WSi_2$-silicon coating on niobium-base alloys.[44c] In the case of the latter coating, the titanium layer was deposited from a fused-salt mixture and the $WSi_2$ and silicon layers by chemical vapor deposition in fluidized beds. "Silicided" chromium electroplates on refractory-metal substrates spalled on thermal cycling.[45] The "siliciding" process[45] made use of monomethylsilanes and tetramethylsilanes as silicon source materials and yielded silicon diffusion type coatings that contained appreciable amounts of SiC. (E. M. Sherwood)

### Ceramic Coatings

The National Bureau of Standards[46] has completed a study of flame spraying. Both rod and powder guns were used to apply aluminum oxide. The coatings were found to be eta alumina that was formed at the high quench rates (800,000°C/sec on stainless steel and 34,000°C/sec on glass). The powder guns sprayed particles continuously; the rod gun sprayed only in bursts. Smaller particles and higher particle speeds were observed with the rod gun. A chemical bond was developed on glass but not on metal. The bond strength between coating and iron increased exponentially with roughness of the metal surface. (B. W. King)

## Explosive Forming

### Forming Characteristics of Refractory Metals

A study of the explosive-forming characteristics of molybdenum–0.5 wt.% titanium and of tungsten has recently been completed by Propellex Division of Chromalloy Corporation.[47] On the basis of this investigation, the following conclusions were drawn:

1. For the range of material thicknesses tested, 10 to 40 mils (and possibly for greater thicknesses), a very low draw-ring pressure must be used to ensure a wrinkle-free part with a minimum thinning of the workpiece.
2. Of the two explosives tested, RDX and 40% dynamite, the latter was found to be superior because the lower detonation velocity permits the maximum possible draw with the least amount of elongation. Cup-shaped specimens formed with RDX showed slightly greater elongations, but there were microscopic cracks around the periphery. For high-temperature (to 1000°F) forming, thermal deterioration can be minimized by encasing the charge in a shaped Fiberglas container.
3. Powdered alumina is a superior transfer medium because its impedance is similar to that of the explosive, which permits only weak reflections from the explosive-alumina interface. The use of alumina slows down the impulse delivery and renders the shape of the charge unimportant.

### Explosive Joining of Dissimilar-Metal Tubes

A program concerning the explosive joining of Zircaloy-2 to type 410 stainless steel has recently been completed by Battelle.[48] This program was concerned with the joining of tubular specimens of Zircaloy-2 and type 410

stainless steel which were prepared from 6-in.-OD by 3.400-in.-ID by 3-in.-long type 410 stainless steel and 3.300- to 3.400-in.-OD by 3.156- to 3.340-in.-ID by 3-in.-long Zircaloy-2 components cut from tubular stock. Various joint designs were investigated during this testing. Sketches of these joint designs are shown in Fig. V-1. The two surface preparations that were used to prepare these specimens for explosive bonding consisted of:

1. (a) Vapor degrease
   (b) Scrub in methyl ethyl ketone
   (c) Place in ultrasonic bath of 200-proof grain alcohol
   (d) Scrub in hot (180°F) distilled water
   (e) Scrub in cold distilled water
   (f) Place in ultrasonic bath of 200-proof grain alcohol
   (g) Hot-distilled-water rinse
   (h) Cold-distilled-water rinse
   (i) Hot-distilled-water rinse
   (j) Air blow dry
   (k) Scrub mating surfaces with 10% MgO-$NaCO_2$ slurry

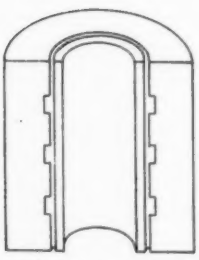

(*a*) Grooved joint

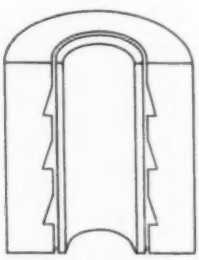

(*b*) Tapered joint — 8, 10, and 12° tapers on inside diameter of stainless steel

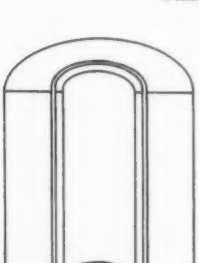

(*c*) Straight joint

Fig. V-1 Joint designs of Zircaloy-2 to type 410 stainless steel.[48]

2. (a) Degrease in methyl ethyl ketone
   (b) Scratch brush mating surfaces with rotating wire brush

Several different charge configurations were used during the explosive impaction of these tubular-joint specimens with both air and water transfer media. Sketches of the charge configurations used are shown in Fig. V-2. Specimens were prepared for detonation in air by simply preparing and locating the desired charge configuration in the specimen and by detonating the charge in air. The specimens that were impacted under water, however, were prepared by (1) placing them in a sock of Gooch tubing, (2) evacuating the assembly, (3) positioning the desired charge configuration in the specimen, (4) submerging the assembly in a tank of water, and (5) detonating the charge.

The bonds produced during this testing were examined metallographically and subjected to bend, tensile-shear, and thermal-cycling tests to determine bond quality and strength. The variables investigated include (1) workpiece configuration, which includes Zircaloy-2 thickness (20 to 100 mils), joint clearance (0 to 50 mils), surface roughness (300 to 1500 $\mu$in.), and joint design (straight, grooved, tapered); (2) explosive process variables, which include standoff distance (0 to $\frac{3}{4}$ in.), transfer medium (air and water), and atmosphere (air and vacuum); and (3) the charge configuration.

A series of tests was conducted in which the thickness of the Zircaloy-2 and the clearance between the Zircaloy-2 and stainless steel were varied. Specimens were impacted in air and under water. Metallographic examination of the joints revealed that 100% bonding was achieved under water with 30-mil-wall Zircaloy-2. In air, however, under similar conditions, only 70% bonding was obtained with 30-mil-wall Zircaloy-2. These bonds are shown in Fig. V-3. In both transfer media, only a minimum amount of bonding was observed in specimens in which the Zircaloy-2 wall thickness was greater than 50 mils. Tensile-shear tests of the bonded material showed a bond strength of approximately 73,000 psi or about the strength of the impacted Zircaloy-2. Thus it appears that Zircaloy-2 wall thickness is a significant factor in bonding since only a constant narrow range of thicknesses showed bonding under a variety of experimental conditions. Also, wall thickness and component clearance appeared interrelated sig-

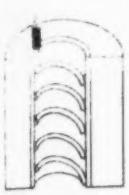

(*a*) Spiraled primacord

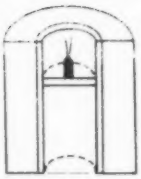

(*b*) Disk. Area above and below disk filled with rubber

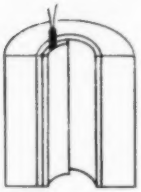

(*c*) Contact charge of sheet explosive covering one-fourth of joint area

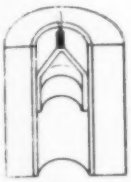

(*d*) Ring and tent

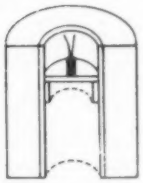

(*e*) Ring and disk. Area below disk filled with rubber

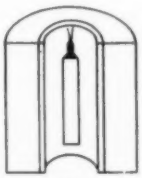

(*f*) Rolled rod

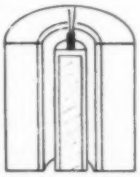

(*g*) Cylindrical charge on mandrel

Fig. V-2 Explosive charge configurations tested.[48]

nificantly since the best results were obtained when clearances and wall thicknesses were in the range of 0.020 to 0.040 in.

Several experiments were conducted for the purpose of determining the optimum amount of clearance required between Zircaloy-2 and type 410 stainless steel. The clearance should allow sufficient expansion for oxide-layer breakup in the Zircaloy but should not be so large that the explosive energy is dissipated in an unnecessary further stretching of the material. Straight- and grooved-joint Zircaloy-2 to stainless-steel specimens with various clearances and Zircaloy thicknesses were explosively impacted both in air and under water. Metallographic examination showed that 100% bonding was obtained in water under vacuum with 20- and 30-mil-wall Zircaloy-2 when joint clearances were 20 to 40 mils and that bonding was reduced to 60% when the clearance was increased to 50 mils. It was also found that very little (10 to 20%) bonding was achieved with 90- to 100-mil Zircaloy-2 either in air or in water under vacuum. Thus it appears that, like Zircaloy-2 wall thickness, joint clearance must be held within a certain narrow range in impacting a particular configuration in order to obtain a good bond.

The effect of surface roughness was investigated to determine the optimum value required. Straight-, tapered-, and grooved-joint specimens with surface finishes of 500, 1000, and 1500 $\mu$ in. rms on the stainless-steel component were evaluated, respectively, with 500-, 500-, and 300-$\mu$ in. rms surface finishes on the Zircaloy-2 components in explosive impaction tests under evacuation in air and water transfer media. Metallographic examination of the impacted specimens revealed that, although 100% bonding was obtained with specimens representing 500-500 and 1000-500 $\mu$ in. rms surface-roughness combinations, more locking was obtained when the 1000-$\mu$ in. rms surface finish on the stainless-steel surfaces was employed. The tensile-shear data obtained indicated a somewhat higher strength with the 1000-$\mu$ in. rms stainless steel to 500-$\mu$ in. rms Zircaloy-2 combination. Thermal cycling 1070 times from 150 to 590°F produced no separation in specimens in which both mating surfaces were finished to 500 $\mu$ in. Therefore it seems that, although surface roughness within the range studied does not appear to be critical, slightly stronger bonds can be expected with rougher surfaces.

Several tests were conducted with various joint designs to determine the joint configuration that would produce the best bonds in Zircaloy-2 to stainless steel and aluminum to mild-steel tubular specimens by explosive impaction. Straight-, grooved-, and tapered-joint configurations were employed with the two material combinations in explosive impaction experiments in air and under evacuation in air and under water. In the experiments conducted with the Zircaloy-2 to stainless-steel specimens, successful bonding was obtained with grooved- and straight-joint specimens. The tensile-shear testing of these specimens revealed that grooved- and straight-joint specimens had about

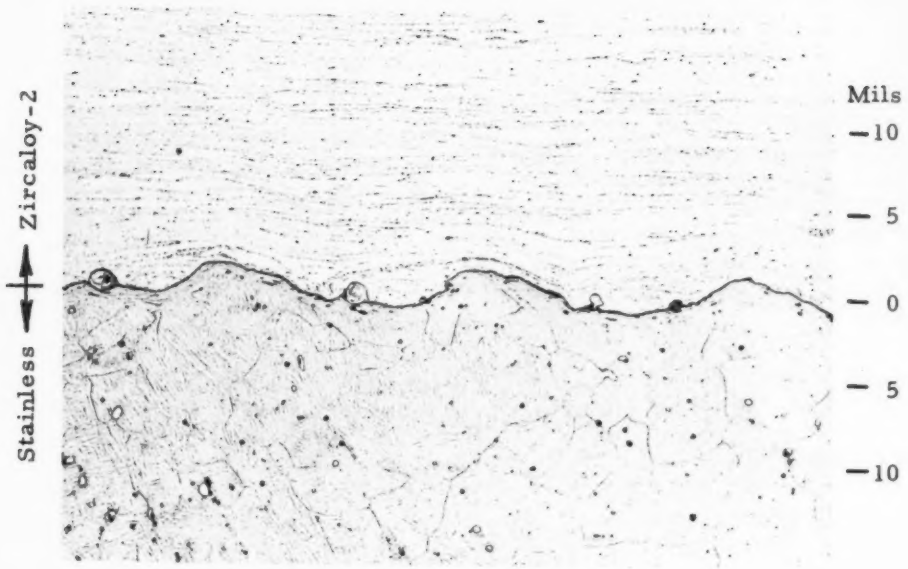


(*a*) Under water (bond covered 100% of surface)

(*b*) In air (bonded at 70% of interface)

Fig. V-3 Explosively bonded Zircaloy-2 to type 410 stainless steel.[48] Bond is shown in the etched condition. The surface finishes of the Zircaloy-2 and stainless steel were 500 and 1000 $\mu$in. rms, respectively.

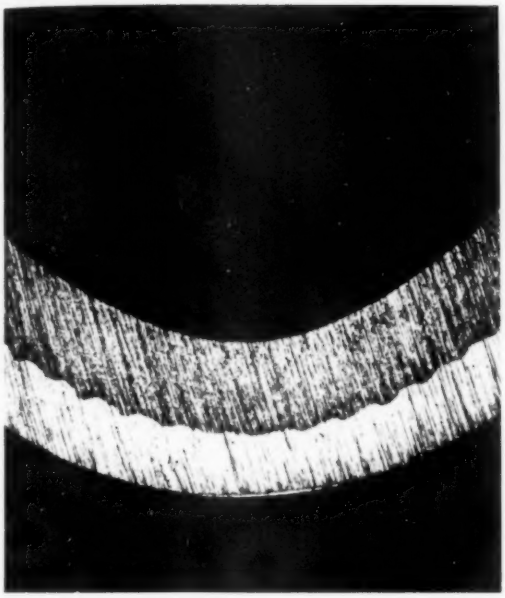

Fig. V-4 Apex of a $\frac{1}{8}$-in.-radius bend of a Zircaloy-2 to type 410 stainless steel straight-joint specimen.[48] The Zircaloy-2 is in tension, and the stainless steel is in compression.

the same strength; however, in bend testing, the grooved-joint specimens ruptured at the edge of the groove shortly after stress initiation, whereas the straight-joint specimens could be bent to a $\frac{1}{8}$-in. radius, as shown in Fig. V-4. There was also no separation visible at the interface of the straight-joint specimens after 1070 thermal cycles from 150 to 590°F. Intermetallic formation at the interface was observed metallographically in all the grooved-joint specimens at the base of the grooves, but only occasionally in the straight-joint specimens. The tapered-joint specimens, however, sheared during explosive impaction; thus no intact bonded examples of this configuration were obtained.

Since apparently there is little difference in facility of bonding between grooved- and straight-joint Zircaloy-2 to type 410 stainless-steel tubular specimens, the superior ductility of the bond interface and the ease of preparation of the straight-joint configuration make it the more promising design.

Several tests were conducted at various standoff distances to determine the optimum charge standoff distance required for explosive bonding of tubular configurations of Zircaloy-2 to type 410 stainless steel and 6061-T-6 aluminum to mild steel. Grooved-joint specimens representing both material combinations were explosively impacted under water in evacuated socks of Gooch tubing. The charges used were 45 g and the standoff distances were 0, $\frac{3}{8}$, $\frac{1}{2}$, $\frac{5}{8}$, and $\frac{3}{4}$ in. Metallographic examination of the impacted specimens revealed that 90 to 100% bonds were obtained with the Zircaloy-2 to stainless-steel specimens at standoff distances of $\frac{1}{2}$ and $\frac{3}{4}$ in., whereas at $\frac{3}{8}$ in. a 70% bond was achieved. However, when contact charges were employed, rupturing occurred.

It was concluded from the results of these tests that, for the Zircaloy-2 to stainless-steel configurations studied, a standoff distance of $\frac{3}{4}$ in. gave best results. The reduction in intermetallic formation followed improvements in the evacuation technique and seemed to confirm earlier conclusions that air entrapped at the interface during impaction produced localized areas of high heat which resulted in a reaction between the two component materials. This can be seen in Figs. V-5 and V-6, which show specimens that were impacted under poor and good evacuations, respectively.

To evaluate the effect of the transfer medium in explosive bonding of Zircaloy-2 to stainless-steel tubular configurations, assemblies were impacted under water and in air with and without evacuation. Metallographic examination of the specimens after impacting revealed that 100% bonding was achieved when impacting was done under evacuation under water, whereas 60 to 70% bonding was achieved under evacuated conditions in air. No bonding occurred when the assemblies were impacted in air without evacuation. These results indicate that water is a more efficient transfer medium than air and that an evacuated atmosphere must be used if good bonding is to be achieved in either medium.

Overall, the work showed that good bonds can be produced relatively inexpensively with prototype materials and geometries since the tensile-shear strengths of the joints produced were nearly equal to that of the base metal. Under optimum joining conditions, no brittle intermetallics or hardness increases were produced in the interface region. Also, no special equipment was needed to effect the joining.

(C. C. Simons)

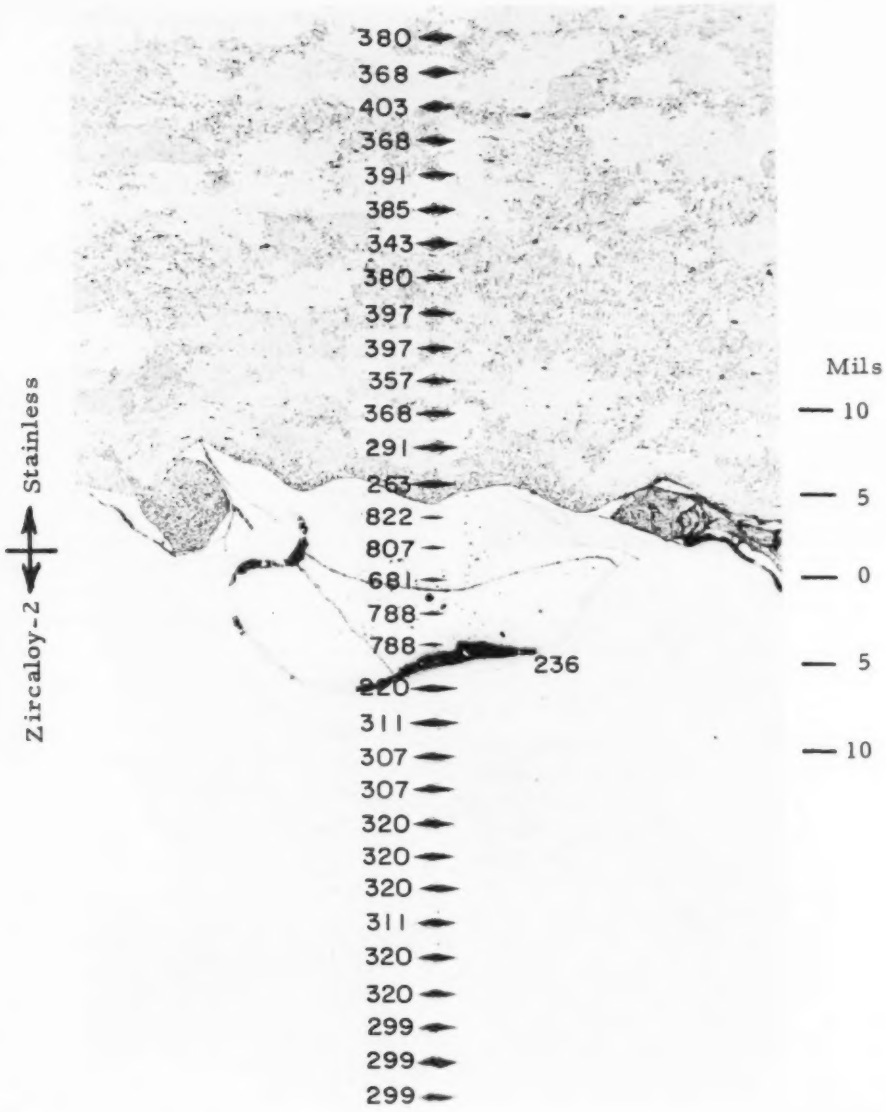


Fig. V-5 Hardness traverse across the explosive-weld interface at the location of the second phase in a Zircaloy-2–type 410 stainless-steel assembly.[48] Note the sharp increase in hardness and cracking in the new phase. Also note the drop in hardness immediately adjacent to either side of the phase. All readings are Knoop hardness made with a diamond-pyramid penetrator and a 100-g load; readings are 0.005 in. apart.

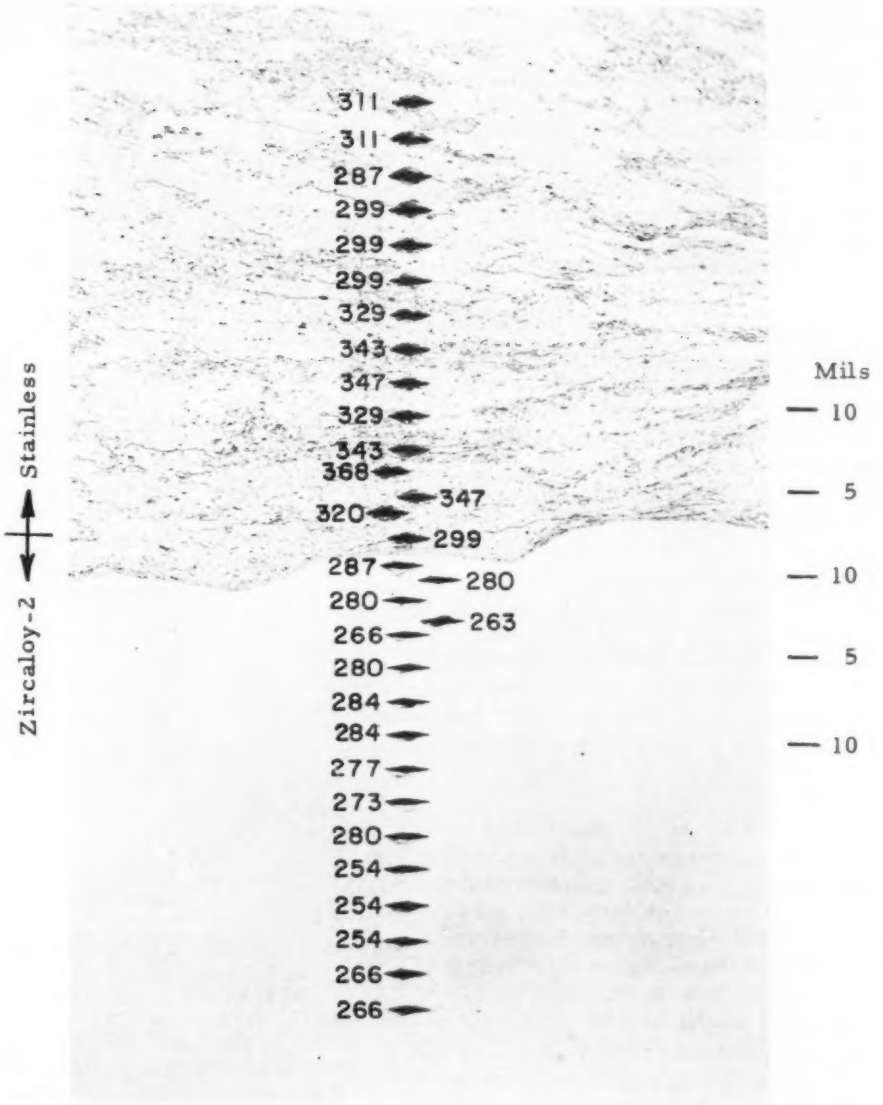


Fig. V-6 Hardness traverse across explosive-weld interface where no second phase is visible in a Zircaloy-2–type 410 stainless-steel assembly.[48] Note that there is very little difference in hardness between the weld interface and base materials. All readings are Knoop hardness made with a diamond-pyramid penetrator and a 100-g load; readings are 0.005 in. apart.

# Nondestructive Testing

Methods of "visualizing" ultrasonic fields to produce images of the interior of materials have been of interest for a long time. According to Jacobs[49] of Northwestern University, charge scanning using an electron beam is capable of obtaining sensitivities in the order of 4% on various metals with thicknesses up to 2 in. The sensitivity of the tubes is limited to the degree of modulation present on the return beam, which in turn is limited by noise in the scanning beam itself.

Charge scanning, as used at Armour Research for the nondestructive evaluation of ceramic coatings on metals,[50] is similar to closed-circuit television. The image-converter tube is analogous to a television-camera tube with the photosensitive surface replaced by a piezoelectric or ferroelectric material.

Measurements of the sensitivity of electronically scanned pickup tubes carried out at Argonne show the tubes to respond to ultrasonic intensities of the order of $10^{-7}$ watt/cm$^2$. Although published theoretical sensitivities are of the order of $10^{-9}$ watt/cm$^2$, $10^{-7}$ watt/cm$^2$ appears to be the threshold sensitivity whether quartz or $BaTiO_2$ faceplates are used. The limiting value appears to be the piezoelectric voltage variation that can be detected by the scanning beam.

Some indications of the sensitivities of charge-scanning techniques are demonstrated in reported figures. Armour[50] claims to obtain visual images of simulated defects $^1/_{32}$ in. in diameter in ceramic coating-metal substrate systems where the defect thickness is only a factor of 3 larger than the average coarse grains found in the coating material.

Argonne workers claim[51] that they can resolve wires 0.005 to 0.007 in. in diameter at frequencies from 2 to 5 Mc. They also report[52] that they can see 3 to 5% thickness variations in 1-in. aluminum.

Argonne[11,52,53] also has investigated imaging techniques other than charge scanning. These have exhibited poor sensitivity. Ultraviolet-excited phosphor, with its luminescence quenched ultrasonically, requires 5 to 10 watts/cm$^2$ of ultrasonic intensity. Photographic film and photographic paper exposed to an ultrasonic field in a developer solution reproduce the ultrasonic field. Each requires intensities of approximately 0.5 watt/cm$^2$. The photographic-paper technique requires 20- to 30-sec exposure times, compared with 5 to 10 min for the photographic-film method. Because of the poor sensitivity of these methods, image quality from metal objects has been poor.

Argonne[11,52,53] has been conducting studies to determine whether the mechanism of beta-to-alpha phase transformation in plutonium is a nucleation and growth mechanism, which is essentially a diffusion-controlled process, or whether it is a martensitic process, where whole groups of atoms move cooperatively, sometimes at nearly sonic speeds. They have succeeded in measuring sound velocity and attenuation in a plutonium sample as a function of temperature. The temperature range has been from room temperature to 320°C. The transformations are from the alpha phase, through the beta and gamma phases, and into the delta phase. The transit time changes abruptly by about 35% during the alpha-to-beta phase change. The other phase changes are also visible, but not in as striking a manner as the alpha-to-beta change. The curves are reproducible. (D. Ensminger)

## References


1. R. Burgett (Ed.), Summary Technical Report for the Period April 1, 1962–June 30, 1962, USAEC Report NLCO-855, National Lead Co. of Ohio, July 25, 1962.
2. Bureau of Mines, Metallurgical Quarterly Progress Report No. 15 for the Period of April 1, 1962, Through June 30, 1962, USAEC Report USBM-U-952.
3. Oak Ridge National Laboratory, Metals and Ceramics Division Annual Progress Report for Period Ending May 31, 1962, USAEC Report ORNL-3313, Aug. 16, 1962.
4. H. Kjoellesdal, T. Lindtveit, and K. Boeye, Mechanical Properties of Niobium. I. Electron-beam Melting and Analytical Methods, Norwegian Report AD-263880, May 1961.
5. T. Hikido, Horizontal Zone Melting of Refractory Metals by Remote Gun Electron Bombardment, pp. 276–283, in Proceedings of the Fourth Symposium on Electron Beam Technology, Alloyd Electronics Corp., 1962.
6. J. Baird and O. J. C. Runnalls, The Preparation of Aluminum-Uranium Alloys by the Aluminum Reduction of Uranium Dioxide, Canadian Report CRRM-1065, December 1961.
7. G. C. Wootton and J. A. Perry, The Gamma-Phase Extrusion of Small Diameter Uranium Bars, Canadian Report CRFD-1094, June 1962.

8. G. C. Wootton, The Fabrication of the Cores for the Mark XIV 19-Element NRU Rod, Canadian Report FD-77, September 1961.
9. Bridgeport Brass Co., Process Development Quarterly Report, July–December 1960, USAEC Report BRB-67, May 31, 1962. (Classified)
10. J. C. Tverberg and J. J. Holmes, Extrusion Characteristics of Uranium-Zirconium and Uranium-Carbon Alloys, USAEC Report HW-62347, Hanford Atomic Products Operation, June 1961.
11. Argonne National Laboratory, Reactor Development Program Progress Report, June 1962, USAEC Report ANL-6580, July 15, 1962.
12. F. E. Weil and J. G. Hill, Investigation of the Technical Feasibility of Cold Extrusion for Zircaloy-2 Tubing Production, Quarterly Technical Progress Report No. 3, April–June 1961, USAEC Report ATL-A-120, Advanced Technology Laboratories.
13. E. Landerman and C. J. Kubit, Development of Fabrication Procedures for Construction of Thermal Baffles, Including Preoxidizing of Zircaloy, USAEC Report CVNA-113, Westinghouse Electric Corp., Atomic Power Dept., Sept. 5, 1961.
14. F. W. Albaugh, Reactor and Fuels Research and Development Operation Monthly Report, June 1962, USAEC Report HW-74153A, Hanford Atomic Products Operation, July 15, 1962. (Classified)
15. W. B. Tuffin, A. R. Gilman, and S. Isserow, Tubular Stainless Steel-Zircaloy Transition Joints Prepared by Tandem Extrusion, USAEC Report NMI-7216, Nuclear Metals, Inc., Feb. 2, 1962.
16. F. Hofmann and B. Liebmann, Fabrication of Oxide-based Fuel Elements by Swaging. Quarterly Progress Report No. 3, January 1–March 31, 1961, Hot Swaging of Uranium Oxide Fuel Elements, USAEC Report EURAEC-60, Nuklear-Chemie und-Metallurgie G.m.b.H., May 17, 1961.
17. FIAT. Sezione Energia Nucleare, Swaging of Uranium Dioxide. Quarterly Progress Report No. 5, July 1, 1961, to September 30, 1961, USAEC Report EURAEC-193, Oct. 31, 1961.
18. FIAT. Sezione Energia Nucleare, Swaging of Uranium Dioxide. Quarterly Progress Report No. 6, October 1, 1961, to December 31, 1961, USAEC Report EURAEC-253, Jan. 31, 1962.
19. S. Goldsmith and P. F. Ashbrook (Eds.), Research and Development Programs Executed for the Division of Reactor Development, Quarterly Progress Report, January–March 1962, USAEC Report HW-73915, Hanford Atomic Products Operation, Aug. 1, 1962.
20. E. S. Hodge et al., Gas-Pressure Bonding, *Ind. Eng. Chem.*, 54(1): 31–35 (January 1962).
21. Westinghouse Electric Corp., Bettis Atomic Power Laboratory, Pressurized Water Reactor (PWR) Project, Technical Progress Report for the Period February 24, 1962–April 23, 1962, USAEC Report WAPD-MRP-97, Apr. 23, 1962.
22. Argonne National Laboratory, Reactor Development Program Progress Report, March 1962, USAEC Report ANL-6544, Apr. 15, 1962.
23. Bureau of Mines, Metallurgical Progress Report No. 14 for the Period of January 1, 1962, to March 31, 1962, USAEC Report USBM-U-921.
24. W. R. Young, J. W. Clark, and E. S. Jones, Investigation of the Physical Metallurgy of Joining Tungsten and Columbium, Report NP-11382, General Electric Co., Flight Propulsion Laboratory Dept., Feb. 9, 1962.
25. E. Blue, A. C. Chapin, and J. H. Ingold, High Temperature Bonding Techniques, Report APED-3870, General Electric Co., Atomic Power Equipment Dept., Dec. 29, 1961.
26. C. B. Graham and H. Hill, Pathfinder Atomic Power Plant Technical Progress Report, October 1961–December 1961, USAEC Report ACNP-62005, Allis-Chalmers Mfg. Co., Apr. 20, 1962.
27. S. Goldsmith (Ed.), Research and Development Programs Executed for the Division of Reactor Development. Quarterly Progress Report, October 1961–December 1961, USAEC Report HW-73100, Hanford Atomic Products Operation, May 1, 1962.
28. Argonne National Laboratory, Metallurgy Division Annual Report for 1961, USAEC Report ANL-6516.
29. J. J. Hauth, Vibration Compacted Ceramic Fuels, *Nucleonics*, 20(9): 50–54 (September 1962).
30. Battelle Memorial Institute, Defense Metals Information Center, Chemical Vapor Deposition, Report DMIC-170, June 4, 1962.
31. R. Bakish et al., Vapor Phase Metallurgy and Ceramics, *J. Metals*, 14(10): 770–774 (October 1962).
32. S. Langer and L. Yang, Carbide Cathode Studies Physical and Chemical Redeposition, USAEC Report GA-3093, General Atomic Div., General Dynamics Corp., Apr. 18, 1962.
33. G. Mandel, Vapor Transport of Solids by Vapor Phase Reactions, *Phys. Chem. Solids*, 23: 587–598 (June 1962).
34. R. F. Lever and G. Mandel, Diffusion and the Vapor Transport of Solids, *Phys. Chem. Solids*, 23: 599–600 (June 1962).
35. M. E. Browning, Deposition for the Production of Structure. Interim Progress Report No. 3 for Feb. 1–May 1, 1962, American Machine and Foundry Co., May 1, 1962.
36. C. P. Talley and G. R. Taylor, Jr., Preparation of High-Purity Single Crystal Boron, Report ASD-TR-61-318, Texaco Experiment Inc., January 1962.
37. C. P. Talley et al., Boron Reinforcements for Structural Composites, Report ASD-TDR-62-257, Texaco Experiment Inc., Mar. 15, 1962.
38. High Temperature Materials, Inc., Development of Boron Pyralloy for Rocket Motor Hardware,

Monthly Progress Report for May 1962, June 27, 1962.

39. B. P. Löcsei, Manufacture of Alkali-Free Corundum of Tabular Crystal Form, *Nature*, 194(4824): 177–178 (Apr. 14, 1962).
40. S. Arnelinckx, Growth of $UO_2$ Single Crystals, USAEC Report EURAEC-245, Centre d'Étude de l'Énergie Nucléaire, Dec. 31, 1961.
41. L. Sama, S. Priceman, and R. Powers, Columbium Coating Program; Informal Progress Report, USAEC Report TID-15087, January 1962. (Classified)
42. F. W. Hoertel, Vapor Deposition of Tungsten and the Effect of Process Variables, Monthly Report No. 8, Bureau of Mines, Rolla Metallurgical Research Center, June 1962.
43. W. H. Cherry et al., Research on the Phenomena of Superconductivity in Metals and Alloys. Quarterly Progress Report No. 1 for Nov. 8, 1961–Jan. 15, 1962, David Sarnoff Research Center, Jan. 31, 1962.
44. Papers presented at Sixth Refractory Composite Working Group Meeting, Dayton, Ohio, June 17–19, 1962:
    *a.* High Temperature Materials, Inc., Research on New and Improved Thermally Protective Fiber Reinforced Composite Materials.
    *b.* G. P. K. Chu, Notes on Siliconizing Molybdenum.
    *c.* R. B. Eaton et al., Deposition of Coatings on Columbium from Fused Salts and Fluid Beds.
45. V. A. Lamb and J. A. Sligh, Coatings for Refractory Metals, Formed by Anodic Treatment and by Vapor Deposition, Report WADD-TR-61-64, National Bureau of Standards, September 1961.
46. D. G. Moore, A. G. Eubanks, H. R. Thornton, W. D. Hayes, Jr., and A. W. Crigler, Studies of the Particle-Impact Process for Applying Ceramic and Cermet Coatings, Report ARL-59, National Bureau of Standards, April 1961.
47. Chromalloy Corp., A Study of Explosive Forming Selected Refractory Metals, Report NP-11621, Apr. 1, 1962.
48. S. J. Paprocki and S. W. Porembka (Eds.), Joining Zircaloy–Stainless Steel and SAP Alloys by Friction, Rolling, and Explosives Techniques, USAEC Report BMI-1594, Battelle Memorial Institute, Sept. 4, 1962.
49. J. E. Jacobs, Ultrasonic Image Converter and Cinesonography in Nondestructive Testing, paper given at Symposium on Physics and Nondestructive Testing Sponsored by Southwest Research Institute, San Antonio, Tex., Oct. 2–4, 1962.
50. K. E. Feith and W. E. Lawrie, Ultrasonic Methods for Nondestructive Evaluation of Ceramic Coating, Report WADD-TR-61-91 (Pt. II), Illinois Institute of Technology, Armour Research Foundation, April 1962.
51. Argonne National Laboratory, Reactor Development Program Progress Report, August 1962, USAEC Report ANL-6610, Sept. 15, 1962.
52. Argonne National Laboratory, Reactor Development Program Progress Report, July 1962, USAEC Report ANL-6597, Aug. 15, 1962.
53. Argonne National Laboratory, Reactor Development Program Progress Report, May 1962, USAEC Report ANL-6573, June 15, 1962.

## LEGAL NOTICE

This document was prepared under the sponsorship of the U. S. Atomic Energy Commission. Neither the United States, nor the Commission, nor any person acting on behalf of the Commission:

A. Makes any warranty or representation, expressed or implied, with respect to the accuracy, completeness, or usefulness of the information contained in this report, or that the use of any information, apparatus, method, or process disclosed in this report may not infringe privately owned rights; or

B. Assumes any liabilities with respect to the use of, or for damages resulting from the use of any information, apparatus, method, or process disclosed in this report.
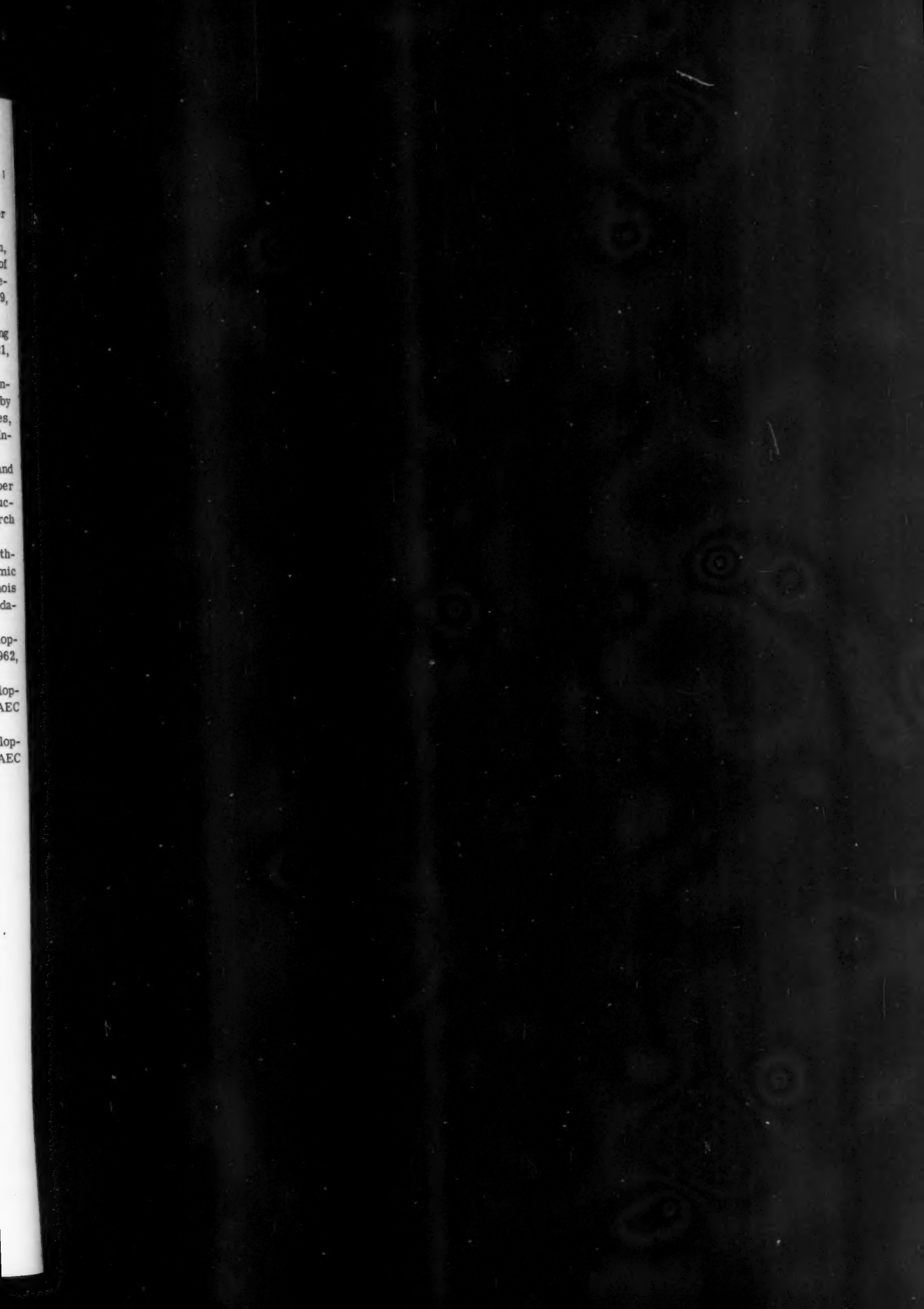
As used in the above, "person acting on behalf of the Commission" includes any employee or contractor of the Commission, or employee of such contractor, to the extent that such employee or contractor of the Commission, or employee of such contractor prepares, disseminates, or provides access to, any information pursuant to his employment or contract with the Commission, or his employment with such contractor.